frontiers | Research Topics

Diving deeper with metabolomics into animal physiology

Edited by
Elda Dervishi and Dagnachew Hailemariam

Published in
Frontiers in Molecular Biosciences
Frontiers in Animal Science

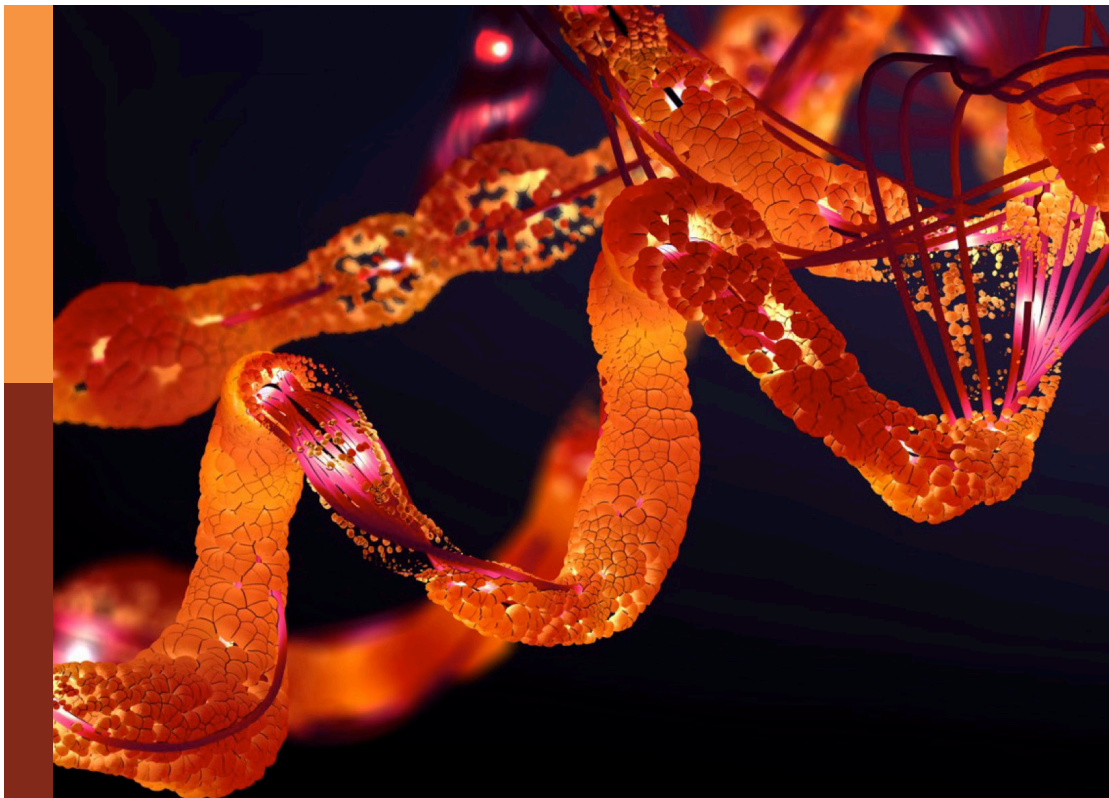

ISSN 1664-8714
ISBN 978-2-8325-5757-0
DOI 10.3389/978-2-8325-5757-0

About Frontiers

Frontiers is more than just an open access publisher of scholarly articles: it is a pioneering approach to the world of academia, radically improving the way scholarly research is managed. The grand vision of Frontiers is a world where all people have an equal opportunity to seek, share and generate knowledge. Frontiers provides immediate and permanent online open access to all its publications, but this alone is not enough to realize our grand goals.

Frontiers journal series

The Frontiers journal series is a multi-tier and interdisciplinary set of open-access, online journals, promising a paradigm shift from the current review, selection and dissemination processes in academic publishing. All Frontiers journals are driven by researchers for researchers; therefore, they constitute a service to the scholarly community. At the same time, the *Frontiers journal series* operates on a revolutionary invention, the tiered publishing system, initially addressing specific communities of scholars, and gradually climbing up to broader public understanding, thus serving the interests of the lay society, too.

Dedication to quality

Each Frontiers article is a landmark of the highest quality, thanks to genuinely collaborative interactions between authors and review editors, who include some of the world's best academicians. Research must be certified by peers before entering a stream of knowledge that may eventually reach the public - and shape society; therefore, Frontiers only applies the most rigorous and unbiased reviews. Frontiers revolutionizes research publishing by freely delivering the most outstanding research, evaluated with no bias from both the academic and social point of view. By applying the most advanced information technologies, Frontiers is catapulting scholarly publishing into a new generation.

What are Frontiers Research Topics?

Frontiers Research Topics are very popular trademarks of the *Frontiers journals series*: they are collections of at least ten articles, all centered on a particular subject. With their unique mix of varied contributions from Original Research to Review Articles, Frontiers Research Topics unify the most influential researchers, the latest key findings and historical advances in a hot research area.

Find out more on how to host your own Frontiers Research Topic or contribute to one as an author by contacting the Frontiers editorial office: frontiersin.org/about/contact

Diving deeper with metabolomics into animal physiology

Topic editors

Elda Dervishi — California State Polytechnic University, Pomona, United States

Dagnachew Hailemariam — University of Alberta, Canada

Citation

Dervishi, E., Hailemariam, D., eds. (2024). *Diving deeper with metabolomics into animal physiology*. Lausanne: Frontiers Media SA. doi: 10.3389/978-2-8325-5757-0

Table of contents

frontiers | Frontiers in Molecular Biosciences

TYPE Editorial
PUBLISHED 29 November 2024
DOI 10.3389/fmolb.2024.1503412

OPEN ACCESS

EDITED BY
Farhana R. Pinu,
The New Zealand Institute for Plant and Food Research Ltd., New Zealand

REVIEWED BY
Seyed Ali Goldansaz,
Agri-Food and Biosciences Institute, Ireland

*CORRESPONDENCE
Elda Dervishi,
edervishi@cpp.edu

RECEIVED 28 September 2024
ACCEPTED 19 November 2024
PUBLISHED 29 November 2024

CITATION
Hailemariam D and Dervishi E (2024) Editorial: Diving deeper with metabolomics into animal physiology.
Front. Mol. Biosci. 11:1503412.
doi: 10.3389/fmolb.2024.1503412

Editorial: Diving deeper with metabolomics into animal physiology

Dagnachew Hailemariam[1] and Elda Dervishi[2]*

[1]Department of Agricultural, Food and Nutritional Science, University of Alberta, Edmonton, AB, Canada, [2]Department of Animal and Veterinary Sciences, California State Polytechnic University Pomona, Pomona, CA, United States

KEYWORDS

animal physiology, metabolomics, health, efficiency, biomarkers, genetics

Editorial on the Research Topic
Diving deeper with metabolomics into animal physiology

This research topic brings together metabolomics based research in different animal species that include dairy cows, goats, pigs, bats, silkworms and parasitic nematodes. The studies in dairy cows, goats and pigs employed metabolomics to understand the physiology of different aspects of the animal that could be applicable to improve sustainability, animal health and welfare, antimicrobial use and fertility. Furthermore, metabolomics was used to compare the metabolites in the cochleae of two bat species. The effect of diet on cocoon yield in silkworms and developmental stage specific mechanisms of survival in parasitic nematode has been investigated using metabolomics.

Feed efficiency and reproductive management are two important aspects of dairy farming which has significant economic contribution to milk production. Hailemariam et al. investigated the physiological underpinnings of residual feed intake (a measure of feed efficiency), identified biomarkers and developed prediction models using targeted milk metabolomics. The authors reported varying mechanisms of feed efficiency during the lactation period and lactation stage-dependent biomarkers and prediction models that can assist in generating large-scale records that can be used to select dairy cows for improved feed efficiency. Some of the lactation stage specific biomarkers include decanoylcarnitine (AUC = 0.81), dodecenoylcarnitine (AUC = 0.81) and phenylalanine (AUC = 0.85) at early, mid and late stages of lactation, respectively. In another study, Pollock et al. explored the relationship between higher estrus associated temperatures (HEAT) and pre-ovulatory follicular fluid metabolome. The study revealed association of follicular fluid metabolome with HEAT, for instance, the maximum vaginal temperature was related to the differential abundances of uracil, uric acid, and 6-phospho-D-gluconate when expressed as change from the baseline. The findings support the concept that HEAT is related to changes in the pre-ovulatory follicular fluid metabolites involved in energy metabolism, thermoregulation, and oxidative stress management. The study by Vasco et al. combines the use of untargeted metabolomics and metagenomics to investigate the effect of intramammary ceftiofur treatment and different lactation stages on the metabolic and microbial profiles of dairy cattle hindgut. The authors reported that the week after treatment, treated cows had elevated levels of stachyose, phosphatidylethanolamine diacylglycerol and inosine. This research provides information into how antibiotic treatments and lactation stages influence the gut microbiome and metabolome in cattle. Furthermore, the dynamics of fecal microbiome and blood metabolites of dairy calves during the first

2 weeks after birth was investigated by Kojima et al. Early microbiomes were dominated by Proteobacteria, while Firmicutes and Bacteroidetes became more prevalent later-on. Blood metabolite profiles changed during the neonatal period, reflecting shifts in energy metabolism, immune response, and gut function as the calves transitioned from colostrum intake to solid feed. The temporal changes observed provide insights into the impacts of gut microbiota maturation on the metabolic health of calves, emphasizing the importance of gut-microbiome interactions during the early stages of life.

Animal welfare is another important aspect of farming that is known to significantly impact animal production. The impact of prolonged transportation on the welfare and health of goats is becoming a growing societal concern. The study by Batchu et al. used targeted metabolomics and demonstrated that extended transportation induces metabolic stress in goats, affecting key metabolic pathways related to amino acids metabolism, energy and stress response. However, habituation to livestock trailers appears to reduce the severity of these effects, suggesting that habituation may be a valuable strategy to improve the welfare and health of livestock during transportation. By identifying specific metabolic markers of stress, the findings offer practical insights into improving livestock management practices and ensuring animal welfare during transport.

Application of metabolomics has expanded in several livestock species, including pigs. For example, combining genomics and metabolomics, Dervishi et al. investigated the genetic and metabolic factors that influence the immune response. Analysis of genetic correlations between plasma metabolites and complete blood count (CBC) traits in young pigs revealed that plasma concentration of L-proline and L-glutamine were genetically positively correlated with hemoglobin and neutrophils concentration, respectively. In addition, metabolites such as dimethylglycine, betaine, and L-methionine were reported as candidate metabolites to improve growth rate of young healthy pigs. This research has practical implications for improving pig health and immunity through selective breeding strategies based on metabolic and blood traits. The study also opens up the potential for precision livestock farming through metabolic profiling to monitor and optimize immune function in pigs.

In this special edition, application of metabolomics expanded beyond livestock species. For example, in bats, echolocation is a complex biological process that involves the production and detection of sound waves, and the cochlea plays a central role in this auditory system. The study by Wang et al. used untargeted metabolomics to identify and compare the metabolites in the cochleae of the two bat species. By identifying specific metabolites related to several biological processes, including signaling pathways, nervous system, and metabolic process, the study advances the understanding of how molecular mechanisms support complex biological functions like echolocation. These findings could have broader implications for studying auditory physiology and evolution in other echolocating mammals and other species.

In this special edition, studies on silkworms and parasitic nematodes that used metabolomics were included. Wu et al. investigated the impact of different diets on cocoon yield in silkworms. Traditionally, silkworms are fed mulberry leaves, which are known to be their natural diet. This study compared the effect of feeding formula feed and mulberry leaves on cocoon production and quality. Distinct metabolic profiles between silkworms fed with mulberry leaves and formula feed were observed in regards to cysteine and methionine metabolism, arginine biosynthesis, and arginine and proline metabolism. This study provides insights into the potential mechanisms through which formula feed may enhance silk production and could provide directions for formula feed optimization in factory-raised silkworms. On the other hand, Polak et al. examined how the parasitic nematode Anisakis simplex adapts to different host environments during its larval stages. Using metabolomic analysis, the study compared the metabolic profiles of Anisakis simplex larvae at various developmental stages, focusing on how these changes help the parasite survive and thrive inside different hosts. Metabolic pathways related to amino acids, starch, and sucrose were mainly activated in the L3 stage, meanwhile the molecules responsible for successful migration within their host, such as pyridoxine and prostaglandins (E1, E2, F1a) were present in the L4 stage. This research enhances the understanding of Anisakis simplex's adaptation mechanisms to different host environments, providing valuable insights into parasite-host interactions. The findings may inform future strategies for controlling parasitic infections in humans and animals by targeting specific metabolic pathways crucial for the parasite's survival.

The research articles presented in this Research Topic contribute to a deeper understanding of metabolic pathways and how they influence physiological, health, and disease states in different animal species. In addition, it highlights the potential of metabolomics to advance our knowledge of animal physiology and improve animal welfare and health, fertility and production practices.

Author contributions

DH: Writing–review and editing. ED: Writing–original draft, Writing–review and editing.

Funding

The author(s) declare that no financial support was received for the research, authorship, and/or publication of this article.

Conflict of interest

The authors declare that the research was conducted in the absence of any commercial or financial relationships that could be construed as a potential conflict of interest.

Generative AI statement

The author(s) declare that no Generative AI was used in the creation of this manuscript.

Publisher's note

frontiers | Frontiers in Molecular Biosciences

TYPE Original Research
PUBLISHED 17 August 2022
DOI 10.3389/fmolb.2022.977047

OPEN ACCESS

EDITED BY
Elda Dervishi,
University of Alberta, Canada

REVIEWED BY
Xiaoming Zhao,
Shanxi University, China
Feng Shang,
Southwest University, China

*CORRESPONDENCE
Wenlin Zhou,
zhouwl@zaas.ac.cn

SPECIALTY SECTION
This article was submitted to Metabolomics, a section of the journal Frontiers in Molecular Biosciences

RECEIVED 24 June 2022
ACCEPTED 18 July 2022
PUBLISHED 17 August 2022

CITATION
Wu X, Chen X, Ye A, Cao J, He R, Pan M, Jin F, Ma H and Zhou W (2022), Multi-tissue metabolomic profiling reveals potential mechanisms of cocoon yield in silkworms (Bombyx mori) fed formula feed versus mulberry leaves. *Front. Mol. Biosci.* 9:977047. doi: 10.3389/fmolb.2022.977047

Multi-tissue metabolomic profiling reveals potential mechanisms of cocoon yield in silkworms (*Bombyx mori*) fed formula feed versus mulberry leaves

Xuehui Wu[1], Xuedong Chen[1], Aihong Ye[1], Jinru Cao[1], Ruimin He[2], Meiliang Pan[3], Feng Jin[2], Huanyan Ma[3] and Wenlin Zhou[1]*

[1]Institute of Sericulture and Tea, Zhejiang Academy of Agricultural Sciences, Hangzhou, Zhejiang, China, [2]Shengzhou Mulsun Biotech Co., Ltd., Shengzhou, Zhejiang, China, [3]Zhejiang Provincial Agricultural Technology Extension and Service Center, Hangzhou, Zhejiang, China

Use of formula feed (FF) for silkworms for all instars, has promoted transformation and progress in traditional sericulture. However, the cocoon yield of FF silkworms has failed to reach that of silkworms fed mulberry leaves (ML). The biological mechanisms underlying this phenomenon have not been well described. This study aimed to identify metabolic mechanisms and potential biomarkers relating to the poor cocoon yield of FF silkworms. In this study, silkworms received treatments of either ML (ML group) or FF (FF group) for all instars. At the 3rd day of the 5th instar, the midgut (MG), hemolymph (HL) and posterior silk gland (PSG) were collected for the metabolome profiles detection. The remaining silkworms were fed ML or FF until cocooning for investigation. The whole cocoon yield (WCY) was significantly higher in the FF group than the ML group ($p < 0.05$), whereas the cocoon shell weight (CSW) and cocoon shell rate (CSR) were significantly lower in the FF group ($p < 0.05$). A total of 845, 867 and 831 metabolites were qualified and quantified in the MG, HL and PSG of the FF silkworms, respectively. Correspondingly, 789, 833 and 730 metabolites were quantified in above three tissues of the ML group. Further, 230, 249 and 304 significantly different metabolites (SDMs) were identified in the MG, HL and PSG between the FF and ML group, respectively. Eleven metabolic pathways enriched by the SDMs were mutual among the three tissues. Among them, cysteine and methionine metabolism, arginine biosynthesis, and arginine and proline metabolism were the top three pathways with the highest impact value in the PSG. Six biomarkers

Abbreviations: CSW, Cocoon shell weight; CSR, Cocoon shell rate; ESI, Electrospray ionization; FF, Formula feed; HL, Hemolymph; IPV, Impact value; MG, Midgut; ML, Mulberry leaves; MVDA, Multivariate data analysis; PSG, Posterior silk gland; QC, Quality control; QQQ, Triple quadrupole; SDM, Significantly different metabolite; WCY, Whole cocoon yield.

were obtained through biomarker analysis and Pearson correlation calculation. Among them, homocitrulline, glycitein, valyl-threonine, propyl gallate and 3-amino-2,3-dihydrobenzoic acid were positively correlated with WCY, but negatively correlated with CSW and CSR ($p < 0.05$). An opposite correlation pattern was observed between 3-dimethylallyl-4-hydroxyphenylpyruvate and the three cocoon performance traits. Overall, three key metabolic pathways and six biomarkers associated with cocoon yield were interpreted, and should provide directions for formula feed optimization in factory-raised silkworms.

KEYWORDS

silkworm, metabolome profile, biomarker, formula feed, mulberry leaves

1 Introduction

The domesticated silkworm (*Bombyx mori*) is a Lepidoptera model organism that has been reared and domesticated on mulberry leaves (ML) for thousands of years (Tao et al., 2022). However, with continual optimization and changes in rural economic structure, Chinese sericulture is facing unprecedented challenges. Silkworm rearing on formula feed (FF), a method that originated in the middle of last century in Japan (Nair and Kumar, 2004), is becoming a major focus in the sericulture industry, because it alleviates season, climate, land and environmental restrictions (Kim et al., 2021). In 2019, rearing the silkworm variety "Zhong 2016×Ri 2016" on FF for all instars was successful in a commercial industry. However, the issue of poor cocoon yield in the FF silkworms remains unresolved, thus hindering sericulture.

It has been acknowledged that the three cocoon yield performance traits: the whole cocoon yield (WCY), the cocoon shell weight (CSW) and the cocoon shell rate (CSR) has drawn much attention in researches (Ruan et al., 2021; Chen et al., 2022), for they being closely related to sericulture profits. The WCY consists of CSW and the pupae weight, which can be utilized to evaluate the growth and development of the silkworm larva and its cocooning ability. The CSW is an indicator to assess the silk synthesis ability, while the CSR is used to evaluate the efficiency of nutrients to silk. However, there is no standard for which levels could be more desirable of these three performance traits in the production owing to the variety differences. For example, the cocoon shell weight of silkworm variety "Zhong 2016×Ri 2016" was more than 0.40 and 0.35 g in the ML and FF silkworms, respectively (Chen et al., 2022). In detail, the CSW and CSR of "Zhong 2016×Ri 2016" were decreased by 13.1 and 4.19% in the FF group, respectively (Chen et al., 2022).

Many studies have been performed to improve the cocoon yield performance of the FF silkworms to the greatest extent possible (Zhang et al., 2020; Kim et al., 2021; Yamamoto et al., 2021). Most have focused on optimizing the FF composition (Kim et al., 2021; Yamamoto et al., 2021) and silkworm variety breeding (Zhang et al., 2020). However, the mechanisms underlying the poor cocoon yield of the FF silkworms have not been well documented. With the rapid development of systems biology, omics methods have been widely used in livestock studies, including the sericulture field (Dong et al., 2018; Fang et al., 2020; Ge et al., 2020; Xiao et al., 2020; Tao et al., 2022). Researchers have explored the molecular differences between the FF and ML silkworms (Zhou et al., 2008; Dong et al., 2017; Dong et al., 2018; Lamberti et al., 2019; Qin et al., 2020; Tao et al., 2022). For instance, the intestinal microbiota diversity was reported to be higher in the ML silkworms than the FF silkworms (Dong et al., 2018). Lamberti et al. (2019) found five differentially expressed proteins associated with diet type through comparative proteomics. Furthermore, the content of pupa proteins in the FF silkworms was markedly higher than that in traditional ML silkworms as reported (Lamberti et al., 2019).

Metabolomics can qualify and quantify thousands of metabolites, and describe the specific metabolomic profiles of certain tissues or biofluids at specific time points in organisms (Saoi and Britz-McKibbin, 2021). Currently used detection platforms are based on gas chromatography-mass spectrometry, liquid chromatography-mass spectrometry (LC-MS) and nuclear magnetic resonance, each of which has its own merits. LC-MS aids in identifying metabolites with high polarity and high formula weight, and can quantify and qualify more metabolites than other platforms (Tao et al., 2022). Metabolomics has been applied in exploring the metabolic profiles of silkworms subjected to two rearing methods (FF versus ML) (Dong et al., 2017; Qin et al., 2020; Tao et al., 2022). However, previous studies have focused mainly on metabolic changes in a single tissue; therefore, the results cannot fully reflect systematic variations of the whole organism. Consequently, multi-tissue studies on modern sericultural research are necessary. Hemolymph (HL), the transporter of nutrients and intermediates, reflects changes in the whole body (Tao et al., 2022). Zhou et al. (2015) have reported that changes in the HL metabolome are closely associated with dietary composition, cell membrane biosynthesis, and protein and energy metabolism. However, the non-specific characteristic of the HL restricts the explain validity to some issues. The midgut (MG) plays a crucial role in nutrient digestion and absorption (Shen et al., 2022), and thus warrants further nutrition metabolism studies. Posterior silk gland (PSG) is the locus of fibroin production (Shigematsu and Koyasako, 1962), which is closely associated with various cocoon performance traits.

Consequently, integrating the metabolomic profiles of the three aforementioned tissues should provide systematic knowledge in silkworm nutritional biology.

This study aimed to identify mechanisms and biomarkers relating to poor cocoon yield in silkworms reared on formula feed for all instars, by integrating systematic metabolomic profiling.

2 Materials and methods

2.1 Animals and rearing

The *B. mori* variety "Zhong 2016×Ri 2016," provided by the Zhejiang Silkworm Egg Quality Inspection Station (Hangzhou, China), was studied. Three thousand silkworms were divided into six groups and were randomly allocated to receive two diet treatments: formula feed (FF group) and fresh mulberry leaves (ML group) for all instars. The FF silkworms were fed once from the newly hatched period to the 2nd instar, and were fed one, one and two times in the 3rd, 4th and 5th instars, respectively. The ML group was fed three times at 7:00 a.m., 13:00 p.m. and 19:00 p.m. per day during five instar periods.

All silkworms were reared in an intelligent and independent room with relatively optimal room temperature and humidity, according to the different requirements of each instar. All remaining experimental silkworms were reared to cocoon stage for further cocoon yield performance investigation, including the WCY, CSW and CSR.

2.2 Diet preparation

The ingredients of the formula feed were based on a report by Dong et al. (2017). The formula contained 33% mulberry leaf powder for silkworms in the 1st -3rd instars, whereas 4th to 5th instar silkworms were fed formula feed containing 25% mulberry leaves. The formula feed powder was mixed with 1.85× (w/w) sterile water. The mixture was placed in a storage bag, pressed to a thickness of approximately 1.00 cm and heated for 50 min at 100°C after sealing. After heating, the formula feed mixture was naturally cooled and stored at 4°C for feeding trials.

Mulberry leaves were picked from the Nongsang No.14 mulberry variety every morning and were stored at 4°C to maintain freshness. Nongsang No.14 with good mulberry leaf quality was provided by Shaoxing Dayu Silkworm Egg Production Co., Ltd. (Shaoxing, China).

2.3 Sample collection and preparation

2.3.1 Sample collection

The 3rd day of the 5th instar is the most active time point of silkworm larval metabolism (Dong et al., 2017). MG, HL and PSG were collected on ice at the 5th instar after feeding for 72 h. HL was gathered by cutting the anal horns of the silkworm larvae. Those silkworm larvae were fixed and cut in a dissecting pan to obtain the experimental MG and PSG with specialized surgical nippers and scissors. Groups of six silkworm tissues were combined into one sample replicate. A total of 12 samples per tissue were analyzed, consisting of six male and six female replicates. To terminate the metabolic activity of each tissue, every sample was frozen in liquid nitrogen as soon as possible and was stored at −80°C for subsequent metabolomic profiling analysis.

2.3.2 Sample preparation for metabolite detection

Sample preparation, including thawing and following procedures before detection, was performed on ice.

2.3.2.1 HL

On the basis of the readily oxidizable property of silkworm HL, nitrogen oxides were inflated to the refrigerated HL sample for 5 s after the experimental samples were removed from −80°C storage. The thawed HL was vortexed for 10 s, and 50 μL of sample was added to an Eppendorf (EP) tube containing 300 μL pure methanol with 0.1% butylated hydroxytoluene and internal standard extract (1 ppm: [^{2}H3]-L-carnitine HCl, 4-fluoro-L-α-phenylglycine, L-phenylalanine (2–13C, 99%), L-2-chlorophenylalanine, [^{2}H5]-kynurenic acid, [^{2}H5]-hippuric acid, [^{2}H5]-phenoxy acetic acid). The above mixtures were vortexed for 3 min and centrifuged for 4 min at 12,000 rpm (r = 0.15 m) and 4°C. Subsequently, 200 μL supernatant was transferred to a new EP tube to silence for 30 min in −20°C. Then, the above supernatants were centrifuged at 12,000 rpm for 10 min at 4°C. Finally, 150 μL supernatant was transferred into a brown injection bottle and stored at −20°C for UHPLC-MS/MS detection.

2.3.2.2 MG and PSG

Tissue samples were thawed, and approximately 50 mg was cut and placed into a clean 1.5 ml EP tube. Steel balls were added to the EP tubes, and samples were homogenized at 30 Hz for 3 min. The mixture was vortexed for 5 min after 1 ml 70% methanol with the aforementioned internal standard extract was added. The mixture was placed on ice for 10 min before centrifugation (4°C, 12,000 rpm, 10 min). Subsequently, 400 μL supernatant was transferred into a new EP tube and stored overnight at −20°C. Finally, the supernatant was centrifuged for 3 min at 12,000 rpm and 4°C, and 200 μL supernatant was transferred to an injection bottle for UHPLC-MS/MS detection.

Of note, after every ten samples. 10 μL of the prepared sample supernatants of each tissue was combined into a mixed sample, which served as the QC for UHPLC-MS/MS detection, to evaluate the manual accuracy, instrument stability and technology replicability.

2.4 UHPLC-MS/MS detection and analysis

2.4.1 Compound detection by UHPLC-MS/MS

The above sample extracts were analyzed with a UHPLC (ExionLC FF, https://sciex.com.cn/)-electrospray ionization (ESI)-MS/MS system (QTRAP® System, https://sciex.com/).

The UHPLC conditions were as follows: Waters ACQUITY UPLC HSS T3 C18 column (1.8 μm, 2.1 mm × 100 mm), A phase: ultrapure water (0.1% formic acid), B phase: acetonitrile (0.1% formic acid), column temperature: 40°C, injection volume: 2 μL. The UHPLC gradient elution was conducted as follows: 95:5 V/V (A phase/B phase) at 0 min, 10:90 V/V at 10.0 min, 10:90 V/V at 11.0 min, 95:5 V/V at 11.1 min and 95:5 V/V at 14.0 min.

The QTRAP® LC-MS/MS system equipped with an ESI Turbo Ion-Spray interface was used to acquire the linear ion trap and triple quadrupole (QQQ) scans. This system was controlled by Sciex Analyst 1.6.3 software (https://sciex.com.cn/), and was operated in positive and negative ion mode. The ESI parameters were set as follows: source temperature: 500°C; ion spray voltage: 5500 V (positive) to 4500 V (negative); ion source gas I, gas II and curtain gas set at 55.0, 60.0 and 25.0 psi, respectively; collision-activated dissociation parameter set high. Equipment tuning and mass calibration were performed with 10 and 100 μmol/L polypropylene glycol solutions in QQQ and linear ion trap modes, respectively. In QQQ scans, each ion pair was detected on the basis of the optimal declustering potential and collision energy (Chen et al., 2013).

2.4.2 Identification and quantification of metabolites

Compound identification was based on the metware database, retention time, macroion and precursor ion information, and secondary spectrum data of specific compounds.

Multiple reaction monitoring of the QQQ system was used to quantify the compounds detected. The areas under each chromatographic peak were calculated and represented the relative content of the detected compound in MultiQuant software (https://sciex.com.cn/). On the basis of the retention time and peak pattern information of the detected compounds, integral correction in different samples was performed to ensure the qualification and quantification accuracy (Fraga et al., 2010). Metabolites were defined as detected if they were present in more than 50% of the QC samples. Similarly, metabolites were considered to exist in a given group if they were detected in at least 50% of the samples in the group.

2.4.3 Unique and mutually present metabolites in the MG, HL and PSG

To identify the metabolic similarities and differences among the MG, HL and PSG, we analyzed the unique and mutual metabolites in different tissues in this study.

2.5 Statistical analysis

2.5.1 Significantly different metabolites identification between the ML and FF group

Metaboanalyst 5.0 (https://www.metaboanalyst.ca/) was used to perform multivariate data analysis (MVDA) under the log transformation of data and auto scaling mode (Pang et al., 2021). Sample normalization was set to "normalized by sum". MVDA, as conducted in this study, included PCA and OPLS-DA. The PCA model was used to observe the global distribution of experimental samples. OPLS-DA was performed to identify the metabolomic differences among treatments, particularly in distinguishing different metabolites. Missing value estimation was performed by default. In detail, missing values were replaced by one-fifth of the minimum positive values in corresponding variables.

The VIP >1.00, FC > 2.00 or < −2.00 and FDR <0.05 were the criteria used to define SDMs, which were further identified, validated and classified in the KEGG and HMDB. Mutual and unique SDMs were analyzed and shown in Venn diagrams. Furthermore, the $|\log_2 FC|$ was the index used to identify the top 15 up-regulated and the top 15 down-regulated SDMs in three tissues.

2.5.2 Pathway analysis based on the significantly different metabolites

Pathway analysis was conducted in Metaboanalyst 5.0, with the fruit fly (*Drosophila melanogaster*) library applied in this step. Sample normalization, data transformation and data scaling was set "Normalization by sum", "Log transformation" and "Data scaling", respectively. In this study, the impact value (IPV) > 0.100 was set as the cutoff for relevance (Sun et al., 2015; Wu et al., 2019).

2.5.3 Biomarker and correlation analysis

Biomarker analysis was conducted in Metaboanalyst 5.0 with the relative concentrations of metabolites detected. To improve the reliability of results, metabolites with level B were discarded in this procedure. SDMs with an AUC = 1 served as the preselected biomarkers to explain and indicate the metabolic differences between the FF and ML silkworms across the three tissues.

Preselected biomarkers mutually present among the MG, HL and PSG were chosen for correlation analysis with the cocoon yield performance traits (WCY, CSW and CSR). Correlation analysis was conducted in the R package (https://www.r-project.org/) using Pearson coefficient.

2.5.4 Performance traits analysis

In sericulture production, male and female silkworms are fed together in nearly all silkworm varieties. Normally, the proportion of male and female silkworms bred is 1:1. So equal number of male and female silkworms were collected together to be consistent with the production. In addition, for the three cocoon performance traits in this study, there was no interaction between the diet and sex in the statistical model. Thus, sex was not included in the model. In detail,

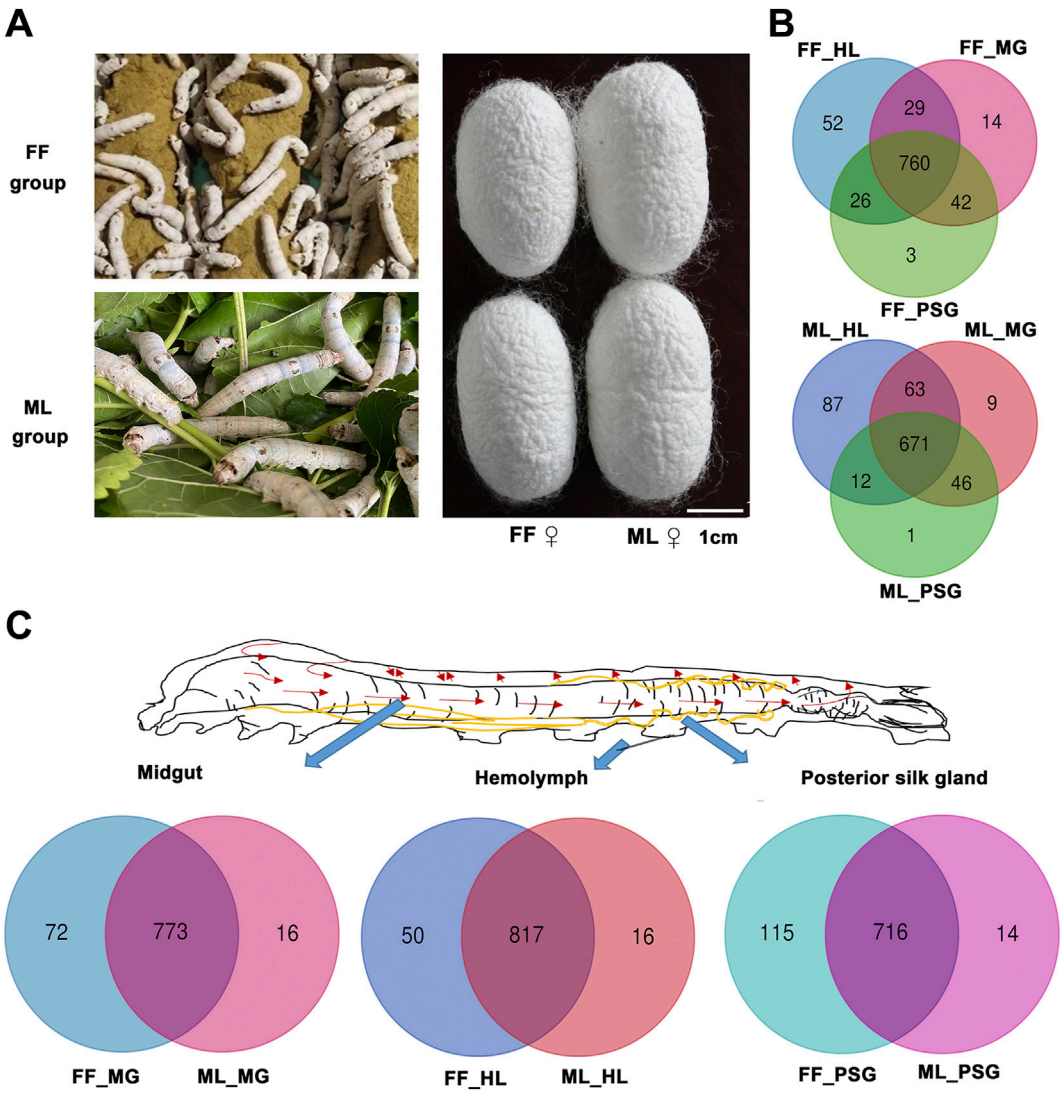

FIGURE 1
Metabolites distribution in the hemolymph (HL), midgut (MG) and posterior silk gland (PSG) between the FF and ML silkworms. **(A)** Silkworms fed formula feed (FF) or mulberry leaves (ML), and corresponding cocoons. **(B)** Metabolites distribution among three tissues in the FF (up) and ML (down) silkworms. **(C)** Unique and mutual metabolites identified in different tissues in the FF and ML groups.

the SAS MIXED model and the univariate statistical analysis was used to analyze the WCY, CSW and CSR between the FF and ML group. Diets was set as the only factor in the statistical model. $p < 0.05$ was defined as the significance threshold, and $p < 0.01$ was regarded as an extremely significant difference.

3 Results

3.1 Cocoon yield performance

In this study, WCY, CSW and CSR, typical cocoon yield performance traits were investigated and analyzed between the FF and ML silkworms (Figure 1A; Table 1). The WCY was 10.6% higher in the FF group than the ML group ($p < 0.05$), whereas the CSW and CSR of the FF group were 11.7 and 20.5% lower than the ML group, respectively ($p < 0.05$). Besides, the pupa of FF group was 17.1% heavier than those of ML group ($p < 0.05$).

3.2 UHPLC-MS/MS detection and analysis

3.2.1 Metabolite identification and quantification

The total ion chromatogram information under positive and negative ion modes are shown in Supplementary Figure

TABLE 1 The cocoon yield performance of silkworms reared on formula feed or mulberry leaves.

Treat[a]	WCY[b], g	CSW[c], g	CSR[d], %	PW[e], g
FF group	2.08 ± 0.114[a]	0.371 ± 0.0228[b]	17.8 ± 0.34[b]	1.71 ± 0.085[a]
ML group	1.88 ± 0.016[b]	0.420 ± 0.0126[a]	22.4 ± 0.62[a]	1.46 ± 0.015[b]

[a]FF group, silkworms reared on formula feed; ML group, silkworms reared on mulberry leaves.
[b]WCY, whole cocoon yield.
[c]CSW, cocoon shell weight.
[d]CSR, cocoon shell rate.
[e]PW, pupae weight.
Data are presented as mean ± standard deviation.
Different letters within a column indicate significant differences between FF and ML groups ($p < 0.05$).

S1. A total of 1,033 compounds were identified by ultra-high performance LC-MS/MS (UHPLC-MS/MS). After filtering, 927 metabolites were finally qualified. The results of compound identification and quantification are described in Supplementary Table S1. Different letters (A or B) in the level column indicate different levels of identified metabolites (Supplementary Table S1), which were associated with subsequent biomarker analysis. Level A indicates that the information on two ion fragments was consistent with the metware database, whereas level B indicates that only one ion fragment was consistent.

3.2.2 Metabolite distribution

The number of metabolites detected in three tissues of silkworms fed the two diets are shown in Figure 1B and Figure 1C. A total of 845, 867 and 831 metabolites were identified in the MG, HL and PSG of the FF silkworms, respectively. Correspondingly, 789, 833 and 730 metabolites were detected in the MG, HL and PSG of the FF group, respectively.

The metabolite distribution in the analyzed tissues in the FF and ML silkworms is depicted in Figure 1B. A total of 760 metabolites were mutual in the MG, HL and PSG of the FF group, whereas 671 metabolites were mutual in the corresponding tissues of the ML silkworms. A total of 52 and 87 specific metabolites were detected in the HL of the FF and ML groups, respectively. Only 14 and three metabolites were specific in the MG and PSG of the FF group. Similarly, nine metabolites and one metabolite were specific in the MG and PSG of the ML group, respectively.

Similarly, the metabolite distributions (Figure 1C) indicated that 773, 817 and 716 metabolites were mutual in the MG, HL and PSG of the FF and ML groups. The numbers of specific metabolites in the FF group were 72, 50 and 115, and those in the ML group were 16, 16 and 14 in the MG, HL and PSG, respectively.

3.2.3 Multivariate statistical comparison of metabolites between the FF and ML groups

Figure 2 shows the multivariate statistical analysis (MVDA) results of the metabolic profiling between the FF and ML silkworms in the MG (A-C), HL (D-F) and PSG (**G-I**). For the MG metabolic profile, a significant separation was observed between the FF and ML groups in the principal component analysis (PCA) score plot. For the HL and PSG, a similar pattern was demonstrated. No outliers were beyond the 95% Hotelling's T-squared ellipse in all PCA score plots. The PCA score plot contained quality control (QC) samples is shown in Supplementary Figure S2 (**A**-MG, B-HL, **C**-PSG). All QC samples clustered together and was separately from the FF and ML samples (Supplementary Figure S2). The orthogonal partial least squares discriminant analysis (OPLS-DA) score plot also showed two clearly distinct clusters, with no samples exceeding the 95% ellipse. Furthermore, 2000 permutation tests indicated that the OPLS-DA model was suitable for significantly different metabolites (SDMs) identification (MG: R2Y = 0.993 and Q2 = 0.985, HL: R2Y = 0.998 and Q2 = 0.996 and PSG: R2Y = 0.995 and Q2 = 0.987).

3.2.4 Significantly different metabolite identification between the FF and ML silkworms

A total of 230, 249 and 304 SDMs (Variable importance for the projection (VIP) > 1.00, fold change (FC) > 2.00 or FC < -2.00, false discovery rate (FDR) < 0.05) were identified in the MG, HL and PSG, respectively, between the FF and ML groups (Supplementary Table S2). In the volcano plot (Figure 3A, Figure 4A, Figure 5A), the upregulated metabolites in the FF silkworms are in red, whereas downregulated metabolites are in blue. A total of 180, 153 and 256 upregulated SDMs were found in the MG, HL and PSG, respectively. In contrast, the numbers of downregulated SDMs of the MG, HL and PSG were 50, 96 and 48, respectively. The above upregulated and downregulated SDMs were categorized and shown in Figure 3B, Figure 4B and Figure 5B, respectively. In the MG metabolic profiling, the class of amino acids, peptides, and analogues; carbohydrates and carbohydrate conjugates; lipids and lipid-like molecules; and coenzymes and vitamins accounted for 50, 15, 66 and 7, respectively. In the HL, 54, 24, 55 and 7 SDMs were classified as amino acids, peptides, and analogues; carbohydrates and carbohydrate conjugates; lipids and lipid-like molecules and coenzymes and vitamins, respectively. In the metabolic profiles of the PSG, a large proportion of SDMs was classified as amino acids and their derivatives (n = 89) and lipids and lipid-like molecules (n = 74). Furthermore, carbohydrates and carbohydrate conjugates, and coenzymes and vitamins accounted for 16 and 4, respectively.

The top 15 upregulated SDMs and top 15 downregulated SDMs of the three tissues with the most significant differences ($|\log_2 FC|$) are displayed in Figure 3C, Figure 4C and Figure 5C, respectively. Among them, 3-dimethylallyl-4-

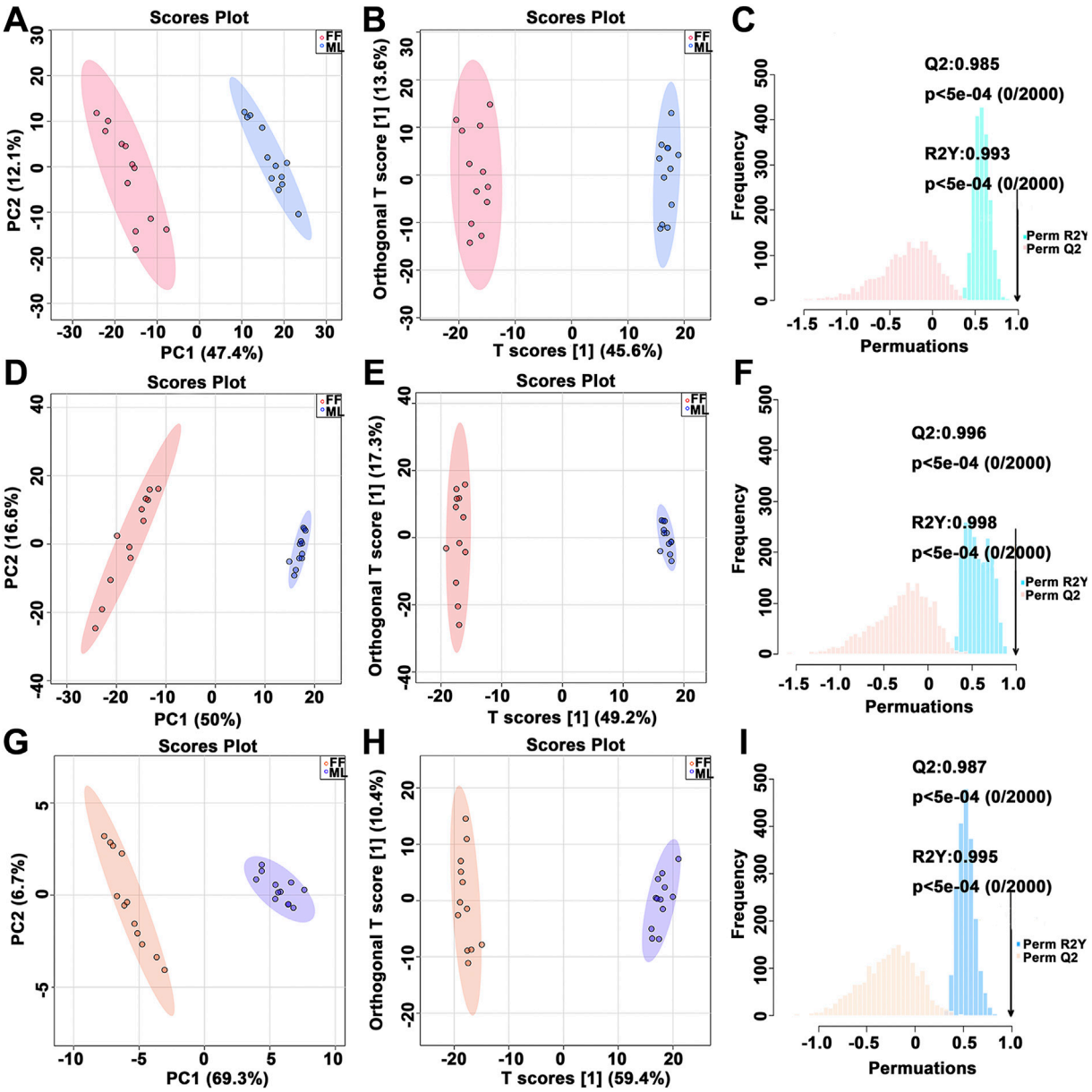

FIGURE 2
PCA score plot, OPLS-DA score plot and corresponding permutation test results of the metabolite profiles. PCA, principal component analysis; OPLS-DA, orthogonal partial least squares discriminant analysis. PCA score plot **(A,D,G)**, OPLS-DA score plot **(B,E,H)** and corresponding permutation test results **(C,F,I)** were derived from the metabolite profiles of the midgut (MG, **(A–C)**, hemolymph (HL, **(D–F)** and posterior silk gland (PSG, **(G–I)**. Red dots represent silkworms fed formula feed (FF), and blue dots represent silkworms fed mulberry leaves (ML).

hydroxyphenylpyruvate was the only top 15 downregulated SDM mutually among the three tissues.

The mutual and specific SDM distribution results among the MG, HL and PSG are depicted in Supplementary Figure S3. A total of 60 SDMs were mutually found in the three tissues (Supplementary Table S3). The numbers of specific SDMs of the MG, HL and PSG were 75, 116 and 144, respectively.

3.2.5 Identification of metabolic pathways related to SDMs

Metabolic pathways were enriched by the SDMs between the FF and ML groups among three tissues (Figure 3D, Figure 4D and Figure 5D, respectively.). In the MG, 23 metabolic pathways were enriched by the 230 SDMs, among which alanine, aspartate and glutamate metabolism

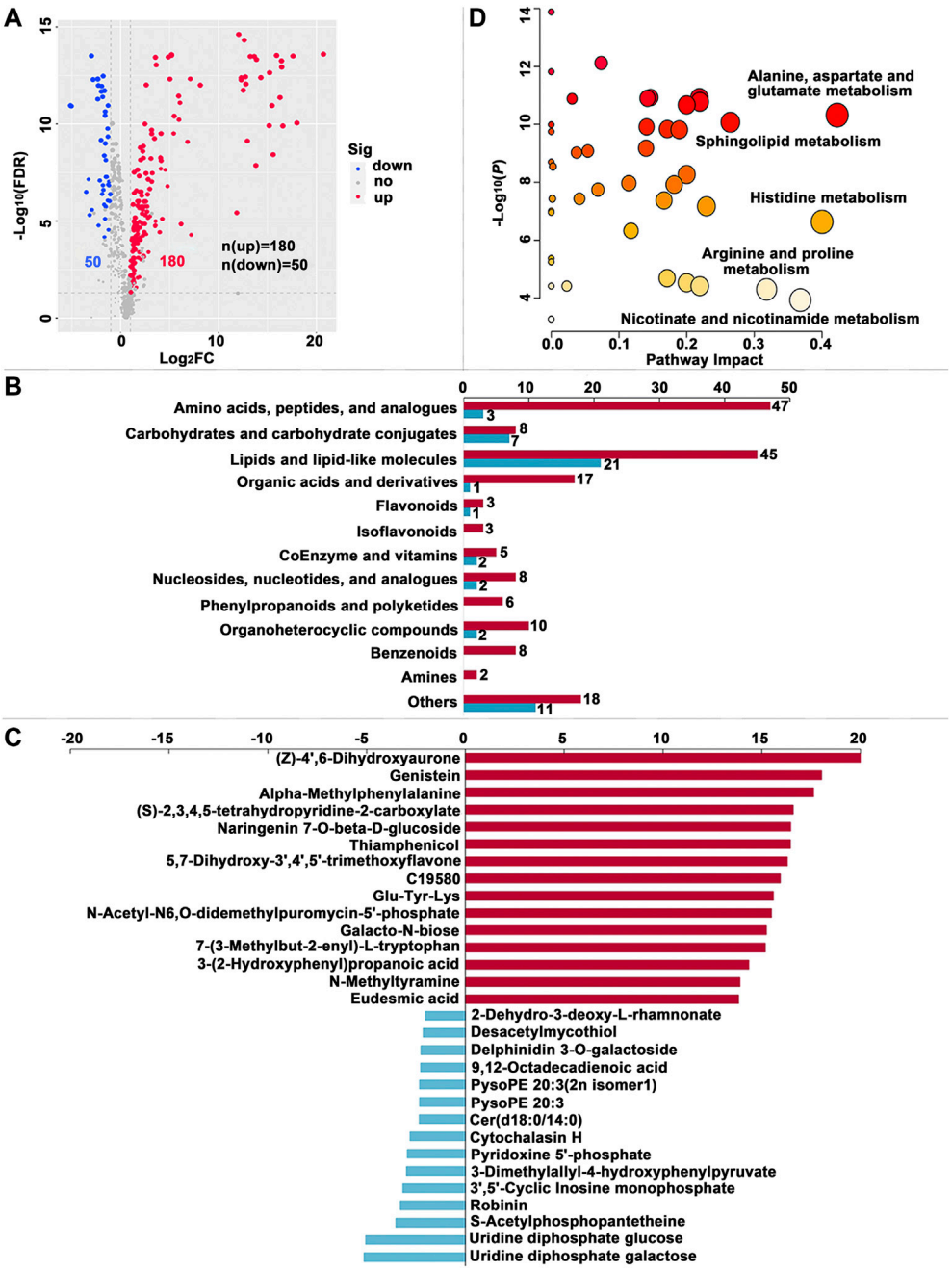

FIGURE 3
Significantly different metabolites (SDMs) and enriched pathways relating to different diets in the midgut (MG). **(A)** Volcano plots of metabolites for the formula feed (FF) and the mulberry leaves (ML) silkworms in the MG. The red dot represents the metabolite is significantly higher in the FF silkworms, and the blue dot indicates a higher abundant metabolite in the ML silkworms. The dot size represents the VIP value. **(B)** SDMs classification and variation between the FF and ML group. The blue and red bar indicate the number of downregulated and upregulated metabolites in the MG of FF group, respectively. **(C)** The top 15 upregulated SDMs and downregulated SDMs in the MG of the FF silkworms. **(D)** Metabolic pathways enriched by the SDMs between the FF and ML groups in the MG. C19580, alpha-[3-[(Hydroxymethyl)nitrosoamino]propyl]-3-pyridinemethanol.

(IPV = 0.422); histidine metabolism (IPV = 0.400); nicotinate and nicotinamide metabolism (IPV = 0.368); arginine, proline metabolism (IPV = 0.318); and sphingolipid metabolism (IPV = 0.265) were the top five enriched pathways (Supplementary Table S4). The SDMs of the HL were mainly enriched in 22 metabolic pathways (impact value

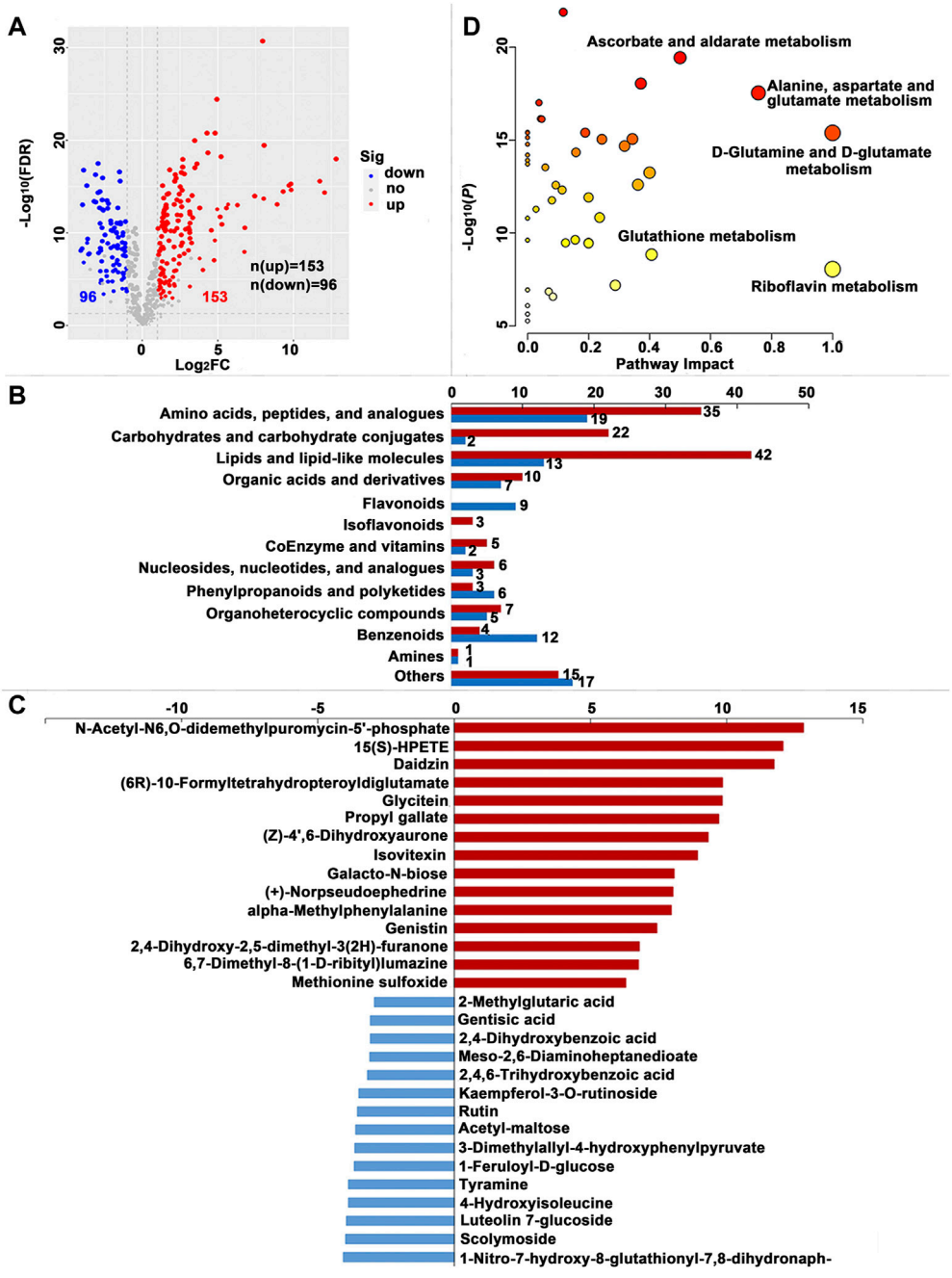

FIGURE 4
Significantly different metabolites (SDMs) and enriched pathways relating to different diets in the hemolymph (HL). **(A)** Volcano plots of metabolites for the formula feed (FF) and the mulberry leaves (ML) silkworms in the HL. The red dot represents the metabolite is significantly higher in the FF silkworms, and the blue dot indicates a higher abundant metabolite in the ML silkworms. The dot size represents the VIP value. **(B)** SDMs classification and variation between the FF and ML group. The blue and red bar indicate the number of downregulated and upregulated metabolites in the HL of the FF group, respectively. **(C)** The top 15 upregulated SDMs and downregulated SDMs in the HL of the FF silkworms. **(D)** Metabolic pathways enriched by the SDMs between the FF and ML groups in the HL.

(IPV) > 0.100). D-glutamine and D-glutamate metabolism (IPV = 1); riboflavin metabolism (IPV = 1.00); alanine, aspartate and glutamate metabolism (IPV = 0.757); ascorbate and aldarate metabolism (IPV = 0.500); and glutathione metabolism (IPV = 0.407) were the top five affected pathways (Supplementary Table S4). A total of

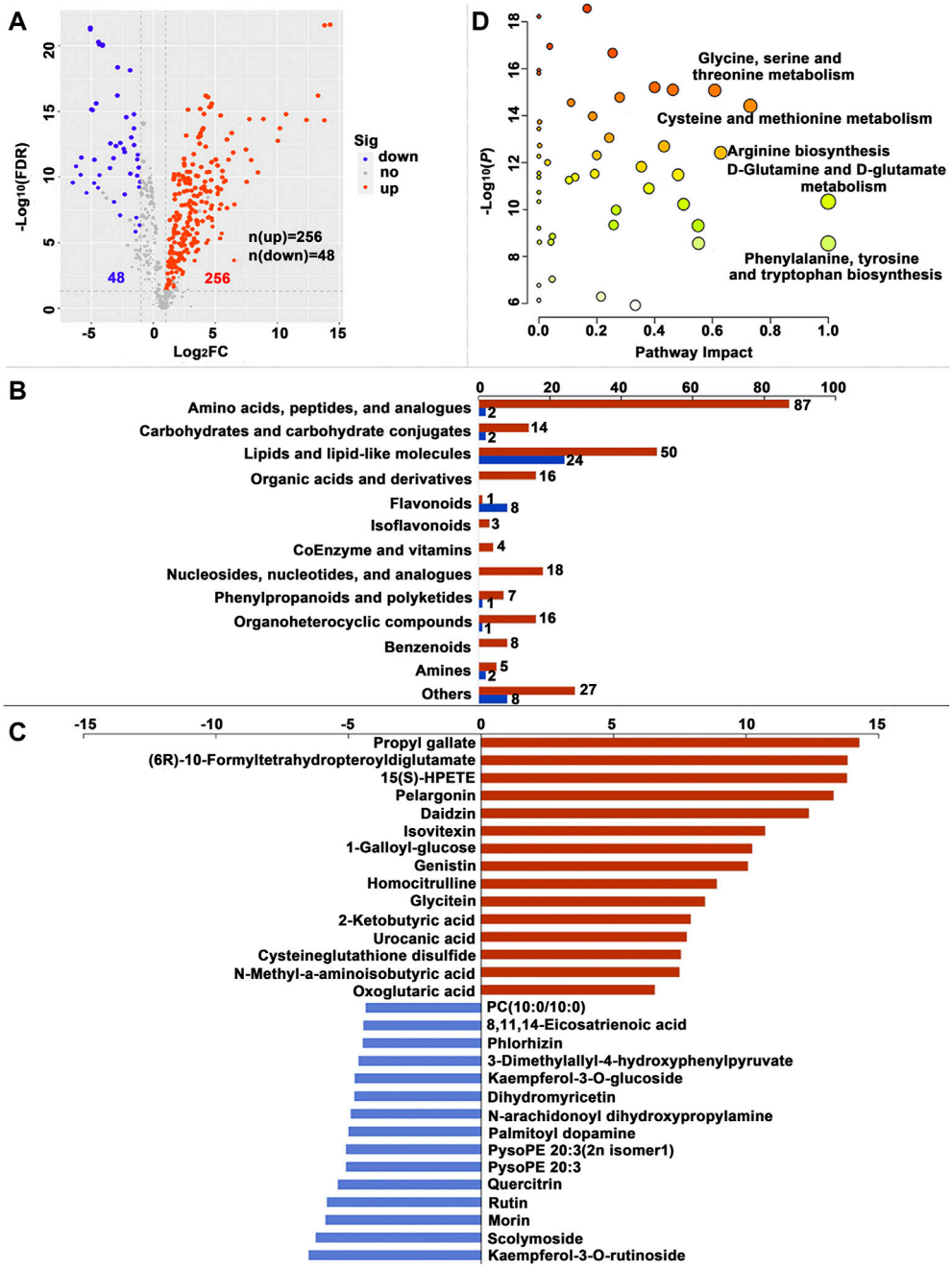

FIGURE 5
Significantly different metabolites (SDMs) and enriched pathways relating to different diets in the posterior silk gland (PSG). **(A)** Volcano plots of metabolites for the formula feed (FF) and the mulberry leaves (ML) silkworms in the PSG. The red dot represents the metabolite is significantly higher in the FF silkworms, and the blue dot indicates a higher abundant metabolite in the ML silkworms. The dot size represents the VIP value. **(B)** SDMs classification and variation between the FF and ML group. The blue and red bar indicate the number of downregulated and upregulated metabolites in the PSG of the FF group, respectively. **(C)** The top 15 upregulated SDMs and downregulated SDMs in the PSG of the FF silkworms. **(D)** Metabolic pathways enriched by the SDMs between the FF and ML groups in the PSG.

28 metabolic pathways were enriched in the SDMs of the PSG, among which D-glutamine and D-glutamate metabolism (IPV = 1.00); phenylalanine, tyrosine and tryptophan biosynthesis (IPV = 1.00); cysteine and methionine metabolism (IPV = 0.731); arginine biosynthesis (IPV = 0.629); and glycine, serine and threonine metabolism

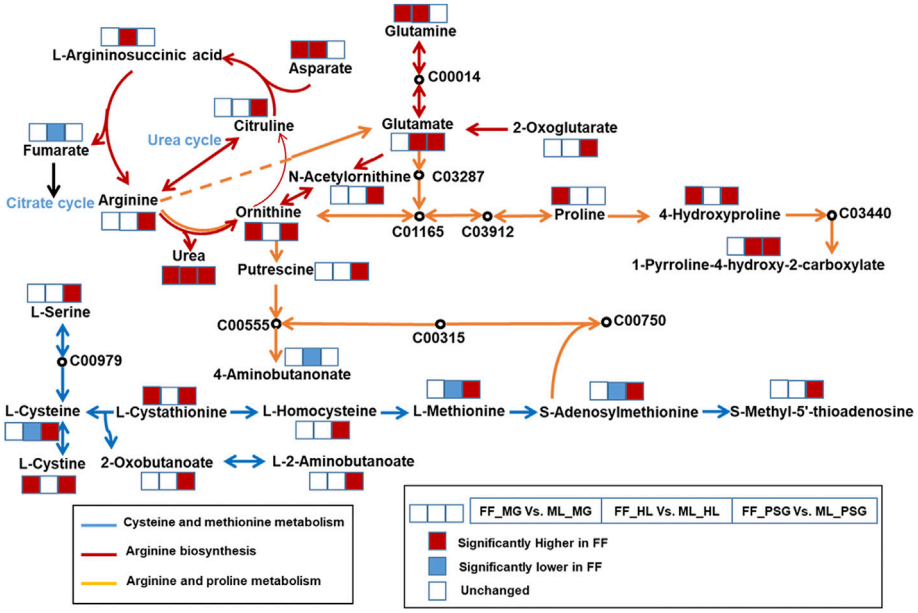

FIGURE 6
The integrated mutual metabolic pathways in the midgut (MG), hemolymph (HL) and posterior silk gland (PSG) of the formula feed (FF) silkworms. The blue, red and yellow line represented different metabolic pathways. The KEGG ID represented those were not detected or were not significantly different between the FF and mulberry leaves (ML) fed silkworms. The three squares with colors showed the different trends of metabolites in the MG, HL and PSG, respectively. The red, blue and blank squares represented the metabolites were significantly higher, lower or unchanged in the FF group, respectively.

(IPV = 0.608) were the top five enriched pathways. Furthermore, phenylalanine metabolism (IPV = 0.552); glutathione metabolism (IPV = 0.550); and ascorbate and aldarate metabolism (IPV = 0.500) also showed high impact values (IPV ≥0.500, Supplementary Table S4).

A total of 11 mutual pathways were enriched in the SDMs across the three tissues. Among them, the top three mutual pathways with the highest IPV in the PSG were listed as follows, which was integrated and depicted in Figure 6. Cysteine and methionine metabolism (IPV = 0.731) was enriched by ten SDMs in the PSG: S-methyl-5′-thioadenosine (Log_2FC = 2.02), S-adenosylmethionine (Log_2FC = 3.15), L-cystathionine (Log_2FC = 2.13), L-serine (Log_2FC = 2.39), L-homocysteine (Log_2FC = 2.74), L-methionine (Log_2FC = 1.29), L-cystine (Log_2FC = 3.46), L-cysteine (Log_2FC = 2.98), L-2-aminobutanoate (Log_2FC = 1.69) and 2-Oxobutanoate (Log_2FC = 7.89). Arginine biosynthesis, with an IPV of 0.629, was enriched by the SDMs: L-glutamate (Log_2FC = 4.09), L-arginine (Log_2FC = 1.71), N-acetylornithine (Log_2FC = 1.78), L-citrulline (Log_2FC = 2.51), 2-oxoglutarate (Log_2FC = 6.54), L-ornithine (Log_2FC = 2.83) and urea (Log_2FC = 5.43). Arginine and proline metabolism (IPV = 0.463) was enriched by the SDMs: L-arginine (Log_2FC = 1.71), putrescine (Log_2FC = 1.26), S-adenosylmethionine (Log_2FC = 3.16), L-glutamate (Log_2FC = 4.09), L-ornithine (Log_2FC = 2.83), 4-hydroxyproline (Log_2FC = 4.41) and 1-pyrroline-4-hydroxy-2-carboxylate (Log_2FC = 2.32).

3.2.6 Biomarkers associated with cocoon yield performance traits

A total of 722 metabolites with level A were used to perform biomarker analysis. Together with the differential trend of each metabolite (the selected metabolites are the SDMs in Results Section), 93, 171 and 163 preselected biomarkers (area under the curve (AUC) = 1) were obtained in the MG, HL and PSG, respectively (Supplementary Table S5). Among them, a total of 24 metabolites could serve as mutual preselected biomarkers across the three tissues (Supplementary Table S6).

The correlation analysis indicated that six mutual preselected biomarkers were significantly associated with the WCY, CSW and CSR ($p < 0.05$, Figure 7). Among them, homocitrulline, glycitein, valyl-threonine, propyl gallate and 3-amino-2,3-dihydrobenzoic acid were positively correlated with WCY, but were negatively correlated with CSW and CSR. In contrast, an opposite correlation pattern was observed between 3-dimethylallyl-4-hydroxyphenylpyruvate and the three cocoon performance traits (WCY, CSR and CSW). In this study, the above six preselected potential candidate biomarkers were defined as biomarkers relating to cocoon yield performance traits, which deserve further study.

10.3389/fmolb.2022.977047

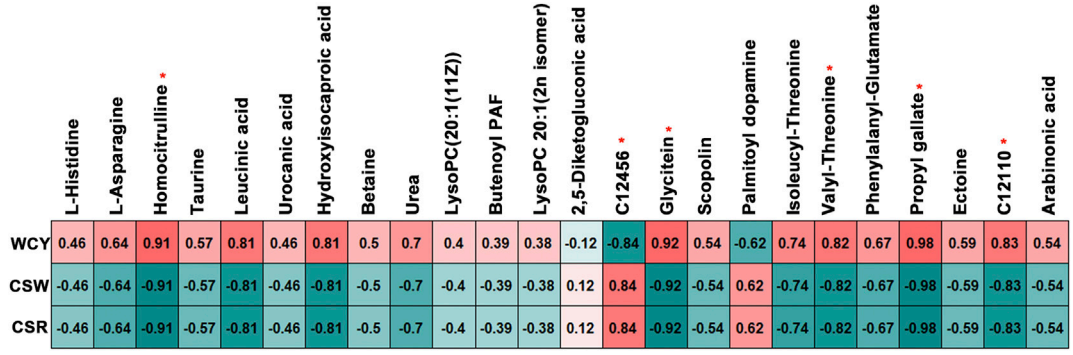

FIGURE 7
Correlation results between the cocoon yield performance traits and the six biomarkers identified. The red "*" indicates biomarkers which was significantly correlated with the cocoon yield performance traits. WCY, whole cocoon yield; CSW, cocoon shell weight; CSR, cocoon shell rate. C12456, 3-Dimethylallyl-4-hydroxyphenylpyruvate; C12110, 3-Amino-2,3-dihydrobenzoic acid.

4 Discussion

To our knowledge, this study is the first to integrate the metabolomic profiles of three tissues (MG, HL and PSG) with cocoon yield performance traits (WCY, CSW and CSR) in factory sericulture research. The current study also provides a method to systematically identify the metabolic reasons for the poor cocoon performance of the FF silkworms. We also performed pathway analysis and biomarker identification to explore the internal metabolic mechanisms and key biomarkers relating to the cocoon yield, thus providing future directions for improving the cocoon performance of the FF silkworms by optimizing the nutrition supply.

4.1 Poor cocoon performance of the FF silkworms

The experimental *B. mori* variety "Zhong 2016×Ri 2016" has been widely reared in a commercial enterprise. Although the CSW and CSR of the FF group were lower than those of the control ML silkworms, they also reached the average levels of the ML silkworms reported in previous studies (Qin et al., 2020; Xiao et al., 2020). Furthermore, given the high feeding adaptability to formula feed, developmental uniformity and silk quality of the silkworm variety with the relatively high efficiency of factory sericulture, feeding silkworms on formula feed has demonstrated practical application value. However, much room remains for cocoon performance improvement in the FF silkworms. Systematic metabolomic research provides a perspective to identify the internal mechanisms relating to cocoon and nutrition supply, which should aid in improving cocoon performance.

4.2 Significantly different metabolites

Regarding the metabolic differences between the FF and ML silkworms in three experimental tissues, we assessed, validated and classified the SDMs in the online Kyoto Encyclopedia of Genes and Genomes database (KEGG: https://www.kegg.jp/) and the Human Metabolome Database (HMDB: https://hmdb.ca/metabolites). Our analysis indicated that a large proportion of SDMs were significantly higher in the FF silkworms, a finding which was inconsistent with a previous report (Tao et al., 2022). Tao et al. (2022) has reported that the FF group had more downregulated metabolites in the HL than the ML group, thus indicating that the formula feed inhibited the metabolic activity of silkworms. This contradictory results might due to the nutrient levels of the formula feed. In our study, the WCY of FF silkworms was greater than the control group (ML group). However, in the report of Tao et al. (2022), the three cocoon performance traits of FF silkworms were much lower than the control, which might indicate the nutrient supply didn't meet the requirement of FF silkworms.

To explore the largest differences in metabolomic profiling, the top 15 upregulated and top 15 downregulated SDMs were considered.

In the MG, N-methyltyramine, a potent stimulant of gastrin release with a role in promoting intestinal secretion and movement (Ohta et al., 2020), was significantly higher in the FF group. Consequently, we inferred that the absorbed energy and nutrients did not satisfy the cocoon requirements in the FF silkworms, thus increasing the release of N-methyltyramine and accelerating the digestion and absorption in the MG. N-methyltyramine is also involved in tyrosine metabolism (Leete and Marion, 1953). On the basis of this finding, combined with lower levels of tyramine (an intermediate metabolite from tyrosine to N-methyltyramine) in the HL, we inferred that more tyrosine was metabolized into

N-methyltyramine in the FF silkworms. Furthermore, tyrosine was significantly higher in the PSG of the FF silkworms. Thus, we inferred that more tyrosine was supplied in the experimental formula feed. Tyrosine, one of the four main components of silk, might not be the limiting factor for silk synthesis in the FF silkworms. Pyridoxine 5′-phosphate was one of the top 15 downregulated SDMs in the FF silkworms, which participates in pyridoxine (vitamin B_6) metabolism (KEGG PATHWAY: map00750). Combined with the significantly diminished pyridoxine in the FF silkworms, the above results indicated that pyridoxine was in short supply in formula feed. Further, pyridoxine 5′-phosphate is involved in cofactor biosynthesis, thus indirectly affecting several amino acids, including serine, glutamine, methionine and cysteine metabolism (KEGG PATHWAY: map01240). Thus, we inferred that insufficient pyridoxine resulted in a lower pyridoxine 5′-phosphate level, which in turn restricted the corresponding amino acid metabolism. Ultimately, the cocoon yield decreased in silkworms reared on formula feed. Moreover, pyridoxine 5′-phosphate can be converted into pyridoxal 5′-phosphate through interaction with the pyridoxine-5′-phosphate oxidase (Huang et al., 2016a; Huang et al., 2016b). Pyridoxine-5′-phosphate oxidase is regulated by development and hormones (juvenile hormone, molting hormone) in silkworms (Huang et al., 2016a). Thus, the lower pyridoxine 5′-phosphate in the FF silkworms might be related to the hormone levels-a possibility requiring further validation.

In the HL, seven of the top SDMs were classified as flavonoids and isoflavonoids, given that flavonoid and isoflavonoid metabolism differs among diet treatments. Among above seven SDMs, all flavonoids were significantly higher in the ML group, whereas all isoflavonoids were much higher in the FF silkworms. (+)-Norpseudoephedrine plays a role in suppressing appetite (Balasubramanian, 2020). Thus, the significantly higher concentration of (+)-norpseudoephedrine in the FF group might indicate lower feed intake of the FF silkworms. The substrate of riboflavin (vitamin B_2), 6,7-dimethyl-8-(D-ribityl)lumazine (Zylberman et al., 2006), was much higher in the FF group. Correspondingly, the riboflavin level in the FF silkworms was significantly higher than that in the ML group. These results indicated that the riboflavin supply was beyond the requirement, a result warranting further validation in the FF silkworms. Tyramine, a monoamine compound derived from nondigestible tyrosine-containing peptides and proteins by bacterial fermentation (Anderegg et al., 2020), was markedly lower in the FF silkworms. Our results showed that the tyrosine to tyramine pathway was less active in the FF group, possibly because of less bacterial fermentation activity. However, this possibility requires further validation.

Among the top 30 SDMs (15 upregulated and 15 downregulated) in the PSG, 11 SDMs were classified as flavonoids and isoflavonoids, thus further validating that the flavonoid and isoflavonoid supply or metabolism markedly differed between the FF and ML groups. Among the 11 SDMs, eight were enriched in the ML group, a result consistent with the high number of flavonoids in mulberry leaves. Higher content of cysteine glutathione disulfide might imply that the FF silkworms were in a state of oxidative stress, because cysteine glutathione disulfide is a product of glutathione oxidation (Eriksson et al., 1967). Thus, the health and immune status of the FF silkworms should be examined with biochemical methods in the future.

A total of 60 mutual SDMs were identified in the three experimental tissues. Among them, 48 up-regulated and two down-regulated SDMs showed the same difference patterns. In silkworm larvae, superfluous amino acids are deaminized in the fat body and MG, thus producing ammonia, which is removed in three forms (Weihrauch and O'Donnell, 2021). Part of the ammonia is excreted in the form of ammonium salt by the Malpighian tubules (Weihrauch and O'Donnell, 2021), and a portion of the ammonia is stored as amides to provide amidogen for amino acid synthesis (Hirayama et al., 1997), or is involved in purine synthesis and eventually metabolized to uric acid or urea (Hirayama et al., 1996; Hiroko et al., 2016). Uric acid and urea, the end-product of amino acid metabolism, were significantly higher in all three tissues in the FF group than the ML group, possibly because of the higher urease activity of mulberry leaves (Hirayama et al., 1999). We speculated that urease was inactivated in the production and heat treatment of formula feed, thus impairing the metabolism of proteins, amino acids and other nitrogen-containing substances, which was consistent with a previous report (Tao et al., 2022). Many amino acids or small peptides including histidine, asparagine, homocitrulline and gamma-glutamylleucine were enriched in the FF tissues, in agreement with the above hypothesis. The difference trends for ascorbic acid were discrepant in three tissues: the levels were markedly lower in the MG and HL of the FF silkworms, but higher in the PSG. Ascorbic acid, also called vitamin C, is a crucial nutrient for the growth and development of silkworm larvae (Sayyad, 2020) and is obtained mainly from the diet. Thus, we inferred that the ascorbic acid supply was insufficient in the FF silkworm larvae, thus restricting the development of silkworms. The discrepant patterns of ascorbic acid in different tissues might be related to ascorbic acid metabolism, as observed for ascorbate and aldarate metabolism in the metabolic pathways enriched in the HL and PSG.

4.3 Metabolic pathways

In this study, the SDMs of different diets were found to be classified and involved mainly in the metabolism of amino acids and other nitrogen-contained intermediates, lipids, carbohydrates, vitamins, flavonoids and isoflavonoids. Some studies have found that insufficient vitamin supply; higher urea and uric acid content; and metabolic disorders related to

amino acid, carbohydrate and lipid metabolism are the main discrepancies between silkworms fed ML and FF (Dong et al., 2017; Qin et al., 2020; Tao et al., 2022). To identify crucial pathways relating to the diet treatments, we put the mutually enriched pathways among three tissues to the first place. The PSG serves as the production locus for fibroin, a main component of silk (Shigematsu and Koyasako, 1962). Besides, the SDM amounts in the PSG were much higher than those in the MG and HL, thus illustrating that the metabolomic differences affected by the rearing method were highest in the PSG; therefore, our analysis was focused on the top three mutual pathways with the highest IPV in the PSG.

With the highest IPV, cysteine and methionine metabolism was enriched by ten SDMs in the PSG. The ten SDMs accounted for approximately one-third of the entire pathway. Notably, the log_2FC values revealed that all SDMs involved in cysteine and methionine metabolism were significantly higher in the FF group. Cysteine is derived from the diet or biosynthesis, with the latter source used serine as the substrate (KEGG Module: M00021, M00338). The serine content was indeed higher in the PSG of the FF silkworms. Serine is one of the four main components of silk (Kensuke et al., 1976). Given the biological function of the PSG, our results might indicate that the higher serine was not integrated into silk as expected but was metabolized into cysteine or other intermediates. This possibility is supported by the higher content of L-cystathionine, 2-oxobutanoate and L-homocysteine, which are intermediate products of serine metabolism in the cysteine and methionine metabolism pathway (KEGG PATHWAY: map00270). Thus, the above possibility might partly explain the contradictory finding of higher serine and lower silk performance traits in the FF silkworms. Methionine has been reported to be upregulated in silkworms reared on formula feed (Tao et al., 2022). As an essential amino acid, methionine cannot be synthesized by silkworms (Ito, 1967). Thus, we inferred that the higher content of methionine might have been derived from the diet or bacterial synthesis.

Arginine biosynthesis (KEGG PATHWAY: map00220), with an impact value of 0.629, was the 2nd mutual metabolic pathway enriched in the three experimental tissues. Arginine, an essential amino acid for silkworms, has been speculated to be synthesized mainly by the microbiota (Ito, 1967). On the one hand, the content of L-glutamate, N-acetylornithine and L-citrulline, which are substrates for arginine synthesis (KEGG Module: M00845), were all higher than those in the ML group. On the other hand, three metabolic products of arginine had higher levels in the FF silkworms: L-ornithine, L-citrulline and urea. Consequently, we speculated that the above arginine pathways involved in synthesis and metabolism might be more active in the FF silkworms. As noted in Discussion section: Significantly different metabolites, the substantially high FC of urea (Log_2FC = 5.43) implied that the free arginine exceeded the requirements for normal growth and development of the FF silkworms. Further, combined with the lack of urease, the higher content of urea could not be hydrolyzed into ammonia to provide nitrogen for silkworm growth and development. Thus, the higher content of arginine might be detrimental indirectly for the silkworm growth and development.

Arginine and proline metabolism, with the 3rd highest IPV, was discussed subsequently. Arginine and proline are essential and semi-essential amino acids for silkworms (Ito, 1967), respectively. In the current study, the metabolic products of arginine, including L-ornithine, putrescine and L-glutamate (KEGG PATHWAY: map00330), all showed higher content in the FF silkworms. Although L-proline was not identified as an SDM in the PSG, owing to its low VIP value (VIP <1.00), it was numerically higher in the FF silkworms (FDR <0.05). Proline can be transformed by arginine and ornithine (Xu et al., 1980) to partly or completely meet the requirement of silkworm growth. In the FF group, proline was significantly higher in the MG, which indicated the high content of proline was partly derived from the diet source. The lack of proline could restricted the development and growth of silkworms (Ito, 1972). In this study, the higher content of proline in the FF group might be helpful to explain the heavier pupae weight of the FF group. The higher proline content was metabolized into hydroxyproline and L-glutamate, both of which were significantly higher than those in the ML silkworms ($p < 0.05$). L-glutamate is an essential amino acid for silkworm (Ito, 1972), which provides amidogen in transaminatin. Under the role of alanine aminotransferase, L-glutamate could be metabolized into pyruvic acid (Fukuda, 1957), which could provide energy for silk synthesis. However, pyruvic acid was not significantly different between the FF and ML silkworms, which might be attributed to the less active alanine aminotransferase in the FF silkworms. It was reported alanine aminotransferase was less active when the vitamin B_6 was insufficient in silkworms (Horie and Nakamura, 1986). In this study, we inferred vitamin B_6 was in short supply in the Discussion section: Significantly different metabolites. Thus, we thought the insufficient vitamin B_6 restricted the activity of alanine aminotransferase which further limited the transformation of L-glutamate to pyruvic acid and restricted the silk synthesis ultimately.

4.4 Biomarkers associated with cocoon yield performance traits

Biomarker analysis combined with a Pearson correlation calculation revealed six biomarkers that showed positive or negative relationships with the WCY, CSW and CSR: homocitrulline (Log_2FC = 4.88, 4.82 and 8.88 in the MG, HL and PSG, respectively), glycitein (Log_2FC = 12.6, 9.83 and 8.43 in the MG, HL and PSG, respectively), valyl-threonine (Log_2FC = 4.56, 4.28 and 5.19 in the MG, HL and PSG, respectively), propyl gallate (Log_2FC = 12.1, 9.70 and 14.3 in the MG, HL and PSG,

respectively), 3-amino-2,3-dihydrobenzoic acid (Log_2FC = 1.93, 2.44 and 3.97 in the MG, HL and PSG, respectively) and 3-dimethylallyl-4-hydroxyphenylpyruvate (Log_2FC = -2.98, -3.64 and -4.60 in the MG, HL and PSG, respectively). Among these six biomarkers identified, the first five showed a positive relationship with WCY, and a negative relationship with CSW and CSR.

Homocitrulline, an L-alpha amino acid, is a post-translational modification product (Mahmoudi et al., 2019). As reported, homocitrulline is closely associated with inflammatory responses, physical condition and diseases (Lac et al., 2018), and has been proposed to serve as a biomarker for identifying patient frailty (Mahmoudi et al., 2019) or oxidative stress relating to myeloperoxidase (Pireaux et al., 2021). In this study, homocitrulline was significantly higher in the FF silkworms, particularly in the PSG (Log_2FC = 8.88). Thus, we speculated that the FF silkworms might have been in a state of oxidative stress or weakness, a possibility warranting further exploration.

Glycitein, an isoflavonoid, was detected only in the FF group in this experiment. It is present in high concentrations in natto, miso and soybeans, according to the HMDB (https://hmdb.ca/metabolites/HMDB0005781). Therefore, our results were reasonable, given that soybean meal was a major component of the experimental formula feed (1st to 3rd instar silkworm feed: 31%, 4th and 5th instar silkworm feed: 40%). Moreover, glycitein, a primary metabolite, is directly associated with the growth, development and reproduction of organisms (Hu et al., 2015; Pastore et al., 2018). The extremely high glycitein might contribute to greater growth and development of silkworm larvae, thus resulting in a positive correlation between glycitein and pupa weight, as included in the WCY.

Valyl-threonine, a dipeptide of valine and threonine, is an incomplete breakdown product in protein digestion or catabolism (https://hmdb.ca/metabolites/HMDB0029137). The high content of valyl-threonine might have indicated incomplete proteolysis in the FF silkworms, thereby restricting the substrate supply for silk synthesis. Thus, this compound was negatively correlated with CSR and CSW. Moreover, some dipeptides have been found to be directly used in organism development (Fedoreyeva et al., 2020), thus possibly explaining the positive relationship with WCY.

Propyl gallate, an antioxidant used in the food industry (Nguyen et al., 2021), was significantly higher in the FF group. Propyl gallate is found in corn, a major component of the experimental formula feed. In addition, gallic acid, a part of propyl gallate, was added in the formula feed as a preservative. Thus, the content of propyl gallate was affected by the diet treatment. Propyl gallate is absorbed after ingestion (Becker, 2007), and thus showed a relatively higher concentration in the MG, which plays important roles in digestion and absorption (Shen et al., 2022). The HL, a circulatory system for nutrients and metabolites, also contained more propyl gallate in the FF group. The biological roles of propyl gallate include scavenging of oxygen free radicals, antimicrobial activity, inhibitory enzyme activity and biosynthetic processes inhibition (Becker, 2007). Thus, the higher concentration of propyl gallate might have resulted in lower microbiota and enzymatic activity, thereby restricting nutrient metabolism and silk synthesis in the FF group. Furthermore, propyl gallate shows slight toxicity when ingested (Becker, 2007) and therefore might have influenced silkworm health status.

The compound 3-amino-2,3-dihydrobenzoic acid, in the category of amino acids, peptides and analogues, showed higher concentrations in all experimental tissues of the FF silkworms. This compound, also known as gabaculin or 5-aminocyclohexa-1,3-diene-1-carboxylic acid, exists in all living organisms and inhibits the activity of γ-aminobutanoic acid-transaminase (Park et al., 2021) and ornithine aminotransferase (Li et al., 2016). Inhibition of ornithine aminotransferase results in restriction of ornithine synthesis with glutamate (KEGG Module: M00028) as a substrate. Thus, the higher content of 3-amino-2,3-dihydrobenzoic acid might have restricted the corresponding amino acid metabolism in the FF silkworms and partially explained the negative correlations between 3-amino-2,3-dihydrobenzoic acid and CSW, and 3-amino-2,3-dihydrobenzoic acid and CSR. In plant research, 3-amino-2,3-dihydrobenzoic acid is used as an inhibitor of chlorophyll biosynthesis, a tetrapyrrole synthesis relating to heme and holocytochrome (Demko et al., 2010).

As the only biomarker which was negatively correlated with WCY and positively correlated with CSW and CSR, 3-dimethylallyl-4-hydroxyphenylpyruvate was significantly lower in the FF silkworms. Of note, 3-dimethylallyl-4-hydroxyphenylpyruvate was also the only top SDM identified mutully in all experimental tissues in this research. On the basis of the KEGG database, 3-dimethylallyl-4-hydroxyphenylpyruvate is involved in novobiocin biosynthesis (KEGG PATHWAY: map00401) and biosynthesis of secondary metabolites (KEGG PATHWAY: map01110). In the novobiocin biosynthesis pathway, 3-dimethylallyl-4-hydroxyphenylpyruvate is indirectly synthesized by L-tyrosine. Given the higher tyrosine and lower 3-dimethylallyl-4-hydroxyphenylpyruvate levels, we inferred that the novobiocin biosynthesis pathway was less active in the FF silkworms.

5 Conclusion

In this study, systematic metabolomic profiles of the MG, HL and PSG were integrated to clarify the metabolic characteristics of silkworms fed formula feed versus mulberry leaves. Cysteine and methionine metabolism; arginine biosynthesis; and arginine and proline metabolism were mutual key pathways affecting cocoon yield performance traits. Homocitrulline, glycitein, valyl-threonine, propyl gallate, 3-amino-2,3-dihydrobenzoic acid were positively correlated with WCY, but negatively correlated with

CSW and CSR, while 3-dimethylallyl-4-hydroxyphenylpyruvate showed an opposite correlation pattern. In other words, the lower level of homocitrulline, glycitein, valyl-threonine, propyl gallate, 3-amino-2,3-dihydrobenzoic acid and the higher level of 3-dimethylallyl-4-hydroxyphenylpyruvate, the higher CSW and CSR might be achieved, which requires further validation by a nutritional experiment further.

Data availability statement

The original contributions presented in the study are included in the article/Supplementary Material, further inquiries can be directed to the corresponding author.

Author contributions

WZ and XW conceived the study. WZ and JC offered valuable suggestions for the study design. XW, AY, and XC performed the procedures, analyzed the metabolic data and wrote the manuscript. RH and FJ provided the silkworm variety, formula feed and much help for the study. MP and HM provide suggestions for revising the manuscript. All authors read and approved the final manuscript.

Funding

The research described in this article was supported by Key Scientific and Technological grant of Zhejiang for Breeding New Agricultural Varieties (2021C02072), China Agriculture Research System of MOF and MARA (CARS-18), Cooperative Extension Project of Major Agricultural Technologies of Zhejiang Province (2020XTTGCS01), Zhejiang Provincial Key R&D project (2019C02044) and Zhejiang Provincial Silkworm and Bee Resources Utilization and Innovation Research Key Laboratory (2020E10025).

Acknowledgments

The authors really thank Tingting Zhang and Lanfang Ye (temporatory worker) for their help in the study trial and sampling.

Conflict of interest

RH and FJ were employed by the Company Shengzhou Mulsun Biotech Co., Ltd.

The remaining authors declare that the research was conducted in the absence of any commercial or financial relationships that could be construed as a potential conflict of interest.

Publisher's note

All claims expressed in this article are solely those of the authors and do not necessarily represent those of their affiliated organizations, or those of the publisher, the editors and the reviewers. Any product that may be evaluated in this article, or claim that may be made by its manufacturer, is not guaranteed or endorsed by the publisher.

Supplementary material

The Supplementary Material for this article can be found online at: https://www.frontiersin.org/articles/10.3389/fmolb.2022.977047/full#supplementary-material

References

Anderegg, J., Constancias, F., and Meile, L. (2020). Effects of sodium chloride on tyramine production in a fermented food model and its inhibition by tyrosine-degrading *Lactobacillus plantarum* JA-1199. *Chimia* 74 (5), 391–397. doi:10.2533/chimia.2020.391

Balasubramanian, K., Perez, C. I., Arroyo, B., Moreno, M. G., and Gutierrez, R. (2020). The appetite suppressant D-norpseudoephedrine (cathine) acts *via* D1/D2-like dopamine receptors in the nucleus accumbens shell. *Front. Neurosci.* 14, 572328–572414. doi:10.3389/fnins.2020.572328

Becker, L. (2007). Final report on the amended safety assessment of propyl gallate. *Int. J. Toxicol.* 26, 89–118. doi:10.1080/10915810701663176

Chen, W., Gong, L., Guo, Z. L., Wang, W. S., Zhang, H. Y., Liu, X. Q., et al. (2013). A novel integrated method for large-scale detection, identification, and quantification of widely targeted metabolites: Application in the study of rice metabolomics. *Mol. Plant* 6 (006), 1769–1780. doi:10.1093/mp/sst080

Chen, X. D., Ye, A. H., Wu, X. H., Qu, Z. G., Xu, S. Q., Sima, Y. H., et al. (2022). Combined analysis of silk synthesis and hemolymph amino acid metabolism reveal key roles for glycine in increasing silkworm silk yields. *Int. J. Biol. Macromol.* 209, 1760–1770. doi:10.1016/j.ijbiomac.2022.04.143

Demko, V., Pavlovic, A., and Hudak, J. (2010). Gabaculine alters plastid development and differentially affects abundance of plastid-encoded DPOR and nuclear-encoded GluTR and FLU-like proteins in spruce cotyledons. *J. Plant Physiol.* 167 (9), 693–700. doi:10.1016/j.jplph.2009.12.008

Dong, H. L., Zhang, S. X., Tao, H., Chen, Z. H., Li, X., Qiu, J. F., et al. (2017). Metabolomics differences between silkworms (*Bombyx mori*) reared on fresh mulberry (*morus*) leaves or artificial diets. *Sci. Rep.* 7 (1), 10972–10988. doi:10.1038/s41598-017-11592-4

Dong, H. L., Zhang, S. X., Chen, Z. H., Tao, H., Xu, S. Q., Qiu, J. F., et al. (2018). Differences in gut microbiota between silkworms (*Bombyx mori*) reared on fresh

mulberry (*Morus alba* var. Multicaulis) leaves or an artificial diet. *RSC Adv.* 8 (46), 26188–26200. doi:10.1039/C8RA04627A

Eriksson, B., Eriksson, S. A., Cyvin, S. J., Brunvoll, J., and Dumanovi, J. (1967). Synthesis and characterization of the L-cysteine-glutathione mixed disulfide. *Acta Chem. Scand.* 21 (5), 1304–1312. doi:10.3891/acta.chem.scand.21-1304

Fang, S. M., Zhou, Q. Z., Yu, Q. Y., and Zhang, Z. (2020). Genetic and genomic analysis for cocoon yield traits in silkworm. *Sci. Rep.* 10, 5682–5693. doi:10.1038/s41598-020-62507-9

Fedoreyeva, L. I., Kononenko, N. V., Baranova, E. N., Dilovarova, T. A., Smirnova, E. A., and Vanyushin, B. F. (2020). Dipeptides and Glycine modulate development of seedlings and regenerants of tobacco *nicotiana tabacum L. Biol. Bull. Russ. Acad. Sci.* 47 (4), 364–373. doi:10.1134/S1062359020030036

Fraga, C. G., Clowers, B. H., Moore, R. J., and Zink, E. M. (2010). Signature-discovery approach for sample matching of a nerve-agent precursor using liquid chromatography-mass spectrometry, XCMS, and chemometrics. *Anal. Chem.* 82 (10), 4165–4173. doi:10.1021/ac1003568

Fukuda, T. (1957). Biochemical studies on the formation of the silkprotein. 4. The conversion of pyruvic acid to alanine in the silkworm larva. *J. Biochem.* 44 (8), 505–510. doi:10.1093/oxfordjournals.jbchem.a126780

Ge, Q., Xiao, R., Yuan, Y., He, S. Q., Chen, L., Ma, S. S., et al. (2020). Transcriptome and proteomics-based analysis to investigate the regulatory mechanism of silk gland differences between reciprocal cross silkworm, *Bombyx mori. J. Asia. Pac. Entomol.* 23 (4), 1101–1113. doi:10.1016/j.aspen.2020.09.002

Hirayama, C., Konno, K., and Shinbo, H. (1996). Utilization of ammonia as a nitrogen source in the silkworm, *Bombyx mori. J. Insect Physiol.* 42 (10), 983–988. doi:10.1016/0022-1910(96)00009-1

Hirayama, C., Konno, K., and Shinbo, H. (1997). The pathway of ammonia assimilation in the silkworm, *Bombyx mori. J. Insect Physiol.* 43 (10), 959–964. doi:10.1016/s0022-1910(97)00045-0

Hirayama, C., Sugimura, M., and Shinbo, H. (1999). Recycling of urea associated with the host plant urease in the silkworm larvae, *Bombyx mori. J. Insect Physiol.* 45 (1), 15–20. doi:10.1016/S0022-1910(98)00095-X

Hiroko, T., Hidemasa, B., Katsuhiko, I., and Takeshi, Y. (2016). Can the silkworm (*Bombyx mori*) Be used as a human disease model? *Drug Discov. Ther.* 10 (1), 3–8. doi:10.5582/ddt.2016.01011

Horie, Y., and Nakamura, M. (1986). Effect of dietary pyridoxine on alanine and aspartate aminotransferases in the silkworm, *Bombyx mori* (Lepidoptera, bombycidae). *Appl. Entomol. Zool.* 21 (1), 164–170. doi:10.1303/aez.21.164

Hu, Y. J., Gao, K. G., Zheng, C. T., Wu, Z. J., Yang, X. F., Wang, L., et al. (2015). Effect of dietary supplementation with glycitein during late pregnancy and lactation on antioxidative indices and performance of primiparous sows. *J. Anim. Sci.* 93 (5), 2246–2254. doi:10.2527/jas.2014-7767

Huang, S. H., Yang, H. H., Yao, L. L., Zhang, J. Y., and Huang, L. Q. (2016a). Effect of exogenous hormones on transcription levels of pyridoxal 5 '-Phosphate biosynthetic enzymes in the silkworm (*Bombyx mori*). *Comp. Biochem. Physiol. B Biochem. Mol. Biol.* 194, 20–24. doi:10.1016/j.cbpb.2016.01.002

Huang, S. H., Yao, L. L., Zhang, J. Y., and Huang, L. Q. (2016b). Direct and indirect effects of RNA interference against pyridoxal kinase and pyridoxine 5 '-Phosphate oxidase Genes in *Bombyx mori*. *Gene* 587 (1), 48–52. doi:10.1016/j.gene.2016.04.035

Ito, T. (1967). Nutritional requirements of the silkworm, *Bombyx mori* L. *Proc. Jpn. Acad.* 43 (1), 57–61. doi:10.2183/pjab1945.43.57

Ito, T. (1972). Amino acid nutrition of the silkworm, *Bombyx mori. Proc. Jpn. Acad.* 48, 613–618. doi:10.2183/pjab1945.48.613

Kensuke, S., Aiko, K., Kohei, O., Yōtarō, K., and Akio, H. (1976). Studies on silk fibroin of *Bombyx mori*. I. fractionation of fibroin prepared from the posterior silk gland. *J. Biochem.* 80 (4), 693–702. doi:10.1093/oxfordjournals.jbchem.a131328

Kim, M. G., Cha, J. M., Kim, J. G., Son, Y. H., Kim, C. R., Kim, M. R., et al. (2021). Effect of acetic acid ester and kumgang medicine stone in silkworm rearing with artificial diet and mulberry. *Int. J. Sci. Res. Sci. Eng. Technol.* 8 (1), 01–11. doi:10.32628/IJSRSET207648

Lac, P., Saunders, S., Tutunea-Fatan, E., Barra, L., Bell, D. A., and Cairns, E. (2018). Immune responses to peptides containing homocitrulline or citrulline in the DR4-transgenic mouse model of rheumatoid arthritis. *J. Autoimmun.* 89, 75–81. doi:10.1016/j.jaut.2017.12.002

Lamberti, C., Gai, F., Cirrincione, S., Giribaldi, M., Purrotti, M., Manfredi, M., et al. (2019). Investigation of the protein profile of silkworm (*Bombyx mori*) pupae reared on a well-calibrated artificial diet compared to mulberry leaf diet. *PeerJ* 1 (7), 6723–6745. doi:10.7717/peerj.6723

Leete, E., and Marion, L. (1953). The biogensis of alkaloids. 7. The formation of horeenine and N-methyltyramine from tyrosine in barley. *Can. J. Chem.* 31 (2), 126–128. doi:10.1139/v53-017

Li, H., Meininger, C. J., Bazer, F. W., and Wu, G. Y. (2016). Intracellular sources of ornithine for polyamine synthesis in endothelial cells. *Amino Acids* 48 (10), 2401–2410. doi:10.1007/s00726-016-2256-6

Mahmoudi, R., Jaisson, S., Badr, S., Jaidi, Y., Bertholon, L. A., Novella, J. L., et al. (2019). Post-translational modification-derived products are associated with frailty status in elderly subjects. *Clin. Chem. Lab. Med.* 57 (8), 1153–1161. doi:10.1515/cclm-2018-1322

Nair, J. S., and Kumar, S. N. (2004). Artificial diet for silkworm *Bombyx mori L.* - a retrospection through the decades. *Indian J. Seric.* 43 (1), 1–17.

Nguyen, V. H., Le, M. N., Nguyen, H. B., Ha, K. O., Pham, T. H. V., Nguyen, T. H., et al. (2021). Propyl gallate. *Molbank* 2021 (2), 1201–1210. doi:10.3390/M1201

Ohta, H., Murakami, Y., Takebe, Y., Murasaki, K., Morimura, S., Yoshihara, H., et al. (2020). N-methyltyramine, a gastrin-releasing factor in beer, and structurally related compounds as agonists for human trace amine-associated receptor 1. *Food Sci. Technol. Res.* 26 (2), 313–317. doi:10.3136/fstr.26.313

Pang, Z., Chong, J., Zhou, G., Morais, D., Xia, J., Barrette, M., et al. (2021). MetaboAnalyst 5.0: Narrowing the gap between raw spectra and functional insights. *Nucleic Acids Res.* 49 (1), 388–396. doi:10.1093/nar/gkab382

Park, M. G., Han, A. R., Kim, S. Y., Kim, T. Y., Kim, H. M., and Lee, C. J. (2021). High-yield synthesis and purification of recombinant human GABA transaminase for high-throughput screening assays. *J. Enzyme Inhib. Med. Chem.* 36 (1), 2016–2024. doi:10.1080/14756366.2021.1975697

Pastore, M. R., Negrato, E., Poltronieri, C., Barion, G., Messina, M., Tulli, F., et al. (2018). Effects of dietary soy isoflavones on estrogenic activity, cortisol level, health and growth in rainbow trout, *Oncorhynchus mykiss*. *Aquac. Res.* 49 (4), 1469–1479. doi:10.1111/are.13602

Pireaux, V., Delporte, C., Rousseau, A., Desmet, J. M., Antwerpen, P. V., Raes, M., et al. (2021). M2 monocyte polarization in dialyzed patients is associated with increased levels of M-CSF and myeloperoxidase-associated oxidative stress: Preliminary results. *Biomedicines* 9 (1), 84–97. doi:10.3390/biomedicines9010084

Qin, D. Y., Wang, G. H., Dong, Z. M., Xia, Q. Y., and Zhao, P. (2020). Comparative fecal metabolomes of silkworms being fed mulberry leaf and artificial diet. *Insects* 11 (12), 851–866. doi:10.3390/insects11120851

Ruan, J. H., Wu, M. Y., Ye, X. G., Zhao, S., Liang, J. S., Ye, L. P., et al. (2021). Comparative mRNA and LncRNA analysis of the molecular mechanisms associated with low silk production in *Bombyx mori. Front. Genet.* 11, 592128–601807. doi:10.3389/fgene.2020.592128

Saoi, M., and Britz-McKibbin, P. (2021). New advances in tissue metabolomics: A review. *Metabolites* 11 (10), 672–697. doi:10.3390/metabo11100672

Sayyad, N. R. (2020). Effects of supplementary nutrients of amla and lime fruit extract on growth of silkworm *Bombyx mori L. Int. J. Entomol. Res.* 5 (5), 40–42.

Shen, Y. W., Zeng, X. Q., Chen, G. P., and Wu, X. F. (2022). Comparative transcriptome analysis reveals regional specialization of gene expression in larval silkworm (*Bombyx mori*) midgut. *Insect Sci.* 8, 1–17. doi:10.1111/1744-7917.13001

Shigematsu, H., and Koyasako, T. (1962). Kinetics of synthesis of fibroin in posterior division of silk-gland of silkworm, *Bombyx mori, L. Nature* 195 (4840), 501–502. doi:10.1038/195501a0

Sun, H. Z., Wang, D. M., Wang, B., Wang, J. K., Liu, H. Y., Guan, L. L., et al. (2015). Metabolomics of four biofluids from dairy cows: potential biomarkers for milk production and quality. *J. Proteome Res.* 14 (2), 1287–1298. doi:10.1021/pr501305g

Tao, S. S., Wang, J., Liu, M. H., Sun, F., Li, B., and Ye, C. J. (2022). Haemolymph metabolomic differences in silkworms (*Bombyx mori L.*) under mulberry leaf and two artificial diet rearing methods. *Arch. Insect Biochem. Physiol.* 109 (2), e21851–25. doi:10.1002/arch.21851

Weihrauch, D., and O'Donnell, M. J. (2021). Mechanisms of nitrogen excretion in insects. *Curr. Opin. Insect Sci.* 47, 25–30. doi:10.1016/j.cois.2021.02.007

Wu, X. H., Sun, H. Z., Xue, M. Y., Wang, D. M., Guan, L. L., and Liu, J. X. (2019). Serum metabolome profiling revealed potential biomarkers for milk protein yield in dairy cows. *J. Proteomics* 184, 54–61. doi:10.1016/j.jprot.2018.06.005

Xiao, R., Yuan, Y., Zhu, F. F., He, S. Q., Ge, Q., Wang, X. Q., et al. (2020). Transcriptomics and proteomics-based analysis of heterosis on main economic traits of silkworm, *Bombyx mori*. *J. Proteomics* 229, 103941–103957. doi:10.1016/j.jprot.2020.103941

Xu, T. S., Zhu, J. H., Lin, H., and Guo, B. X. (1980). Studies on the metabolism of amino acids in the silkworm: Arginase, ornithine-delta transaminase and side chain transaminases. *Acta Entomol. Sin.* 23, 1–8. doi:10.16380/j.kcxb.1980.01.001

Yamamoto, M., Machida, J., Shinohara, M., Igarashi, A., and Kawahara, Y. (2021). Influence of tobiko-mixed artificial diet on textile properties of *Bombyx mori* silkworm cocoons. *J. Nat. Fibers*, 1–11. doi:10.1080/15440478.2021.1901829

Zhang, Y. L., Bi, L. H., Cui, W. Z., Huang, W. J., We, W., Wei, B. Y., et al. (2020). Breeding of new silkworm variety guican 5 suitable for young silkworm rearing with artificial diet. *Acta Sericol Sin.* 46 (5), 584–593. doi:10.13441/j.cnki.cykx.2020.05.008

Zhou, Z. H., Yang, H. J., Chen, M., Lou, C. F., Zhang, Y. Z., Chen, K. P., et al. (2008). Comparative proteomic analysis between the domesticated silkworm (*Bombyx mori*) reared on fresh mulberry leaves and on artificial diet. *J. Proteome Res.* 7 (12), 5103–5111. doi:10.1021/pr800383r

Zhou, L. H., Li, H. H., Hao, F. H., Li, N., Liu, X., Wang, G. L., et al. (2015). Developmental changes for the hemolymph metabolome of silkworm (*Bombyx mori L.*). *J. Proteome Res.* 14 (5), 2331–2347. doi:10.1021/acs.jproteome.5b00159

Zylberman, V., Klinke, S., Haase, I., Bacher, A., Fischer, M., and Goldbaum, F. A. (2006). Evolution of vitamin B_2 biosynthesis: 6, 7-Dimethyl-8-ribityllumazine synthases of Brucella. *J. Bacteriol.* 188 (17), 6135–6142. doi:10.1128/JB.00207-06

frontiers | Frontiers in Animal Science

TYPE Original Research
PUBLISHED 01 November 2022
DOI 10.3389/fanim.2022.934204

OPEN ACCESS

EDITED BY
Georgios Oikonomou,
University of Liverpool,
United Kingdom

REVIEWED BY
Halima Sultana,
University of Florida, United States
Fabio Abeni,
Consiglio per la Ricerca in Agricoltura e l'Analisi dell'Economia Agraria (CREA), Italy

*CORRESPONDENCE
Kentaro Nagaoka
nagaokak@cc.tuat.ac.jp

SPECIALTY SECTION
This article was submitted to Animal Physiology and Management, a section of the journal Frontiers in Animal Science

RECEIVED 02 May 2022
ACCEPTED 07 October 2022
PUBLISHED 01 November 2022

CITATION
Kojima M, Liu H, Takemoto S, Suda Y, Inoue R, Watanabe G, Jin W and Nagaoka K (2022) Temporal changes in the fecal microbiome and blood metabolites of early neonatal calves. *Front. Anim. Sci.* 3:934204. doi: 10.3389/fanim.2022.934204

Temporal changes in the fecal microbiome and blood metabolites of early neonatal calves

Miyu Kojima[1], Hong Liu[1], Satoshi Takemoto[2], Yoshihito Suda[3], Ryo Inoue[4], Gen Watanabe[1], Wanzhu Jin[5] and Kentaro Nagaoka[1]*

[1]Laboratory of Veterinary Physiology, Tokyo University of Agriculture and Technology, Tokyo, Japan, [2]Central Research Institute for Feed and Livestock, ZEN-NOH (National Federation of Agricultural Cooperative Associations), Ibaraki, Japan, [3]Department of Food, Agriculture and Environment, Miyagi University, Miyagi, Japan, [4]Laboratory of Animal Science, Department of Applied Biological Sciences, Setsunan University, Osaka, Japan, [5]Institute of Zoology, Chinese Academy of Sciences, Beijing, China

The initial colonization and early development of the intestinal microbiome are important stages in the growth of calves during pre-weaning. This study investigated temporal changes in the diversity and composition of the fecal microbiota, focusing on the first 2 weeks after birth, with the aim of identifying intestinal bacteria and blood metabolites that are associated with calf diarrhea. In this study, 10 calves were fed colostrum on day 0 after birth, whole milk from days 2 to 5, and milk replacer from day 6. Six calves showed mild diarrhea in the second week (i.e., from day 8 to 14). We observed dramatic changes in the development of the fecal microbiome from day 2 to 14 and found several bacterial species, such as *Lactobacillus* and *Collinsella*, changing significantly in abundance during the milk transition (i.e., from day 4 to 10). In investigating whether there is an association between the microbiome and the milk transition, we found the level of hypotaurine and D-xylose to be significantly higher in whole milk from days 4 and 5 than in milk replacer. A comparison of four healthy calves and six diarrheal calves revealed that the diarrheal calves had a low abundance of *Collinsella* on day 10. Furthermore, we explored plasma metabolites statistically correlated with the change of fecal *Collinsella* and found a high level of dimethylglycine in healthy calves. Taken together, these findings suggest a possible link between temporary changes in the fecal microbiome and neonatal diarrhea during the milk transition in calves.

KEYWORDS

16S rRNA, neonatal diarrhea, whole milk, milk replacer, dairy cows

Introduction

The gastrointestinal microbiome has been proven to be a key feature in the relationship between health and disease across animal species. A balanced microbiome composition, characteristic of each host species, is necessary for maintaining the intestinal mucosal barrier, antagonizing the colonization of pathogenic bacteria, and contributing to metabolism and immune homeostasis (O'Hara & Shanahan, 2006). Disruption of the composition of microbiota, known as "dysbiosis," can trigger several diseases, including gastrointestinal disorders (Sommer et al., 2017). Neonatal diarrhea is predominantly caused by enteric infections during the early stages of life in mammals, when the gastrointestinal microbiome starts to colonize and develop (Bauer et al., 2006).

Dairy cattle are known to have a diverse community of ruminal bacteria that provides energy for growth and milk production, whereas the rumen of neonatal calves is non-functional but starts growing on the addition of cereal to their diets at 3 or 4 weeks of age (Baldwin et al., 2004). It has been suggested that the intestinal (not ruminal) microbiome plays an instrumental role in maintaining calf health by not only providing nutrients and energy, but also stimulating the host immune system to combat pathogens (Yeoman & White, 2014; Malmuthuge & Guan, 2017; Malmuthuge et al., 2019). Neonatal diarrhea is one of the major causes of calf morbidity and mortality and has a large impact on the economics of dairy farms (Uetake, 2013; USDA, 2018). Although enteric infection is often observed, the cause of neonatal diarrhea is difficult to define because it commonly presents with coinfections and most pathogens, consistent with the occurrence of neonatal diarrhea, can also be found in healthy individuals (Cho et al., 2013; Adaska et al., 2017). Recently, studies have reported differences in fecal microbial communities between healthy and diarrheal calves during the first few weeks of life (Oikonomou et al., 2013; Gomez et al., 2017; Zeineldin et al., 2018).

The development of a healthy intestinal microbiome is profoundly influenced by the calf's diet, which is essential in preventing calf diarrhea (Malmuthuge & Guan, 2017; Badman et al., 2019). In general, dairy calves are fed colostrum within a few hours of birth and their diet is changed from whole milk to milk replacer or a solid diet within 2–7 days. There are various management protocols to optimize the process of milk transition and weaning (Khan et al., 2011). However, even under a proper management protocol, neonatal diarrhea is often observed after the milk transition. More importantly, some calves develop diarrhea and others do not, even under the same management protocol. These observations prompted us to investigate changes in the intestinal microbiota before and after the milk transition, and to explore whether there is an association between changes in the microbiome and neonatal diarrhea.

In this study, we analyzed the change in the fecal microbiome by next-generation sequencing and determined the metabolite profiles of colostrum, whole milk, and milk replacer by untargeted metabolomics using gas chromatography–mass spectrometry (GC-MS). The abundance of bacteria significantly changed during the milk transition, and there were different levels of one species of bacterium, *Collinsella*, between healthy and diarrheal calves. In addition, we found that levels of dimethylglycine in plasma, which show a positive correlation with the abundance of *Collinsella*, decreased in the diarrheal calves. This study suggests that a temporary change in the fecal microbiome during the milk transition may be associated with diarrhea in early neonatal calves.

Materials and methods

Animals and sample collection

A total of 10 female Holstein calves born from March to June 2019 were randomly enrolled in this study for fecal and plasma sampling. In addition, the calves' mothers (10 Holstein cows) were used for collecting corresponding milk samples. The newborn calves were moved to the calf hutch 1 h after birth. From each cow, colostrum was obtained within 1 h after birth (day 0), and whole milk was collected daily at 8:00 and 16:30 with a bucket milker from days 1 to 5 after parturition. The milk was warmed to approximately 38°C and artificially fed twice a day to the calves using a feeding bottle. The calves were fed the milk collected from their respective mothers. Milk replacer containing 28% crude protein (CP) and 4.23 Mcal/kg metabolizable energy (ME) (for composition see Supplementary Table S1) was fed to the calves at 9:30 and 16:30 from days 6 to 48 after birth. Calf starter, including 19% CP and 2.89 ME (for composition see Supplementary Table S1), and roughage (timothy hay) were fed *ad libitum* from day 6 after birth. A summary of the feeding procedure is shown in Supplementary Figure S1. Feces and blood samples were collected from calves at 9:00 on days 2, 4, 6, 8, 10, and 14 after birth and stored at –20°C until analysis. Fecal consistency was monitored, and feces showing a liquid appearance were recorded as diarrhea. All experiments were performed in accordance with the guidelines of the University Animal Care and Use Committee of the Tokyo University of Agriculture and Technology (Fuchu, Japan) (R03-176).

DNA extraction from fecal samples

Genomic DNA from the collected fecal samples was extracted using a QuickGene DNA tissue kit S (Kurabo Industries Ltd, Osaka, Japan) in accordance with the manufacturer's instructions. In brief, 40 mg of feces, 15 mg of 0.2-mm glass beads (No.02, Toshin Riko Co., Ltd, Tokyo, Japan),

and 200 µl of tissue lysis buffer were mixed and bead homogenized at 3,000 rpm for 120 s using a Micro Smash Cell Disrupter (MS-100, Tomy Seiko Co., Ltd, Tokyo, Japan). Proteinase K (25 µl) was added to the homogenized sample and the sample was incubated at 55°C for 1 h. The sample was then centrifuged for 10 min at 16,000 × g at 20°C, and the supernatant was transferred to another microtube containing 180 µl of lysis buffer and incubated at 70°C for 10 min. After incubation, 240 µl of > 99% ethanol was added to the microtube and vortexed at the maximum speed for 15 s. The whole lysate was transferred to a QuickGene Mini480 cartridge and pressurized. Wash buffer (750 µl) was applied three times to the cartridge. After the third wash, 200 µl of elution buffer was added and the mixture was incubated at 20°C. DNA was extracted after the third pressurization. The DNA concentration was adjusted to 20 ng/µl using elution buffer.

Library preparation and DNA sequencing

16S ribosomal RNA (rRNA) metagenomic analysis of fecal samples was performed. Briefly, a PCR targeting the variable regions 3 and 4 (V3–4) of the 16S rRNA gene was performed using the primers 341F (5′-CCTACGGGNGGCWGCAG-3′) and 805R (5′-GACTACHVGGGTATCTAATCC-3′), followed by a second PCR to attach dual indices. The amplicon of the second PCR was purified and the concentration was normalized with a SequalPrep Normalization Plate Kit (Life Technologies, Tokyo, Japan). The size and quantity of the library were assessed with a Bioanalyzer 2100 (Agilent Technologies Japan Ltd, Tokyo, Japan) and a Library Quantification Kit for Illumina (Kapa Biosystems, Inc., Wilmington, MA, USA), respectively. The library was mixed with phiX control and sequenced using a MiSeq v3 kit (Illumina Inc., San Diego, CA, USA) in accordance with the manufacturer's instructions. Data from the sequences were processed using QIIME 2™ (version 2021.11), and the imported reads were denoised using the DADA2 plugin to generate the amplicon sequence variant (ASV) feature table. Singleton and ASVs assigned to mitochondria and chloroplasts were excluded from further analysis. Taxonomy was assigned to filtered ASVs using a pretrained QIIME 2-compatible SILVA version 138 database (99% full-length sequences). We assayed for microbial variance using the MicrobiomeAnalyst software with default settings (URL: www.microbiomeanalyst.ca). All 16S rRNA sequencing data were deposited in September 2022 and are available under the accession number PRJNA835625.

Sample preparation for metabolomic analysis

The whole-milk samples collected from individual calves' mothers were centrifuged at 21,500 × g for 60 min at 4°C, and the middle layer was collected as skimmed milk. The milk replacers, prepared for each of the calves, were also centrifuged. Blood anticoagulated with ethylenediaminetetraacetic acid (EDTA) was centrifuged at 2,000 × g for 20 min at 4°C, and plasma samples were collected.

An untargeted metabolomics analysis was performed using GC-MS, as described previously, with some modifications (Usuda et al., 2018). For the pretreatment solution of the plasma, 50 µl of filtered plasma was mixed with 250 µl of methanol–chloroform–water (2.5 : 1 : 1) and 5 µl of 1 mg/ml 2-isopropylmalic acid as an internal standard. The samples were subsequently mixed in a shaker at 1200 rpm at 37°C for 30 min and centrifuged at 16,000 × g at 4°C for 5 min, and 225 µl of the supernatant was mixed with 200 µl of distilled water and vortexed. This was followed by centrifugation at 16,000 × g at 4°C for 5 min, and 250 µl of the supernatant was partially dried using a centrifugal evaporator CVE-2200 (Tokyo Rikakikai Co., Ltd, Tokyo, Japan) for 30 min and frozen at –80°C. The frozen samples were completely dried using vacuum freeze-drying equipment FDU-1200 (Tokyo Rikakikai Co., Ltd, Tokyo, Japan) for 16 h. The dried samples were dissolved in 40 µl of 20 mg/ml pyridine-containing methoxamine hydrochloride (Sigma-Aldrich Co. LLC, St. Louis, MO, USA) and incubated in a shaker at 1,200 rpm at 30°C for 90 min. To this, 20 µl of *N*-methyl-*N*-trimethylsilyl-trifluoroacetamide (MSTFA, Thermo Fisher Scientific, Waltham, MA, USA) was added and the samples further incubated in a shaker at 1,200 rpm at 37°C for 45 min.

For pretreatment of the skimmed milk, 50 µl of filtered skimmed milk was mixed with 50 µl of water, 800 µl of acetonitrile, and 5 µl of 1 mg/ml 2-isopropylmalic acid. The samples were subsequently mixed in a shaker at 1200 rpm at 37°C for 30 min and centrifuged at 16,000 × g at 4°C for 5 min. After centrifugation, the derivatization of skimmed milk samples was performed using a solid-phase derivatization kit for metabolome analysis (AiSTI SCIENCE Co., Ltd, Wakayama, Japan).

Metabolomic analysis using gas chromatography–mass spectrometry

One microliter (plasma) or 2 µl (milk) of the derivatized sample was injected splitless into a GC-MS QP2020 NX (Shimadzu Corporation, Kyoto, Japan). The capillary column was a 1.00-µm DB5 column (30 m × 0.25 mm i.d.; Agilent Technologies, Inc., Santa Clara, CA, USA). The temperature of the vaporizing chamber was 280°C, and the gas flow rate through the column was maintained at 5 ml/min. The temperature program was as follows: 4 min of isothermal heating at 100°C, which was then increased to 320°C at 10°C/min and held at 320°C for 11 min. Ions were generated at 70 eV using electron ionization and recorded at intervals of 0.2 s over the mass range of 45–600 m/z. The metabolites were identified using the standard Smart

Metabolites Database (Shimadzu Corporation, Kyoto, Japan), with each peak being identified manually using LabSolution (Shimadzu Corporation, Kyoto, Japan), and data analysis conducted using MetaboAnalyst (URL: www.metaboanalyst.ca/) (Chong et al., 2019).

Statistical analysis

The data presented were analyzed and visualized using MicrobiomeAnalyst, MetaboAnalyst, and GraphPad Prism 9 (GraphPad Software Inc., San Diego, CA, USA). In microbiome analysis, the beta diversity of the fecal microbiome was plotted by principal coordinate analysis (PCoA) on unweighted unique fraction metric (UniFrac) distance and permutational multivariate analysis of variance. A linear discriminant analysis effect size (LEfSe) analysis was performed to discriminate microbial features among groups. In metabolomics analysis, partial least-squares discriminant analysis (PLS-DA) was used to visualize the separation among the groups [i.e., colostrum (day 0), whole milk (days 1, 2, 3, 4, and 5 after parturition), and milk replacer], and to identify important metabolites responsible for the separation. To further analyze the differences between the whole milk and milk replacer, a volcano plot selected significant metabolites with a fold change threshold of 10 and a *t*-test threshold of $p < 0.05$. Correlations between the selected microbial and serum metabolites were analyzed by Pearson's correlation test. The identified bacteria and metabolites were statistically compared between healthy and diarrheal calves using Bonferroni correction with Dunn's test. Differences were considered statistically significant at a p-value < 0.05.

Results

Changes in fecal microbiome composition during milk transition

To investigate the compositional changes in the fecal microbiome during the milk transition, 16S rRNA gene sequencing was conducted using fecal samples from day 2 to 14 after birth. In total, 1,376,154 (mean ± SD: 22,936 ± 5,020 reads/sample) sequence reads were obtained from 60 samples. As shown in Figure 1A, the alpha diversity index represents the dynamics of the microbiome composition. Chao1, which is defined as "richness," and Shannon, which is defined as "evenness," increased from day 2 to 14 after birth. Similarly, in the PCoA plot based on the unweighted UniFrac distance, beta diversity gradually changed from day 2 to 14 (Figure 1B). In this study, all calves were fed whole milk from their mothers until day 5 after birth, but were switched to a milk replacer on day 6 (Supplementary Figure S1 and Figure 2A). To detect the specific bacteria associated with the milk transition, we conducted the LEfSe using samples from days 4, 6, 8, and 10, and identified four bacterial genera, namely *Clostridium sensu stricto 2*, *Lactobacillus*, *Collinsella*, and *Phascolarctobacterium*, showing high logarithmic linear discriminant analysis scores (Figures 2B, C).

Differences in metabolic components between whole milk and milk replacer

Untargeted metabolomic analysis of the milk samples detected 113 metabolites, and PLS-DA showed that colostrum on day 0 had a high variability among the mother cows, but the variation decreased each day and the metabolite composition in whole milk was stable on day 4 and day 5 after parturition. Milk replacer formed a separate cluster from the whole-milk sample (Figure 3A). The patterns in the abundance of several metabolites were identified by PLS-DA. For example, fructose 6-phosphate, mannose 6-phosphate, and glucose 6-phosphate decreased, whereas orotic acid and ureidosuccinic acid increased, from day 0 (in colostrum) to 5 (in whole milk and the milk replacer) (Figure 3B). To identify further differences in metabolites between the whole milk (days 4 and 5) and the milk replacer, we constructed a volcano plot, which identified seven metabolites, as shown in Figure 3C ($p < 0.05$, fold change threshold 10). Histograms denoting the relative abundance of the metabolites hypotaurine, D-xylose, and ureidosuccinic acid in the milk replacer and whole milk (days 4 and 5) are shown in Figure 3C (right).

Differences in the fecal microbiome between healthy and diarrheal calves

One calf in the first week after birth and six calves in the second week after birth showed mild diarrhea (Figure 4A and Supplementary Table S2). Diarrhea observed during this period was temporary and all animals recovered the next day, and body weight gain was normal for all calves (Supplementary Figure S2). Calves were divided into two groups (i.e., four healthy calves and six diarrheal calves) based on the observation of diarrhea in the second week after birth. There was no difference in the Chao1 index between healthy and diarrheal calves (Figure 4B). Of the four bacteria that change their abundance during the milk transition, *Collinsella* revealed a different trend in comparing healthy and diarrheal calves. As shown in Figure 4C, *Collinsella* on day 10, after milk transition, was lower in diarrheal calves than in healthy calves.

Differences in plasma metabolites between healthy and diarrheal calves

We hypothesized that *Collinsella* is an important bacterium in the early development of calves; therefore, we explored plasma

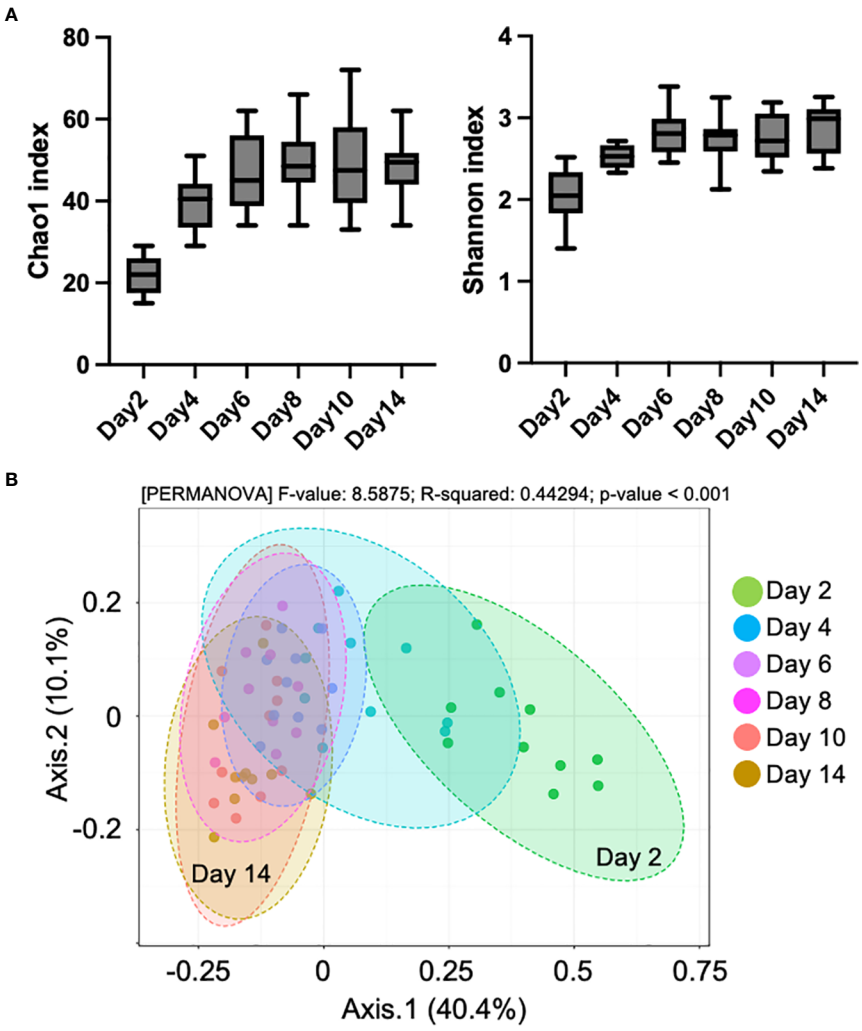

FIGURE 1
Changes in fecal microbiome composition in pre-weaned calves. **(A)** Chao1 and Shannon index of alpha diversity in fecal samples from day 2 to 14 after birth (n = 10). **(B)** Plots of principle coordinate analysis based on the unweighted unique fraction metric (UniFrac) distance of microbial communities.

metabolites that correlate with the abundance of *Collinsella* in calf feces. Pearson's correlation analysis revealed that dimethylglycine, beta-alanine, and glyoxylic acid were positively correlated with the abundance of *Collinsella* (Figure 5A). As shown in Figure 5B, plasma dimethylglycine showed a different trend when comparing healthy and diarrheal calves.

Discussion

The gut microbiome encompasses the bacteria inhabiting the gastrointestinal tract. The gut microbiome plays a critical role in the development and functioning of the gastrointestinal tract and overall gut health across animal species. The disruption of this optimal bacterial community (i.e., dysbiosis) can contribute to gastrointestinal disorders. Neonatal diarrhea is often observed in calves with an immature rumen and has been associated with intestinal microbiome colonization and development during the pre-weaning period. In this study, we focused in particular on the first 2 weeks after birth, when the milk transition, from whole milk to milk replacer, took place, and found that the levels of several fecal bacteria, such as *Lactobacillus* and *Collinsella*, changed significantly during the milk transition. A comparison of healthy and diarrheal calves indicated that *Collinsella* decreased after the milk transition in diarrheal calves. Furthermore, we found that plasma dimethylglycine, which shows a positive correlation with *Collinsella*, also decreased in the diarrheal calves. This study suggests a link between temporary changes in the fecal

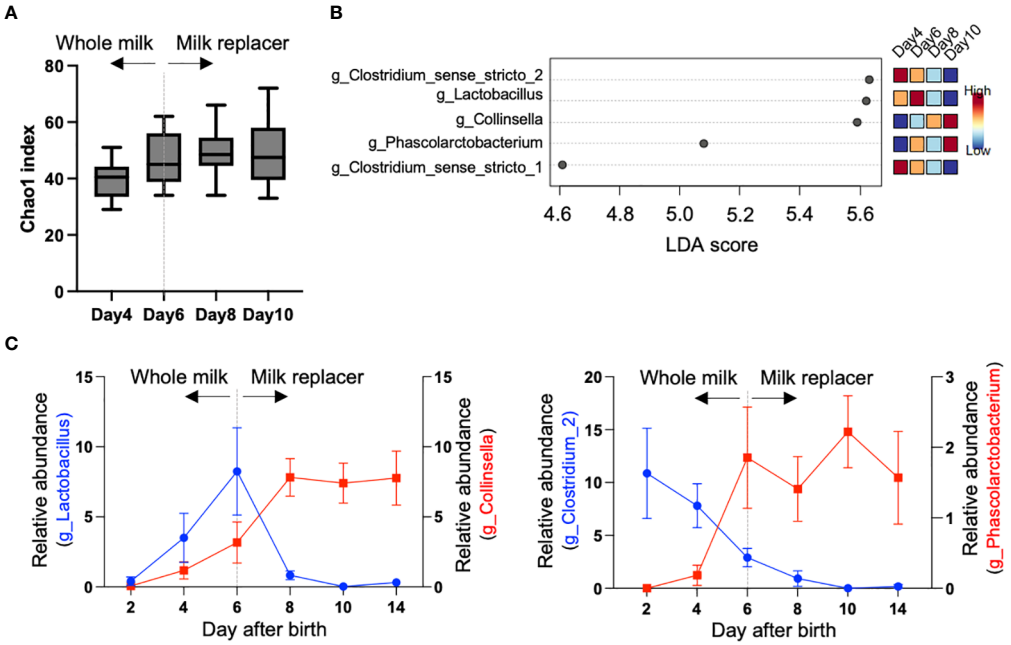

FIGURE 2
Changes of specific bacteria during milk transition. **(A)** Chao1 index of alpha diversity during milk transition (n = 10). All calves were switched from whole milk from their mother to a milk replacer on day 6. **(B)** Specific genera identified by linear discriminant analysis effect size (LEfSe). The colored boxes on the right indicate the relative abundance of the corresponding genera each day. **(C)** Changes of *Clostridium_sense_stricto_2*, *Lactobacillus*, *Collinsella*, and *Phascolarctobacterium* during milk transition.

microbiome and neonatal diarrhea during the milk transition in calves.

A calf's intestinal microbiome has a simple and less diverse bacterial community at birth and it increases in complexity and diversity with growth (Mayer et al., 2012; Oikonomou et al., 2013; Dill-McFarland et al., 2017). We observed dramatic development of the fecal microbiome, with an increase in the alpha diversity (Chao1 and Shannon), from day 2 to 14 after birth. Analysis of the beta diversity also showed that the composition gradually changed as the calves grew. LEfSe identified four bacterial genera that showed significant changes during the milk transition, with a linear discriminant analysis score >5.0. It was reported that the postnatal intestinal microbiome is profoundly influenced by the type of milk (Deng et al., 2017; Badman et al., 2019) and, therefore, we also investigated the compositional differences between whole milk (from days 4 and 5 after birth) and milk replacer. Untargeted metabolomic analysis found that the milk replacer was deficient in hypotaurine and D-xylose compared with whole milk. Hypotaurine, a precursor of taurine, is known as an antioxidant and is involved in a variety of crucial biological functions, including cell proliferation, immunomodulation, and oxidative stress inhibition (Green et al., 1991; Bouckenooghe et al., 2006; Sakuragawa et al., 2010). A recent report indicated that dietary polyphenols, a major group of antioxidants, are relevant in the modulation of the human gut microbiome and that gut bacteria convert polyphenols into active and bioavailable metabolites for host health (Tomás-Barberán et al., 2016). In addition, hypotaurine and D-xylose can be utilized by bacteria as a source of carbon, nitrogen, and energy for growth; therefore, a milk replacer deficient in hypotaurine and D-xylose might alter development of the intestinal microbiome. These findings suggest that these metabolites could be used to supplement milk replacers as a means of promoting a beneficial microbiome in the early development of calves.

In this study, one calf in the first week after birth and six calves in the second week after birth showed mild diarrhea. Ma et al. (2020) reported that most of the diarrhea incidence in veal calves occurred between 7 and 21 days of age and speculated that this might be associated with the lower relative abundance of *Blautia* and higher relative abundance of *Escherichia-Shigella* at 14 days of age. Although we could not detect those two bacterial changes by LEfSe, we found that the abundance of *Collinsella* was significantly higher in healthy calves than in diarrheal calves on day 10. In humans, *Collinsella* and *Bifidobacterium* are

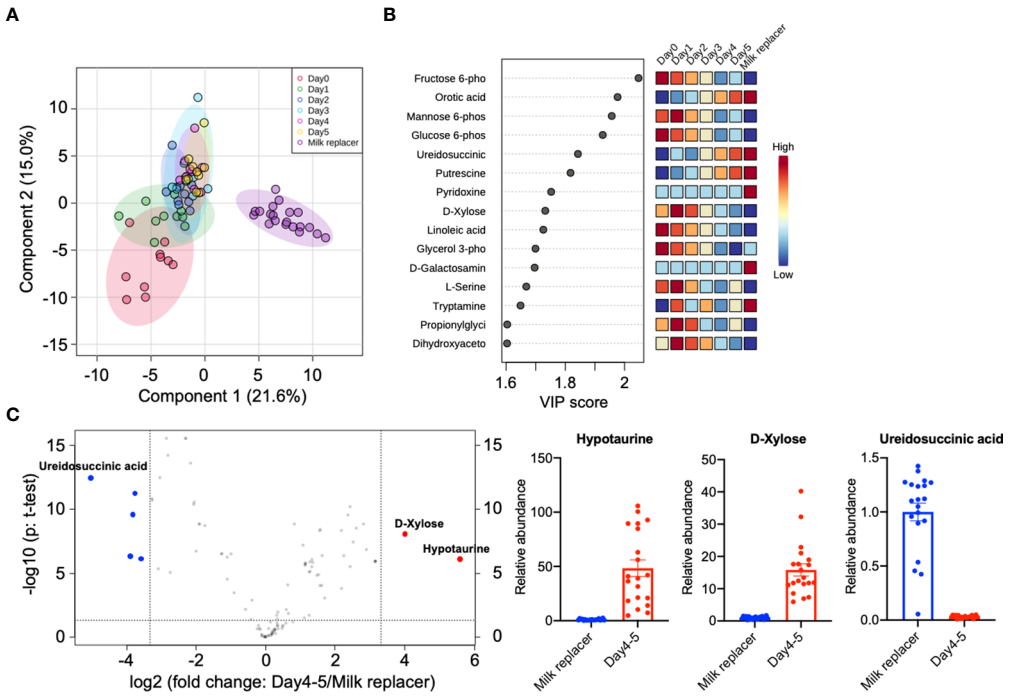

FIGURE 3
Differences in metabolic components between whole milk and milk replacer. **(A)** 2D principal component analysis score plot of colostrum (day 0, *n* = 10), whole milk (days 1, 2, 3, 4, and 5 after parturition, *n* = 10 each), and milk replacer (*n* = 20). **(B)** Important features identified by partial least-squares discriminant analysis (PLS-DA). The colored boxes on the right indicate the relative concentrations of the corresponding metabolites in each group. **(C)** Statistically significant features with a fold change threshold of 10 (*x*-axis) and a *t*-test threshold of $p < 0.05$ (*y*-axis) selected by a volcano plot. The red circles represent higher metabolites in whole milk on days 4 and 5 and the blue circles represent higher metabolites in milk replacer. On the right, histograms show the relative abundance of hypotaurine, D-xylose, and ureidosuccinic acid in milk replacer and whole milk on days 4 and 5.

known as the major lactose utilizers. *Collinsella* and *Bifidobacterium* act to modify the bile acids of the host and modulate the virulence and pathogenicity of enteric pathogens (Rajilić-Stojanović & De Vos, 2014). It was also reported that zinc supplementation to newborn calves for 14 days reduced the incidence of diarrhea, and the relative abundance of *Collinsella* was higher in those calves (Chang et al., 2020). Taken together, this study further suggests that low levels of *Collinsella* abundance during the milk transition may be associated with an increased incidence of diarrhea.

Further investigation revealed that plasma metabolites, such as dimethylglycine, beta-alanine, and glyoxylic acid, were positively correlated with the abundance of fecal *Collinsella*. Further experiments are required to determine the detailed relationship between these metabolites in plasma and *Collinsella* in the fecal microbiota; however, dimethylglycine is known as an anti-stress nutrient with antioxidant properties, and it has been reported to improve offspring growth performance in piglets (Bai et al., 2022). It is also known that dimethylglycine can be derived from gut microbiota, and microbiome- and smoking cessation-induced weight gain involves a concerted host and microbiome shunting of dietary choline to dimethylglycine, which drives an increased gut energy harvest (Fluhr et al., 2021). These observations suggest that dimethylglycine may be an essential nutrient for the early development of calves and healthy growth.

In conclusion, we investigated the temporal changes in the fecal microbiome and plasma metabolites during the milk transition in early neonatal calves. We found that the bacterium *Collinsella* and the metabolite dimethylglycine were key factors associated with the milk transition and/or diarrhea. However, the number of animals used in this study was small, and, because it was primarily an observational study using next-generation sequencing, further research is warranted to verify the validity of the suggested links between the bacteria, the metabolite, and diarrheal incidence in the early lives of calves.

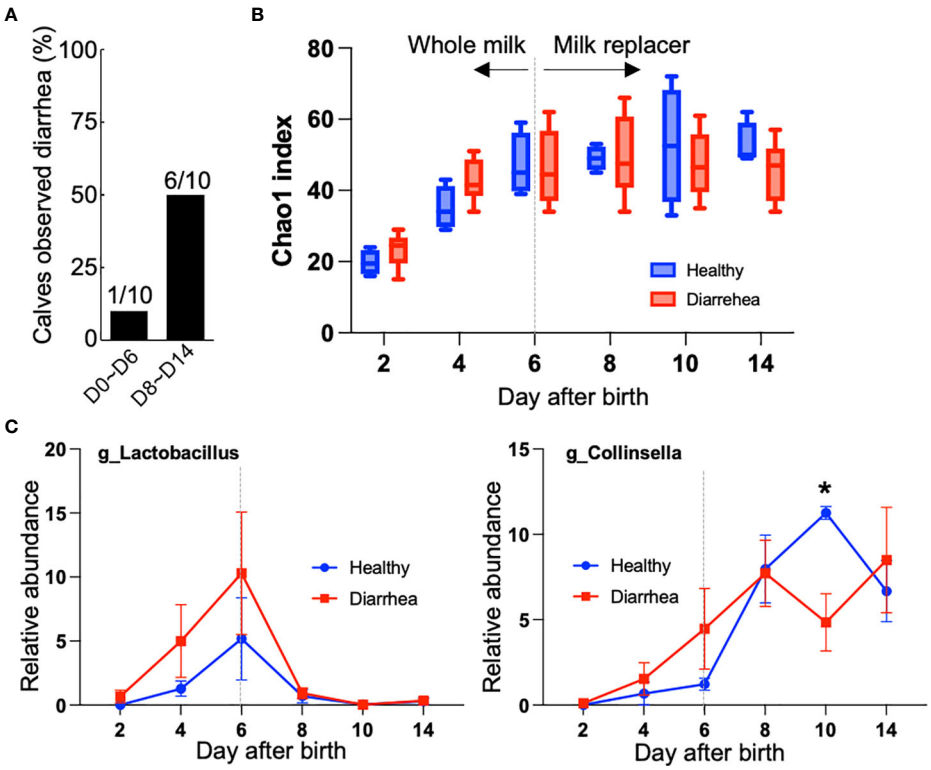

FIGURE 4
Differences in fecal microbiome between healthy calves and diarrheal calves. **(A)** Number of calves with diarrhea in the first or second week after birth. **(B)** Chao1 index of alpha diversity during milk transition. Calves were divided into two groups (i.e., four healthy calves and six diarrheal calves) based on the observation of diarrhea in the second week after birth. **(C)** Changes of *Lactobacillus* and *Collinsella* in feces from healthy and diarrheal calves during milk transition. Asterisk indicates significant difference between healthy calves and diarrheal calves using the Bonferroni Correction with Dunn Test method ($p < 0.05$).

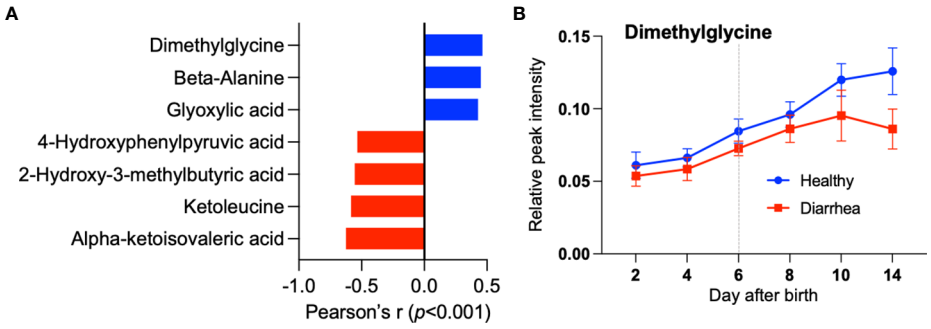

FIGURE 5
Differences in plasma metabolites between healthy and diarrheal calves. **(A)** Identified serum metabolites correlated with the abundance of *Collinsella* by Pearson's correlation analysis. **(B)** Change of dimethylglycine in serum from healthy and diarrheal calves during milk transition.

Data availability statement

The datasets presented in this study can be found in online repositories. The names of the repository/repositories and accession number(s) can be found below: https://www.ncbi.nlm.nih.gov/genbank/, PRJNA835625.

Ethics statement

The animal study was reviewed and approved by Animal Care and Use Committee of the Tokyo University of Agriculture and Technology (R03-176).

Author contributions

MK, ST, and KN contributed to the conception and design of the study. HL and RI conducted next-generation sequencing analyses. YS performed the statistical analysis. MK wrote the first draft of the manuscript. GW and WJ wrote sections of the manuscript. All authors contributed to manuscript revision, read, and approved the submitted version.

Acknowledgments

We would like to thank Editage (Karnataka, India; URL: www.editage.com) for English language editing.

Conflict of interest

The authors declare that the research was conducted in the absence of any commercial or financial relationships that could be construed as a potential conflict of interest.

Publisher's note

Supplementary material

The Supplementary Material for this article can be found online at: https://www.frontiersin.org/articles/10.3389/fanim.2022.934204/full#supplementary-material

SUPPLEMENTARY FIGURE 1
Diet of calves (n = 10) until day 56. Bar graph: Intake of milk feed per day (colostrum, whole milk, and milk replacer). Line graph: Intake of solid diet per day (calf starter pellet and roughage).

SUPPLEMENTARY FIGURE 2
Weight of individual calf until day 56. The average weight gain rate showed no significant difference.

SUPPLEMENTARY TABLE 1
Composition of milk replacer and calf starter.

SUPPLEMENTARY TABLE 2
Diarrhea incidence and antibiotic treatment during the 2 weeks after birth.

SUPPLEMENTARY TABLE 3
Comparison of feed intake of healthy and diarrheal calves.

References

Adaska, J. M., Moeller, R. B., Blanchard, P. C., and Aly, S. S. (2017). Cecal infarction in neonatal calves. *J. Veterinary Diagn. Invest.* 29, 242–244. doi: 10.1177/1040638716688046

Badman, J., Daly, K., Kelly, J., Moran, A. W., Cameron, J., Watson, I., et al. (2019). The effect of milk replacer composition on the intestinal microbiome of pre-ruminant dairy calves. *Front. Veterinary Sci.* 6. doi: 10.3389/fvets.2019.00371

Bai, K., Jiang, L., and Wang, T. (2022). Dimethylglycine sodium salt alleviates intrauterine growth restriction-induced low growth performance, redox status imbalance, and hepatic mitochondrial dysfunction in suckling piglets. *Front. Veterinary Sci.* 9. doi: 10.3389/fvets.2022.905488

Baldwin, V. I. R. L., McLeod, K. R., Klotz, J. L., and Heitmann, R. N. (2004). Rumen development, intestinal growth and hepatic metabolism in the pre- and postweaning ruminant. *J. Dairy Sci.* 87, E55–E65. doi: 10.3168/jds.S0022-0302(04)70061-2

Bauer, E., Williams, B. A., Smidt, H., Verstegen, M. W., and Mosenthin, R. (2006). Influence of the gastrointestinal microbiota on development of the immune system in young animals. *Curr. Issues Intestinal Microbiol.* 7, 35–51.

Bouckenooghe, T., Remacle, C., and Reusens, B. (2006). Is taurine a functional nutrient? *Curr. Opin. Clin. Nutr. Metab. Care* 9, 728–733. doi: 10.1097/01.mco.0000247469.26414.55

Chang, M. N., Wei, J. Y., Hao, L. Y., Ma, F. T., Li, H. Y., Zhao, S. G., et al. (2020). Effects of different types of zinc supplement on the growth, incidence of diarrhea, immune function, and rectal microbiota of newborn dairy calves. *J. Dairy Sci.* 103, 6100–6113. doi: 10.3168/jds.2019-17610

Cho, Y. I., Han, J. I., Wang, C., Cooper, V., Schwartz, K., Engelken, T., et al. (2013). Case-control study of microbiological etiology associated with calf diarrhea. *Veterinary Microbiol.* 166, 375–385. doi: 10.1016/j.vetmic.2013.07.001

Chong, J., Wishart, D. S., and Xia, J. (2019). Using MetaboAnalyst 4.0 for comprehensive and integrative metabolomics data analysis. *Curr. Protoc. Bioinf.* 68, e86. doi: 10.1002/cpbi.86

Deng, Y. F., Wang, Y. J., Zou, Y., Azarfar, A., Wei, X. L., Ji, S. K., et al. (2017). Influence of dairy by-product waste milk on the microbiomes of different gastrointestinal tract components in pre-weaned dairy calves. *Sci. Rep.* 7, 42689. doi: 10.1038/srep42689

Dill-McFarland, K. A., Breaker, J. D., and Suen, G. (2017). Microbial succession in the gastrointestinal tract of dairy cows from 2 weeks to first lactation. *Sci. Rep.* 7, 40864. doi: 10.1038/srep40864

Fluhr, L., Mor, U., Kolodziejczyk, A. A., Dori-Bachash, M., Leshem, A., Itav, S., et al. (2021). Gut microbiota modulates weight gain in mice after discontinued smoke exposure. *Nature* 600, 713–719. doi: 10.1038/s41586-021-04194-8

Gomez, D. E., Arroyo, L. G., Costa, M. C., Viel, L., and Weese, J. S. (2017). Characterization of the fecal bacterial microbiome of healthy and diarrheic dairy calves. *J. Veterinary Internal Med.* 31, 928–939. doi: 10.1111/jvim.14695

Green, T. R., Fellman, J. H., Eicher, A. L., and Pratt, K. L. (1991). Antioxidant role and subcellular location of hypotaurine and taurine in human neutrophils. *Biochim. Biophys. Acta* 1073, 91–97. doi: 10.1016/0304-4165(91)90187-l

Khan, M. A., Weary, D. M., and von Keyserlingk, M. A. (2011). Invited review: Effects of milk ration on solid feed intake, weaning, and performance in dairy heifers. *J. Dairy Sci.* 94, 1071–1081. doi: 10.3168/jds.2010-3733

Malmuthuge, N., and Guan, L. L. (2017). Understanding the gut microbiome of dairy calves: Opportunities to improve early-life gut health. *J. Dairy Sci.* 100, 5996–6005. doi: 10.3168/jds.2016-12239

Malmuthuge, N., Liang, G., Griebel, P. J., and Guan, L. L. (2019). Taxonomic and functional compositions of the small intestinal microbiome in neonatal calves provide a framework for understanding early life gut health. *Appl. Environ. Microbiol.* 85, e02534-18. doi: 10.1128/AEM.02534-18

Ma, T., Villot, C., Renaud, D., Skidmore, A., Chevaux, E., Steele, M., et al. (2020). Linking perturbations to temporal changes in diversity, stability, and compositions of neonatal calf gut microbiota: Prediction of diarrhea. *ISME J.* 14, 2223–2235. doi: 10.1038/s41396-020-0678-3

Mayer, M., Abenthum, A., Matthes, J. M., Kleeberger, D., Ege, M. J., Hölzel, C., et al. (2012). Development and genetic influence of the rectal bacterial flora of newborn calves. *Veterinary Microbiol.* 161, 179–185. doi: 10.1016/j.vetmic.2012.07.023

O'Hara, A. M., and Shanahan, F. (2006). The gut flora as a forgotten organ. *EMBO Rep.* 7, 688–693. doi: 10.1038/sj.embor.7400731

Oikonomou, G., Teixeira, A., Foditsch, C., Bicalho, M. L., Machado, V. S., and Bicalho, R. C. (2013). Fecal microbial diversity in pre-weaned dairy calves as described by pyrosequencing of metagenomic 16S rDNA. associations of faecalibacterium species with health and growth. *PloS One* 8, e63157. doi: 10.1371/journal.pone.0063157

Rajilić-Stojanović, M., and De Vos, W. M. (2014). The first 1000 cultured species of the human gastrointestinal microbiome. *FEMS Microbiol. Rev.* 38, 996–1047. doi: 10.1111/1574-6976.12075

Sakuragawa, T., Hishiki, T., Ueno, Y., Ikeda, S., Soga, T., Yachie-Kinoshita, A., et al. (2010). Hypotaurine is an energy-saving hepatoprotective compound against ischemia-reperfusion injury of the rat liver. *J. Clin. Biochem. Nutr.* 46, 126–134. doi: 10.3164/jcbn.09-91

Sommer, F., Anderson, J. M., Bharti, R., Raes, J., and Rosenstiel, P. (2017). The resilience of the intestinal microbiome influences health and disease. *Nat. Rev. Microbiol.* 15, 630–638. doi: 10.1038/nrmicro.2017.58

Tomás-Barberán, F. A., Selma, M. V., and Espín, J. C. (2016). Interactions of gut microbiome with dietary polyphenols and consequences to human health. *Curr. Opin. Clin. Nutr. Metab. Care* 19, 471–476. doi: 10.1097/MCO.0000000000000314

Uetake, K. (2013). Newborn calf welfare: A review focusing on mortality rates. *Anim. Sci. J.* 84, 101–105. doi: 10.1111/asj.12019

USDA (2018). *dairy 2014: Health and management proctices on U.S. dairy operation* (Fort Collins, CO: USDA–APHIS–VS–CEAH–NAHMS).

Usuda, K., Kawase, T., Shigeno, Y., Fukuzawa, S., Fujii, K., Zhang, H., et al. (2018). Hippocampal metabolism of amino acids by l-amino acid oxidase is involved in fear learning and memory. *Sci. Rep.* 8, 11073. doi: 10.1038/s41598-018-28885-x

Yeoman, C. J., and White, B. A. (2014). Gastrointestinal tract microbiome and probiotics in production animals. *Annu. Rev. Anim. Biosci.* 2, 469–486. doi: 10.1146/annurev-animal-022513-114149

Zeineldin, M., Aldridge, B., and Lowe, J. (2018). Dysbiosis of the fecal microbiota in feedlot cattle with hemorrhagic diarrhea. *Microbial Pathogenesis* 115, 123–130. doi: 10.1016/j.micpath.2017.12.059

frontiers | Frontiers in Molecular Biosciences

TYPE Original Research
PUBLISHED 17 November 2022
DOI 10.3389/fmolb.2022.1027069

OPEN ACCESS

EDITED BY
Dagnachew Hailemariam,
University of Alberta, Canada

REVIEWED BY
Guanshi Zhang,
The University of Texas Health Science Center at San Antonio, United States
Tiago S. Valente,
University of Alberta, Canada

*CORRESPONDENCE
Govind Kannan,
govindak@fvsu.edu

SPECIALTY SECTION
This article was submitted to Metabolomics, a section of the journal Frontiers in Molecular Biosciences

RECEIVED 24 August 2022
ACCEPTED 01 November 2022
PUBLISHED 17 November 2022

CITATION
Batchu P, Naldurtiker A, Kouakou B, Terrill TH, McCommon GW and Kannan G (2022), Metabolomic exploration of the effects of habituation to livestock trailer and extended transportation in goats.
Front. Mol. Biosci. 9:1027069.
doi: 10.3389/fmolb.2022.1027069

Metabolomic exploration of the effects of habituation to livestock trailer and extended transportation in goats

Phaneendra Batchu, Aditya Naldurtiker, Brou Kouakou, Thomas H. Terrill, George W. McCommon and Govind Kannan*

Agricultural Research Station, Fort Valley State University, Fort Valley, GA, United States

Goats raised for meat production are often transported long distances. Twelve-month-old male Spanish goats were used to determine the effects of habituation to trailers on plasma metabolomic profiles when transported for extended periods. In a split-plot design, 168 goats were separated into two treatment (TRT; whole plot) groups and maintained on two different paddocks. Concentrate supplement was fed to one group inside two livestock trailers (habituated group, H), while the other group received the same quantity of concentrate, but not inside the trailers (non-habituated, NH). Goats were subjected to a 10-h transportation stress in 4 replicates (n = 21 goats/replicate/TRT) after 4 weeks of habituation period. Blood samples were collected prior to loading, 20 min after loading (0 h), and at 2, 4, 6, 8, and 10 h of transportation (Time; subplot). A targeted quantitative metabolomics approach was employed to analyze the samples. The data were analyzed using R software and MIXED procedures in SAS. Several amino acids (alanine, serine, glycine, histidine, glutamate, trans-hydroxyproline, asparagine, threonine, methylhistidine, ornithine, proline, leucine, tryptophan) were higher ($p < 0.05$) in the H group compared to the NH group. Six long-chain acylcarnitines were higher ($p < 0.05$), while free (C0) and short-chain (C3, C5) carnitines were lower ($p < 0.05$) in the NH goats compared to the H goats. In general, amino acid concentrations decreased and long-chain acylcarnitine (>C10) levels increased with transportation time ($p < 0.05$). Butyric acid, α-ketoglutaric acid, and α-aminoadipic acid concentrations were lower ($p < 0.05$) and β-hydroxybutyric acid concentrations were higher in the NH goats compared to the H goats. Plasma glucose, non-esterified fatty acid (NEFA) and urea nitrogen concentrations were significantly influenced by Time ($p < 0.01$). Plasma NEFA concentrations were significantly lower ($p < 0.01$) in the H group than the NH group. Habituation to trailers can be beneficial in enhancing stress coping abilities in goats due to higher concentrations of metabolites such as butyrate and certain amino acids that support antioxidant activities and immune function. Plasma long-chain acylcarnitines may be good indicators of stress during long-distance transportation in goats.

KEYWORDS

goats, habituation, plasma metabolomics, stress, transportation

Introduction

In the US, goats raised for meat production are often transported long distances under commercial situations. Long-distance transportation results in physiological changes in animals to maintain body homeostasis, and adverse effects of stress become evident when physiological mechanisms fail to counterbalance. Assuring the well-being of animals during transportation is becoming a growing societal concern since the negative effects of stress can be prolonged for days after transportation.

Food animals are exposed to various stress factors, such as handling, loading and unloading, novel environment, noise, motion, and vibration, disruption of social structure, food and water deprivation, and extreme temperature and humidity conditions (Kannan et al., 2000; Minka and Ayo, 2009). Severe preslaughter stress related to transportation has been reported as one of the major factors affecting meat quality in small ruminants (Kannan et al., 2003). Evidence from previous studies suggests that transportation stress elicits metabolic changes that impact adrenocortical activity, energy balance, immune response, and body weight in goats (Kannan et al., 2000).

To evaluate stress in food animals, researchers have used a wide range of physiological indicators, and studies have also focused on the validity of these animal welfare indices (Verbeke and Viaene, 2000). Increase in plasma non-esterified fatty acid (NEFA) concentrations have been observed in goats after feed deprivation and transportation (Kannan et al., 2002, 2003) and in sheep after 8 h of transportation (Zhong et al., 2011). Blood glucose and urea nitrogen (BUN) concentrations increase due to transportation in goats and remain elevated after transportation during the initial hours of holding (Kannan et al., 2000). Stress due to heat and transportation causes higher β-hydroxybutyrate concentrations in goats and other ruminants (Salama et al., 2014; Batchu et al., 2021).

The metabolome is a collection of small molecular mass components found in biological media, and metabolomic analysis involves large-scale detection and quantification of metabolites (Junot et al., 2014). Advanced analytical techniques and chemometrics are used to identify a vast number of metabolites in a sample, including amino acids, sugars, ketones, fatty acids, organic acids, and exogenous small molecules. Our previous study indicated that stress has a significant impact on the plasma metabolome in goats, with the amino acid levels decreasing and medium- and long-chain acylcarnitine concentrations increasing with increasing duration of stress (Batchu et al., 2021). Therefore, plasma acylcarnitine concentrations could reflect oxidation rate of fatty acids and amino acids in tissues, particularly in liver and muscle (Xu et al., 2011).

The behavioral and physiological responses of an animal can be negatively affected when exposed to a novel situation, and repeated exposure to the same stressor such as handling can attenuate these responses (Ujita et al., 2021). Habituating to transportation has been reported to significantly decrease the frequencies of behaviors indicative of stress as well as physiological stress responses in donkeys (Dai et al., 2020). These authors further observed that habituation to transportation reduced the time needed to load donkeys onto the vehicle. Weeks et al. (2012) also reported that regardless of the age of horses, habituation made the loading process considerably easier. Habituating animals to transportation may help animals cope with the detrimental effects of stress (Stockman et al., 2011); however, to what extent this can be applied in commercial conditions is questionable. We propose habituating goats to livestock trailers may be a more practicable method that could be easily adopted by goat producers worldwide, who invariably operate on smaller-scale and with limited resources.

There are no data available on the effects of conditioning goats to livestock trailers on stress responses during transportation. Recent studies conducted in other livestock species have confirmed the positive effects of habituation to handing and transportation in reducing stress-related physiological responses (Dai et al., 2020; Ujita et al., 2021). The objective of this study was to determine the effects of habituation to livestock trailers on plasma metabolomic profiles in goats.

Materials and methods

Animals

The protocol for this research was reviewed and approved by Fort Valley State University's Animal Care and Use Committee prior to beginning the experiment. Twelve-month-old male Spanish goats were used to determine the effects of habituation to trailers on plasma metabolomic profiles when transported for long periods. The goats were dewormed 3 weeks before the study. All animals were examined for general health status and were determined to be healthy prior to beginning of the experiment. In a split-plot design, 168 uncastrated male Spanish goats (12-month old; Average BW = 31.6 ± 0.34 kg) were separated into two treatment (TRT; whole plot) groups and maintained on two different grass paddocks (predominantly Bermudagrass, *Cyanodon dactylon*). Concentrate supplement (commercial goat pellet, 14% crude protein) was fed to one group inside two livestock trailers (5.3 × 2.3 m each; habituated group, H), while the other group received the same quantity of concentrate, but not inside the trailers (non-habituated, NH). Habituation to trailer was conducted during feeding time between 8:30 a.m. and 9:30 a.m. every day during the months of March-April. The average high/low temperatures in March were 21.1°C/7.2°C and in April were 25.0°C/10.6°C. Every day, the animals remained in the trailer for a 50 ± 10 min-period until all the concentrate feed was consumed. Goats were subjected to a 10-h transportation stress on 4 consecutive days (replicates; n = 21 goats/

replicate/TRT) after 4 weeks of habituation period. The livestock trailers used for habituation and transportation were identical in dimensions and positions of windows provided for ventilation. The average temperatures on the days 1, 2, 3, and 4 of transportation trials were 17.8, 21.7, 22.5, and 23.1°C, respectively. The average relative humidity percentages were 68.0, 73.5, 68.5, and 79.0, respectively, on days 1, 2, 3, and 4. Each trailer was partitioned into two compartments with H goats in one compartment and the NH goats in the other. The order of loading of goats onto the trailer was alternated on each day, such that H goats were in the front compartment on 1 day and they were in the rear compartment on the next day. The floor space allocated was 0.29 m^2/animal during transportation in all replicates that allowed adequate air circulation. The goats were transported approximately 550 km at an average speed of 61 km/h with a 10-min stop every 2 h for blood sampling. To be consistent and to minimize vehicular vibrations, the same route that comprised of paved roads was followed during transportation on all 4 days.

Blood sampling

Blood samples were collected prior to loading (Preload, PL), 20 min after loading (0 h), and at 2, 4, 6, 8, and 10 h of transportation (Time; subplot). For 2, 4, and 8 h sampling, the truck was stopped for 10 min at each time period and blood samples were collected inside the trailer to avoid repeated unloading and loading animals. Only two individuals had to enter the trailer, one animal handler and one blood sampler, for blood sampling. All efforts were made not to agitate the goats, including avoiding loud noise and rough handling. After blood sampling, each goat was marked on the horns with a colored marker to avoid being sampled again. Blood samples were collected by a trained individual by jugular venipuncture into K_2EDTA-coated vacutainer tubes and kept on ice until separation of plasma. Blood samples were collected without any time lapse after the goats were caught in order to avoid confounding of the effect of blood sampling. The individual who collected the blood samples at all time points was so proficient such that it took only a few seconds (<30 s) to draw a sample from each animal. The tubes were then centrifuged at 1,000 × g for 20 min for separation of plasma. Plasma samples were pipetted into screw-cap vials and stored at −80°C until analysis. For blood glucose, BUN, and creatine concentrations, samples were obtained separately in 3 ml vacutainer tubes coated with EDTA (K3) and kept on ice until analysis.

Plasma NEFA, BUN, creatine, and glucose concentrations

The NEFA-HR (2) Kit (Fujifilm, Mountain View, CA) was used to determine plasma NEFA concentrations. The colorimetric assay was conducted using 96-well micro-titer plates according to the instructions provided by the manufacturer. Briefly, plasma samples (5 µL) were placed in the wells, followed by 200 µL of color reagent A solution. The plates were then incubated for 5 min at 37°C before the first optical density measurement was made using a microplate reader at a wavelength of 550 nm (Synergy HTX Microplate Reader, Bio-Tek, Winooski, VT). Then, 100 µL of color reagent B solution was added to each well, and the optical density was measured again at 550 nm. By measuring against a standard curve generated using the manufacturer's instructions and following the manufacturer's directions, the difference between the optical density readings was used to estimate NEFA concentrations in each sample. The concentrations of glucose, BUN, and creatine were determined using the VETSCAN HM5 Hematology Analyzer (Abaxis, Union City, CA) according to the manufacturer's protocol.

Plasma metabolomics

All 168 plasma samples (n = 21 goats/replicate/TRT) were shipped on dry ice to The Metabolomics Innovation Center (TMIC) at the University of Alberta, Edmonton, Canada for metabolomics analysis. The samples were analyzed utilizing a targeted quantitative metabolomics technique that combined direct injection mass spectrometry with a reverse-phase LC–MS/MS custom assay. This custom assay, in combination with a mass spectrometer, was used to identify and quantify up to 150 different endogenous metabolites, such as amino acids, acylcarnitines, biogenic amines and derivatives, uremic toxins, glycerophospholipids, sphingolipids, and sugars. Derivatization and extraction of analytes were combined with selective mass-spectrometric detection using multiple reaction monitoring (MRM) pairs in this approach.

Samples were thawed on ice, vortexed and centrifuged at 13,000 × g for all metabolites except organic acids. The center of the filter on the upper 96-well plate was loaded with 10 µL of each sample, which was then dried in a nitrogen stream. Then, phenyl-isothiocyanate was added for derivatization. The filter spots were dried again with an evaporator after incubation. The metabolites were extracted using 300 µL of extraction solvent. Centrifugation into the lower 96-deep well plate yielded the extracts, which were then diluted with MS running solvent.

For organic acid analysis, 50 µL of sample was mixed with 150 µL of ice-cold methanol and 10 L isotope-labeled internal standard mixture for overnight protein precipitation. It was then centrifuged for 20 min at 13000 × g. A 96-deep well plate was loaded with 50 µL of supernatant, followed by the addition of 3-nitrophenylhydrazine (NPH) reagent. Before LC-MS injection, BHT stabilizer and water were added after a 2-h incubation.

An ABSciex 4000 Qtrap® tandem mass spectrometry instrument (Applied Biosystems/MDS Analytical

Technologies, Foster City, CA) with an Agilent 1260 series UHPLC system (Agilent Technologies, Palo Alto, CA) was used for mass spectrometric analysis. An LC approach was used to deliver the samples to the mass spectrometer, followed by a direct injection (DI) method. Analyst 1.6.2 was used to analyze the data.

Statistical analysis

Plasma glucose, NEFA, BUN, and creatine concentration data were analyzed using MIXED procedures in SAS. When significant by ANOVA, the means were separated using the pdiff procedure.

Data from all 168 samples were used for metabolomics analysis. The metabolites with identical concentrations for all samples (ex. 0 μM) and those with more than 20% of missing concentrations were removed from the datasets. For multivariate analysis, data were scaled by range scaling with Metaboanalyst R. Samples with missing time points were removed and the data were log-transformed for analysis of variance. For two-group comparisons, the data from different time points were combined and univariate T-test and effect size calculation were performed for each metabolite. Because different sets of animals were used at different time points, one-way ANOVA tests were performed for longitudinal analysis of time points, followed by post-hoc tests and effect size calculations. For comparison of TRT (H vs. NH) at different time points, two-way ANOVA was conducted. For all types of comparisons, PCA and PLS-DA tests were performed.

Since the data for all groups were not normally distributed, univariate analysis was conducted using a non-parametric version of statistical tests. Specifically, T test for two independent samples was conducted with Mann-Whitney U rank method. The effect size was calculated with the Cliff's Delta method. Fold change was determined by calculating the ratio between group medians. One-way ANOVA was performed using Kruskal–Wallis test. ANOVA post-hoc tests were conducted using the Dunn's test with Benjamini Hochberg False Discovery Rate correction for multiple comparisons. The effect size was calculated with the Cliff's Delta method (Vargha and Delaney, 2000; Macbeth et al., 2011). Fold change was determined by calculating the ratio between group medians. Two-way ANOVA and post-hoc tests were conducted on log-transformed data, using Benjamini Hochberg False Discovery Rate method to correct *p*-values for multiple comparisons. To balance the risk of Type 1 and Type 2 errors, thresholds of 0.05 for raw *p*-values and 0.1 for FDR values were used to identify statistically significant changes in metabolite concentrations from the T test.

Metaboanalyst R was used to perform principal component analysis (PCA) and partial least square discriminant analysis (PLS-DA). The PLS-DA, a multivariate supervised pattern recognition method, maximizes discriminating variation between classes. The models were tested for performance and the absence of overtraining with 10-fold cross-validation. The model accuracy was considered satisfactory when R2 and Q2 were above 0.66 and considered not over-trained when R2 and Q2 were comparable with each other (within 20%). A permutation test was conducted to assess statistical significance of PLS-DA model. A model was considered statistically significant if $p < 0.05$. The metabolites were then plotted according to their importance in separating the different treatment groups and transportation time groups based on the PLS-DA results using variable importance in projection (VIP) scores. A VIP score of >1.0 indicates that the metabolite is significantly involved in separation of the classes.

Day (replicate) effects were removed by the commonly used median batch effect correction (Rusilowicz et al., 2016). Median concentrations of metabolites were calculated and a batch with the largest median value was selected as the reference per metabolite. For the remaining batches, correction factors for

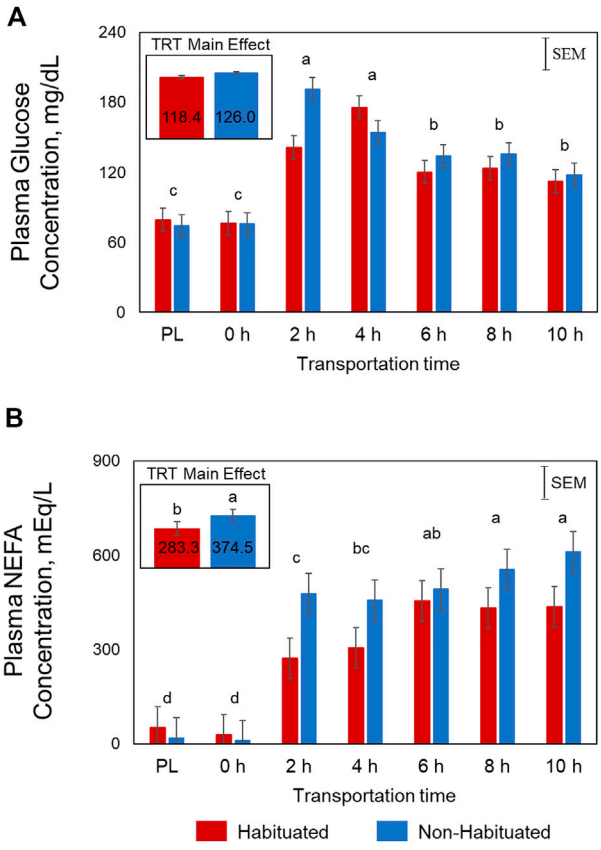

FIGURE 1
Effects of habituation treatment (TRT) and transportation time (Time; PL = Preload) on plasma **(A)** glucose (TRT, $p = 0.14$; Time, $p < 0.01$; TRT × Time, $p < 0.05$) and **(B)** non-esterified fatty acid (NEFA; TRT, $p < 0.05$; Time, $p < 0.05$) concentrations in goats.

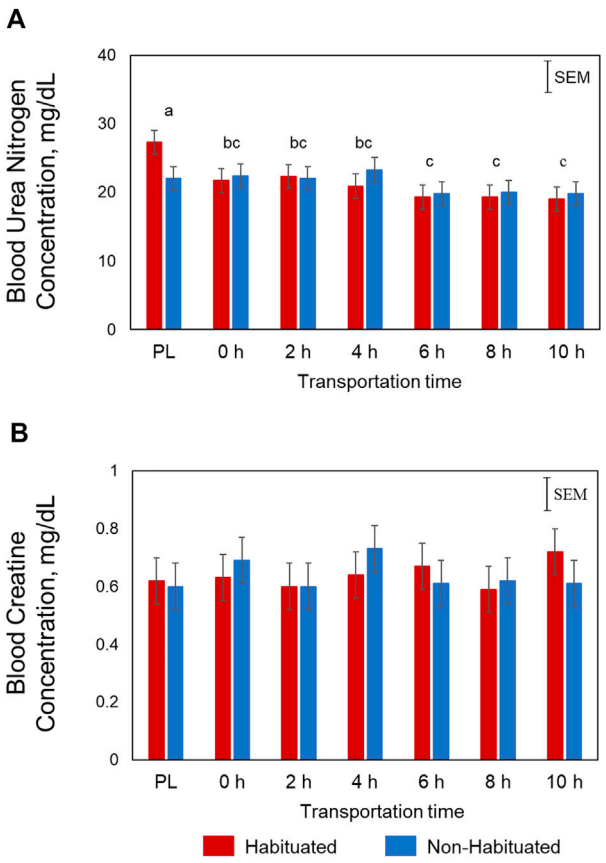

FIGURE 2
Effects of habituation treatment (TRT) and transportation time (Time; PL = Preload) on plasma **(A)** urea nitrogen (Time, $p < 0.05$), and **(B)** creatine concentrations in goats.

each metabolite were calculated by subtracting the batch median value from the reference median value. Finally, concentrations of each metabolite in the remaining batches were adjusted by adding the corresponding correction factors.

Results

Plasma glucose concentrations were significantly influenced by Time ($p < 0.01$) and TRT × Time ($p < 0.05$; Figure 1A). In the NH goats, glucose concentrations spiked at 2 h before gradually decreasing, yet remained higher than PL and 0 h levels. However, in the H group, the glucose concentrations increased gradually and peaked at 4 h. The Time main effects showed that the concentrations were highest at 2 and 4 h, lowest at PL and 0 h sampling, and intermediate at 6, 8, and 10 h for both groups. Plasma NEFA concentrations were significantly higher ($p < 0.05$; Figure 1B) in the NH group compared to the H group. Plasma NEFA concentrations were low at PL and 0 h sampling, significantly increased at 2 h, and further increased with increasing transportation time ($p < 0.05$) in both groups (Time main effect). The overall BUN concentrations were high at PL sampling, low at 6, 8, and 10 h, and intermediate at 0, 2, and 4 h ($p < 0.05$; Figure 2A). Plasma creatine concentrations were not affected by any of the factors (Figure 2B).

At the metabolome level, 13 amino acids, 12 acylcarnitines, 25 phosphatidylcholines, and sphingomyelins, and 13 other metabolites were significantly affected ($p < 0.05$) by TRT. Of the 13 amino acids, 12 (alanine, serine, glycine, tryptophan, histidine, glutamic acid, trans-hydroxyproline, asparagine, threonine, ornithine, proline, and leucine) were significantly lower in the NH group, while methylhistidine was higher in the NH group compared to the H group (Table 1). Eight of the acylcarnitines were higher in the NH group and 4 were lower in the NH group compared to the H group (Table 1). All 25 phosphatidylcholines and sphingomyelins that were significantly influenced by TRT were higher in the NH group compared to the H group (Table 2). In addition, HPHPA, β-hydroxybutyrate, creatinine, and acetyl-ornithine concentrations were higher in the NH groups, while methylmalonic acid, kynurenine, indole acetic acid, α-ketoglutaric acid, propionic acid, uric acid, putrescine, butyric acid, and α-aminoadipic acid were lower in the NH group compared to the H group (Table 3).

Visualization of metabolites clustered by means of a heatmap also revealed that the majority of the amino acids were higher in the H group, while most of the phoshatidylcholines and sphingomyelins and acylcarnitines were lower in the H group compared to the NH group, as evidenced by the intensity of red color (Supplementary Figure S1). When averaged across all time points, stearoylcarnitine, β-hydroxybutyric acid, alanine, lysophosphatidylcholine C18:0, hydroxysphingomyelin C22:1, diacylphasphotidylcholine C36:0, sphingomyelin C18:1, serine, methyl malonic acid, acetylcarnitine, kynurenine, sphingomyelin C18:0, lysophosphatidylcholine C18:2, and hexadecanoylcarnitine were the top 15 metabolites identified by PLS-DA multivariate model ($p < 0.05$) and VIP values with the highest influence (VIP scores >1.5) in separating the H and NH groups, as shown in Figure 3.

Time had a significant effect ($p < 0.05$) on 20 amino acids, with the concentrations decreasing with increasing transportation time as shown in the box plots (Supplementary Figure S2). Several long-chained acylcarnitine concentrations increased ($p < 0.05$; Supplementary Figure S3) with increasing transportation time, while this pattern was not apparent with short-chained acyl carnitines. In addition, carnosine, pyruvic acid, α-amino adipic acid, butyric acid, hippuric acid, lactic acid, kynurenine, indole acetic acid, spermine, citric acid, serotonin, and HPHPA were also significantly ($p < 0.05$) affected by Time (Supplementary Figure S4). The changes in concentrations of all metabolites that were significantly influenced by Time are shown

10.3389/fmolb.2022.1027069

TABLE 1 Amino acids and acylcarnitines significantly ($p < 0.05$) affected by treatment (H = Habituated; NH = Non-habituated) in goats.

Metabolite	*p*-value	FDR[a]	Fold change	Cliff's delta effect size	Cliff's delta effect level	Direction of change
Amino Acids						
Alanine	9.31e-05	2.04e-03	0.85	0.33	Medium	↓ in NH
Serine	1.12e-04	2.04e-03	0.81	0.33	Small	↓ in NH
Glycine	1.42e-04	2.04e-03	0.90	0.32	Small	↓ in NH
Tryptophan	4.90e-04	4.24e-03	0.86	0.29	Small	↓ in NH
Histidine	1.13e-03	8.11e-03	0.91	0.27	Small	↓ in NH
Glutamic acid	0.013	0.043	0.85	0.20	Small	↓ in NH
trans-Hydroxyproline	0.013	0.044	0.92	0.20	Small	↓ in NH
Asparagine	0.017	0.054	0.79	0.19	Small	↓ in NH
Threonine	0.021	0.062	0.85	0.18	Small	↓ in NH
Methylhistidine	0.027	0.075	1.04	−0.17	Small	↑ in NH
Ornithine	0.032	0.078	0.91	0.17	Small	↓ in NH
Proline	0.036	0.085	0.91	0.16	Small	↓ in NH
Leucine	0.039	0.086	0.93	0.16	Small	↓ in NH
Acylcarnitines						
Octadecanoylcarnitine (C18)	1.40e-05	5.80e-04	1.22	−0.37	Medium	↑ in NH
Propionylcarnitine (C3)	4.77e-04	4.24e-03	0.88	0.30	Small	↓ in NH
Dodecanedioylcarnitine (C12DC)	4.82e-04	4.24e-03	0.89	0.30	Small	↓ in NH
Acetylcarnitine (C2)	7.36e-04	5.58e-03	1.17	−0.28	Small	↑ in NH
Hexadecanoylcarnitine (C16)	1.71e-03	0.011	1.15	−0.26	Small	↑ in NH
Tetradecenoylcarnitine (C14:1)	1.79e-03	0.011	1.14	−0.26	Small	↑ in NH
Octadecenoylcarnitine (C18:1)	4.54e-03	0.020	1.14	−0.23	Small	↑ in NH
Isovalerylcarnitine (C5)	0.016	0.050	0.97	0.19	Small	↓ in NH
Hydroxyisovalerylcarnitine (C5OH)	0.024	0.067	0.96	0.18	Small	↓ in NH
Tetradecanoylcarnitine (C14)	0.038	0.086	1.07	−0.16	Small	↑ in NH
Decanoylcarnitine (C10)	0.043	0.093	1.07	−0.15	Small	↑ in NH
Carnitine (C0)	0.047	0.098	0.95	0.15	Small	↓ in NH

[a]False Discovery Rate.

using a heatmap (Supplementary Figure S5). The PCA plot created to visualize the separation of metabolites by Time in principal components 1 and 2 showed that the clusters corresponding to different time periods overlapped; however, the clusters representing PL and 0 h spaced slightly apart from clusters of other time periods (Figure 4). The top 15 metabolites identified by PLS-DA multivariate model ($p < 0.05$) and VIP values are shown in Figure 5. Aspartic acid, total dimethylarginine, lysine, carnitine, propionylcarnitine, glutamine, propenoylcarnitine, betaine, trans-hydroxyproline, tiglylcarnitine, asymmetric dimethylarginine, lysophosphatidylcholine C26:1, diacylphosphatidylcholine C40:6, spermine, and acyl alkylphosphatidylcholine C36:0 had the highest influence (VIP scores >1.5) in separating the different time periods.

Interaction effects (TRT × Time) were significant ($p < 0.05$; Figure 6) for α-ketoglutaric acid, kynurenine, 4 amino acids (alanine, trans-hydroxyproline, isoleucine, ornithine), and 3 acylcarnitines (hexadecanoylcarnitine, octadecenoylcarnitine, octadecanoylcarnitine). The increases in concentrations of the 3 acylcarnitines over transportation time was greater in the NH group compared to the H group. The concentrations of the

TABLE 2 Phosphatidylcholines and sphingomyelins significantly ($p < 0.05$) affected by treatment (H = Habituated; NH = Non-habituated) in goats.

Metabolite	*p*-value	FDR[a]	Fold change	Cliff's delta effect size	Cliff's delta effect level	Direction of change
Diacylphosphatidylcholine C36:0	1.40e-04	2.04e-03	1.17	−0.32	Small	↑ in NH
Hydroxysphingomyelin C22:1	2.61e-04	3.37e-03	1.16	−0.31	Small	↑ in NH
Sphingomyelin C18:0	4.71e-04	4.24e-03	1.12	−0.30	Small	↑ in NH
Sphingomyelin C18:1	4.93e-04	4.24e-03	1.19	−0.29	Small	↑ in NH
Lysophosphatidylcholine C18:0	5.36e-04	4.33e-03	1.12	−0.29	Small	↑ in NH
Lysophosphatidylcholine C28:1	1.68e-03	0.011	1.15	−0.26	Small	↑ in NH
Diacylphosphatidylcholine C36:6	1.90e-03	0.011	1.08	−0.26	Small	↑ in NH
Diacylphosphatidylcholine C40:1	1.98e-03	0.011	1.08	−0.26	Small	↑ in NH
Lysophosphatidylcholine C18:2	2.12e-03	0.011	1.18	−0.26	Small	↑ in NH
Diacylphosphatidylcholine C32:2	2.71e-03	0.014	1.09	−0.25	Small	↑ in NH
Lysophosphatidylcholine C26:1	2.77e-03	0.014	1.12	−0.25	Small	↑ in NH
Diacylphosphatidylcholine C38:0	3.11e-03	0.015	1.22	−0.24	Small	↑ in NH
Hydroxysphingomyelin C24:1	4.50e-03	0.020	1.06	−0.23	Small	↑ in NH
Lysophosphatidylcholine C26:0	7.32e-03	0.029	1.13	−0.22	Small	↑ in NH
Acyl alkylphosphatidylcholine C36:0	7.39e-03	0.029	1.12	−0.22	Small	↑ in NH
Sphingomyelin C16:0	8.64e-03	0.033	1.09	−0.21	Small	↑ in NH
Sphingomyelin C16:1	9.74e-03	0.036	1.10	−0.21	Small	↑ in NH
Lysophosphatidylcholine C24:0	0.011	0.039	1.08	−0.20	Small	↑ in NH
Hydroxysphingomyelin C16:1	0.021	0.062	1.09	−0.18	Small	↑ in NH
Lysophosphatidylcholine C20:4	0.023	0.067	1.08	−0.18	Small	↑ in NH
Lysophosphatidylcholine C18:1	0.028	0.075	1.07	−0.17	Small	↑ in NH
Hydroxysphingomyelin C14:1	0.030	0.077	1.06	−0.17	Small	↑ in NH
Sphingomyelin C20:2	0.031	0.078	1.07	−0.17	Small	↑ in NH
Lysophosphatidylcholine C16:0	0.044	0.094	1.03	−0.15	Small	↑ in NH
Lysophosphatidylcholine C28:0	0.047	0.098	1.07	−0.15	Small	↑ in NH

[a]False Discovery Rate.

3 amino acids decreased to a greater extent after 10 h in the NH group compared to the H group. The α-ketoglutaric acid concentration at PL sampling was significantly higher ($p < 0.05$) in the H group compared to the NH group but decreased rapidly at 0 h and remained at that level throughout the transport duration. However, α-ketoglutaric acid concentrations remained low at all sampling periods.

Discussion

Stress indicators

When an animal is exposed to a stressor, catecholamine release from adrenal medulla causes glycogenolysis in the liver and lipolysis of adipose tissue that lead to increase in both blood glucose and NEFA concentrations (Kannan et a., 2000; 2002; Saeb et al., 2010). Adipocytes are lipase sensitive during stress, and the stored triacylglycerol is split into glycerol and NEFA. Changes in blood glucose concentrations result in glucocorticoid release that stimulates liver to convert fat and protein to intermediary metabolites that are used for energy production (Saeb et al., 2010). Gluconeogenic substrates, such as amino acids and short-chain fatty acids, also decrease during prolonged energy demand and deficit. As a result, fatty acids may be the main source of energy during these situations, and the primary fatty acid metabolic organ is the liver.

Plasma NEFA concentrations were significantly lower in the H group compared to NH group as shown in Figure 1. These effects suggest that habituation to livestock trailer was efficient in reducing stress responses in goats during long-distance transportation. Mobilization of fatty acids from adipose tissue

TABLE 3 Metabolites significantly ($p < 0.05$) affected by treatment (H = Habituated; NH = Non-habituated) in goats.

Metabolite	*p*-value	FDR[a]	Fold change	Cliff's delta effect size	Cliff's delta effect level	Direction of change
HPHPA	7.00e-07	9.03e-05	1.32	−0.43	Medium	↑ in NH
Methylmalonic acid	6.22e-06	4.01e-04	0.84	0.39	Medium	↓ in NH
β-Hydroxybutyric acid	1.80e-05	5.80e-04	1.24	−0.37	Medium	↑ in NH
Kynurenine	1.26e-04	2.04e-03	0.77	0.33	Small	↓ in NH
Indole acetic acid	6.33e-03	0.027	0.75	0.22	Small	↓ in NH
α-Ketoglutaric acid	6.64e-03	0.028	0.96	0.22	Small	↓ in NH
Propionic acid	0.011	0.038	0.91	0.21	Small	↓ in NH
Uric acid	0.015	0.050	0.91	0.19	Small	↓ in NH
Putrescine	0.029	0.076	0.94	0.17	Small	↓ in NH
Butyric acid	0.032	0.078	0.95	0.17	Small	↓ in NH
Creatinine	0.036	0.085	1.05	−0.16	Small	↑ in NH
α-Aminoadipic acid	0.038	0.086	0.92	0.16	Small	↓ in NH
Acetyl-ornithine	0.048	0.098	1.04	−0.15	Small	↑ in NH

[a]False Discovery Rate.

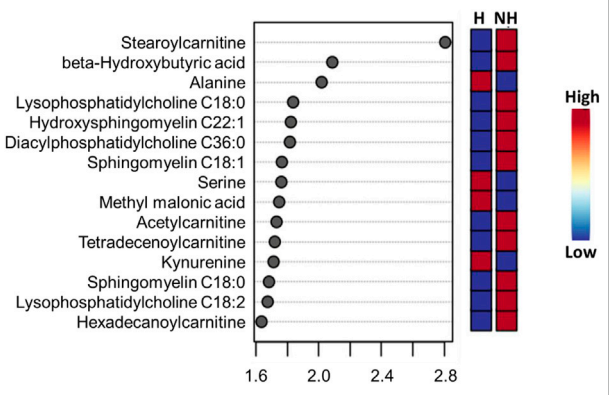

FIGURE 3
PLS-DA VIP plot showing differences between treatment (H = Habituated; NH = Non-habituated) groups and the metabolites (VIP scores >1.5) that significantly contribute to the difference. The metabolite concentrations averaged across all time points were used in the PLS-DA model ($p < 0.05$).

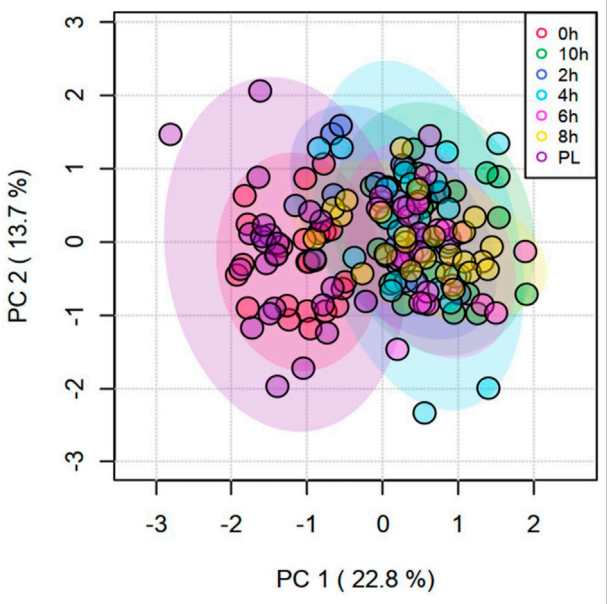

FIGURE 4
Principal Component Analysis (PCA) plot of principal components 1 and 2 of transportation time for metabolites.

and higher NEFA blood concentrations may provide energy for the animals. Blood urea nitrogen concentrations decreased with increasing transportation time in both H and NH treatment groups (Figure 2). The BUN concentrations were highest at PL and lowest at 6 h, 8 h and 10 h samplings. Any situation that causes protein catabolism, including elevated blood glucocorticoid concentrations and feed deprivation, will likely increase BUN (Finco, 1997; Kannan et al., 2000). Transport stress causes increase in BUN concentrations in farm animals (Hurtung, 2003) since feed deprivation is confounded with transportation stress and the process invariably increases glucocorticoids (Kannan et al., 2000).

Amino acids

Several amino acids were lower in the NH group compared to the H group in our study (Table 1). In addition to protein synthesis, amino acids are metabolized to compounds that enter the tricarboxylic acid (TCA) cycle to produce adenosine triphosphate. The amino acids that do not enter the TCA cycle are either ketogenic, glucogenic, or both (Litwack, 2021).

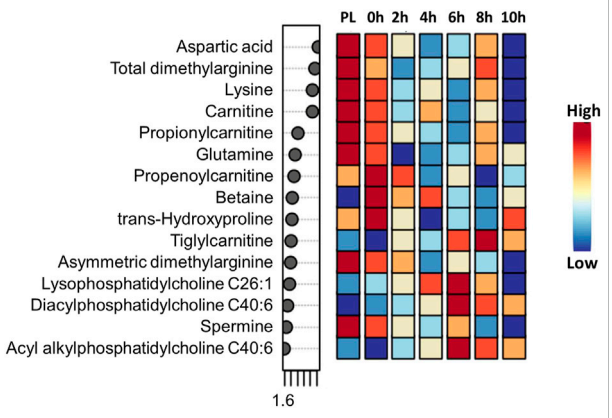

FIGURE 5
PLS-DA VIP plot showing differences among transportation time (PL = Preload) groups and the metabolites (VIP scores >1.5) that significantly contribute to the difference. The metabolite concentrations averaged across the two treatments were used in the PLS-DA model ($p < 0.05$).

Alanine, serine, glycine, histidine, asparagine, proline, and glutamic acid that forms glutamine, are glucogenic amino acids and were probably used for glucose production due to higher stress and energy demand in the NH group. Decreased amino acid concentrations in circulation may indicate their being used in gluconeogenesis, particularly in stressful situations (Coleman et al., 2020). For instance, during feed deprivation, alanine regulates gluconeogenesis to replenish glucose in dairy cattle (Guo et al., 2018). Leucine is a ketogenic amino acid that was used up for fatty acid production due to elevated stress in the NH goats. In addition, tryptophan and threonine were also lower in the NH groups and could have been involved in both glucose and fatty acid formations. Glucose concentrations were not significantly different between the two treatments in our study.

Almost all of the 20 amino acids affected by Time decreased slightly after loading (0 h), further decreased after the beginning of transportation, and stayed at a lower level throughout the rest of the transportation period (Supplementary Figure S2). A progressive decrease with increasing transportation time was noticed only for arginine, ornithine, and isoleucine. Based on interaction effects, the differences in alanine, trans-hydroxyproline, isoleucine, and ornithine concentrations at different time points became significant after 4 h of transportation. While the concentrations of these amino acids decreased or continued to decrease after 4 h in the NH group, the levels increased or stabilized after 4 h in the H group (Figure 6). This may indicate that habituating goats to transportation trailer could result in lower amino acid catabolism.

In addition to their function in protein building, amino acids have several important roles, such as immunomodulatory and immunometabolic activities (Li et al., 2007; Coleman et al., 2020). Glycine and serine concentrations were significantly lower in the NH goats compared to the H goats. Glycine is involved in protein and heme synthesis, as well as in bile acid conjugation (Wang et al., 2013). Its functions also include purine synthesis, glutathione synthesis, cell proliferation and differentiation, and regulating oxidative stress (Chen et al., 2013; Wang et al., 2013). Serine supports glutathione production and has also been reported to support T cell proliferation by supplying glycine and maintaining 1-carbon metabolism (Newsholme et al., 1999; Ma et al., 2017). Histidine that was lower in the NH group plays important roles in immune and antioxidant responses and energy metabolism. In addition, histidine produces glycoproteins that play an important role in immune function-related activities, such as phagocytosis and removal of antibody complexes (Wakabayashi, 2013).

Other amino acids with anti-inflammatory and immune support functions include glutamate and ornithine, whose concentrations were also lower in the NH goats during transportation. Glutamate is a nonessential amino acid and is required for the synthesis of glutathione, NADPH, and α-ketoglutarate (Wu et al., 2004; Newsholme et al., 2003). Glutamic acid converts to glutamine, a purine and pyrimidine precursor, which is required for nitric oxide, cytokine, and NADPH production and accelerated interleukin-6 production by macrophages (Yassad et al., 1997; Newsholme et al., 2003). Ornithine that is synthesized from arginine is required for polyamine synthesis and plays an important role in urea cycle. Arginine concentrations sharply decreased after beginning of transportation and stayed at low levels throughout the transportation period in goats in the present study. Modulating immune function is one of the important functions of arginine, which is synthesized from citrulline (Zhao et al., 2018). Arginine catabolism also produces polyamines through the arginase pathway (Wu et al., 2009) that can activate toll-like receptors (TLRs) and in turn activate innate immunity (Handa et al., 2018). The essential amino acid threonine, which was also lower in the NH goats, is needed for immunoglobulin production and influences glutathione synthesis (Li et al., 2007). Leucine concentrations were lower in the NH goats compared to the H goats, while the three branched-chain amino acids, leucine, isoleucine, and valine, decreased with transportation time. These amino acids also have multiple roles, such as regulation of immunity and energy homeostasis (Coleman et al., 2020). The lower concentrations of these amino acids in goats not habituated to trailers indicate that these animals could have compromised anti-inflammatory and immune capacities, which could collectively make them more susceptible to infections after long journeys.

Methionine, which decreased with transportation time in goats, is needed for glutathione and taurine synthesis (Lushchak, 2012). Methionine could support phosphatidylcholine and carnitine by providing methyl groups to form S-adenosyl methionine (Vance et al., 1997). Lysine is one of the conserved amino acids due to its ability for slower catabolism (Flodin, 1997). Smirga et al. (2002) reported that dietary lysine

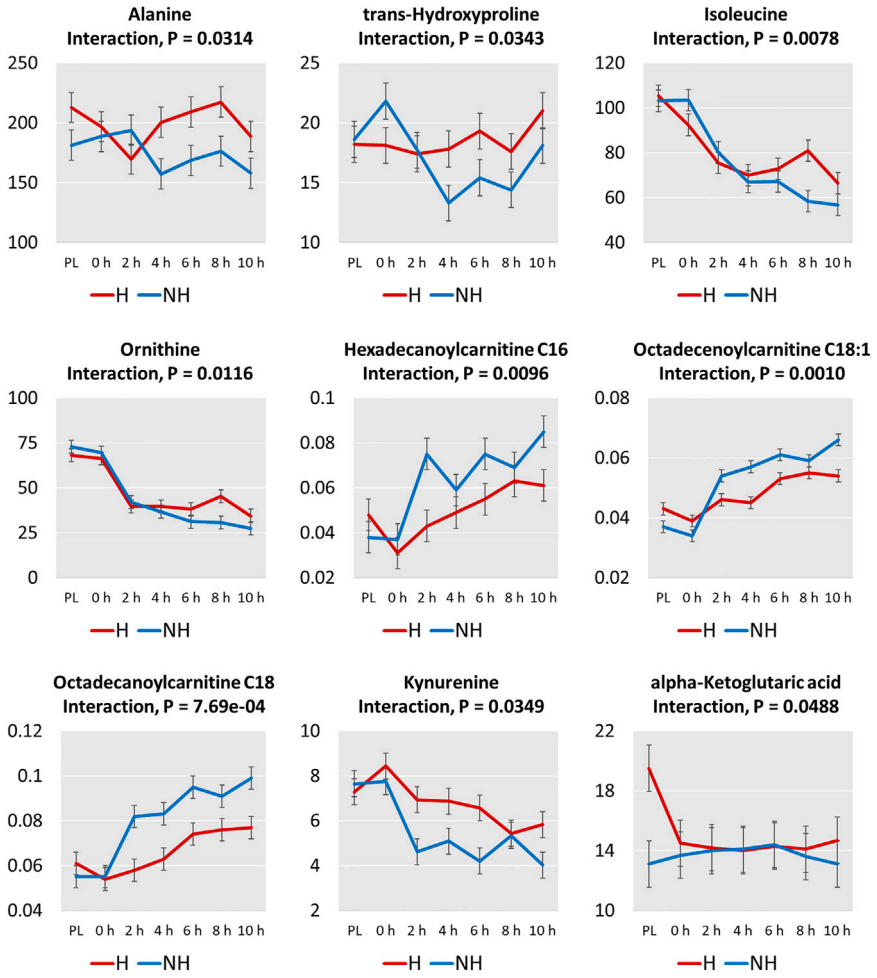

FIGURE 6
Plots of means (± SEM) of metabolites with significant treatment (H = Habituated; NH = Non-habituated) × transportation time (PL = Preload) interaction effects ($p < 0.05$).

deficiency increases stress-induced anxiety by enhancing serotonin release from amygdala. In our study, lysine concentrations decreased over transportation time in goats; however, serotonin concentrations did not increase with time. Lysine acts akin to a receptor competitor of serotonin and inhibits serotonin receptor-mediated anxiety, although lysine does not influence plasma serotonin concentrations (Venzi et al., 2016), which explains the pattern of serotonin concentrations over transportation time. It is not clear if these metabolites had an influence on the emotional status of goats in the present study.

Acylcarnitines

The NH goats had significantly higher octadecanoylcarnitine (C18), hexadecanoylcarnitine (C16), tetradecenoylcarnitine (C14:1), octadecenoylcarnitine (C18:1), tetradecanoylcarnitine (C14, and decanoylcarnitine (C10) concentrations than the H goats (Table 1). Also, plasma long-chain acylcarnitines invariably increased with increasing transportation time (Supplementary Figure S3). In addition to energy expenditures due to maintaining posture and balance in a moving livestock trailer, extended transportation also imposes metabolic stress in goats since they are deprived of feed and water. The animal's ability to cope up with metabolic stress depends on energy-production pathways, such as fatty acid oxidation in mitochondria and the TCA cycle (McCoin et al., 2015; Ghaffari et al., 2020).

The carnitine system, consisting of carnitine, acylcarnitines, carnitine enzymes and carnitine transporters, plays a crucial role in energy generation in cells (Peluso et al., 2000). The endogenous carnitine pool is comprised of the water-soluble compound L-carnitine and its esters, acylcarnitines. Although carnitine is present in highest quantity in muscle, it is mainly

synthesized in the liver from the amino acids lysine and methionine and then transported through circulation. Medium and long-chain acylcarnitines that increased during transportation, particularly in the NH goats, are produced by fatty acid oxidation, while short-chain acylcarnitines are mainly synthesized from amino acids and fatty acids (Makrecka-Kuka et al., 2017). The mitochondrial carnitine system plays an indispensable role in β-oxidation of long-chain fatty acids (Calo et al., 2006). The long-chain fatty acids are transferred from the cytoplasm to the mitochondrial matrix by carnitine and acylcarnitines regulated by carnitine palmitoyltransferase 1, which is present in the mictochondrial outer membrane. After being transferred into the mictochondria, the enzyme carnitine palmitoyltransferase 2, present in the matrix, regulate regeneration of carnitine and long-chain acyl-CoA (Schooneman et al., 2013). The β-oxidation of fatty acyl CoA produces acetyl CoA, which enters the TCA cycle to generate $NADH/FADH_2$ for utilization in the electron transport chain. Acylcarnitine reconversion in mitochondria is an important step that controls the amounts of fatty acids entering mitochondria from cytoplasm for β-oxidation. During times of intense workload, the acylation state of cytoplasmic carnitine pool increases more than the mitochondrial carnitine pool, suggesting that acylcarnitines are exported out of muscle cells (Ramsey and Andruini, 1993). This cellular efflux may cause increase in circulating acylcarnitine concentrations (Veld et al., 2009). Acylcarnitines in blood is the total from different tissues, as they are utilized by tissues such as skeletal muscle, cardiac muscle, and liver (Simcox et al., 2017). Increased concentrations of acylcarnitines in circulation is primarily due to muscle contraction during exercise that increases glucose and fatty acid oxidation (Hiatt et al., 1989).

Elevation in blood long-chain acylcarnitine concentrations can occur if there is a deficiency of carnitine palmitoyltransferases, incomplete β-oxidation of long-chain fatty acids, or depletion of TCA cycle intermediates (Schooneman et al., 2013; Yang et al., 2018; Ghaffari et al., 2020). Acylcarnitine concentrations can increase when the rates of β-oxidation are greater than those of the TCA cycle (Yang et al., 2019). Another reason for elevated long-chain acylcarnitine concentrations in plasma of goats during extended transportation, particularly in NH group, is elevated NEFA concentrations to meet the energy demand. The intense mobilization of fat is also reflected in elevated β-hydroxybuyrate in the NH group due to higher stress experienced during transportation than for the H group. Animal studies have indicated that approximately one-third of NEFA taken up by muscle is directly converted to long-chain acylcarnitines to meet oxidative needs (Sun et al., 2006). Xu et al. (2011) observed that high NEFA concentrations curb carnitine palmitoyltranferase-1 activity and fatty acid oxidation in cultured bovine hepatocytes. Ghaffari et al. (2019) reported that increased serum acylcarnitine concentrations coincided with increased NEFA concentrations in periparturient cows with high body condition. The increase in long-chain acylcarnitines may reflect enhanced lipolysis and the resultant β-oxidation rate that is greater than that of the TCA cycle (Ghaffari et al., 2019). The ensuing accumulation of fatty acids in the matrix could result in mitochondrial stress and incomplete fatty acid oxidation leading to acylcarnitines entering the circulation (Koves et al., 2008). In the present study, the rate of fatty acid oxidation was likely not able to cope up with the rate of accumulation of long-chain fatty acyl CoA in the mitochondrial matrix, that could have resulted in the increase in long-chain acylcarnitine concentrations in the blood.

Prolonged stress due to extended transportation can also promote inflammatory reactions in goats, particularly in those not habituated to transport trailers. Rutkowsky et al. (2014) reported that long-chain acylcarnitines activate pro-inflammatory pathways in rodent macrophages. These authors found that elevated palmitoylcarnitine (C16) concentrations increase release of interleukin-6 (IL-6) in monocytes and adenylate kinase (AK) in macrophages, the latter being a death marker. Long-chain acylcarnitines have also been reported to be associated with increased reactive oxygen species, apoptosis, and endoplasmic reticulum stress in cardiac muscle (Son et al., 2010). However, McCoin et al. (2015) did not observe markers for endoplasmic reticulum stress with increased C16 carnitine in their study, although the authors found increases in intracellular calcium and caspase-3 activity, and rapidly activated JNK/ERK/p38 MAPK stress pathways. McCoin et al. (2015) also opined that increase in long-chain acylcarnitines could promote muscle cell inflammation and stress under conditions that affect fatty acid oxidation. These reactions as a result of higher plasma long-chain acylcarnitines, if also occurring in goats, could negatively impact muscle metabolism and possibly meat quality characteristics. Conditioning goats to livestock trailers could attenuate the negative effects, such as inflammation and compromised immune function due to transportation stress. Further studies are needed to understand the potential effects of elevated plasma long-chain acylcarnitines on muscle cell inflammation, muscle metabolism, and meat quality characteristics in goats.

The beneficial effects of habituating goats to livestock trailers is clearly seen in the pattern of increase in the three long-chain acylcarnitines (C16, C18, C18:1) in the plasma (Figure 6). In the NH goats, these three long-chain acylcarnitines increased steeply with transportation time, while in the H goats, the increase was moderate, explaining the significant TRT × Time interaction effects.

Carnitine concentration was also lower in the NH goats compared to the H goats. The lower free carnitine concentrations in serum could be due to enhanced utilization by skeletal muscle fibers (Yang et al., 2019) for transferring long-chain fatty acids from cytosol into mitochondrial matrix because of intense stress and energy need. Carnitine maintains the balance between free and esterified CoA (Sharma and Black, 2009).

Phosphatidylcholines and sphingomyelins

The phosphatidylcholines and sphingomyelins significantly affected by TRT were lower in the H goats compared to the NH goats (Table 2). In mammalian cells, the primary phospholipid that forms membranes is phosphatidylcholine, a glycerophospholipid that has a polar phosphocholine head group and two non-polar hydrocarbon chains (Taylor et al., 2007). Lyso-phosphatidylcholine is usually formed when the enzyme phospholipase 2 cleaves the fatty acid from the cell membrane phosphatidylcholine glycerol backbone. Small variations in phospholipid levels can have significant effects on lipid profiles and insulin signaling (van der Veen et al., 2017). In hepatocytes, 1-palmitoyl-2-oleoyl-*sn*-glycerol-3-phosphocholine acts as an endogenous ligand for PPATα, a transcription factor that regulates expression of multiple genes that are involved in lipid metabolism (Kersten, 2014). This nuclear hepatocyte receptor has also been reported to control a lipogenic pathway that regulates fatty acid uptake and β-oxidation by muscle (Furse and de Kroon, 2015). The elevated levels of phosphatidylcholines and lyso-phosphatidylcholines are likely associated with increased fatty acid metabolism in NH goats, as these animals experienced higher stress compared to the H goats, based on plasma NEFA concentrations.

Lyso-phosphatidylcholine (20:4) has been suggested as a marker of stress and depression in rats and humans (Adams et al., 1996; Wu et al., 2019). Although phosphatidylcholines are involved in normal cognition (Haus et al., 2009), and chronic stress can cause depression due to decreases in phosphatidylcholines (Ren et al., 2018), high levels as seen in the present experiment are due to enhanced fatty acid metabolism. Increases in plasma sphingosine and sphinganine could also result in increase in ceramide, which can cause depression (Gulbins et al., 2013).

Other metabolites

Ketone bodies have a glucose-sparing role in ruminants and are used as a source of energy in the small intestines and peripheral tissues in ruminants (Penner et al., 2011). In the NH group of goats, β-hydroxybutyrate concentrations were higher compared to the H goats (Table 3). The metabolic precursor of β-hydroxybutyric acid, acetoacetate, is a metabolite of fatty acids (ex. butyrate) and ketogenic amino acids (ex. Leucine and isoleucine). Both butyrate and leucine concentrations were significantly lower in the NH goats in the present study (Tables 1, 3), indicating both fatty acids and amino acids were used up to a higher degree in the NH goats in producing energy during transportation. Some animal species may have a unique way of coping up with ketosis, for instance, β-hydroxybutyrate was not significantly affected as a result of 5-h transportation in dromedary camels (Wensvoort et al. (2004).

α-ketoglutarate is an important molecule that determines the rate of the TCA cycle (Wu et al., 2016). Under normal conditions, it promotes protein synthesis and curbs protein breakdown. In the present study, α-ketoglutarate was lower in the NH groups compared to the H group (Table 3), and the significant TRT × Time interaction effect noticed was because of the rapid decline of this metabolite in the H goats after loading onto the trailer (Figure 6). Decrease of this key TCA cycle intermediate could have also contributed to the possible enhanced level of β-oxidation, resulting in fatty acid overload and the consequent increase in long-chain acylcarnitines in circulation. α-ketglutarate could synthesize glutamate, which was also lower in the NH group (Table 1). α-ketoglutaric acid plays an important role in immune function of the organism. Glutamine, that is formed by glutamate, is an important fuel for lymphocytes and macrophages (Parry-Billings et al., 1990) that are part of the innate defense system. In addition, α-ketoglutarate can enhance cellular antioxidant capacity by increasing superoxide dismutase and glutathione peroxidase activities and preventing lipid peroxidation, as well as by scavenging reactive oxygen species (Velvizhi et al., 2002; Mailloux et al., 2009). The lower α-ketoglutarate levels in goats during transportation could negatively impact immune function and antioxidant activities.

α-aminoadipic acid was lower in the NH group and decreased with transportation time in goats in our study (Table 3). Under normal resting conditions, lower α-aminoadipic acid and higher lysine levels will result in protein synthesis (Goldansaz et al., 2020). α-aminoadipic acid is a breakdown product of lysine (Guidetti and Schwarcz, 2003), a ketogenic and indispensable amino acid. The decrease in plasma aminoadipic acid concentrations with transportation time corresponded with decrease in lysine concentrations in our study. This suggests that the breakdown of lysine *via* the saccharophine pathway does not stop with the formation of aminoadipic acid due to the energy demand during stress. The initial step in the catabolism of α-aminoadipic acid is transamination with α-ketoglutarate to form glutamate and then 2-ketoadipic acid. Subsequently, glutaryl-CoA is formed by decarboxylation of 2-ketadipic acid, which is then metabolized through the CoA esters to form acetyl-CoA (Matthews, 2020). The lower α-ketoglutaric acid noticed in the NH goats in the present study is likely due to the intensity of this catabolic process during extended transportation.

Tryptophan, that has both ketogenic and glucogenic properties was lower in the NH goats and decreased with transportation time in our study, which also corresponded with the decrease in kynurenine concentrations (Table 3). Kynurenine is degraded during tryptophan catabolism. Butyric acid concentrations were lower in the NH group compared to the H group (Table 3), and the concentrations also decreased over transportation time (Supplementary Figure S4). Butyric acid is produced from rumen microbial fermentation of dietary fiber, and its concentrations in blood negatively correlates with certain inflammatory markers (Juanola et al., 2019). Butyrate has also been shown to have anti-inflammatory and immune boosting

capacities, in addition to its crucial role in energy homeostasis (Kasubuchi et al., 2015). The metabolite profiles together suggest the goats that have been previously conditioned to livestock trailers before a long-distance transportation may have better ability to cope with the negative effects of stress.

The limitation in this study was that other potential factors such as weather, noise, and vehicular vibration could not be evaluated separately due to the confounding nature of these stressors. The extent to which these factors influenced the metabolic profiles of individual goats is therefore not clear in this study.

Conclusion

Habituation to trailers could be beneficial to goats in maintaining energy metabolism during transportation as glucogenic and ketogenic amino acid levels in blood were lower, and their decrease over transportation time was greater in the non-habituated goats compared to habituated goats. There is evidence in this study that both gluconeogenesis and fatty acid oxidation pathways are upregulated and that there is possible mitochondrial overload and incomplete fatty acid oxidation during prolonged intense stress, such as transportation, that results in elevated blood long-chain acylcarnitine concentrations. We suggest that long-chain acylcarntines could be good indicators of prolonged stress in goats as these metabolites increased with increasing transportation time, more so in the non-habituated goats, although further studies focusing on biomarker sensitivity and specificity are required. The potential negative effects of elevated long-chain acylcarnitines on myofiber inflammation, muscle metablolism, and meat quality characteristics also require further investigation. Habituation to trailers can also be beneficial in enhancing stress coping abilities in goats during long-distance transportation due to higher concentrations of metabolites that support energy homeostasis, antioxidant activities, and immune function.

Data availability statement

The original contributions presented in the study are included in the article/Supplementary Material, further inquiries can be directed to the corresponding author.

Ethics statement

The animal study was reviewed and approved by the Agricultural and Laboratory Animal Care and Use Committee at FVSU.

Author contributions

PB and AN participated in blood sample collection and laboratory analysis of stress indicators. BK and TT assisted in blood sampling and review of manuscript, and PB assisted in data processing. GM provided partial funding and lab support for blood analysis. GK, TT, and PB conceived the project hypothesis. GK acquired the funds and directed the project by designing the study, advising on blood sample analysis, conducting part of the statistical analysis, interpreting the data, creating figures, and preparing the manuscript for submission based on the preliminary draft developed by PB.

Funding

Experimental animals were provided by the Agricultural Research Station at Fort Valley State University and the study was partially supported by the USDA-NIFA Evans-Allen Program.

Acknowledgments

The authors thank Gregory Dykes and Leah Brooks for their assistance during blood sample collection and laboratory analysis. The authors also thank Mark Berjanski for assistance with statistical analysis.

Conflict of interest

The authors declare that the research was conducted in the absence of any commercial or financial relationships that could be construed as a potential conflict of interest.

Publisher's note

Supplementary material

The supplementary material for this article can be found online at: https://www.frontiersin.org/articles/10.3389/fmolb.2022.1027069/full#supplementary-material

References

Adams, P. B., Lawson, S., Sanigorski, A., and Sinclair, A. J. (1996). Arachidonic acid to eicosapentaenoic acid ratio in blood correlates positively with clinical symptoms of depression. *Lipids* 31, S157–S161. doi:10.1007/BF02637069

Batchu, P., Terrill, T. H., Kouakou, B., Estrada-Reyes, Z. M., and Kannan, G. (2021). Plasma metabolomic profiles as affected by diet and stress in Spanish goats. *Sci. Rep.* 11, 12607. doi:10.1038/s41598-021-91893-x

Calo, L. A., Pagnin, E., Davis, P. A., Semplicini, A., Nicolai, R., Calvani, M., et al. (2006). Antioxidant effect of L-carnitine and its short chain esters relevance for the protection from oxidative stress related cardiovascular damage. *Int. J. Cardiol.* 107, 54–60. doi:10.1016/j.ijcard.2005.02.053

Chen, Y., Dong, H., Thompson, D. C., Shertzer, H. G., Nebert, D. W., and Vasiliou, V. (2013). Glutathione defense mechanism in liver injury: Insights from animal models. *Food Chem. Toxicol.* 60, 38–44. doi:10.1016/j.fct.2013.07.008

Coleman, D. N., Lopreiato, V., Alharthi, A., and Loor, J. J. (2020). Amino acids and the regulation of oxidative stress and immune function in dairy cattle. *J. Anim. Sci.* 98, S175–S193. doi:10.1093/jas/skaa138

Dai, F., Mazzola, S., Cannas, S., Heinzl, E. U. L., Padalino, B., Minero, M., et al. (2020). Habituation to transport helps reducing stress-related behavior in donkeys during loading. *Front. Vet. Sci.* 7, 593138. doi:10.3389/fvets.2020.593138

Finco, D. R. (1997). "Kidney function," in *Clinical biochemistry of domestic animals*. Editor J. J. Kaneko (New York, NY: Academic Press), 441–484.

Flodin, N. W. (1997). The metabolic roles, pharmacology and toxicology of lysine. *J. Am. Coll. Nutr.* 16, 7–21. doi:10.1080/07315724.1997.10718644

Furse, S., and de Kroon, A. I. P. M. (2015). Phosphatidylcholine's functions beyond that of a membrane brick. *Mol. Membr. Biol.* 32, 117–119. doi:10.3109/09687688.2015.1066894

Ghaffari, M. H., Jahanbekam, A., Sadri, H., Schuh, K., Dusel, G., Prehn, C., et al. (2019). Metabolomics meets machine learning: Longitudinal metabolite profiling in serum of normal versus overconditioned cows and pathway analysis. *J. Dairy Sci.* 101, 11561–11585. doi:10.3168/jds.2019-17114

Ghaffari, M. H., Sadri, H., Schuh, K., Dusel, G., Prehn, C., Adamski, J., et al. (2020). Alterations of the acylcarnitine profiles in blood serum and in muscle from periparturient cows with normal or elevated body condition. *J. Dairy Sci.* 103, 4777–4794. doi:10.3168/jds.2019-17713

Goldansaz, S. A., Marcus, S., Berjanskii, M., Rout, M., Guo, A. C., Wang, Z., et al. (2020). Candidate serum metabolite biomarkers of residual feed intake and carcass merit in sheep. *J. Anim. Sci.* 98, skaa298–15. doi:10.1093/jas/skaa298

Guidetti, P., and Schwarcz, R. (2003). Determination of α-aminoadipic acid in brain, peripheral tissues, and body fluids using GC/MS with negative chemical ionization. *Brain Res. Mol. Brain Res.* 118, 132–139. doi:10.1016/j.molbrainres.2003.08.004

Gulbins, E., Palmada, M., Reichel, M., Luth, A., Bohmer, C., Amato, D., et al. (2013). Acid sphingomyelinase-ceramide system mediates effects of antidepressant drugs. *Nat. Med.* 19, 934–938. doi:10.1038/nm.3214

Guo, J., Gao, S., Quan, S., Zhang, Y., Bu, D., and Wang, J. (2018). Blood amino acids profile responding to heat stress in dairy cows. *Asian-Australas. J. Anim. Sci.* 31, 47–53. doi:10.5713/ajas.16.0428

Handa, A. K., Fatima, T., and Mattoo, A. K. (2018). Polyamines: Bio-Molecules with diverse functions in plant and human health and disease. *Front. Chem.* 6, 10. doi:10.3389/fchem.2018.00010

Haus, J. M., Kashyap, S. R., Kasumov, T., Zhang, R., Kelly, K. R., Defronzo, R. A., et al. (2009). Plasma ceramides are elevated in obese subjects with type 2 diabetes and correlate with the severity of insulin resistance. *Diabetes* 58, 337–343. doi:10.2337/db08-1228

Hiatt, W. R., Regensteiner, J. G., Wolfel, E. E., Ruff, L., and Brass, E. P. (1989). Carnitine and acylcarnitine metabolism during exercise in humans. Dependence on skeletal muscle metabolic state. *J. Clin. Invest.* 84, 1167–1173. doi:10.1172/JCI114281

Hurtung, J. (2003). Effects of transport on health of farm animals. *Vet. Res. Commun.* 27, 525–527. doi:10.1023/b:verc.0000014212.81294.78

Juanola, O., Ferrusquía-Acosta, J., García-Villalba, R., Zapater, P., Magaz, M., Marín, A., et al. (2019). Circulating levels of butyrate are inversely related to portal hypertension, endotoxemia, and systemic inflammation in patients with cirrhosis. *FASEB J.* 33, 11595–11605. doi:10.1096/fj.201901327R

Junot, C., Fenaille, F., Colsch, B., and Bécher, F. (2014). High resolution mass spectrometry based techniques at the crossroads of metabolic pathways. *Mass Spectrom. Rev.* 33, 471–500. doi:10.1002/mas.21401

Kannan, G., Kouakou, B., Terrill, T. H., and Gelaye, S. (2003). Endocrine, blood metabolite, and meat quality changes in goats as influenced by short-term, preslaughter stress. *J. Anim. Sci.* 81, 1499–1507. doi:10.2527/2003.8161499x

Kannan, G., Terrill, T. H., Kouakou, B., Gazal, O. S., Gelaye, S., Amoah, E. A., et al. (2000). Transportation of goats: Effects on physiological stress responses and live weight loss. *J. Anim. Sci.* 78, 1450–1457. doi:10.2527/2000.7861450x

Kannan, G., Terrill, T. H., Kouakou, B., Gelaye, S., and Amoah, E. A. (2002). Simulated preslaughter holding and isolation effects on stress responses and live weight shrinkage in meat goats. *J. Anim. Sci.* 80, 1771–1780. doi:10.2527/2002.8071771x

Kasubuchi, M., Hasegawa, S., Hiramatsu, T., Ichimura, A., and Kimur, I. (2015). Dietary gut microbial metabolites, short-chain fatty acids, and host metabolic regulation. *Nutrients* 7, 2839–2849. doi:10.3390/nu7042839

Kersten, S. (2014). Integrated physiology and systems biology of PPARα. *Mol. Metab.* 3, 354–371. doi:10.1016/j.molmet.2014.02.002

Koves, T. R., Ussher, J. R., Noland, R. C., Slentz, D., Mosedale, M., Ilkayeva, O., et al. (2008). Mitochondrial overload and incomplete fatty acid oxidation contribute to skeletal muscle insulin resistance. *Cell Metab.* 7, 45–56. doi:10.1016/j.cmet.2007.10.013

Li, P., Yin, Y. L., Li, D., Kim, S. W., and Wu, G. (2007). Amino acids and immune function. *Br. J. Nutr.* 98, 237–252. doi:10.1017/S000711450769936X

Litwack, G. (2021). "Matabolism of amino acids," in *Human biochemistry* (Cambridge, MA: Elsevier), 357–394.

Lushchak, V. I. (2012). Glutathione homeostasis and functions: Potential targets for medical interventions. *J. Amino Acids* 2012, 736837. doi:10.1155/2012/736837

Ma, E. H., Bantug, G., Griss, T., Condotta, S., Johnson, R. M., Samborska, B., et al. (2017). Serine is an essential metabolite for effector T cell expansion. *Cell Metab.* 25, 345–357. doi:10.1016/j.cmet.2016.12.011

Macbeth, G., Razumiejczyk, E., and Ledesma, R. D. (2011). Cliff's delta calculator: A non-parametric effect size program for two groups of observations. *Univ. Psychol.* 10, 545–555. doi:10.11144/javeriana.upsy10-2.cdcp

Mailloux, R. J., Singh, R., Brewer, G., Auger, C., Lemire, J., and Appanna, V. D. (2009). Alpha-ketoglutarate dehydrogenase and glutamate dehydrogenase work in tandem to modulate the antioxidant alpha-ketoglutarate during oxidative stress in Pseudomonas fluorescens. *J. Bacteriol.* 191, 3804–3810. doi:10.1128/JB.00046-09

Makrecka-Kuka, M., Sevostjanovs, E., Vilks, K., Volska, K., Antone, U., Kuka, J., et al. (2017). Plasma acylcarnitine concentrations reflect the acylcarnitine profile in cardiac tissues. *Sci. Rep.* 7, 17528. doi:10.1038/s41598-017-17797-x

Matthews, D. E. (2020). Review of lysine metabolism with a focus on humans. *J. Nutr.* 150, 2548S–2555S. doi:10.1093/jn/nxaa224

McCoin, C. S., Knotts, T. A., Ono-Moore, K. D., Oort, P. J., and Adams, S. H. (2015). Long-chain acylcarnitines activate cell stress and myokine release in C2C12 myotubes: Calcium-dependent and –independent effects. *Am. J. Physiol. Endocrinol. Metab.* 308, E990–E1000. doi:10.1152/ajpendo.00602.2014

Minka, N. S., and Ayo, J. O. (2009). Physiological responses of food animals to road transportation stress. *Afr. J. Biotechnol.* 8, 7415–7427.

Newsholme, P., Curi, R., Pithon Curi, T. C., Murphy, C. K., Garcia, C., and Pires de Melo, M. (1999). Glutamine metabolism by lymphocytes, macrophages, and neutrophils: Its importance in health and disease. *J. Nutr. Biochem.* 10, 316–324. doi:10.1016/s0955-2863(99)00022-4

Parry-Billings, M., Calder, P., Newsholme, E., and Evans, J. (1990). Does glutamine contribute to immunosuppression after major burns? *Lancet* 336, 523–525. doi:10.1016/0140-6736(90)92083-t

Peluso, G., Barbarisi, A., Savica, V., Reda, E., Nicolai, R., Benatti, P., et al. (2000). Carnitine: An osmolyte that plays a metabolic role. *J. Cell. Biochem.* 80, 1–10. doi:10.1002/1097-4644(20010101)80:1<1:aid-jcb10>3.0.co;2-w

Penner, G. B., Steele, M. A., Aschenbach, J. R., and McBride, B. W. (2011). Ruminant Nutrition Symposium: Molecular adaptation of ruminal epithelia to highly fermentable diets. *J. Anim. Sci.* 89, 1108–1119. doi:10.2527/jas.2010-3378

Ramsey, R. R., Andruini, A., and Arduini, A. (1993). The carnitine acyltransferases and their role in modulating acyl-CoA pools. *Arch. Biochem. Biophys.* 302, 307–314. doi:10.1006/abbi.1993.1216

Ren, Y., Yang, C., Li, Z., Yang, Z., Xiao, Z., Duan, J., et al. (2018). Chronic stress disturbs metabolome of blood plasma and urine in diabetic rats. *Front. Psychiatry* 9, 525. doi:10.3389/fpsyt.2018.00525

Rusilowicz, M., Dickinson, M., Charlton, A., O'Keefe, S., and Wilson, J. (2016). A batch correction method for liquid chromatography–mass spectrometry data that

does not depend on quality control samples. *Metabolomics.* 12, 56. doi:10.1007/s11306-016-0972-2

Rutkowsky, J. M., Knotts, T. A., Ono-Moore, K. D., McCoin, C. S., Huang, S., Schneider, D., et al. (2014). Acylcarnitines activate proinflammatory signaling pathways. *Am. J. Physiol. Endocrinol. Metab.* 306, E1378–E1387. doi:10.1152/ajpendo.00656.2013

Saeb, M., Baghshani, H., Nazifi, S., and Saeb, S. (2010). Physiological response of dromedary camels to road transportation in relation to circulating levels of cortisol, thyroid hormones, and some serum biochemical parameters. *Trop. Anim. Health Prod.* 42, 55–63. doi:10.1007/s11250-009-9385-9

Salama, A. A. K., Caja, G., Hamzaoui, S., Badaoui, B., Castro Costa, A., Façanha, D. A. E., et al. (2014). Different levels of response to heat stress in dairy goats. *Small Rumin. Res.* 121, 73–79. doi:10.1016/j.smallrumres.2013.11.021

Schooneman, M. G., Vaz, F. M., Houten, S. M., and Soeters, M. R. (2013). Acylcarnitines: Reflecting or inflicting insulin resistance? *Diabetes* 62, 1–8. doi:10.2337/db12-0466

Sharma, S., and Black, S. M. (2009). Carnitine homeostasis, mitochondrial function, and cardiovascular disease. *Drug Discov. Today. Dis. Mech.* 6, e31–e39. doi:10.1016/j.ddmec.2009.02.001

Simcox, J., Geoghegan, G., Maschek, J. A., Bensard, C. L., Pasquali, M., Miaoet, R., et al. (2017). Global analysis of plasma lipids identifies liver-derived acylcarnitines as a fuel source for Brown fat thermogenesis. *Cell Metab.* 26, 509–522. doi:10.1016/j.cmet.2017.08.006

Smirga, M., Kameishi, M., Uneyama, H., and Torii, K. (2002). Dietary L-lysine deficiency increases stress-induced anxiety and fecal excretion in rats. *J. Nutr.* 132, 3744–3746. doi:10.1093/jn/132.12.3744

Son, N. H., Yu, S., Tuinei, J., Arai, K., Hamai, H., Homma, S., et al. (2010). PPARγ-induced cardiolipotoxicity in mice is ameliorated by PPARα deficiency despite increases in fatty acid oxidation. *J. Clin. Invest.* 120, 3443–3454. doi:10.1172/JCI40905

Stockman, C. A., Collins, T., Barnes, A. L., Miller, D., Wickham, S. L., Beatty, D. T., et al. (2011). Qualitative behavioural assessment and quantitative physiological measurement of cattle naïve and habituated to road transport. *Anim. Prod. Sci.* 51, 240–249. doi:10.1071/an10122

Sun, D., Cree, M. G., Zhang, X. J., Boersheim, E., and Wolfe, R. R. (2006). Measurement of stable isotopic enrichment and concentration of long-chain fatty acyl-carnitines in tissue by HPLC-MS. *J. Lipid Res.* 47, 431–439. doi:10.1194/jlr.D500026-JLR200

Taylor, L. A., Arends, J., Hodina, A. K., Unger, C., and Massing, U. (2007). Plasma lyso-phosphatidylcholine concentration is decreased in cancer patients with weight loss and activated inflammatory status. *Lipids Health Dis.* 6, 17. doi:10.1186/1476-511X-6-17

Ujita, A., Seekford, Z., Kott, M., Goncherenko, G., Dias, N. W., Feuerbacher, E., et al. (2021). Habituation protocols improve behavioral and physiological responses of beef cattle exposed to students in an animal handling class. *Animals.* 11, 2159. doi:10.3390/ani11082159

van der Veen, J. N., Kennelly, J. P., Wan, S., Vance, J. E., Vance, D. E., and Jacobs, R. L. (2017). The critical role of phosphatidylcholine and phosphatidylethanolamine metabolism in health and disease. *Biochim. Biophys. Acta. Biomembr.* 1859, 1558–1572. doi:10.1016/j.bbamem.2017.04.006

Vance, D. E., Walkey, C. J., and Cui, Z. (1997). Phosphatidylethanolamine N-methyltransferase from liver. *Biochim. Biophys. Acta* 1348, 142–150. doi:10.1016/s0005-2760(97)00108-2

Vargha, A., and Delaney, H. D. (2000). A critique and improvement of the CL common language effect size statistics of McGraw and Wong. *J. Educ. Behav. Stat.* 25, 101–132. doi:10.2307/1165329

Veld, F., Primassin, S., Hoffmann, L., Mayatepek, E., and Spickerkoetter, U. (2009). Corresponding increase in long-chain acyl-CoA and acylcarnitine after exercise in muscle from VLCAD mice. *J. Lipid Res.* 50, 1556–1562. doi:10.1194/jlr.M800221-JLR200

Velvizhi, S., Nagalashmi, T., Essa, M. M., Dakshayani, K. B., and Subramanian, P. (2002). Effects of α-ketoglutarate on lipid peroxidation and antioxidant status during chronic ethanol administration in wistar rats. *Pol. J. Pharmacol.* 54, 231–236.

Venzi, M., David, F., Bellet, J., Cavaccini, A., Bombardi, C., Crunelli, V., et al. (2016). Role for serotonin2A (5-HT2A) and 2C (5-HT2C) receptors in experimental absence seizures. *Neuropharmacology* 108, 292–304. doi:10.1016/j.neuropharm.2016.04.016

Verbeke, W. A., and Viaene, J. (2000). Ethical challenges for livestock production: Meeting consumer concerns about meat safety and animal welfare. *J. Agric. Environ. Ethics* 12, 141–151. doi:10.1023/a:1009538613588

Wakabayashi, S. (2013). New insights into the functions of histidine-rich glycoprotein. *Int. Rev. Cell Mol. Biol.* 304, 467–493. doi:10.1016/B978-0-12-407696-9.00009-9

Wang, W., Wu, Z., Dai, Z., Yang, Y., Wang, J., and Wu, G. (2013). Glycine metabolism in animals and humans: Implications for nutrition and health. *Amino Acids* 45, 463–477. doi:10.1007/s00726-013-1493-1

Weeks, C., McGreevy, P., and Waran, N. (2012). Welfare issues related to transport and handling of both trained and unhandled horses and ponies. *Equine Vet. Educ.* 24, 423–430. doi:10.1111/j.2042-3292.2011.00293.x

Wensvoort, J., Kyle, D. J., Orskov, E. R., and Bourke, D. A. (2004). Biochemical adaptation of camelids during fasting. *J. Camel Sci.* 1, 71–75.

Wu, G., Bazer, F. W., Davis, T. A., Kim, S. W., Li, P., Marc Rhoads, J., et al. (2009). Arginine metabolism and nutrition in growth, health and disease. *Amino Acids* 37, 153–168. doi:10.1007/s00726-008-0210-y

Wu, G., Fang, Y. Z., Yang, S., Lupton, J. R., and Turner, N. D. (2004). Glutathione metabolism and its implications for health. *J. Nutr.* 134, 489–492. doi:10.1093/jn/134.3.489

Wu, N., Yang, M., Gaur, U., Xu, H., Yao, Y., and Li, D. (2016). Alpha-ketoglutarate: Physiological functions and applications. *Biomol. Ther.* 24, 1–8. doi:10.4062/biomolther.2015.078

Wu, Q., Xia, D., Lan, F., Wang, Y., Tan, X., Sun, J., et al. (2019). UPLC–QTOF/MS-based metabolomics reveals the mechanism of chronic unpredictable mild stress-induced hypertension in rats. *Biomed. Chromatogr.* 33, e4619. doi:10.1002/bmc.4619

Xu, C., Wang, Z., Zhang, R., Zhang, H., Fu, S., and Xia, C. (2011). Effect of NEFA and glucose levels on CPT-I mRNA expression and translation in cultured bovine hepatocytes. *J. Vet. Med. Sci.* 73, 97–101. doi:10.1292/jvms.10-0164

Yang, Y., Sadri, H., Prehn, C., Adamski, J., Rehage, J., Danicke, S., et al. (2019). Acylcarnitine profiles in serum and muscle of dairy cows receiving conjugated linoleic acids or a control fat supplement during early lactation. *J. Dairy Sci.* 102, 754–767. doi:10.3168/jds.2018-14685

Yassad, A., Lavonine, A., Bion, A., Daveau, M., Husson, A., and Lavoinne, A. (1997). Glutamine accelerates interleukin-6 production by rat peritoneal macrophages in culture. *FEBS Lett.* 413, 81–84. doi:10.1016/s0014-5793(97)00881-8

Zhao, F. F., Wu, T. Y., Wang, H. R., Ding, L. Y., Ahmed, G., Li, H. W., et al. (2018). Jugular arginine infusion relieves lipopolysaccharide-triggered inflammatory stress and improves immunity status of lactating dairy cows. *J. Dairy Sci.* 101, 5961–5970. doi:10.3168/jds.2017-13850

Zhong, R. Z., Liu, H. W., Zhou, W., Sun, H. X., and Zhao, C. S. (2011). The effects of road transportation on physiological responses and meat quality in sheep differing in age. *J. Anim. Sci.* 89, 3742–3751. doi:10.2527/jas.2010-3693

frontiers | Frontiers in Molecular Biosciences

TYPE Original Research
PUBLISHED 13 March 2023
DOI 10.3389/fmolb.2023.1140375

OPEN ACCESS

EDITED BY
Evagelos Gikas,
National and Kapodistrian University of Athens, Greece

REVIEWED BY
Shilpita Karmakar,
Jackson Laboratory, United States
Katerina Iliou,
National and Kapodistrian University of Athens, Greece

*CORRESPONDENCE
G. Plastow,
plastow@ualberta.ca

SPECIALTY SECTION
This article was submitted to Metabolomics, a section of the journal Frontiers in Molecular Biosciences

RECEIVED 09 January 2023
ACCEPTED 27 February 2023
PUBLISHED 13 March 2023

CITATION
Dervishi E, Bai X, Dyck MK, Harding JCS, Fortin F, Dekkers JCM and Plastow G (2023), GWAS and genetic and phenotypic correlations of plasma metabolites with complete blood count traits in healthy young pigs reveal implications for pig immune response. *Front. Mol. Biosci.* 10:1140375. doi: 10.3389/fmolb.2023.1140375

GWAS and genetic and phenotypic correlations of plasma metabolites with complete blood count traits in healthy young pigs reveal implications for pig immune response

E. Dervishi[1], X. Bai[1], M. K. Dyck[1], J. C. S. Harding[2], F. Fortin[3], J. C. M. Dekkers[4] and G. Plastow[1]* on behalf of PigGen Canada Members

[1]Livestock Gentec, Department of Agriculture, Food and Nutritional Science, Faculty of Agricultural, Life and Environmental Sciences, University of Alberta, Edmonton, AB, Canada, [2]Department of Large Animal Clinical Sciences, University of Saskatchewan, Saskatoon, SK, Canada, [3]Centre de Developpement du porc du Quebec inc (CDPQ), Quebec City, QC, Canada, [4]Department of Animal Science, Iowa State University, Ames, IA, United States

Introduction: In this study estimated genetic and phenotypic correlations between fifteen complete blood count (CBC) traits and thirty-three heritable plasma metabolites in young healthy nursery pigs. In addition, it provided an opportunity to identify candidate genes associated with variation in metabolite concentration and their potential association with immune response, disease resilience, and production traits.

Methods: The blood samples were collected from healthy young pigs and Nuclear Magnetic Resonance (NMR) was used to quantify plasma metabolites. CBC was determined using the ADVIA® 2120i Hematology System. Genetic correlations of metabolite with CBC traits and single step genome-wide association study (ssGWAS) were estimated using the BLUPF90 programs.

Results: Results showed low phenotypic correlation estimates between plasma metabolites and CBC traits. The highest phenotypic correlation was observed between lactic acid and plasma basophil concentration (0.36 $\pm$ 0.04; $p < 0.05$). Several significant genetic correlations were found between metabolites and CBC traits. The plasma concentration of proline was genetically positively correlated with hemoglobin concentration (0.94 $\pm$ 0.03; $p < 0.05$) and L-tyrosine was negatively correlated with mean corpuscular hemoglobin (MCH; −0.92 $\pm$ 0.74; $p < 0.05$). The genomic regions identified in this study only explained a small percentage of the genetic variance of metabolites levels that were genetically correlated with CBC, resilience, and production traits.

Discussion: The results of this systems approach suggest that several plasma metabolite phenotypes are phenotypically and genetically correlated with CBC traits, suggesting that they may be potential genetic indicators of immune response following disease challenge. Genomic analysis revealed genes and pathways that might interact to modulate CBC, resilience, and production traits.

KEYWORDS

metabolomics, complete blood count, pigs, genetic correlation, GWAS-genome-wide association study

Introduction

Immunity refers to the immune system's capacity to protect individuals from disease by recognizing and eliminating potentially pathogenic agents, including bacteria, bacterial toxins, viruses, parasites and fungi (Stanfield and Germann, 2008). The earliest line of defence against microbes and pathogens it is provided by innate immunity which is a non-specific response. The principal components of innate immunity include: 1) physical and chemical barriers example: skin, epithelia, the gastrointestinal tract and antimicrobial chemicals produced at epithelial surfaces 2) cellular components include: neutrophils, eosinophils, monocytes, macrophages, dendritic cells, and natural killer (NK) cells; 3) other innate lymphoid cells and blood proteins, including members of the complement system and other mediators of inflammation (Janeway et al., 2001; Stanfield and Germann, 2008). Adaptive immunity is a more sophisticated defense response which uses specific antigens to strategically mount an immune response. Cellular components of adaptive immune system include lymphocytes: B cells and T cells. B cells are made and mature in bone marrow and are responsible for production of antibodies and release them into the blood. T cells migrate from the bone marrow through the blood stream and mature in the thymus (Janeway et al., 2001). T lymphocytes are distinguished by the presence of cell surface molecules CD4 and CD8 and are a major source of cytokines production. T lymphocytes expressing CD4 are known as helper T cells and are subdivided into Th1, Th2, Th17 and inducible regulatory T cells (Paul and Zhu, 2010). The cytokines produced by Th1 and Th2 cells are known as Th1-type cytokines and Th2-type cytokines (Berger, 2000). The cytokines produced by Th1 cells, tend to produce an inflammatory response. Th1 cells mount a host defense against intracellular pathogens such as protozoa, bacteria, and viruses (Butcher and Zhu, 2021) meanwhile Th2 cells participate in different types of allergic disease, but they important in helping to mount a defense against extracellular parasites infections and exposure to venoms (Paul and Zhu, 2010).

Other component of blood such as platelets, possess immune receptors and produce inflammatory molecules (Semple et al., 2011). Platelets also contribute in recruiting leukocytes, principally neutrophils, to the affected site (Kolaczkowska and Kubes, 2013). New findings suggest that red blood cells (RBCs), which develop in bone marrow, are also components of inflammatory responses, as Lam et al. (2021) showed that RBCs serve as critical immune sensors through surface expression of the nucleic acid–sensing Toll-like receptor 9 (TLR9).

In humans, metabolic reprogramming of immune cells has a critical influence on their function (Rodriguez-Coira et al., 2021). For example, sphingolipids are involved in dendritic cell maturation, activation, and migration (Park and Im, 2019). Metabolites such as succinate and citrate have been identified to be involved in innate immune responses by acting as signals in inflammation (Corcoran and O'Neill, 2016). In addition, short chain fatty acids (SCFA) and biogenic amines, enhance dendritic cell regulatory activity (Tan et al., 2014).

Therefore, understanding the impact of different metabolites on metabolic reprogramming of immune cells is important to improve diagnosis, prognosis, and therapeutic personalized medicine strategies in humans (Rodriguez-Coira et al., 2021). In this regard, pigs serve in biomedical research as an animal model because of their similarity with human physiology. Therefore, understanding the relationship of metabolites and immune response cells in pigs can offer insights for human physiology and immune response.

In the last decade, metabolomics has been used to discover biomarkers of disease in different livestock species as well as in animal genetic studies because it provides the potential to identify new phenotypes or traits which can be used to select for more efficient and resilient animals (Montgomery et al., 2009; Widmann et al., 2013; Karisa et al., 2014; Dervishi et al., 2018a; Dervishi et al., 2018b; Carmelo et al., 2020; Li et al., 2020). It is therefore important to understand the genetic architecture of these potential new phenotypes and their relationship with immune response.

The importance of health and the immune system in relation to productivity in pigs facing disease challenge has been described (Bai et al., 2020; Cheng et al., 2020). Bai et al. (2020) reported that pigs classified as resilient initiated a faster adaptive immune response and recovered earlier following infection showing a greater increase in lymphocyte concentration in blood collected 2- weeks before and 2-weeks after the disease challenge, compared to susceptible pigs. In addition, Bai et al. (2020) reported estimates of heritability of CBC traits and the phenotypic and genetic correlations of CBC traits with growth rate and veterinary treatment rate. Estimates of the heritability of 44 metabolites on young healthy pigs along with estimates of the phenotypic and genetic parameters of plasma metabolite concentration with subsequent performance, disease resilience, and carcass traits under the same natural disease challenge described by Bai et al. (2020) was reported by Dervishi et al. (2021).

The present study is part of a larger project which has identification of predictors of disease resilience in young healthy pigs prior to a disease challenge as its main objective. For this purpose, a natural polymicrobial disease challenge model (Cheng et al., 2020; Bai et al., 2020) was established and numerous samples and traits were collected before and after challenge, including complete blood count traits (CBC), average daily gain (ADG), feed intake and feed intake duration (ADFI and ADFD), number of individual health treatments (nTRT), mortality, residual feed intake (RFI), and feed conversion ratio (FCR) (Dervishi et al., 2021; Bai et al., 2020; Cheng et al., 2020).

The purpose of this study was to estimate the phenotypic and genetic parameters between CBC traits and plasma metabolite concentrations in plasma samples collected on young healthy pigs, prior to the disease challenge. Furthermore, we attempted to identify genomic regions that control the genetic variance of metabolites that are genetically correlated with CBC, resilience, and production traits.

Material and methods

Ethics statement

The experiment was carried out in accordance with the Canadian Council on Animal Care guidelines (CCAC, 1993) and (Kilkenny et al., 2010) Animal Research: Reporting of *In Vivo*

Experiments guidelines ARRIVE; https://arriveguidelines.org; (Percie du Sert et al., 2020). The animal experiments were performed with the approval of the Animal Protection Committee of the Centre de Recherche en Sciences Animales de Deschambault (15PO283) and the Animal Care and Use Committee at the University of Alberta (AUP00002227).

Experimental design

All the details of the polymicrobial challenge together with phenotypes/traits that were collected were described by Putz et al. (2019), Cheng et al. (2020) and Bai et al. (2020). Briefly, healthy F1 crossbred (Landrace × Yorkshire) castrated male weaned pigs were provided in rotation by seven genetic suppliers, all members of the PigGen Canada research consortium. Each batch consisted of approximately 65 or 75 pigs from a healthy multiplier farm from one of the genetic suppliers (Bai et al., 2020). All weaned pigs arrived at an average age of 21 days and were housed in a quarantine nursery (Supplementary Figure S1). At approximately 40 days of age, pigs were transferred to the test station late nursery (challenge nursery) and exposed to multiple pathogens through contact with the previous batch that entered 3-weeks prior. Pigs were sent for slaughter when they reached the slaughter weight of 130 kg, at approximately 181 days of age (Bai et al., 2020).

Jugular blood was collected into K2 ethylenediaminetetraacetic acid (EDTA) tubes (BD Vacutainer, Blood Collection Tubes, United States) from all pigs in the quarantine nursery 5 days post-arrival at average 26 days of age (Bai et al., 2020) for CBC and metabolomics analysis. Complete blood count, number of treatments, mortality, growth rate, feed intake and feed efficiency, were collected from a total of 3,205 F1 crossbred pigs, either when sent to slaughter or euthanized at humane end points specified for animal welfare.

All animals were genotyped using a 650 k Affymetrix Axiom Porcine Genotyping Array at Delta Genomics (Edmonton AB, Canada). Raw Affymetrix SNP data were processed by Delta Genomics, separately for each cycle, using the Axiom Analysis Suite. All the details of genotyping and quality control have been previously described (Putz et al., 2019; Bai et al., 2020; Cheng et al., 2020). A total of 417,443 SNPs for 3,205 pigs remained after quality control and were used for analysis (Dervishi et al., 2021).

Complete blood count and metabolomics traits

In this study we used CBC and metabolomics data obtained from blood samples collected in the quarantine nursery from 968 pigs. Details of the CBC and metabolomic data have been described by Bai et al. (2020) and Dervishi et al. (2021) respectively. CBC analysis was performed using the ADVIA® 2120i Hematology System (Siemens Healthineers, Erlangen, Germany). A total of 15 CBC traits were included: concentration of total white blood cell concentration (WBC, 10^3/μL), neutrophils (NEU, 10^3/μL), lymphocytes (LYM, 10^3/μL), monocytes (MONO, 10^3/μL), eosinophils (EOS, 10^3/μL), basophils (BASO, 10^3/μL), red blood cells (RBC, 10^6/μL), hemoglobin (HGB, g/L), hematocrit (HCT, %), mean corpuscular volume (MCV, fL), mean corpuscular hemoglobin (MCH, pg), mean corpuscular hemoglobin concentration (MCHC, g/L), red blood cell distribution width (RDW, %), platelet concentration (PLT, 10^3/μL), and mean platelet volume (MPV, fL). Descriptive statistics including mean and standard deviation values of CBC traits by batch, for the pigs included in the analysis, are shown in Supplementary Table S1.

Details of metabolomics analysis are described in Dervishi et al. (2021). In order to remove plasma macromolecules, samples were thawed on ice and a deproteinization step, involving ultra-filtration was performed (Psychogios et al., 2011). Prior to filtration process, a 3 kDa cut-off centrifugal filter units (Amicon Microcon YM-3), were rinsed five times each with 0.5 mL of H_2O and centrifuged (10,000 rpm for 10 min) to remove residual glycerol bound to the filter membranes. To remove macromolecules from the sample (primarily protein and lipoproteins), aliquots of each sample were transferred into the centrifuge filter devices and spun at 10,000 rpm during 20 min (Dervishi et al., 2021). After collecting the filtrates, the volumes for each sample were recorded. If the total volume of the sample was under 250 μL an appropriate amount of 150 mM KH_2PO_4 buffer (pH 7) was added and the dilution factor was annotated and metabolite concentrations were corrected in the subsequent analysis. Thereafter, 46.5 μL of a standard buffer solution (54% D_2O:46% 1.75 mM KH_2PO_4 pH 7.0 v/v containing 5.84 mM DSS (2,2-dimethyl-2-silcepentane-5-sulphonate), 5.84 mM 2-chloropyrimidine-5 carboxylate, and 0.1% NaN_3 in H_2O) was added to the sample (Dervishi et al., 2021). After preparation step, plasma samples (250 μL) were transferred in 3 mm SampleJet NMR tubes for spectral analysis and ^{1}H-NMR spectra were collected on a 700 MHz Avance III (Bruker) spectrometer equipped with a 5 mm HCN Z-gradient pulsed-field gradient (PFG) cryoprobe (Dervishi et al., 2021). ^{1}H-NMR spectra were acquired at 25°C using the first transient of the NOESY pre-saturation pulse sequence (noesy1dpr), chosen for its high degree of quantitative accuracy (Saude et al., 2006). All free induction decays (FID's) were zero-filled to 250 K data points. The singlet produced by the DSS methyl groups was used as an internal standard for chemical shift referencing (set to 0 ppm). The quantification all ^{1}H-NMR spectra were processed and analyzed using an in-house version of the MAGMET automated analysis software package using a custom metabolite library (Dervishi et al., 2021). MAGMET allows for qualitative and quantitative analysis of an NMR spectrum by automatically fitting spectral signatures from an internal database to the spectrum. This fitting procedure provides absolute concentration accuracy of 90% or better (Ravanbakhsh et al., 2015). An NMR spectroscopist inspected all spectra to minimize compound misidentification and misquantification (Dervishi et al., 2021). A representative NMR spectrum with assignments it is provided in Supplementary Figure S2.

Forty-four metabolites were quantified: amino acids (AAs), short chain fatty acids (SCFA), sugars, alcohols, organic acids, amines, TCA cycle intermediates and urea cycle intermediates (Dervishi et al., 2021). In addition, two indexes were calculated: 1) ketogenic amino acids (ketoAA), calculated as the sum of L-lysine and L-leucine and 2) the sum of branched amino acids (BCAA) that was calculated as the sum of L-leucine, L-isoleucine and L-valine (Dervishi et al., 2021). Dervishi et al. (2021) reported that the concentrations of 33 metabolites were heritable; in the present

study we only considered these for estimation of genetic correlations between CBC and metabolite traits and subsequent GWAS. The observations for leukocyte count (white blood cells) and concentrations of 2-hydroxybutyrate and L-alpha aminobutyric acid were not normally distributed and, therefore, were log-transformed before statistical analyses.

Estimation of genetic correlations

Genetic correlations of metabolite with CBC traits were estimated using AIREMLF90 of the BLUPF90 programs (Misztal et al., 2002), with the following bivariate mixed linear model described by Dervishi et al. (2021):

$$\Upsilon_{ijk} = Batch_i + Age_{ijk} + Pen_j + Litter_{ijk} + u_{ijk} + e_{ijk}$$

where Υ_{ijk} is the phenotype for the trait (metabolite, CBC) for one of the 968 analyzed pigs; $Batch_i$ is the fixed effect (i = 1, . . ., 15); Age_{ijk} is the covariate of age when the pig entered the quarantine nursery; Pen_j is the random effect of nursery pen by batch, with $Pen_j \sim N(0, \sigma^2_P)$, where σ^2_P is pen variance; $Litter_{ijk}$ is the common environmental effect associated with litter, with $Litter_{ijk} \sim N(0, \sigma^2_L)$, where σ^2_L is the litter environmental variance; u_{ijk} is the random additive genetic effect, with the vector $\boldsymbol{u} \sim N(\mathbf{0}, \mathbf{G}\sigma^2_A)$, where $\mathbf{G}$ is the genomic relationship matrix and σ^2_A is the additive genetic variance; and e_{ijk} is the residual effect, with $e_{ijk} \sim N(0, \sigma^2_e)$, where σ^2_e is the residual variance (Dervishi et al., 2021). Environmental enrichment was included as fixed effect for 3-methyl 2-oxovaleric acid and amino acids L-ornithine, L-leucine, L-valine, L-asparagine because it was previously found to be significant ($p \leq 0.05$; Dervishi et al., 2021). The genomic relationship matrix, **G**, was created using the software preGSf90 (Misztal et al., 2002) and the method described by VanRaden (2008). Matrix **G**, was first created separately for pigs from each of the seven companies and thereafter combined into one **G** matrix. In order to focus on the within-company variance components, genetic relationships between companies was set to zero as described by Cheng et al. (2020). In addition, we estimated phenotypic and genetic correlations among metabolites that belong to the same pathway. Genetic correlations between two traits were estimated as the estimate of the genetic covariance from the bivariate analysis divided by the product of the genetic standard deviations for the two traits. A likelihood ratio test with 1 degree of freedom was used to determine the significance of correlation estimates (Dervishi et al., 2021).

GWAS and functional analyses

Phenotypic data (concentration of 33 plasma metabolites) were available for 968 F1 crossbred pigs and genotypic data were available for 3,205 F1 crossbred pigs. The complete pedigree for 3,205 pigs was unavailable due to the use of pooled semen in some batches (Bai et al., 2020), however dam information was available for 3,194 pigs and sire information was available for 1,138 pigs.

Single step genome-wide association study (ssGWAS), was performed using the programs of BLUPF90 software family (Misztal et al., 2002; Wang et al., 2014), modified to account for genomic information (Geiger et al., 2016). Single step GWAS integrates pedigree and genomic data in a single step (**H** matrix; Geiger et al., 2016). The inverse of **H** matrix needed for mixed model equations is given by:

$$\mathbf{H}^{-1} = \mathbf{A}^{-1} + \begin{bmatrix} 0 & 0 \\ 0 & \mathbf{G}^{-1} - \mathbf{A}_{22}^{-1} \end{bmatrix}$$

where $\mathbf{A}^{-1}$ is the inverse of the numerator relationship matrix; $\mathbf{A}_{22}^{-1}$ is the inverse of the pedigree relationship matrix; and $\mathbf{G}^{-1}$ is the inverse of the genomic relationship matrix. The genomic relationship matrix (**G**) was constructed as: G = ZDZ′q (VanRaden, 2008); where Z is the incidence matrix containing genotypes (aa = 0, Aa = 1 and AA = 2) adjusted for allele frequency, **D** is a diagonal matrix of weights for SNP markers (initially D = I), and q is a weighting factor. The weighting factor was as in Vitezica et al. (2011), ensuring that the average diagonal in G is close to that of A_{22}. The genomic estimated breeding value (GEBV, $\hat{\mathbf{a}}_\mathbf{g}$) was calculated by ssGBLUP and the solutions of the SNP effects ($\hat{\mathbf{u}}$) were obtained using the AIREMLF90 (Wang et al., 2012) algorithm. Briefly, on the first step, set **D** = **I**, which gives a weight of 1 to all SNP, and **G** = ZDZ′q where **G** is the genomic relationship matrix. On the second step we estimated $\hat{\mathbf{a}}_\mathbf{g}$, which were converted to SNP effects: $\hat{\mathbf{u}}$ = λDZ'G−1 $\hat{a}_g$, where $\hat{a}_g$ is the GEBV of genotyped animals. This process was run for one iteration.

In this study, SNPs located within 0.5 Mb were grouped as a single window, and the percentage of genetic variance (GV) explained by each window was calculated using the postGSF90 module as: $[Var(a_i)/\sigma^2 a]$ x 100%, where a_i is the genetic value of the ith SNP window and $\sigma^2 a$ is the additive GV (Wang et al., 2014). The results of GWAS were reported as the proportion of the genetic variance explained by non-overlapping genomic windows (0.5 Mb). The windows that explained equal to or greater than 0.5% of the genetic variance from ssGWAS were considered as QTL regions (Hong et al., 2020). The model for GWAS was as follow:

$$\boldsymbol{Y} = \boldsymbol{Xb} + \boldsymbol{Wc} + \boldsymbol{Ul} + \boldsymbol{Za} + \boldsymbol{e}$$

where $\boldsymbol{Y}$ is the vector of the phenotypes (metabolite concentration); $\boldsymbol{b}$ is the vector of fixed effects (batch and covariate of age when the pig entered the quarantine nursery); $\boldsymbol{X}$ is the incidence matrix relating observations to the fixed effects, $\boldsymbol{c}$ is the vector for the random pen effect; $\boldsymbol{W}$ is the incidence matrix of the random pen effect; $\boldsymbol{l}$ is the vector of for the random litter effect; $\boldsymbol{U}$ is the incidence matrix of the random litter effects; **a** is the vector of direct additive genetic effects; **Z** is the incidence matrix of random animal effects; and **e** is a vector of the random residuals.

Batches were nested within farms and coded uniquely; therefore population stratification was accounted for in the association analysis by fitting batch as the fixed effect in the model (Bai et al., 2020).

The identification of candidate genes was performed using *Sus scrofa* genome version 11.1 in BioMart (http://uswest.ensembl.org/biomart/martview/73240e1280d6d0c946725fde6eb27af9). Genecards (https://www.genecards.org/) was used to investigate the gene function based on orthologous genes of humans. Candidate genes were also compared with the information about QTLs reported in QTLdb (Hu et al., 2016; http://www.animalgenome.org/cgi-bin/QTLdb/index).

The Metscape plugin (Karnovsky et al., 2012) in Cytoscape 3.8.2 (Shannon et al., 2003) was used to explore and visualize the biochemical pathway that metabolites are involved in. Metabolites that had significant ($p \leq 0.05$) genetic correlations with traits of interest (example: NEU, MONO, EOS, BASO, LYM, ADG) were used for network visualization. In order to generate a gene-compound network, a file containing the list of KEGG elements was loaded into Metscape following instructions provided by (Karnovsky et al., 2012). In a gene-compound network, genes and metabolites are represented as nodes and reactions are represented as edges. A compound node with an outgoing edge is a substrate, while a compound node with an incoming edge is the product of a specific biochemical reaction (Dervishi et al., 2021).

Results

Phenotypic correlations

In general, estimates of phenotypic correlations of the metabolites with CBC were small (Supplementary Figure S3). The estimate of greatest magnitude was between L-glutamic acid and PLT. L-lactic acid was positively correlated with BASO, WBC, NEU, EOS, and MPV, while it showed negative phenotypic correlation with MCHC ($p < 0.05$). Pyruvic acid showed positive phenotypic correlation estimates with HCT, MCV, MCH ($p < 0.05$), and negative correlations with PLT, RDW, and MPV ($p < 0.05$). D-glucose showed negative phenotypic correlation estimates with NEU, BASO, EOS, MONO, LYM, and MPV. Furthermore, L-alanine showed negative phenotypic correlation with MCHC (Supplementary Table S2; $p < 0.05$). Finally, oxoglutarate was positively correlated with HGB ($p < 0.05$). A scatter plot showing the negative correlations between pyruvic acid, D-glucose and CBC traits is shown in Supplementary Figure S4.

The phenotypic correlation between metabolites that are involved in the same pathway (betaine, dimethylglycine, L-glycine, L-glutamic acid, L-serine, oxoglutarate, L-glutamine and methionine) are shown in Table 3. The highest significant positive correlation was observed between oxoglutarate an L-glutamic acid.

Genetic correlations

Overall, estimates of genetic correlations of the metabolites with CBC traits were larger than phenotypic correlations (Tables 1, 2) but had larger SE. Table 1 shows the estimates of genetic correlation between metabolites and white blood cell traits. Some metabolites showed significant correlation estimates ($p < 0.05$) with white blood cell traits. For example, a high negative genetic correlation between NEU and plasma L-lysine was observed ($p < 0.05$). L-glutamine was positively correlated with NEU ($p < 0.05$) and L-aspartate was positively correlated with MONO ($p < 0.05$). 2-hydroxybutyrate, 3-methyl-2-oxovaleric acid and L-alpha aminobutyric acid had positive genetic correlation estimates with EOS, while dimethylglycine was negatively correlated with EOS concentration ($p < 0.05$). Positive genetic correlations were estimated for WBC with the amino acids L-asparagine and L-glutamic acid ($p < 0.05$). Lymphocyte concentration was positively correlated with isobutyric acid and L-histidine ($p < 0.05$), while LYM was negatively correlated with hypoxanthine and L-ornithine ($p < 0.05$; Table 1).

Overall, we found a higher number of significant genetic correlation between metabolites and leukocytes than RBC or platelets traits. Therefore, metabolites that were genetically correlated with leukocytes traits are visualized in a compound network in Figure 1. These metabolites are involved in different metabolic pathways, including vitamin H (biotin) metabolism, vitamin B9 (folate) metabolism, urea cycle and metabolism of arginine, proline, glutamate, aspartate and asparagine, histidine metabolism, glycine, serine, alanine and threonine metabolism.

Estimates of genetic correlations between metabolites and RBC and platelet traits are shown in Table 2. L-proline was highly genetically positively correlated with HGB ($p < 0.05$) and HCT ($p < 0.05$). A high negative genetic correlation was observed for L-tyrosine with MCV ($p < 0.05$) and MCH ($p < 0.05$). In addition, L-glycine was positively correlated at the genetic level with MCH ($p < 0.05$). L-alanine (-$p < 0.05$) and L-alpha-aminobutyric acid ($p < 0.05$) were negatively correlated with RDW. Furthermore L-alanine was positively correlated with PLT ($p < 0.05$). Finally, the amino acid L-methionine was negatively correlated with MPV ($p < 0.05$). Basophils, RBC, platelets, MCHC, and MCV were not genetically correlated with any of the metabolites. The genetic correlation between metabolites that are involved in the same pathway are shown in Table 3 (below diagonal). The highest significant positive correlation was observed between oxoglutarate and L-glutamic acid followed by the correlation between L-serine and L-glycine.

GWAS

GWAS was performed for L-alpha aminobutyric acid, L-aspartate, L-asparagine, L-glutamic acid, L-glutamine, L-glycine, L-histidine, L-lysine, L-methionine, L- ornithine, L-serine, betaine, creatinine, dimethylglycine, hypoxanthine, isobutyric acid, oxoglutarate, 2-hydroxybutyrate and 3-methyl-2 oxovaleric acid because in the present study they were estimated to be genetically correlated with CBC, and in a previous study they were genetically correlated with resilience, or production traits (Dervishi et al., 2021).

For L-glutamic acid, the five most important windows were located on SSC14 and explained 7% of the genetic variance (Table 4). In addition, for L-tyrosine two windows on SSC1 explained 1.4% and 2.56% of the genetic variance. For L-asparagine, the most important window explained 1.1% of the genetic variance was found on SSC6. For creatinine a window on SSC12 explained 1.2% of the genetic variance and for hypoxanthine a window on SSC4 explained 1.2% of the genetic variance. One window on SSC6 explained 1.1% of the genetic variance for L-aspartate. Finally, one window on SSC2 explained 1.1% of the genetic variance of isobutyric acid.

The results of GWAS showed that some windows overlapped for some of the metabolites. For example, the window on SSC14

TABLE 1 Estimates and standard errors (SE) of genetic correlations of metabolite correlations[a] with white blood cells traits[b].

Metabolite	NEU	MONO	EOS	BASO	LYM	WBC
2-Hydroxybutyrate	0.07 (0.73)	−0.21 (0.70)	**0.86 (0.78)****	0.51 (0.80)	0.31 (0.79)	0.11 (0.02)
3-Methyl-2-oxovaleric acid	−0.04 (0.63)	0.41 (1.0)	**0.68 (0.05)***	0.37 (2.32)	−0.45 (0.85)	−0.30 (0.79)
Betaine	−0.25 (0.27)	0.06 (0.28)	0.06 (0.20)	−0.12 (0.9)	−0.013 (0.23)	−0.12 (0.29)
Citric acid	-	0.22 (0.34)	-	−0.45 (0.78)	-	−0.01 (0.37)
Creatinine	−0.09 (0.27)	−0.08 (0.26)	−0.08 (0.20)	0.35 (0.78)	0.12 (0.22)	−0.09 (0.30)
D-glucose	−0.28 (0.34)	−0.29 (0.35)	0.04 (0.3)	−0.65 (0.77)	−0.006 (0.31)	-
Dimethylglycine	−1.06 (1.48)	0.20 (0.40)	**−0.37 (0.20)***	−0.5 (0.80)	0.59 (0.60)	−0.29 (0.29)
Hypoxanthine	0.11 (0.28)	−0.22 (0.29)	0.12 (0.18)	−0.33 (3.81)	**−0.42 (0.23)***	−0.02 (0.29)
Isobutyric acid	0.10 (0.42)	−0.06 (0.45)	0.043 (0.06)	0.85 (1.32)	**0.69 (0.35)*****	0.37 (0.40)
L-alanine	0.45 (0.52)	0.02 (0.5)	−0.72 (1.05)	−0.06 (0.04)	-	0.12 (0.47)
L-alpha-aminobutyric acid	0.56 (0.44)	0.40 (0.36)[X]	**0.75 (0.51)***	0.70 (0.87)	**1.0 (0.90)***	0.86 (0.86)
L-asparagine	0.41 (0.54)	−0.01 (0.51)	0.19 (0.40)	0.73 (1.54)	0.56 (0.69)	**0.74 (0.58)***
L-aspartate	0.34 (0.85)	**0.66 (0.58)***	0.09 (0.30)	0.86 (1.89)	0.10 (0.36)	0.15 (0.50)
L-glutamine	**0.75 (0.30)*****	−0.08 (0.25)	0.11 (0.18)	0.56 (0.89)	0.06 (0.20)	**0.51 (0.29)***
L-glutamic acid	-	0.01 (0.27)	0.27 (0.12)	0.61 (0.92)	−0.0035 (0.2)	**0.41 (0.06)****
L-glycine	0.02 (0.26)	0.02 (0.35)	−0.14 (0.20)	0.06 (0.64)	0.26 (0.23)	−0.04 (0.29)
L-histidine	−0.006 (0.38)	−0.04 (0.35)	0.01 (0.02)	0.67 (3.09)	**0.33 (0.29)***	-
L-isoleucine	−0.08 (0.86)	0.11 (6.0)	0.50 (0.69)	0.33 (1.18)	−0.58 (0.69)	0.11 (0.02)
L-Lactic acid	0.19 (0.42)	0.0003 (0.4)	0.13 (0.26)	0.57 (0.68)	−0.01 (0.30)	−0.17 (0.50)
L-lysine	**−0.81 (0.4)***	−0.17 (0.32)	0.19 (0.24)	−0.02 (0.72)	0.16 (0.26)	−0.32 (0.56)
L-leucine	−0.09 (0.46)	0.77 (0.81)	0.27 (0.30)	0.43 (0.95)	−0.07 (0.36)	−0.26 (0.56)
L-methionine	0.22 (0.45)	−0.51 (0.52)	0.39 (0.29)[X]	−0.08 (0.1)	−0.26 (0.36)	-
L-ornithine	−0.34 (0.33)	-	−0.10 (0.21)	−0.39 (0.64)	**−0.42 (0.21)***	-
L-phenylalanine	−0.56 (0.95)	0.79 (0.51)	-	0.43 (1.08)	−0.15 (0.49)	−0.51 (1.35)
L-proline	0.34 (0.69)	0.004 (1.01)	−0.04 (0.01)	0.45 (1.03)	-	0
L-serine	−0.23 (0.48)	−0.26 (0.44)	−0.04 (0.31)	−0.19 (0.96)	0.37 (0.43)	0.006 (0.4)
Oxoglutarate	-	−0.32 (0.55)	0.25 (0.20)	0.56 (0.94)	−0.20 (0.1)	−0.33 (0.71)
Pyruvic acid	−0.03 (0.32)	0.18 (0.33)	0.13 (0.23)	0.70 (0.97)	0.36 (0.24)[X]	0.42 (0.36)
L-threonine	−0.49 (1.57)	−0.24 (0.86)	−0.75 (1.12)	−0.03 (1.37)	0.07 (0.52)	−0.31 (0.65)
L-tyrosine	-	0.12 (0.93)	−0.1 (0.33)	0.28 (1.0)	−0.16 (0.40)	−0.15 (0.97)
L-valine	−0.14 (0.55)	0.03 (0.54)	0.08 (0.37)	0.52 (0.81)	−0.06 (0.41)	−0.06 (0.67)
BCAA	−0.12 (0.48)	-	0.22 (0.34)	0.45 (0.81)	−0.18 (0.39)	−0.25 (1.24)
KetoAA	**−0.81 (0.59)***	0.21 (1.27)	0.25 (0.27)	0.10 (0.87)	0.12 (0.30)	−0.33 (0.71)

[a]BCAA, Branched-chain amino acid index was calculated as the sum of L-leucine, L-isoleucine and L-valine and ketoAA, ketogenic amino acids was calculated as the sum of L-lysine and L-leucine.

[b]NEU, neutrophil concentration (10^3/μL); MONO, monocyte concentration (10^3/μL); EOS, eosinophil; BASO, basophil concentration (10^3/μL); LYM, lymphocyte concentration (10^3/μL); WBC, total white blood cell concentration (10^3/μL).

Significance of the genetic correlations are highlighted in bold based on the likelihood ratio test and indicated as ***, **, *, [X], corresponding to $p < 0.001$, $p < 0.01$ and $p \leq 0.05$, and $0.05 < p < 0.10$ respectively; "-" indicates not estimable.

(49,337,114–49,836,497 bp) explained some of the genetic variance for both L-glutamic acid and glutamine. In this window a total of 10 genes were found (*SPECC1L, ADORA2A, UPB1, GUCD1, LRRC75B, GGT5, SUSD2, CABIN1, DDT, GSTT4*). Another window on SSC2 (87,468,329–87,968,307 bp) was found to explain genetic variance for both betaine and dimethylglycine.

10.3389/fmolb.2023.1140375

TABLE 2 Estimates and standard errors (SE) of genetic correlations of metabolite concentrations[a] with red blood cell and platelet traits[b].

Metabolite	RBC	HGB	HCT	MCV	MCH	MCHC	RDW	PLT	MPV
2-Hydroxybutyrate	0.05 (0.41)	0.05 (1.27)	0.21 (1.27)	0.03 (0.4)	−0.25 (0.37)	0.07 (0.7)	−0.83 (0.03)	−0.78 (0.83)	−0.2 (0.42)
3-Methyl-2-oxovaleric acid	0.29 (0.64)	0.62 (2.06)	0.51 (2.0)	−0.36 (0.45)	−0.48 (0.07)	−0.08 (0.74)	0.43 (0.08)	−1.02 (2.25)	0.52 (0.80)
Betaine	0.26 (0.25)	0.37 (0.50)	0.68 (1.09)	−0.07 (0.20)	0.03 (0.19)	−0.01 (0.31)	0.45 (0.30)	*0.48 (0.46)*	−0.04 (0.26)
Citric acid	0.007 (0.26)	−0.17 (0.57)	0.37 (0.58)	0.11 (0.20)	−0.18 (0.21)	−0.11 (0.4)	−0.78 (1.48)	0.13 (0.42)	−0.14 (0.26)
Creatinine	0.04 (0.23)	0.19 (0.47)	−0.12 (0.68)	0.11 (0.18)	0.19 (0.18)	0.04 (0.28)	−0.75 (0.90)	−0.08 (0.34)	−0.06 (0.33)
D-glucose	−0.05 (0.30)	−0.56 (0.72)	−0.25 (0.58)	−0.11 (0.26)	−0.06 (0.27)	0.33 (0.54)	−0.22 (1.15)	-	0.02 (0.34)
Dimethylglycine	−0.03 (0.24)	0.07 (0.4)	0.21 (0.49)	0.08 (0.18)	0.18 (0.18)	−0.17 (0.27)	0.50 (0.10)	-	0.17 (0.25)
Hypoxanthine	0.21 (0.22)	0.48 (0.52)	**0.63 (0.49)***	0.21 (0.16)	0.08 (0.28)	0.08 (0.28)	−0.30 (0.76)	−0.42 (0.4)	−0.02 (0.23)
Isobutyric acid	−0.20 (0.35)	0.27 (0.66)	−0.13 (0.71)	0.17 (0.31)	0.18 (0.34)	0.49 (0.52)	−0.76 (0.04)[X]	−0.44 (0.90)	−0.17 (0.36)
L-alanine	0.54 (0.48)[X]	0.44 (1.06)	0.17 (0.06)	0.11 (0.28)	0.09 (0.28)	−0.36 (0.43)	**−0.64 (0.05)***	**0.98 (0.05)****	0.07 (0.39)
L-alpha-aminobutyric acid	0.14 (0.32)	0.24 (0.67)	0.56 (0.69)	0.26 (0.31)	0.06 (0.30)	−0.07 (0.37)	**−0.98 (0.03)****	−0.85 (1.54)	−0.13 (0.33)
L-asparagine	−0.02 (0.55)	0.07 (1.33)	0.29 (0.92)	0.32 (0.52)	0.40 (0.59)	0.2 (0.81)	−0.10 (1.41)	−0.30 (2.17)	−0.42 (0.91)
L-aspartate	0.05 (0.40)	−0.36 (0.59)	−0.35 (0.73)	−0.24 (0.29)	−0.16 (0.38)	0.25 (0.44)	−0.52 (1.23)	−0.54 (0.73)	0.01 (0.04)
L-glutamine	0.07 (0.22)	0.37 (0.62)	0.36 (0.60)	0.18 (0.17)	0.16 (0.18)	0.16 (0.28)	−0.32 (0.88)	−0.56 (0.55)	−0.21 (0.23)
L-glutamic acid	0.03 (0.23)	0.03 (0.39)	−0.08 (0.48)	−0.12 (0.16)	−0.01 (0.17)	0.22 (0.26)	−0.42 (0.06)	−0.47 (0.07)	−0.10 (0.23)
L-glycine	0	0.09 (0.59)	0.27 (0.59)	0.13 (0.18)	**0.45 (0.17)****	0.26 (0.29)	−0.19 (0.94)	0.16 (0.45)	0.23 (0.25)
L-histidine	−0.02 (030)	0.19 (0.56)	−0.73 (0.88)	−0.20 (0.24)	0.17 (0.23)	0.37 (0.34)	−0.36 (0.80)	−0.72 (1.05)	−0.21 (0.39)
L-isoleucine	0.55 (0.75)	0.97 (0.25)[X]	0.82 (1.78)	−0.26 (0.50)	−0.34 (0.52)	−0.03 (0.78)	0.08 (1.35)	−0.68 (1.11)	0.33 (0.77)
L-Lactic acid	0.61 (0.71)	0.93 (1)	0.67 (0.85)	−0.002 (0.38)	−0.02 (0.39)	−0.26 (0.54)	−0.25 (2.09)	-	−0.38 (0.61)
L-lysine	0.15 (0.32)	0.04 (0.59)	−0.02 (0.71)	−0.27 (0.25)	−0.19 (0.24)	0.29 (0.33)	−0.65 (0.05)	−0.24 (0.44)	−0.17 (0.29)
L-leucine	0.42 (0.43)	0.82 (0.90)	0.35 (0.79)	−0.23 (0.32)	−0.12 (0.33)	−0.38 (0.78)	−0.21 (1.45)	−0.14 (0.78)	0.17 (0.48)
L-methionine	0.13 (0.35)	−0.27 (3.57)	0.018 (0.72)	−0.10 (0.39)	−0.33 (0.25)	−0.49 (0.45)	0.75 (0.70)	−0.56 (0.83)	**−0.56 (0.41)***
L-ornithine	−0.11 (0.25)	−0.07 (0.46)	−0.19 (0.62)	*−0.34 (0.21)*	−0.24 (0.22)	−0.07 (0.11)	−0.23 (1.52)	−0.09 (0.40)	0.36 (0.28)
L-phenylalanine	0	−0.14 (1.38)	−0.41 (0.95)	−0.32 (0.47)	−0.34 (0.36)	−0.01 (0.51)	−0.03 (1.25)	−0.49 (0.66)	0.18 (0.60)
L-proline	0.90 (0.97)	**0.94 (0.03)***	**0.70 (0.04)****	0.18 (0.32)	0.08 (0.57)	−0.39 (0.30)	−0.68 (0.06)	0.02 (0.04)	0.20 (0.66)
L-serine	0.01 (0.35)	−0.04 (0.68)	0.6 (1.13)	0.05 (0.27)	0.17 (0.35)	0.27 (0.49)	0.79 (0.70)	−0.007 (0.71)	0.18 (0.38)
Oxoglutarate	0.08 (0.24)	0.12 (0.64)	0.32 (0.61)	−0.007 (0.19)	0.18 (0.19)	0.31 (0.28)	−0.82 (0.10)[X]	−0.54 (0.48)[X]	−0.08 (0.28)
Pyruvic acid	0.18 (0.31)	0.52 (0.83)	0.57 (0.64)	0.07 (0.74)	0.01 (0.26)	−0.47 (0.63)	−0.75 (0.29)	−0.12 (0.51)	−0.06 (0.28)
L-threonine	−0.06 (0.56)	0.01 (0.96)	0.26 (1.63)	0.09 (0.50)	0.04 (0.48)	−0.1 (0.84)	0.92 (0.16)	0.62 (1.63)	−0.12 (0.55)
L-tyrosine	0.44 (0.45)	−0.10 (1.14)	0.37 (0.95)	**−0.73 (0.68)***	**−0.92(0.74)****	−0.42 (0.54)	0.66 (1.02)	−0.20 (0.52)	−0.22 (0.46)
L-valine	0.11 (0.49)	0.48 (1.25)	0.16 (0.98)	−0.15 (0.67)	−0.02 (0.63)	0	-	0.26 (0.97)	0.13 (0.59)
BCAA	0.33 (0.46)	0.69 (0.78)	0.34 (0.99)	−0.21 (0.32)	−0.12 (0.31)	−10 (0.46)	−0.04 (1.32)	−0.12 (0.93)	0.16 (0.42)
KetoAA	0.24 (0.33)	0.24 (0.91)	0.07 (0.65)	−0.33 (0.32)	−0.22 (0.39)	0.17 (0.58)	−0.68 (0.05)[X]	−0.27 (0.63)	−0.16 (0.36)

[a]BCAA, branched-chain amino acid index was calculated as the sum of L-leucine, L-isoleucine and L-valine; ketoAA, ketogenic amino acids was calculated as the sum of L-lysine and L-leucine.
[b]RBC, red blood cell concentration (10^6/μL); HGB, hemoglobin concentration (g/L); HCT, hematocrit (%); MCV, mean corpuscular volume (fL); MCH, mean corpuscular hemoglobin (pg); MCHC, mean corpuscular hemoglobin concentration (g/L); RDW, red blood cell distribution width (%). PLT, platelet concentration (10^3/μL) and MPV, mean platelet volume (fL).
Significance of the genetic correlations are highlighted in bold based on the likelihood ratio test and indicated as ***, **, *, [X], corresponding to $p < 0.001$, $p < 0.01$ and $p \leq 0.05$, and $0.05 < p < 0.10$ respectively; "-" indicates not estimable.

Four genes were located in this window (*ARSB, DMGDH, BHMT2* and *BHMT*). In addition, one window on SSC1 (73,972,391–74,471,148 bp) was found to explain some of percentages of the genetic variance for L-ornithine, L-proline, and L-tyrosine. A total of 5 genes were found in this region (*SEC63, OSTM1, NR2E1, SNX3* and *AFG1L*).

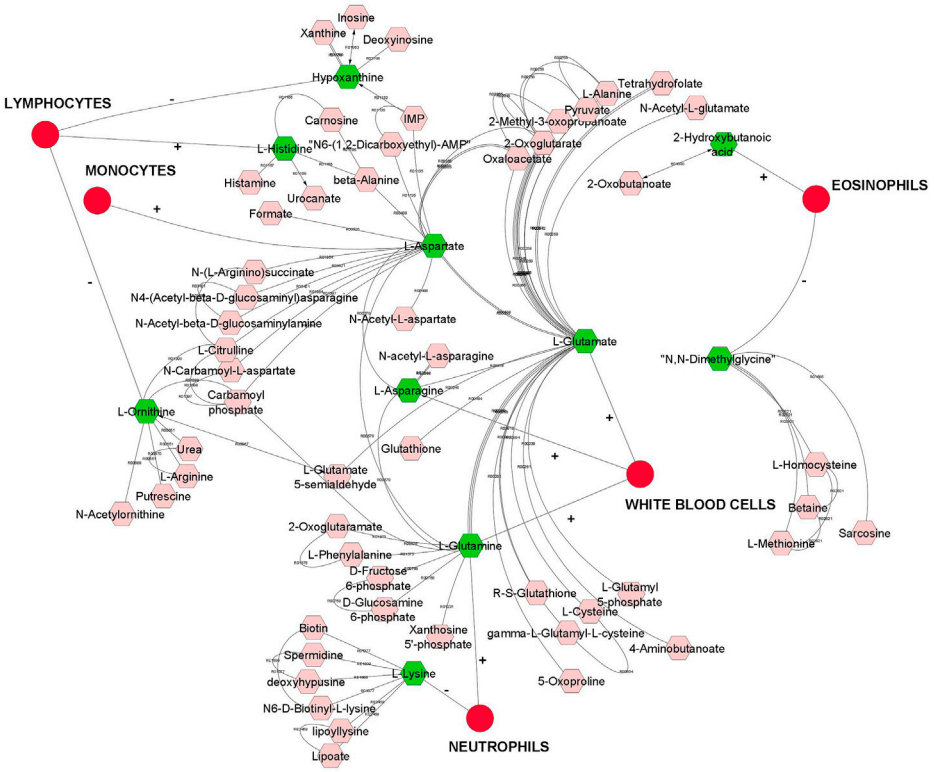

FIGURE 1
A compound network of metabolites that are significantly ($p < 0.05$) genetically correlated with leukocytes (white blood cells). Input metabolites are shown in green color and chemical reactions are represented as edges. Positive or negative sign on the edges represent positive or negative genetic correlation.

TABLE 3 Estimates and standard errors (SE) of genetic correlations (below diagonal) and phenotypic correlation (above diagonal) between metabolites involved in the same pathway.

Metabolites	Betaine	Dimethylglycine	Glycine	L-glutamic acid	L-Serine	Oxoglutarate	L-Glutamine	Methionine
Betaine	1	**0.40 (0.03)****	**0.33 (0.04)***	−0.03 (0.03)	**0.35 (0.03)****	0.01 (0.04)	−0.002 (0.04)	**0.24 (0.04)****
Dimethylglycine	0.28 (0.14)	1	0.09 (0.04)	-	**0.13 (0.04)***	−0.06 (0.04)	**−0.12 (0.04)****	0.029 (0.03)
L-glycine	0.19 (0.19)	0.16 (0.21)	1	**0.20 (0.03)*****	-	**0.25 (0.05)*****	**0.18 (0.03)*****	0.01 (0.04)
L-glutamic acid	−0.14 (0.20)	−0.22 (0.26)	−0.007 (0.18)	1	**0.27 (0.03)****	**0.69 (0.02)*****	**0.42 (0.034)*****	0.09 (0.04)
L-serine	−0.02 (0.47)	0.21 (0.33)	**0.76 (0.52)*****	0.14 (0.29)	1	0.27 (0.03)	**0.22 (0.04)*****	**0.19 (0.04)***
Oxoglutarate	0.002 (0.22)	−0.18 (0.20)	0.22 (0.18)	**0.79 (0.09)*****	0.39 (0.34)	1	**0.27 (0.03)*****	0.05 (0.04)
L-glutamine	**−0.37 (0.20)*****	**−0.28 (0.17)**^{x}	−0.23 (0.21)	0.2 (0.16)	−0.16 (0.34)	**0.38 (0.18)***	1	**0.33 (0.03)*****
L-methionine	0.07 (2.25)	0.07 (0.22)	**−0.59 (0.29)****	0.13 (0.40)	−0.46 (1.43)	0.11 (0.30)	0.3 (0.26)	1

Significance of the genetic and phenotypic correlations are highlighted in bold based on the likelihood ratio test and indicated as ***, **, *, ^{x}, corresponding to $p < 0.001$, $p < 0.01$ and $p \leq 0.05$, and $0.05 < p < 0.10$ respectively; "-" indicates not estimable.

Discovery of common genomic regions for different metabolites led us to further investigate some genes that control the genetic variance of different metabolites. Thus, a compound-gene network of metabolites that had significant ($p < 0.05$) genetic correlations with traits of interest (example: neutrophils, EOS, MCH, ADG and number of veterinary treatments), and for which had overlapping genomic windows that explained genetic variance. Figure 2 shows the input metabolites (in dark purple color) and chemical reactions are represented as edges. The

TABLE 4 Chromosome position (in basepairs) and the proportion of additive genetic variance explained for each metabolite and genes located in the region.

Metabolite	Chromosome	Start (bp)	End (bp)	Variance explained by adjacent SNPs	Gene name
L-alanine	1	77,666,621	78,166,009	0.7	*FYN, U6, CCN6, TUBE1*
	13	148,254,310	148,753,746	0.6	*NECTIN3*
	14	98,696,648	99,196,606	0.54	*PRKG1, A1CF, N-acylsphingosine amidohydrolase 2*
L-asparagine	1	134,389,442	134,886,597	0.71	*CDIN1*
	6	63,321,290	63,818,847	0.65	*NOC2L, KLHL17, PLEKHN1, HES4, ISG15, AGRN, RNF223, ssc-mir-200b, ssc-mir-429, TNFRSF4, SDF4, B3GALT6, C1QTNF12, UBE2J2, ACAP3, PUSL1, INTS11, TAS1R3, DVL1, MXRA8, AURKAIP1, CCNL2, MRPL20, TMEM88B, VWA1, ATAD3A, TMEM240, SSU72, MIB2, MMP23B*
	6	65,142,458	66,987,107	2.49	*TPRG1L, WRAP73, TP73, CCDC27, SMIM1, LRRC47, CEP104, ssc-mir-2320, DFFB, C1orf174, ssc-mir-4331-1, AJAP1, NPHP4, KCNAB2*
L-aspartate	6	24,433,478	24,931,615	1.06	*U2*
	6	25,256,424	25,751,462	0.63	*None*
	6	70,267,482	70,764,647	0.88	*LZIC, NMNAT1, RBP7, UBE4B, KIF1B, U6, PGD, CENPS*
	14	43,982,025	44,481,714	0.82	*SEZ6L, ASPHD2, HPS4, SRRD, TFIP11, TPST2, CRYBB1, CRYBA4*
	14	106,941,420	107,439,174	0.61	*SORBS1, ALDH18A1, TCTN3, ENTPD1, CC2D2B*
	14	107,490,232	107,987,938	0.96	*CC2D2B, CCNJ, ZNF518A, BLNK, DNTT, OPALIN*
L-glutamic Acid	14	44,945,208	45,444,193	1.10	*MN1, PITPNB, TTC28*
	14	46,222,942	46,720,805	1.54	*ZNRF3, C22orf31, KREMEN1, EMID1, RHBDD3, EWSR1, GAS2L1, RASL10A, AP1B1, SNORD125, NEFH, THOC5, NIPSNAP1, NF2*
	14	46,863,516	47,363,323	1.36	*MTMR3, HORMAD2, LIF, OSM, CASTOR1, TBC1D10A, SF3A1, RNF215*
	14	47,569,039	48,065,569	2.06	*OSBP2, MORC2, TUG1, SMTN, SELENOM, INPP5J, PLA2G3, RNF185, LIMK2, PIK3IP1*
	14	49,337,114	49,836,497	0.89	*SPECC1L, ADORA2A, UPB1, GUCD1, LRRC75B, GGT5, SUSD2, CABIN1, DDT, GSTT4*
L-glutamine	12	9,686,276	10,186,144	0.57	*None*
	14	47,589,083	48,088,498	0.65	*OSBP2, MORC2, TUG1, SMTN, SELENOM, INPP5J, PLA2G3, RNF185, LIMK2, PIK3IP1, PATZ1*
	14	49,337,114	49,836,497	0.72	*SPECC1L, ADORA2A, UPB1, GUCD1, LRRC75B, GGT1, GGT5, SUSD2, CABIN1, DDT, GSTT4*
	14	107,490,232	107,987,938	0.54	*CC2D2B, CCNJ, ZNF518A, BLNK, DNTT, OPALIN, TLL2, TM9SF3*
L-glycine	6	41,826,913	42,324,310	0.54	*ZNF507*
	7	85,729,010	86,228,917	0.82	*RGMA, CHD2*
	13	67,207,607	67,707,171	0.53	*HRH1, ATG7, VGLL4*
L-histidine	2	134,063,036	134,562,065	0.53	*FNIP1, MEIKIN, ACSL6, CSF2, P4HA2, PDLIM4*
	6	66,977,105	67,476,230	0.6	*KCNAB2, CHD5, RPL22, RNF207, ICMT, HES3, GPR153, ACOT7, HES2, ESPN, TNFRSF25, PLEKHG5, NOL9, TAS1R1, ZBTB48, KLHL21, PHF13, THAP3, DNAJC11*
	7	49,996,822	50,495,753	0.69	*IL16, STARD5, TMC3*
	10	8,877,853	9,376,716	0.58	*LYPLAL1*
	14	9,447,641	9,946,090	0.6	*GNRH1, KCTD9, CDCA2, EBF2*

(Continued on following page)

TABLE 4 (*Continued*) Chromosome position (in basepairs) and the proportion of additive genetic variance explained for each metabolite and genes located in the region.

Metabolite	Chromosome	Start (bp)	End (bp)	Variance explained by adjacent SNPs	Gene name
L-lysine	1	73,972,391	74,471,148	1.02	*SEC63, OSTM1, NR2E1, SNX3, AFG1L*
	1	74,474,926	74,974,129	0.58	*AFG1L, FOXO3, ARMC2*
	15	107,259,807	107,753,851	0.74	*CTLA4, ICOS*
	16	25,159,487	25,656,089	0.63	*None*
L-methionine	4	72,410,298	72,909,455	0.51	*CHD7, RAB2A*
	14	99,323,188	99,821,978	0.54	*MINPP1, PAPSS2, ATAD1*
L-ornithine	1	73,972,391	74,471,148	0.92	*SEC63, OSTM1, NR2E1, SNX3, AFG1L*
	1	8,554,166	9,054,053	0.89	*DYNLT1, TMEM181, GTF2H5, SERAC1, SYNJ2*
	3	9,162,389	9,658,871	0.56	*collagen type XXVI alpha 1 chain, MYL10, CUX1*
L-proline	1	73,972,391	74,471,148	0.58	*SEC63, OSTM1, NR2E1, SNX3, AFG1L*
	1	116,533,603	117,031,491	0.57	*RAB27A, RSL24D1*
	6	65,802,953	66,302,936	0.58	*AJAP1*
L-Serine	6	65,676,029	66,175,375	0.65	*AJAP1*
	14	46,499,201	46,998,737	0.54	*AP1B1, NEFH, THOC5, NIPSNAP1, NF2, CABP7, ZMAT5, UQCR10, ASCC2, MTMR3*
	14	47,569,039	48,065,569	0.62	*OSBP2, MORC2, TUG1, SMTN, SELENOM, INPP5J, PLA2G3, RNF185, LIMK2, PIK3IP1*
	17	31,756,334	32,255,590	0.7	*RNF24, PANK2, ssc-mir-103-2, AP5S1, CDC25B, CENPB, SPEF1, C20orf27, HSPA12B, HSPA12B, SIGLEC1, ADAM33, GFRA4, ATRN, U6*
L-tyrosine	1	73,972,391	74,471,148	1.16	*SEC63, OSTM1, NR2E1, SNX3, AFG1L*
	1	74,642,280	75,141,490	1.4	*FOXO3, ARMC2, SESN1*
	1	75,293,381	75,793,269	0.65	*CD164, PPIL6, SMPD2, MICAL1, ZBTB24, FIG4*
	1	80,371,029	80,869,342	0.68	*None*
	3	28,372,233	28,869,026	0.55	*ABCC1, BFAR, PARN*
Betaine	1	37,056,251	37,556,077	0.58	*NCOA7, HEY2*
	2	86,542,827	87,041,852	0.53	*TBCA, AP3B1*
	2	87,468,329	87,968,307	0.53	*ARSB, DMGDH, BHMT2, BHMT*
	6	82,101,618	82,599,859	0.57	*STPG1, NIPAL3, RCAN3, U6, SRRM1, CLIC4, RUNX3*
	15	124,184,229	124,681,509	0.69	*PAX3, SGPP2, MOGAT1*
	17	26,471,906	26,969,482	0.82	*PET117, KAT14, U6, ZNF133, DZANK1, POLR3F, RBBP9, SEC23B, SMIM26, DTD1*
Creatinine	2	149,629,454	150,127,355	0.74	*SPINK9, FBXO38, HTR4, ADRB2*
	12	2,562,992	3,060,017	1.15	*CBX8, CBX2, ENPP7, U6*
Dimethylglycine	2	85,842,752	86,340,606	0.51	*AGGF1, PDE8B, SNORA47*
	2	86,505,377	87,003,259	0.93	*OTP, TBCA, AP3B1*
	2	87,468,329	87,968,307	0.60	*ARSB, DMGDH, BHMT2, BHMT*
	6	82,101,618	82,599,859	0.64	*STPG1, NIPAL3, RCAN3, U6, SRRM1, CLIC4, RUNX3*
	15	129,051,568	129,551,348	0.86	*SCYGR5, SCYGR6, SCYGR8, C-C motif chemokine ligand 20, DAW1, SPHKAP, U6*

(Continued on following page)

TABLE 4 (*Continued*) Chromosome position (in basepairs) and the proportion of additive genetic variance explained for each metabolite and genes located in the region.

Metabolite	Chromosome	Start (bp)	End (bp)	Variance explained by adjacent SNPs	Gene name
Hypoxanthine	3	10,293,739	10,789,778	0.70	*RHBDD2, CCL26, HIP1, NSUN5, TRIM50, FKBP6, FZD9, BAZ1B*
	4	129,471,881	129,968,024	1.18	*CLCA1, CLCA2, ODF2L, COL24A1*
	4	130,191,423	130,690,509	0.76	*COL24A1, ZNHIT6, CCN1, DDAH1, BCL10, C1orf52*
	5	69,586,920	70,086,295	0.60	*CECR2, BCL2L13, BID, MICAL3*
	17	31,589,919	32,084,533	0.66	*SMOX, U6, RNF24, PANK2, ssc-mir-103-2, AP5S1, CDC25B, CENPB, SPEF1, C20orf27, HSPA12B, SIGLEC1, ADAM33, GFRA4, ATRN*
	17	32,123,118	32,620,235	1.14	*ATRN, U6, DNAAF9, SLC4A11, ITPA, DDRGK1, LZTS3, FASTKD5, UBOX5, AVP, OXT*
Isobutyric acid	2	149,658,663	150,158,529	1.10	*FBXO38, HTR4*
	4	129,471,881	129,968,024	0.52	*CLCA1*
	12	2,562,992	3,060,017	0.59	*CBX8, CBX2, ENPP7, U6*
L-alpha-aminobutyric acid	14	107,490,232	107,987,938	0.62	*CC2D2B, CCNJ, ZNF518A, BLNK, DNTT, OPALIN*
	14	110,517,873	111,017,235	0.54	*CNNM1, GOT1, NKX2-3, SLC25A28, ENTPD7, ENTPD7, COX15, CUTC, ABCC2*
Oxoglutarate	1	25,502,333	26,001,840	0.83	*REPS1, ECT2L, CCDC28A, NHSL1, SNORA70, heme binding protein 2*
	1	24,945,041	25,443,993	0.61	*U6, CITED2, TXLNB, HECA, ABRACL*
	2	134,496,051	134,994,766	0.64	*P4HA2, PDLIM4, SLC22A4, SLC22A5, RAD50, IRF1, IL5, KIF3A, IL13, IL4*
	14	46,622,301	47,118,015	0.58	*THOC5, NIPSNAP1, NF2, CABP7, ZMAT5, UQCR10, ASCC2, MTMR3, HORMAD2*
	14	47,569,039	48,065,569	0.85	*OSBP2, MORC2, TUG1, SMTN, SELENOM, INPP5J, PLA2G3, RNF185, LIMK2, PIK3IP1*
	14	49,337,114	49,836,497	0.56	*SPECC1L, ADORA2A, UPB1, GUCD1, LRRC75B, GGT5, SUSD2, CABIN1, DDT, GSTT4*
2-hydroxybutyrate	7	85,799,632	86,298,534	0.55	*RGMA, CHD2*
3-methyl-2-oxovaleric acid	1	4,465,007	4,963,404	0.95	*QKI*
	13	26,247,606	26,746,605	0.54	*CCDC13, HIGD1A, ACKR2, CYP8B1, ZNF662, POMGNT2, SNRK, ANO10*
	15	122,986,770	123,486,192	0.53	*EPHA4*
	16	18,909,569	19,408,454	0.84	*NPR3*

genes that are associated with these metabolites are displayed in bright green. For example, Figure 2 shows that betaine and dimethylglycine metabolism are interconnected. Genes located in same window on SSC2, (*DMGDH, BHMT2, BHMT*), are associated with both metabolites, suggesting pleiotropic effects of genes on multiple metabolites.

Discussion

To our best knowledge, this is the first study reporting genetic correlation between metabolites and CBC traits in healthy young pigs. The aims of the present study were to estimate 1) genetic correlations between thirty-three heritable metabolites with CBC traits in healthy young pigs, and 2) identify genomic regions controlling the genetic variance of metabolites that were genetically correlated with CBC and production and disease resilience traits. Identification of genetic predictors/markers of resilience and production traits under disease challenge by using samples from healthy pigs is necessary for genetic selection programs in high health nucleus farms. This study contributes to our understanding of the relationship of metabolites and immune response cells in pigs. The results of phenotypic and genetic correlations increase our understanding of the crosstalk between

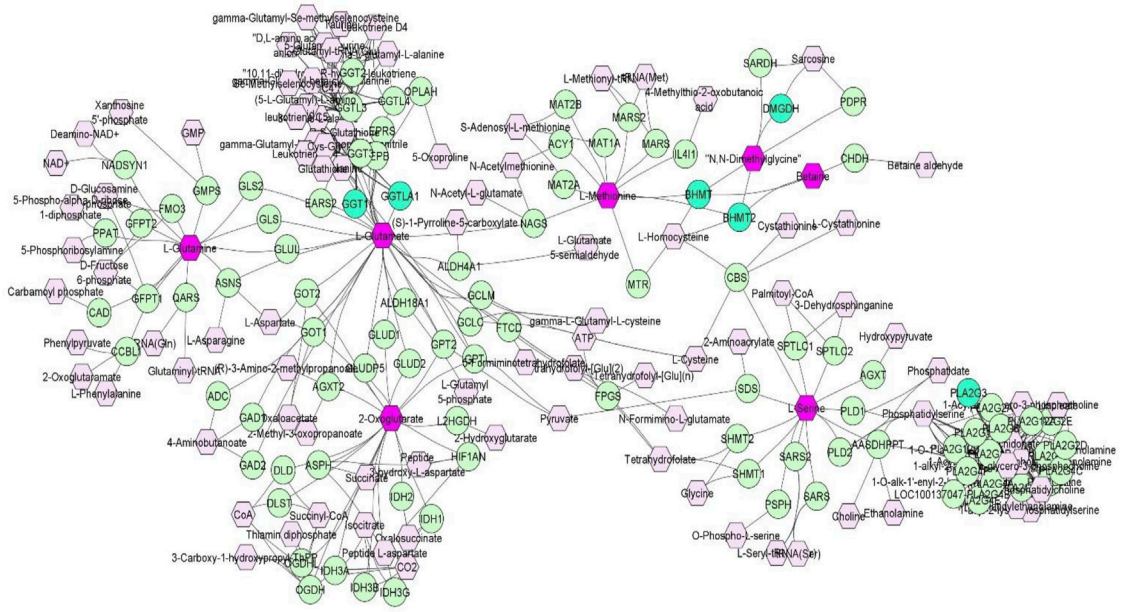

FIGURE 2
A compound-gene network of metabolites that are significantly ($p < 0.05$) genetically correlated with traits of interest (NEU, EOS, MCH, ADG and number of veterinary treatments). Input metabolites are shown in dark purple hexagonal and input genes are shown in bright green circles. Chemical reactions are represented as edges.

metabolites and immune cells in healthy animals, which might help design nutritional and selection strategies to improve resilience. Meanwhile, it is possible to estimate the genetic correlations between different traits, it is often not clear what molecular processes contributes to these genetic correlations. Thus, this study deepens our understanding to what contributes to the genetic correlations at a molecular level in young healthy pigs.

Phenotypic and genetic correlations

Phenotypic correlations of metabolites with CBC traits were generally very low. D-glucose had negative phenotypic correlation estimates with NEU, LYM, MONO, EOS, BASO, and MPV, while lactic acid was phenotypically positively correlated with WBC, NEU, LYM, BASO, EOS, RBC, HGB and MPV. Lactic acid is a hydroxycarboxylic acid and is mainly produced in muscle cells and red blood cells during anaerobic glycolysis (Connor et al., 1983). During glycolysis, glucose is metabolized into pyruvate, ATP, and NADHs. In the presence of oxygen, pyruvate is converted to acetyl-CoA in the tricarboxylic acid (TCA) cycle. Under oxygen-deprived conditions, pyruvate is reduced to lactate. However, the conversion of pyruvate to lactate also occurs under aerobic conditions, under which glucose uptake increases and preferential production of lactic acid takes place and it is known as the "Warburg effect" (Manca et al., 2021). In humans, increased levels of lactic acid are often used as biomarkers for various diseases, including autoimmune diseases, sepsis and neoplasia malignancy (Jansen et al., 2009; Ippolito et al., 2019). Lactic acid has been observed to be released by neutrophils in humans and mice (Stanfield and Germann, 2008; Kilkenny et al., 2010), acting as a critical regulator of neutrophil mobilization from the bone marrow. In ruminants, a greater concentration of lactic acid in blood is associated with ruminal acidosis (Hernández et al., 2014) and other health issues. In addition, lactic acid is reported to decrease platelet aggregation in horses and dogs (Lam et al., 2021; Lanier et al., 2022). Interestingly, our earlier work on these same data showed that lactic acid concentration in healthy pigs was found to be heritable (Dervishi et al., 2021), however, in this study we did not find significant genetic correlation estimates between lactic acid and CBC traits. Nonetheless, the results of phenotypic correlation are consistent with the possible role of lactic acid in exerting immunomodulatory effects that regulate the inflammatory response (Hoque et al., 2014; Pucino et al., 2017; Manca et al., 2021).

Overall, estimates of genetic correlations between metabolites and CBC traits ranged from moderate to high. We found high negative genetic correlation between plasma L-lysine and NEU (−0.81 ± 0.4), which is in agreement with previous studies reporting that lysine can modulate the neutrophil metabolism (Hu et al., 2016). L-Lysine is an essential amino acid in protein biosynthesis. Pigs have a high requirement for lysine (Liao et al., 2015) and supplementation with lysine can improve muscle protein accretion in pigs (Wu et al., 2014). On the other hand, impaired immune function, and increase susceptibility to infectious diseases have been reported in animals receiving a diet deficient in lysine (Chen et al., 2003). In pigs, (Brooks et al., 1964) found that lysine supplementation resulted in reductions in white blood cell counts, gamma globulin levels, and sedimentation rates, and increases in hematocrit values, red cell counts, hemoglobin levels, total serum protein levels, and serum albumin levels. In rats, supplementation of

lysine significantly reduced the neutrophil, lymphocyte counts, the tumor necrosis factor alpha (TNF-α), interleukin-8 (IL-8), and migration inhibitory factor (MIF) levels and protected against sepsis-induced chronic lung injury (Zhang et al., 2019). Lysine is found in high abundance in histones and lysine residues in the histones are accessible to several post translational modifications, including methylation and acetylation. Neutrophils are key participant in the innate immune response with a short half-life varying from 8–20 h and the regulation of neutrophil death rate is essential for maintaining hemostasis under physiological conditions (Perez- Figueroa et al., 2021). One of the defense mechanism of neutrophils is the formation of neutrophil extracellular traps (NETs; Brinkmann et al., 2004), which consist of DNA fibers associated with histones, enzymes from neutrophil granules and anti-microbial peptides which are released in the extracellular environment. The release of NETs is also a part of programmed cell-death process called NETosis. Lysine is important amino acid which is involved in histone modification process that take place during NETosis which will result in the formation of dispersed chromatin (Poli et al., 2021; Pérez-Figueroa et al., 2021). This molecular process might explain the negative genetic correlation between lysine and neutrophils. Our results suggest that L-lysine modulates neutrophil concentration and hence the immune response in pigs. The molecular aspect of it needs to be clarified and deserve further investigation.

We found that L-glutamine was genetically positively highly correlated with NEU and L-aspartate was positively correlated with MONO. Positive genetic correlation estimates were observed for the amino acids L-asparagine and L-glutamic acid with WBC. Lymphocyte concentration was negatively correlated with hypoxanthine and L-ornithine. Extensive research conducted in human and animal studies have demonstrated the role of amino acids in immune cell maturation, modulation, and function. For example, amino acids such as glutamic acid, glutamine, histidine, methionine, leucine, isoleucine, and valine are functional regulators of macrophages, dendritic cells, and T cells (Yoneda et al., 2009; McGaha et al., 2012; Wu, et al., 2012; Liu et al., 2017).

One of our most interesting results is the high positive genetic correlation between L-proline and hemoglobin concentration (0.94 ± 0.03). Using NMR spectroscopy and mutagenesis Gell et al. (2009) identified the importance of an evolutionary conserved proline residue in α-hemoglobin stabilizing protein. The results of genetic correlation between hemoglobin and proline may reflect the fact that proline is necessary for the structural reorganization of α-hemoglobin (Gell et al., 2009) and for the synthesis of iron related proteins such as hemoglobin, ferritin, and transferrin (Kitajima et al., 2003). Indeed, in rats, supplementation with proline enhanced a significant increase in the number of red blood cells and hemoglobin (Kitajima et al., 2003).

In addition, isobutyric acid was found to be positively genetically correlated with LYM concentration (0.69 ± 0.35) in healthy pigs. Previously, Dervishi et al. (2021), using the same pig population, reported that isobutyric acid in these pigs is heritable and negatively genetically correlated with residual feed intake under disease (RFI; −0.38). Furthermore, LYM concentration in young healthy pigs was found to be negatively genetically correlated with veterinary treatment rate under disease (Bai et al., 2020) in the same pig population. These results suggests that isobutyric acid might modulate both traits, LYM in young healthy pigs and RFI in pigs under disease conditions. Further research is necessary to investigate the relationship between isobutyric acid and LYM levels in blood of young healthy pigs, and RFI under disease.

Other metabolites such as 2-hydroxybutyrate, 3-methyl-2-oxovaleric acid and L-alpha aminobutyric acid were estimated to have positive genetic correlations with LYM and EOS concentration meanwhile dimethylglycine was negatively correlated with EOS. Furthermore, we found that the amino acids L-alanine and L-alpha-aminobutyric acid, also called homoalanine, are negatively genetically correlated with RDW. The red blood cell distribution width is a measure of size variability and heterogeneity of erythrocytes in the pheripheral blood and reflects the degree of anysocytosis. At present it is not clear why L-alpha aminobutyric and L-alanine are genetically correlated with RDW, but it is worth further investigation. For many other metabolites such as 2-hydroxybutyrate and 3-methyl-2-oxovaleric acid, literature on genetic correlations is lacking, making the interpretation of our results difficult.

GWAS

We performed a GWAS for 22 metabolites in young healthy pigs that were genetically correlated either with production or resilience traits or with CBC traits and investigated the genomic regions that explained a sizeable proportion of the variance for each metabolite. GWAS with CBC traits, were previously reported by Bai et al. (2020). Interestingly, Bai et al. (2020) proposed Member RAS Oncogene Family (*RAB32*) located on SSC1 as a candidate gene for RBC concentration. In the present study we found Member RAS Oncogene Family (*RAB27A*), located on SSC1 as a candidate gene for L-proline. In addition, proline was found to be genetically correlated with HGB concentration and HCT. These results might suggest that member RAS oncogene family (RAB32 and RAB27A) and proline modulate RBC traits, however further functional studies are necessary to validate our results. In addition, Bai et al. (2020) proposed tubulin beta class VI coded by TUBB1 (tubulin beta 1 class VI) on SSC17 as candidate gene for mean platelet volume (MPV fL). In our study we found that TUBE1 (tubulin epsilon 1) on SSC1, explains a small percentage of genetic variation of L-alanine which is positively genetically correlated with platelet concentration (PLT 10^3/μL) suggesting a possible role of L-alanine and tubulin superfamily in platelets concentration.

Furthermore, in our study we found that a window on SSC1 containing five genes (*SEC63*, *OSTM1, NR2E1, SNX3* and *AFG1L*), explained 1.02% of genetic variation of L-lysine concentration which was negatively genetically correlated with NEU concentration. Interestingly NR2E1 (Nuclear Receptor Subfamily 2, Group E, Member) functions as a repressor and activator of gene transcription (Corso-Díaz et al., 2016). As repressor of gene expression, NR2E1 interacts with co-repressor histone Lysine-specific demethylase 1 (LSD1) (Yokoyama et al., 2008). There is evidence that acetylation of lysine residues of other transcription factor such as C/EBPε is necessary for terminal neutrophil differentiation (Bartels et al., 2015). Our results suggest a possible epigenetic role of L-lysine and NR2E1 gene in modulating NEU concentration. However functional studies are necessary to validate our results.

Overall, the percentage of genetic variance explained by each window was small (<2%) for all metabolites. For L-glutamic acid, there were five important neighboring windows on SSC14 that together explained 6.9% of the genetic variance. Interestingly, we found overlapping windows on SSC14 that explained variance for L-glutamic acid, L-glutamine, L-serine, and oxoglutarate (example: 47,569,039–48,065,569 bp; 49,337,114–49,836,497 bp). These overlapping genomic windows might explain the positive genetic correlation between L-glutamic acid and oxoglutarate. Other overlapping windows were detected on SSC1 for L-lysine, L-ornithine, L-proline, and L-tyrosine (73,972,391–74,471,148 pb), on SSC2 for betaine and dimethylglycine (87,468,329–8768,307), on SSC6 for L-asparagine, L-proline, and L-serine (65,676,029–66,175,375 pb), and on SSC12 for creatinine and isobutyric acid (2,562,992–3060017 pb). These overlapping windows on SSC2 might contribute to the positive genetic correlation observed between betaine and dimethylglycine. These results suggest pleiotropic effects of loci on metabolite concentrations, i.e., that the same gene may control variation in more than one metabolite. Pleiotropy effects of loci on metabolites have been previously described in human studies (Smith et al., 2022). To further investigate, we attempted to integrate metabolites and genes in a single network (Figure 2). Indeed, we found that some of the genetic variation of metabolites such as L-glutamic acid, L-glutamine, oxoglutarate, dimethylglycine, betaine, and L-serine were explained by the same loci. For example, on SSC14 the window 47,569,039–48,065,569 pb contains *phospholipase A2 group III* (PLA2G3). PLA2G3 is involved in L-serine metabolism and lipid metabolism. It catalyzes the calcium-dependent hydrolysis of the sn-2 acyl bond of phospholipids to release arachidonic acid and lysophospholipids. Phosphatidylserine is a phospholipid that consists of two fatty acids attached in ester linkage to the first and second carbon of glycerol and serine attached through a phosphodiester linkage to the third carbon of the glycerol (Nelson and Cox, 2008). In a previous study on these same pigs, Dervishi et al. (2021) reported that L-serine was positively genetically correlated with average daily gain in the quarantine nursery (0.54). This might suggest *PLA2G3* as a candidate gene for ADG in healthy young pigs. Additionally, the window 87,468,329–87,968,307 pb on SSC2 includes *arylsulfatase B* (ARSB), *dimethylglycine dehydrogenase* (DMGDH), *betaine-homocysteine S-methyltransferase* (BHMT), and *betaine-homocysteine S-methyltransferase 2* (BHMT2). DMGDH is involved in the catabolism of choline, catalyzing the oxidative demethylation of dimethylglycine to form sarcosine. BHMT and BHMT2 are methyl transferases. *BHMT* encodes a cytosolic enzyme that catalyzes the conversion of betaine and homocysteine to dimethylglycine and methionine, respectively. BHMT2 can catalyze the transfer of the methyl group from betaine to homocysteine to create methionine (Ganu et al., 2015). The metabolism of dimethylglycine, of betaine, and of methionine are intertwined, as is shown in Figure 2, suggesting pleiotropic effect of these genes on metabolites. Previously, in pigs *DMGDH* has been associated with total weight of live neonates per litter (Wu et al., 2018) and *BHMT* has been associated with number of muscle fibers per unit area (Wimmers et al., 2006). Interestingly, using the same pig population, Dervishi et al. (2021) showed that betaine, dimethylglycine, and methionine concentrations in blood of young healthy pigs were genetically positively correlated with growth rate in the quarantine nursery. Here we found that, in blood of healthy young pigs, dimethylglycine was genetically negatively correlated with EOS and the amino acid L-methionine was negatively correlated with MPV, suggesting a genetic connection between immune response and growth. Our results suggest *PLA2G3, DMGDH*, *BHMT,* and *BHMT2* as candidate genes for variation in L-serine, dimethylglycine, betaine, and L-methionine concentration. Furthermore, serine, dimethylglycine, betaine, and L-methionine might be candidate metabolites to improve nursery growth rate of young healthy pigs. Future Mendelian randomization analysis and/or functional experiments should be performed in order to confirm that the metabolite mediates the effect of the SNP/gene on the phenotype and to establish a causal relationship.

We previously reported that isobutyric acid concentration in blood of young healthy pigs is negatively genetically correlated with RFI under disease challenge, suggesting that young healthy pigs that have higher plasma isobutyric acid content genetically have lower RFI under disease conditions (Dervishi et al., 2021). The GWAS for isobutyric acid showed that the most important windows on SSC2 explained 1.1% of the genetic variance for isobutyric acid. Two genes have been annotated for this window; *F-box protein 38* (FBXO38) and *5-hydroxytryptamine receptor 4* (HTR4). *5-hydroxytryptamine receptor 4* is a member of the family of serotonin receptors, which are G protein coupled receptors that stimulate cAMP production in response to serotonin (5-hydroxytryptamine). Interestingly Yao et al. (2013) identified a significant SNP in *HTR4* to be associated with RFI in dairy cattle using the Random Forests (RF) algorithm. In addition, GWAS performed by Manca et al. (2021) suggested *HTR4* as a candidate gene for residual concentrate intake (RCI) in dairy cattle. In pigs there is no evidence in the literature to connect isobutyric acid with *HTR4* and RFI, making interpretation of our results challenging. However, 5-hydroxytryptamine receptor 2B, (*HTR2B*), which belongs to the same family of serotonin receptors as *HTR4,* was proposed as functional candidate gene for feed conversion ratio (FCR) in pigs (Horodyska et al., 2017). We think that further research is necessary to elucidate the relationship between isobutyric acid, *HTR4* and RFI.

Conclusion

Phenotypic correlation estimates of plasma metabolites levels with CBC traits in young healthy pigs were generally low. Lactic acid might exert immunomodulatory effects that regulate the inflammatory response in pigs, which deserves further research and validation. This study showed significant genetic correlation estimates between metabolites and CBC traits in blood of young healthy pigs, demonstrating a potential role of metabolites in modulating the immune system. We identified candidate genes for part of the genetic variation of plasma metabolite concentrations. The GWAS demonstrated that the regulation of metabolites concentration is polygenic with no individual region, explaining a large proportion of the total genetic variation. Results of

GWAS suggest that *DMGDH*, *BHMT,* and *BHMT2* are candidate genes for dimethylglycine, betaine and L-methionine concentration in blood of young healthy pigs, while dimethylglycine, betaine, and L-methionine are candidate metabolites to improve growth rate of young healthy pigs.

This study contributes to understanding the relationship of metabolites and immune response cells in pigs and can offer insights for human physiology and immune response, however replication studies and validation of our results in human samples are necessary.

PigGen Canada Members

ALPHAGENE (2200, Pratte Avenue, Saint-Hyacinthe QC J2S 4B6 Canada), Hypor Canada (Spoorstraat 69, 5831CK, Boxmeer, Netherlands), Topigs Canada (20 South Landing, Unit 1, Oak Bluff, MB. R4G 0C4, Canada), Alliance Genetics (PO Box 24039 Edward RPO 107 Edward St. St. Thomas, ON N5P 1Y0, Canada), Fast Genetics (8—4003 Millar Avenue, Saskatoon, SK S7K 2K6, Canada), DNA Genetics (4438 Old Mill Court, Columbus, NE 68601, United States), Genesus Genetics (101 2nd St, Oakville, MB R0H 0Y0, Canada).

Data availability statement

The data analyzed in this study is subject to the following licenses/restrictions: The data analyzed in this study are not publicly available, because the data were generated on samples from commercially owned animals, however, they can be made available by the corresponding author on reasonable request. Requests to access these datasets should be directed to plastow@ualberta.ca.

Ethics statement

The animal study was reviewed and approved by Animal Protection Committee of the Centre de Recherche en Sciences Animales de Deschambault (15PO283) and the Animal Care and Use Committee at the University of Alberta (AUP00002227). Written informed consent was obtained from the owners for the participation of their animals in this study.

Author contributions

GP, JD, MD, FF, PGC, and JH conceived the experiment and obtained funding as the main applicants. ED and XB analyzed the results and ED wrote the first draft of the manuscript. All authors collaborated in the interpretation of results and discussion of the manuscript. All authors have read, reviewed and approved the final manuscript.

Funding

This project was funded by Genome Canada, Genome Alberta (ALGP2), Genome Prairie, PigGen Canada, and USDA-NIFA grant # 2017-67007-26144.

Acknowledgments

The authors thank the members of PigGen Canada (Canadian Centre for Swine Improvement, Fast Genetics, Genesus, Hypor, ALPHAGENE, Topigs Norsvin, DNA Genetics, the Canadian Swine Breeders Association, and Alliance Genetics Canada) for providing the pigs and insightful feedback. The authors thank The Metabolomics Innovation Center (TMIC) at University of Alberta, AB, Canada and Rupasri Mandal, for their service during metabolomics work and input on the methodological description. Yan Meng, Ziqi Yang and Jiehan Lim contributed in blood sample collection and preparation.

Conflict of interest

The authors declare that the research was conducted in the absence of any commercial or financial relationships that could be construed as a potential conflict of interest.

Publisher's note

Supplementary material

The Supplementary Material for this article can be found online at: https://www.frontiersin.org/articles/10.3389/fmolb.2023.1140375/full#supplementary-material

SUPPLEMENTARY FIGURE S1
Time line and collected phenotypes during natural polymicrobial disease challenge model.

SUPPLEMENTARY FIGURE S2
A representative of NMR spectrum with assignments. represents full spectrum; **(B–D)** are the partial zoom views.

SUPPLEMENTARY FIGURE S3
Phenotypic correlation between metabolites and complete blood count traits.

SUPPLEMENTARY FIGURE S4
Scatter plot showing the negative phenotypic correlations between D-glucose, pyruvic acid and CBC traits.

References

Bai, X., Putz, A. M., Wang, Z., Fortin, F., Harding, J. C. S., Dyck, M. K., et al. (2020). Exploring phenotypes for disease resilience in pigs using complete blood count data from a natural disease challenge model. *Front. Genet.* 11, 216. doi:10.3389/fgene.2020.00216

Bartels, M., Govers, A. M., Fleskens, V., Lourenço, A. R., Pals, C. E., Vervoort, S. J., et al. (2015). Acetylation of C/EBPε is a prerequisite for terminal neutrophil differentiation. *Blood* 125 (11), 1782–1792. doi:10.1182/blood-2013-12-543850

Berger, A. (2000). Th1 and Th2 responses: What are they? *BMJ* 321 (7258), 424. doi:10.1136/bmj.321.7258.424

Brinkmann, V., Reichard, U., Goosmann, C., Fauler, B., Uhlemann, Y., Weiss, D. S., et al. (2004). Neutrophil extracellular traps kill bacteria. *Science* 303, 1532–1535. doi:10.1126/science.1092385

Brooks, C. C., Davis, J. W., Thomas, H. R., and Vipperman, P. E. Jr. (1964). Effect of dietary lysine level on certain blood patterns in growing swine. *J. Anim. Sci.* 23 (2), 385–391. doi:10.2527/jas1964.232385x

Butcher, M. J., and Zhu, J. (2021). Recent advances in understanding the Th1/Th2 effector choice. *Fac. Rev.* 15 (10), 30. doi:10.12703/r/10-30

Carmelo, V. A. O., Banerjee, P., da Silva Diniz, W. J., and Kadarmideen, H. N. (2020). Metabolomic networks and pathways associated with feed efficiency and related-traits in Duroc and Landrace pigs. *Sci. Rep.* 10, 255. doi:10.1038/s41598-019-57182-4

CCAC (1993). Canadian Council on animal Care guidelines (CCAC). Available at: https://www.ccac.ca/en/certification/about-certification.

Chen, C., Sander, J. E., and Dale, N. M. (2003). The effect of dietary lysine deficiency on the immune response to Newcastle disease vaccination in chickens. *Avian Dis.* 47, 1346–1351. doi:10.1637/7008

Cheng, J., Putz, A. M., Harding, J. C. S., Dyck, M. K., Fortin, F., Plastow, G. S., et al. (2020). Genetic analysis of disease resilience in wean-to-finish pigs from a natural disease challenge model. *J. Anim. Sci.* 98, 244. doi:10.1093/jas/skaa244

Connor, H., Woods, H. F., and Ledingham, J. G. G. (1983). Comparison of the kinetics and utilisation of D(-)- and L(+)-sodium lactate in normal man. *Ann. Nutr. Metab.* 27, 481–487. doi:10.1159/000176723

Corcoran, S. E., and O'Neill, L. A. J. (2016). HIF1α and metabolic reprogramming in inflammation. *J. Clin. Invest.* 126 (10), 3699–3707. doi:10.1172/JCI84431

Corso-Díaz, X., de Leeuw, C. N., Alonso, V., Melchers, D., Wong, B. K. Y., Houtman, R., et al. (2016). Co-activator candidate interactions for orphan nuclear receptor NR2E1. *BMC Genomics* 17, 832. doi:10.1186/s12864-016-3173-5

Dervishi, E., Zhang, G., Hailemariam, D., Mandal, R., Wishart, D. S., and Ametaj, B. N. (2018b). Urine metabolic fingerprinting can be used to predict the risk of metritis and highlight the pathobiology of the disease in dairy cows. *Metabolomics* 14, 83. doi:10.1007/s11306-018-1379-z

Dervishi, E., Zhang, G., Mandal, R., Wishart, D. S., and Ametaj, B. N. (2018a). Targeted metabolomics: New insights into pathobiology of retained placenta in dairy cows and potential risk biomarkers. *Animal* 12, 1050–1059. doi:10.1017/S1751731117002506

Dervishi, E., Yang, T., Dyck, M. K., Harding, J. C. S., Fortin, F., PigGen Canada., et al. (2021). Heritability and genetic correlations of plasma metabolites of pigs with production, resilience and carcass traits under natural polymicrobial disease challenge. *Sci. Rep.* 11. doi:10.1038/s41598-021-99778-9

Ganu, R. S., Ishida, Y., Koutmos, M., Kolokotronis, S. O., Roca, A. L., Garrow, T. A., et al. (2015). Evolutionary analyses and natural selection of betaine-homocysteine S methyltransferase (BHMT) and BHMT2 genes. *PloS One* 10 (7), e0134084. doi:10.1371/journal.pone.0134084

Geiger, R., Rieckmann, J. C., Wolf, T., Basso, C., Feng, Y., Fuhrer, T., et al. (2016). L-arginine modulates T cell metabolism and enhances survival and anti-tumor activity. *Cell* 167 (3), 829–842. doi:10.1016/j.cell.2016.09.031

Gell, D. A., Feng, L., Zhou, S., Jeffrey, P. D., Bendak, K., Gow, A., et al. (2009). A cis-proline in alpha-hemoglobin stabilizing protein directs the structural reorganization of alpha-hemoglobin. *J. Biol. Chem.* 284 (43), 29462–29469. doi:10.1074/jbc.M109.027045

Hernández, J., Benedito, J. L., Abuelo, A., and Castillo, C. R. (2014). Ruminal acidosis in feedlot: From aetiology to prevention. *Sci. World J.* 2014, 1–8. doi:10.1155/2014/702572

Hong, J. K., Lee, J. B., Ramayo-Caldas, Y., Kim, S. D., Cho, E. S., Kim, Y. S., et al. (2020). Single-step genome-wide association study for social genetic effects and direct genetic effects on growth in Landrace pigs. *Sci. Rep.* 10, 14958. doi:10.1038/s41598-020-71647-x

Hoque, R., Farooq, A., Ghani, A., Gorelick, F., and Mehal, W. Z. (2014). Lactate reduces liver and pancreatic injury in Toll-like receptor- and inflammasome-mediated inflammation via GPR81-mediated suppression of innate immunity. *Gastroenterology* 146, 1763–1774. doi:10.1053/j.gastro.2014.03.014

Horodyska, J., Hamill, R. M., Varley, P. F., Reyer, H., and Wimmers, K. (2017). Genome-wide association analysis and functional annotation of positional candidate genes for feed conversion efficiency and growth rate in pigs. *PloS ONE* 12 (6), e0173482. doi:10.1371/journal.pone.0173482

Hu, Z. L., Park, C. A., and Reecy, J. M. (2016). Developmental progress and current status of the Animal QTLdb. *Nucleic Acids Res.* 44, D827–D833. doi:10.1093/nar/gkv1233

Ippolito, L., Morandi, A., Giannoni, E., and Chiarugi, P. (2019). Lactate: A metabolic driver in the tumour landscape. *Trends biochem. Sci.* 44, 153–166. doi:10.1016/j.tibs.2018.10.011

Janeway, C. A., Traver, P., Walport, M., and Schlomchik, M. J. (2001). *Immunobiology: The immune system in health and disease*. 5th Edn. New York: Taylor & Francis.

Jansen, T. C., Van Bommel, J., and Bakker, J. (2009). Blood lactate monitoring in critically ill patients: A systematic health technology assessment. *Crit. Care. Med.* 37, 2827–2839. doi:10.1097/CCM.0b013e3181a98899

Karisa, B. K., Thomson, J. M., Wang, Z., Li, C., Mantanholi, Y., Miller, S. P., et al. (2014). Plasma metabolites associated with residual feed intake and other productivity performance traits in beef cattle. *Livest. Sci.* 165, 200–211. doi:10.1016/j.livsci.2014.03.002

Karnovsky, A., Weymouth, T., Hull, T., Tarcea, V. G., Scardoni, G., Laudanna, C., et al. (2012). Metscape 2 bioinformatics tool for the analysis and visualization of metabolomics and gene expression data. *Bioinformatics* 28 (3), 373–380. doi:10.1093/bioinformatics/btr661

Kilkenny, C., Ki, C., Browne, W., Cuthill, I. C., Emerson, M., and Altman, D. G. (2010). Animal research: Reporting of *in Vivo* experiments the ARRIVE guidelines. *Br. J. Pharmacol.* 160, 1577–1579. doi:10.1111/j.1476-5381.2010.00872.x

Kitajima, H., Shiomoto, H., Osada, K., and Yokogoshi, H. (2003). Co-administration of proline and inorganic iron enhance the improvement of behavioral and hematological function of iron-deficient anemic rats. *J. Nutr. Sci. Vitaminol.* 49 (1), 7–12. doi:10.3177/jnsv.49.7

Kolaczkowska, E., and Kubes, P. (2013). Neutrophil recruitment and function in health and inflammation. *Nat. Rev. Immunol.* 13 (3), 159–175. doi:10.1038/nri3399

Lam, L. K. M., Murphy, S., Kokkinaki, D., Venosa, A., Sherrill-Mix, S., Casu, C., et al. (2021). DNA binding to TLR9 expressed by red blood cells promotes innate immune activation and anemia. *Sci. Transl. Med.* 13 (616), eabj1008. doi:10.1126/scitranslmed.abj1008

Lanier, C. J., Taintor, J. S., Christopherson, P. W., and Spangler, E. A. (2022). Effect of lactic acid addition to equine whole blood on platelet aggregation measured by impedance aggregometry. *Clin. Pathol.* 51 (1), 65–69. doi:10.1111/vcp.13034

Li, J., Akanno, E., Valente, T. S., Abo-Ismail, M., Karisa, B. K., Wang, A., et al. (2020). Genomic heritability and Genome-Wide Association studies of plasma metabolites in crossbred beef cattle. *Front. Gen.* 11, 538600. doi:10.3389/fgene.2020.538600

Liao, S. F., Wang, T., and Regmi, N. (2015). Lysine nutrition in swine and the related monogastric animals: Muscle protein biosynthesis and beyond. *Springerplus* 27, 147. doi:10.1186/s40064-015-0927-5

Liu, Y., Wang, X., Hou, Y., Yin, Y., Qiu, Y., Wu, G., et al. (2017). Roles of amino acids in preventing and treating intestinal diseases: Recent studies with pig models. *Amino Acids* 49, 1277–1291. doi:10.1007/s00726-017-2450-1

Manca, E., Cesarani, A., Falchi, L., Atzori, A. S., Gaspa, G., Rossoni, A., et al. (2021). Genome-wide association study for residual concentrate intake using different approaches in Italian Brown Swiss. *Ital. J. Anim. Sci.* 20, 1957–1967. doi:10.1080/1828051X.2021.1963864

McGaha, T. L., Huang, L., Lemos, H., Metz, R., Mautino, M., Prendergast, G. C., et al. (2012). Amino acid catabolism: A pivotal regulator of innate and adaptive immunity. *Immun. Rev.* 249, 135–157. doi:10.1111/j.1600-065X.2012.01149.x

Misztal, I., Tsuruta, S., Strabel, T., Auvray, B., Druet, T., and Lee, D. H. (2002). "BLUPF90 and related programs (BGF90)," in Proceedings of 7th World Congress of Genetics Applied to Livestock Production, Montpellier, France, 19-23 August 2002, 1–10.

Montgomery, S. P., Sindt, J. J., Greenquist, M. A., Miller, W. F., Pike, J. N., Loe, E. R., et al. (2009). Plasma metabolites of receiving heifers and the relationship between apparent bovine respiratory disease, body weight gain, and carcass characteristics. *J. Anim. Sci.* 87, 328–333. doi:10.2527/jas.2008-0969

Nelson, D., and Cox, M. (2008). *Lehninger principles of biochemistry*. 5 ed. New York: W.H Freeman and company, 350.

Park, S. J., and Im, D. S. (2019). Blockage of sphingosine-1-phosphate receptor 2 attenuates allergic asthma in mice. *Br. J. Pharmacol.* 176 (7), 938–949. doi:10.1111/bph.14597

Paul, W. E., and Zhu, J. (2010). How are T(H)2-type immune responses initiated and amplified? *Nat. Rev. Immunol.* 10 (4), 225–235. doi:10.1038/nri2735

Percie du Sert, N., Hurst, V., Ahluwalia, A., Alam, S., Avey, M. T., Baker, M., et al. (2020). The ARRIVE guidelines 2.0: Updated guidelines for reporting animal research. *PLoS Biol.* 18 (7), e3000410. doi:10.1371/journal.pbio.3000410

Pérez-Figueroa, E., Álvarez-Carrasco, P., Ortega, E., and Maldonado-Bernal, C. (2021). Neutrophils: Many ways to die. *Front. Immunol.* 4 (12), 631821. doi:10.3389/fimmu.2021.631821

Poli, V., Ma, V. P. Y., Di Gioia, M., Broggi, A., Benemar, M., Chen, Q., et al. (2021). Zinc-dependent histone deacetylases drive neutrophil extracellular trap formation and potentiate local and systemic inflammation. *iScience* 24 (11), 103256. doi:10.1016/j.isci.2021.103256

Psychogios, N., Hau, D. D., Peng, J., Guo, A. C., Mandal, R., Bouatra, S., et al. (2011). The human serum metabolome. *PloS One* 6 (2), e16957. doi:10.1371/journal.pone.0016957

Pucino, V., Bombardieri, M., Pitzalis, C., and Mauro, C. (2017). Lactate at the crossroads of metabolism, inflammation, and autoimmunity. *Eur. J. Immunol.* 47 (1), 14–21. doi:10.1002/eji.201646477

Putz, A. M., Harding, J. C. S., Dyck, M. K., Fortin, F., Plastow, G. S., Dekkers, J. C. M., et al. (2019). Novel resilience phenotypes using feed intake data from a natural disease challenge model in wean-to-finish pigs. *Front. Genet.* 9, 660. doi:10.3389/fgene.2018.00660

Ravanbakhsh, S., Liu, P., Bjorndahl, T. C., Mandal, R., Grant, J. R., Wilson, M., et al. (2015). Accurate, fully-automated NMR spectral profiling for metabolomics. *PloS One* 10 (5), e0124219. doi:10.1371/journal.pone.0124219

Rodriguez-Coira, J., Villaseñor, A., Izquierdo, E., Huang, M., Barker-Tejeda, T. C., Radzikowska, U., et al. (2021). The Importance of metabolism for immune homeostasis in allergic diseases. *Front. Immunol.* 28 (12), 692004. doi:10.3389/fimmu.2021.692004

Saude, E. J., Slupksy, C. M., and Sykes, B. D. (2006). Optimization of NMR analysis of biological fluids for quantitative accuracy. *Metabolomics* 2, 113–123. doi:10.1007/s11306-006-0023-5

Semple, J. W., Italiano, J. E., and J Freedman, J. (2011). Platelets and the immune continuum. *Nat. Rev. Immunol.* 11 (4), 264–274. doi:10.1038/nri2956

Shannon, P., Markiel, A., Ozier, O., Baliga, N. S., Wang, J. T., Ramage, D., et al. (2003). Cytoscape: A software environment for integrated models of biomolecular interaction networks. *Genome Res.* 13, 2498–2504. doi:10.1101/gr.1239303

Smith, C. J., Sinnott-Armstrong, N., Cichonska, A., Julkunen, H., Fauman, E., Wurtz, P., et al. (2022). Integrative analysis of metabolite GWAS illuminates the molecular basis of pleiotropy and genetic correlation. *eLife* 11, e79348. doi:10.7554/eLife.79348

Stanfield, L. C., and Germann, W. J. (2008). *Principles of human physiology*. 3rd Edn. San Francisco: Pearson education, Inc.

Tan, J., McKenzie, C., Potamitis, M., Thorburn, A. N., Mackay, C. R., and Macia, L. (2014). The role of short-chain fatty acids in health and disease. *Adv. Immunol.* 121, 91–119. doi:10.1016/B978-0-12-800100-4.00003-9

VanRaden, P. M. (2008). Efficient methods to compute genomic predictions. *J. Dairy Sci.* 91, 4414–4423. doi:10.3168/jds.2007-0980

Vitezica, Z. G., Aguilar, I., Misztal, I., and Legarra, A. (2011). Bias in genomic predictions for populations under selection. *Genet. Res.* 93, 357–366. doi:10.1017/S001667231100022X

Wang, H., Misztal, I., Aguilar, I., Legarra, A., Fernando, R. L., Vitezica, Z., et al. (2014). Genome-wide association mapping including phenotypes from relatives without genotypes in a single-step (ssGWAS) for 6-week body weight in broiler chickens. *Front. Genet.* 5, 134. doi:10.3389/fgene.2014.00134

Wang, H., Misztal, I., Aguilar, I., Legarra, A., and Muir, W. M. (2012). Genome-wide association mapping including phenotypes from relatives without genotypes. *Genet. Res.* 94, 73–83. doi:10.1017/S0016672312000274

Widmann, P., Reverter, A., Fortes, M. R. S., Weikard, R., Suhre, K., Hammon, H., et al. (2013). A systems biology approach using metabolomic data reveals genes and pathways interacting to modulate divergent growth in cattle. *BMC Genom* 14, 798. doi:10.1186/1471-2164-14-798

Wimmers, K., Fiedler, I., Hardge, T., Murani, E., Schellander, K., and Ponsuksili, S. (2006). QTL for microstructural and biophysical muscle properties and body composition in pigs. *BMC Genet.* 7, 15. doi:10.1186/1471-2156-7-15

Wu, G., Bazer, F. W., Dai, Z. L., Li, D. F., Wang, J. J., and Wu, Z. L. (2014). Amino acid nutrition in animals: Protein synthesis and beyond. *Annu. Rev. Anim. Biosci.* 2, 387–417. doi:10.1146/annurev-animal-022513-114113

Wu, P., Yang, Q., Wang, K., Zhou, J., Ma, J., Tang, Q., et al. (2018). Single step genome-wide association studies based on genotyping by sequence data reveals novel loci for the litter traits of domestic pigs. *Genomics* 110 (3), 171–179. doi:10.1016/j.ygeno.2017.09.009

Wu, X., Zhang, Y., Liu, Z., Li, T. J., and Yin, Y. L. (2012). Effects of oral supplementation with glutamate or combination of glutamate and N-carbamylglutamate on intestinal mucosa morphology and epithelium cell proliferation in weanling piglets. *J. Anim. Sci.* 90, 337–339. doi:10.2527/jas.53752

Yao, C., Spurlock, D. M., Armentano, L. E., Page, C. D., Jr VandeHaar, M. J., Bickhart, D. M., et al. (2013). Random Forests approach for identifying additive and epistatic single nucleotide polymorphisms associated with residual feed intake in dairy cattle. *J. Dairy Sci.* 96 (10), 6716–6729. doi:10.3168/jds.2012-6237

Yokoyama, A., Takezawa, S., Schüle, R., Kitagawa, H., and Kato, S. (2008). Transrepressive function of TLX requires the histone demethylase LSD1. *Mol. Cell Biol.* 28 (12), 3995–4003. doi:10.1128/MCB.02030-07

Yoneda, J., Ayatoshi Andou, A., and Takehana, K. (2009). Regulatory roles of amino acids in immune response. *Curr. Rheumat. Rev.* 5, 252–258. doi:10.2174/157339709790192567

Zhang, Y., Wu, Y., Han, D., Meng, J., Wang, H., and andCao, G. (2019). L–lysine ameliorates sepsis-induced acute lung injury in a lipopolysaccharide-induced mouse model. *Biomed. Pharmacother.* 118, 109307. doi:10.1016/j.biopha.2019.109307

frontiers | Frontiers in Molecular Biosciences

TYPE Original Research
PUBLISHED 04 April 2023
DOI 10.3389/fmolb.2023.1146069

OPEN ACCESS

EDITED BY
Young Hae Choi,
Leiden University, Netherlands

REVIEWED BY
Kateryna Goncharova Pierzynowska,
Lund University, Sweden
Alessia Vignoli,
University of Florence, Italy

*CORRESPONDENCE
Dagnachew Hailemariam,
✉ hailemar@ualberta.ca

SPECIALTY SECTION
This article was submitted
to Metabolomics,
a section of the journal
Frontiers in Molecular Biosciences

RECEIVED 16 January 2023
ACCEPTED 20 March 2023
PUBLISHED 04 April 2023

CITATION
Hailemariam D, Hashemiranjbar M, Manafiazar G, Stothard P and Plastow G (2023), Milk metabolomics analyses of lactating dairy cows with divergent residual feed intake reveals physiological underpinnings and novel biomarkers. *Front. Mol. Biosci.* 10:1146069. doi: 10.3389/fmolb.2023.1146069

Milk metabolomics analyses of lactating dairy cows with divergent residual feed intake reveals physiological underpinnings and novel biomarkers

Dagnachew Hailemariam[1]*, Mohsen Hashemiranjbar[1], Ghader Manafiazar[1,2], Paul Stothard[1] and Graham Plastow[1]

[1]Department of Agricultural, Food, and Nutritional Science, University of Alberta, Edmonton, AB, Canada, [2]Animal Science and Aquaculture Department, Faculty of Agriculture, Dalhousie University, Halifax, NS, Canada

The opportunity to select for feed efficient cows has been limited by inability to cost-effectively record individual feed efficiency on an appropriate scale. This study investigated the differences in milk metabolite profiles between high- and low residual feed intake (RFI) categories and identified biomarkers of residual feed intake and models that can be used to predict residual feed intake in lactating Holsteins. Milk metabolomics analyses were undertaken at early, mid and late lactation stages and residual feed intake was calculated in 72 lactating dairy cows. Cows were ranked and grouped into high residual feed intake (RFI >0.5 SD above the mean, n = 20) and low residual feed intake (RFI <0.5 SD below the mean, n = 20). Milk metabolite profiles were compared between high residual feed intake (least efficient) and low residual feed intake (most efficient) groups. Results indicated that early lactation was predominantly characterized by significantly elevated levels of medium chain acyl carnitines and glycerophospholipids in high residual feed intake cows. Citrate cycle and glycerophospholipid metabolism were the associated pathways enriched with the significantly different metabolites in early lactation. At mid lactation short and medium chain acyl carnitines, glycerophospholipids and amino acids were the main metabolite groups differing according to residual feed intake category. Late lactation was mainly characterized by increased levels of amino acids in high residual feed intake cows. Amino acid metabolism and biosynthesis pathways were enriched for metabolites that differed between residual feed intake groups at the mid and late lactation stages. Receiver operating characteristic curve analysis identified candidate biomarkers: decanoylcarnitine (area under the curve: AUC = 0.81), dodecenoylcarnitine (AUC = 0.81) and phenylalanine (AUC = 0.85) at early, mid and late stages of lactation, respectively. Furthermore, panels of metabolites predicted residual feed intake with validation coefficient of determination (R^2) of 0.65, 0.37 and 0.60 at early, mid and late lactation stages, respectively. The study sheds light on lactation stage specific metabolic differences between high-residual feed intake and low-residual feed intake lactating dairy cows. Candidate biomarkers that distinguished divergent residual feed intake groups and panels of metabolites that predict individual residual feed intake phenotypes were identified. This result supports the potential of milk metabolites to select for more efficient

cows given that traditional residual feed intake phenotyping is costly and difficult to conduct in commercial farms.

KEYWORDS

milk metabolome, biomarker, feed efficiency, physiology, dairy cows

Introduction

Feed cost represents a large proportion of the variable costs of dairy production and it has increased substantially over time (Berry and Crowley, 2013). Selection for feed efficiency has both economic and environmental benefits by addressing the increasing cost of feed and environmental concerns over the carbon footprint of dairy cattle production (Basarab et al., 2013). Residual feed intake (RFI) is a measure of feed efficiency and is defined as the difference between actual and predicted feed intake after accounting for production and maintenance (Koch et al., 1963). Low RFI (the most efficient) cows consume less feed for the same milk output and emit less methane compared to the high RFI (least efficient) cows (Hailemariam et al., 2021). Despite its importance, RFI is difficult and costly to include in an industry wide recording scheme for the purpose of generating accurate estimates for direct selection in the breeding program. Therefore, RFI is designated as a hard-to-measure trait for the dairy industry. Alternatively, low cost and easy-to-measure biomarker models associated with underlying metabolic differences in RFI could provide a potential alternative. Biomarkers offer indirect measurement of traits that would otherwise be expensive to directly measure.

The between-animal differences in RFI could be determined by digestive ability (Potts et al., 2017) ruminal microbial composition (Jewell et al., 2015), feed intake pattern, fermentation and digestion of feed, anabolic and catabolic metabolism, physical activity and thermoregulation (Herd and Arthur, 2009). It has been proposed that variation in RFI may represent inherent variation in basic metabolic processes that determine production efficiency (Cantalapiedra-Hijar et al., 2018). Potts et al. (2017) speculated differences in post absorptive metabolic processes, heat production, or energy utilization for maintenance account for more of the variation in RFI than digestibility.

The mammary gland becomes metabolically active and is an energetically demanding tissue during lactation (Hanigan et al., 2009). Hanigan and Baldwin (1994) constructed a model of energy metabolism in the udder of lactating cows and showed that ATP generated was used for maintenance and synthesis of milk components. Milk components are synthesized in mammary epithelial cells and milk precursors are constantly absorbed from blood (Knight et al., 1994). Proteins, some amino acids, fats and lactose are synthesized and secreted by the mammary epithelial cells (Xiao and Cant, 2005; Rezaei et al., 2016). Branched-chain amino acids are catabolized to support milk production (Li et al., 2009).

Given the vital role of the mammary gland in the energy metabolism of lactating dairy cows, we used a milk metabolomics approach to study the biological mechanisms of divergence in feed efficiency. High-throughput milk metabolomics have been used to study the metabolism (Tian et al., 2016) and pathophysiology (Klein et al., 2011; Sun et al., 2017) of dairy cows. To the best of our knowledge milk metabolomics data had not been used to study the physiology of feed efficiency in dairy cows. In this study, we investigated the differences in milk metabolite profiles between high and low RFI cows at early, mid and late lactation stages. In addition, candidate biomarkers that can distinguish cows between high and low RFI groups and panels of metabolites that can be used to predict individual RFI phenotypes at each stage of lactation were identified.

Materials and methods

Animals and diet

The experiment was conducted at the University of Alberta, Dairy Research and Technology Center (DRTC) from June 2017 to October 2018. The study was undertaken on mixed parity lactating Holsteins managed in a tie-stall system. The layout of the study is shown in Figure 1. All the experimental procedures for this study were approved by the University of Alberta Animal Policy and Welfare Committee for Livestock (Study ID: AUP00000170), and animals were cared for in accordance with the guidelines of the Canadian Council on Animal Care (2009). We used 72 mixed parity lactating Holstein cows 3–240 days in milk (DIM). Out of the 72 cows that were used in the study, 40 cows (20 least efficient and 20 most efficient) were selected for comparison. Cows that were culled/died due to disease/s or any other reason before last milk sampling point (240 DIM) were excluded from the experiment. Disease incidences in the window of 2 weeks before each sampling dates were considered in the analysis. The number of cows affected by different diseases during the experimental period varied with the sampling points. At 50 DIM, a total of 6 cows (out of 40) were sick and they had lameness (n = 1), milk fever (n = 3), and mastitis (n = 3). Out the 6 sick cows, 1 had both milk fever and mastitis. At 150 DIM, a total of 4 cows had lameness (n = 2), milk fever (n = 1) and mastitis (n = 2). One cow had both lameness and mastitis. At 240 DIM 2 cows had lameness and 2 had mastitis. One of these had both lameness and mastitis. The forty cows (19 primiparous, 21 multiparous) had parity ranging from one to four and all cows with parity >3 were categorized as "3+" during the analyses.

All cows were fed the same diet and daily ration was offered as total mixed ration (TMR) for *ad libitum* intake to allow approximately 5% feed refusals throughout the experiment. All cows were fed once daily in the morning at 08:00 a.m. Individual offered feed weight in the morning and refusal feed weight left on the next morning were recorded daily. Feed composition, including dry matter (%), crude protein (%), and neutral detergent fiber (%), acid detergent fiber (%), and net energy lactation were determined when the TMR ingredients were changed. The ingredients and chemical composition of the TMR is described in Table 1.

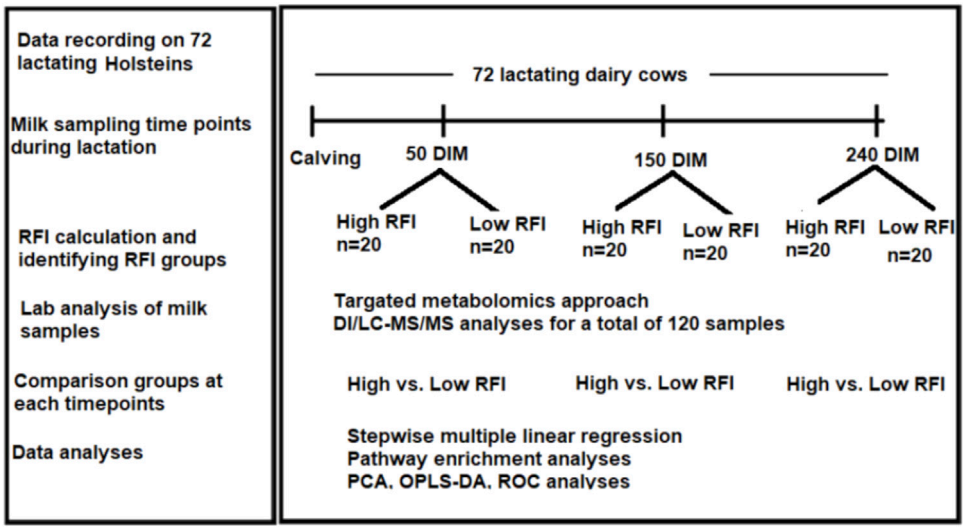

FIGURE 1
Workflow of the study showing calculation of RFI in 72 cows from 3–240 DIM and milk samples collection at three time points (50, 150, 240 DIM) during lactation. Cows were ranked and the high and low RFI groups were identified. Milk samples from high and low RFI groups in all the three time points were analyzed using DI/LC-MS/MS method.

TABLE 1 Diet ingredients and chemical composition of total mixed ration for the study cows. Average values of ingredients and chemical composition are presented.

Diet ingredients, % (DM basis)	Ration
Alfalfa hay	11.55
Barley silage[a]	35.28
Rolled grain[b]	33.58
Protein supplement	19.59
Chemical composition	
DM, %	50.57
Crude protein, % of DM	17.09
Acid detergent fiber, % of DM	20.71
Neutral detergent fiber, % of DM	32.26
NE lactation, Mcal/kg	1.81

DM, dry matter; NE, net energy for lactation.
[a]Rolled gran: Corn and barley.
[b]Protein supplement: 26.61% amino plus (high bypass soy), 26.25% soy bean meal-47%, 25.75% canola meal, 8.15% F 100 Dairy fat, 4% corn distiller 2010, 2.3% limestone, 2% AFA/canola oil, 1.5% SOD, bicarbonate, 1.2% DICAL PHOS-21%, 1% salt, 0.58% MAG OX-56%, 0.4% nutritec-diamond V mills, 0.1% selenium 1,000 mg/kg, 0.1% ruminant TM, pak, 0.05% ADE VIT, PAK-30% and 0.02% biotin 2%-Rovimix H-2.

Feed intake, milk yield and composition, and body weight recording

Daily feed intake, weekly milk composition and yield and monthly body weight data were collected on 72 lactating dairy cows from 3–240 days in milk (DIM) at DRTC. Feed intake was calculated as the difference between the amount of feed offered and refused for individual cows on a daily basis. Dry matter percentage of the feed was analyzed every week and daily individual dry matter intake (DMI) was calculated as a product of feed intake and dry matter percentage. Cows were milked twice per day and both PM and AM milk samples were collected separately once per week. Milk samples were collected with bar-coded plastic vials. Samples were stored at +4^{O}C temporarily and shipped to Lactanet Canada, Edmonton for milk composition analyses. Mid-infrared (MIR) spectrometry (Foss MilkoScan FT6000; Foss Electric A/S, Hillerød, Denmark) was used to determine milk composition (milk fat, protein and lactose). Milk yield (for the dates of milk sampling) data was obtained from the DRTC where it is recorded as a routine farm activity. Animals were weighed once per month at 7:

00 a.m. after milking using Myscale Pro-W810 scale (Gallagher, Canley, United Kingdom).

Milk sample collection for DI/LC-MS/MS analyses

Milk samples were collected from 72 mixed parity lactating cows at DRTC. Sampling was undertaken 03:00 to 06:00 a.m. before feeding at 3 time points during the lactation period (50, 150 and 240 DIM) and hereafter named as early, mid and late lactation stages, respectively. All the milk samples were collected using a 50 mL tube and temporarily maintained on ice. Following homogenization of the milk sample in each 50 mL tube, aliquots of 500 µL were prepared and stored at −80^{O}C until DI/LC-MS/MS analyses.

Trait derivation for RFI calculation

Metabolic body weight and empty body weight were derived from body weight data recorded once per month. Similarly, milk production energy requirement was derived from milk yield, fat, protein and lactose percentages that were recorded weekly. The daily values of metabolic body weight and empty body weight were predicted from monthly values and daily values of milk production energy requirement were predicted from weekly values using a random regression model. The details of the Legendre polynomial random regression model and calculations of the parameters were described in Manafiazar et al. (2013). After predicting daily values of metabolic body weight from monthly values, empty body weight change was calculated as a difference in empty body weight between two consecutive days (days after minus day before, e.g., empty body weight at fourth -third DIM) from 3–240 DIM. Cows that lose weight after calving had negative empty body weight change values while cows that gain weight had positive values. Empty body weight change was calculated to account for the body tissue mobilization in the RFI calculation during the study period (3–240 DIM). A multiple linear and quadratic regression model was used to predict expected energy intake values from 3–240 DIM.

Calculation of residual feed intake

Residual feed intake values were calculated for 72 lactating Holsteins as the difference between the actual and expected net energy intake as described in our previous study (Hailemariam et al., 2021). In short, daily actual energy intake, metabolic body weight, empty body weight, empty body weight change and milk production net energy requirements were used to calculate RFI. Mixed parity cows were used in the study and parity was included in the RFI calculation model. The daily average lactation RFI for each individual over 237 days (3—240 DIM) was obtained by dividing the total lactation RFI by the number of days recorded for each cow. Then, the 72 RFI predicted cows were ranked and categorized into most efficient (low RFI: RFI <0.5 SD from the mean) and least efficient (high RFI: RFI >0.5 SD from the mean) at all the three time points (50, 150, 240 DIM) using the same average (3–240 DIM) RFI values.

Targeted milk metabolomics using TMIC prime assay DI/LC-MS/MS method

All the milk samples were analyzed at The Metabolomics Innovation Center (TMIC, University of Alberta, Edmonton, AB) using a TMIC prime custom assay (DI/LC-MS/MS). A targeted quantitative metabolomics approach was used to analyze the samples using a combination of direct injection mass spectrometry with a reverse-phase LC-MS/MS custom assay. This custom assay, in combination with an ABI 4000 Q-Trap (Applied Biosystems/MDS Sciex) mass spectrometer, was used for the targeted identification and quantification of up to 143 different endogenous metabolites including amino acids, acylcarnitines, organic acids, biogenic amines and derivatives, uremic toxins, glycerophospholipids, sphingolipids and sugars. The method combines the derivatization and extraction of analytes and selective mass-spectrometric detection using multiple reaction monitoring (MRM) pairs. Isotope-labeled and other internal standards were used for metabolite quantification. The custom assay contains a 96 deep-well plate with a filter plate attached with sealing tape and reagents and solvents used to prepare the plate assay. The first 14 wells were used for one blank, three zero samples, seven standards and three quality control samples. For all metabolites except organic acids, samples were thawed on ice and were vortexed and centrifuged at ×13,000 g. Ten µL of each sample was loaded onto the center of the filter on the upper 96-well plate and dried in a stream of nitrogen. Subsequently, phenyl-isothiocyanate was added for derivatization. After incubation, the filter spots were dried again using an evaporator. Extraction of the metabolites was then achieved by adding 300 µL of extraction solvent. The extracts were obtained by centrifugation into the lower 96-deep well plate, followed by a dilution step with MS running solvent.

For organic acid analysis, 150 µL of ice-cold methanol and 10 µL of isotope-labeled internal standard mixture was added to 50 µL of milk sample for overnight protein precipitation. After centrifugation at 13,000 g for 20 min 50 µL of supernatant was loaded into the center of wells of a 96-deep well plate, followed by the addition of 3-nitrophenylhydrazine (NPH) reagent. After incubation for 2 h, BHT stabilizer and water were added before LC-MS injection. Mass spectrometric analysis was performed on an API4000 Qtrap® tandem mass spectrometry instrument (Applied Biosystems/MDS Analytical Technologies, Foster City, CA) equipped with an Agilent 1,100 series HPLC system (Agilent Technologies, Palo Alto, CA). The samples were delivered to the mass spectrometer by a liquid chromatography (LC) method followed by direct injection (DI). Data analysis was done using Analyst 1.6.2.

Statistical analyses

A step wise multiple linear regression analysis in R was used to analyse the differences of milk metabolites between low and high

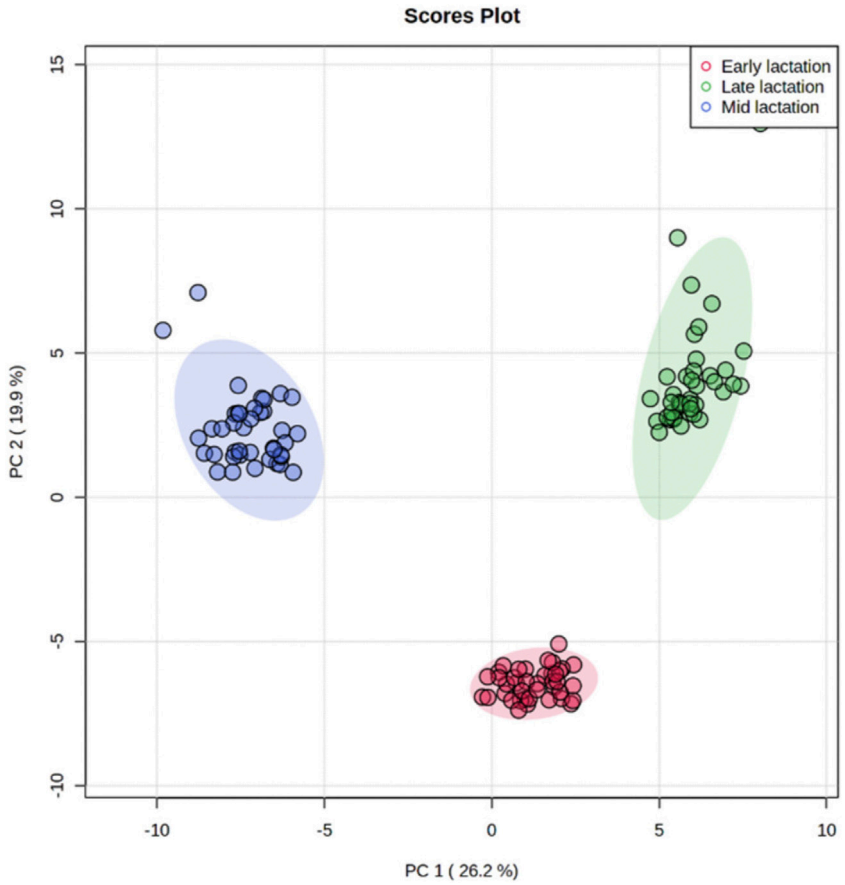

FIGURE 2
Principal component analysis showing a clear separation in the milk metabolite profiles of cows among early, mid and late lactation stages.

RFI groups. The model was fitted for each metabolite concentration as dependant variable and RFI groups (R), parity (P), age at first calving (AFC), health status (HS), and month and year of sampling (MY) as independent variables. A total of 118 metabolites were analysed using the following model:

$$Y_{ijklmn} = \mu + R_i + P_j + MY_k + AFC_l + HS_m + e_{ijklmn},$$

where Yijklmn is the metabolite concentration for the *n*th cow tested from the *i*th RFI group (low and high RFI) and *j*th parity (1–3+), *k*th MY, lthAFC, *m*th HS and eijklm is the deviation due to the ijklmth cow or error term.

Each metabolite was tested for normal distribution and where appropriate, for data that were not normally distributed, the natural log-transformation was used and back-transformed results are presented. The results were presented as least squares means ± standard error of mean per RFI category. Benjamini Hochberg False Discovery Rate (FDR) method was used to correct the raw *p*-values for multiple comparisons. A threshold of $p < 0.05$ for raw *p*-values and FDR <0.1 were used to identify statistically significant changes in metabolite concentration between RFI groups. Tendencies were declared at $0.05 \leq p < 0.1$ for raw *p*-values.

The disease incidences were not equally distributed during the lactation period or in RFI groups. Because of this we coded cows as sick and healthy and included this factor in the model. The concentration of milk metabolites at all the three time points were adjusted for significant fixed effects including health status. To avoid potential bias for the analyses other than the regression, we used metabolome data adjusted for significant fixed effects. Therefore, in all the analyses the effect of disease or other fixed effects on milk metabolite concentration has been taken care of.

Multiple linear regression analyses were used to predict average RFI phenotypes from milk metabolite profiles at early, mid and late lactation stages. Only the metabolites that were significantly different and tended to differ between high vs. low RFI comparisons were fitted in the model. Leave-one-out cross validation (LOOCV) of linear models were done using caret package (Kuhn, 2005).

Metabolite pathway analyses were performed using MetaboAanalyst (Xia et al., 2013) to identify pathways that were enriched for the metabolites that had differential concentration between high vs. low RFI comparison groups. A hypergeometric test was used for over representation analysis and relative–betweenness centrality for pathway topology analysis. *Homo sapiens* was used as a reference with Human Metabolome Database (HMDB) ID since a high proportion of metabolites affected by RFI at early stage of lactation were missing from the bovine metabolome database (BMDB).

TABLE 2 List of milk metabolites with altered concentrations in the high vs. low RFI comparisons at early lactation stage. The metabolite concentrations were described in least square means (LSM) and corresponding standard error of mean (SEM) in each group with *p*-values and false discovery rate (FDR).

Metabolite (μM)	High RFI (n = 20)	Low RFI (n = 20)	*p*-value	FDR
Decenoylcarnitine (C10:1)	0.13 ± 0.01	0.10 ± 0.01	0.001	0.024
lysoPC a C20:4	0.12 ± 0.02	0.04 ± 0.01	0.001	0.012
lysoPC a C18:1	3.30 ± 0.22	2.12 ± 0.25	0.001	0.008
lysoPC a C18:2	1.40 ± 0.16	0.61 ± 0.23	0.003	0.018
PC aa C40:1	0.05 ± 0.00	0.03 ± 0.01	0.004	0.019
Decadienylcarnitine (C10:20)	0.01 ± 0.00	0.008 ± 0.00	0.008	0.032
Decanoylcarnitine (C10)	0.05 ± 0.00	0.04 ± 0.00	0.009	0.031
Hydroxyhexadecenoylcarnitine (C16:1-OH)	0.13 ± 0.01	0.11 ± 0.01	0.009	0.027
lysoPC a C16:1	0.40 ± 0.03	0.28 ± 0.03	0.009	0.024
lysoPC a C18:0	0.99 ± 0.06	0.75 ± 0.06	0.010	0.024
Total dimethyl arginine	0.55 ± 0.05	0.72 ± 0.05	0.013	0.028
Spermidine	0.45 ± 0.03	0.37 ± 0.02	0.019	0.038
lysoPC a C28:1	0.30 ± 0.03	0.20 ± 0.04	0.021	0.039
Butyric acid	28.8 ± 2.32	21.4 ± 2.26	0.023	0.039
Acetylornithine	0.27 ± 0.05	0.47 ± 0.09	0.027	0.043
Betaine	36.7 ± 3.96	26.5 ± 3.72	0.040	0.060
lysoPC a C26:0	0.16 ± 0.02	0.22 ± 0.02	0.052	0.073
Citric acid	3,897 ± 127	4,271 ± 175	0.060	0.080
Fumaric acid	23.4 ± 1.56	19.5 ± 1.30	0.060	0.076
Butenylcarnitine (C4:1)	0.04 ± 0.00	0.031 ± 0.00	0.070	0.084
SM C16:0	16.1 ± 0.75	14.1 ± 0.75	0.070	0.080
lysoPC a C16:0	5.21 ± 0.32	4.44 ± 0.39	0.082	0.089
PC aa C38:6	0.07 ± 0.01	0.05 ± 0.01	0.084	0.088
Methylmalonic acid	0.13 ± 0.02	0.10 ± 0.01	0.091	0.091

Multivariate analyses were performed using MetaboAnalyst (Xia et al., 2013). Principal component analysis (PCA) were used to visualize the change in milk metabolite profiles with lactation stage. Orthogonal partial least squares discriminant analysis (OPLS-DA) was used to assess whether the high and low RFI groups cluster separately on the basis of milk metabolite profiles. To minimize the possibility that any observed separation for an OPLS-DA plot was due to chance, permutation testing involving repeated (2,000 times) OPLS-DA calculations using different random labeling of the samples was performed. A *p*-value (<0.05) was considered significant for the separation observed between the two groups. Metabolites with VIP score >1 were considered as the metabolite significantly contributed for separation of RFI groups. Biomarker profiles and the quality of the biomarkers were determined using receiver-operator characteristic (ROC) curves. A receiver operator characteristic curve shows the sensitivity and specificity of the test and often summarized into a single metric known as the area under the curve (AUC). A rough guide for assessing the utility of a biomarker based on its AUC is 0.9–1.0 = excellent; 0.8 to 0.9 = good; 0.7 to 0.8 = fair; 0.6 to 0.7 = poor; 0.5 to 0.6 = fail (Hailemariam et al., 2014). For this study, we presented the top five metabolites (on the basis of AUC values) at early, mid and late lactation stages.

Results

Dynamics of milk metabolites during lactation

Using targeted DI/LC-MS/MS, 118 milk metabolites were identified and quantified at each of the lactation stages (early, mid and late). To obtain a global perspective on metabolic changes during the lactation period, principal component analysis (PCA) of milk metabolites profiled at early, mid and late lactations were performed without considering RFI grouping. The first two principal components (PCs) accounted for 46.1% of the

10.3389/fmolb.2023.1146069

TABLE 3 List of milk metabolites with altered concentrations in the high vs. low RFI comparisons at mid lactation stage. The metabolite concentrations were described in least square means (LSM) and corresponding standard error of mean (SEM) in each group with *p*-values and false discovery rate (FDR).

Metabolites (μM)	High RFI (n = 20)	Low RFI (n = 20)	*p*-value	FDR
Dodecenoylcarnitine (C12:1)	0.40 ± 0.02	0.50 ± 0.02	0.001	0.028
PC aa C36:6	0.03 ± 0.00	0.02 ± 0.00	0.002	0.028
Methylglutarylcarnitine (C5-M-DC)	0.07 ± 0.00	0.08 ± 0.00	0.003	0.028
Hydroxypropionylcarnitine (C3-OH)	0.04 ± 0.00	0.05 ± 0.00	0.004	0.028
LysoPC a C28:1	0.40 ± 0.03	0.30 ± 0.03	0.004	0.022
Hydroxyhexadecenoylcarnitine (C16:1-OH)	0.02 ± 0.00	0.03 ± 0.00	0.005	0.023
PC aa C38:6	0.09 ± 0.01	0.06 ± 0.00	0.005	0.020
Methionine	1.90 ± 0.19	1.20 ± 0.12	0.006	0.021
Histidine	2.70 ± 0.53	1.20 ± 0.24	0.006	0.019
Dodecanoylcarnitine (C12)	4.70 ± 0.29	5.70 ± 0.30	0.008	0.022
Glucose	33,823 ± 1,136	38,742 ± 1,301	0.008	0.020
PC aa C32:2	0.90 ± 0.07	0.70 ± 0.08	0.019	0.044
Tryptophan	0.60 ± 0.11	0.40 + 0.06	0.029	0.063
PC ae C40:6	0.02 ± 0.00	0.03 ± 0.00	0.032	0.064
Pimelylcarnitine (C7-DC)	0.05 ± 0.00	0.08 ± 0.01	0.033	0.062
Valine	6.00 ± 1.20	3.30 ± 0.65	0.035	0.061
PC ae C36:0	0.60 ± 0.04	0.50 ± 0.03	0.039	0.064
Hexenoylcarnitine (C6:1)	0.05 ± 0.00	0.06 ± 0.00	0.044	0.068
SM C20:2	0.10 ± 0.00	0.08 ± 0.00	0.048	0.071
SM C16:0	23.2 ± 1.31	19.6 ± 1.31	0.055	0.077
SM C18:1	0.74 ± 0.05	0.62 ± 0.04	0.06	0.080
Arginine	11.5 ± 1.16	8.50 ± 0.89	0.066	0.084
Creatine	460 ± 36.3	556 ± 36.3	0.068	0.083
Methylmalonic acid	0.12 ± 0.00	0.10 ± 0.00	0.071	0.083
Phenylalanine	3.10 ± 0.32	2.40 ± 0.29	0.073	0.082
LysoPC a C26:1	0.08 ± 0.00	0.05 ± 0.00	0.073	0.079
SM C16:1	0.70 ± 0.05	0.60 ± 0.04	0.074	0.077
Creatinine	66.1 ± 3.19	76.5 ± 4.47	0.081	0.081

total variation among samples (Figure 2). The three stages of lactation were clearly distinguished from one another based on the top 2 PCs. Since the three lactation stages strikingly clustered in a non-overlapping manner, we performed the high vs. low RFI comparison independently for each lactation stage.

Next, we compared the high (n = 20) vs. low (n = 20) RFI groups for all 118 metabolites at each lactation stage. In the comparisons of each metabolite concentration between high and low RFI groups, fixed effects such as parity (P), age at first calving (AFC), sampling month and year (MY), health status (HS) were adjusted whenever significant ($p < 0.05$). The result indicated that different sets of metabolites differed ($p < 0.05$) between high-and low RFI groups at each lactation stage. At early lactation, the concentrations of 4 acyl carnitines, 7 glycerophospholipids, 3 biogenic amines, 1 organic acid and betaine were significantly ($p < 0.05$) different between the high and low RFI groups (Table 2). A similar comparison at mid lactation (high vs. low RFI) revealed the differential ($p < 0.05$) concentration of 7 acyl carnitines, 4 amino acids, 7 glycerophospholipids and glucose between the comparison groups (Table 3). The late lactation stage was characterized by differential ($p < 0.05$) concentration of 14 amino acids, 2 biogenic amines, 6 glycerophopholipids, 2 acyl carnitines, 3 organic acids, carnosine and betaine between high and low RFI cows (Table 4).

TABLE 4 List of milk metabolites with altered concentrations in the high vs. low RFI comparisons at late lactation stage. The metabolite concentrations were described in least square means (LSM) and corresponding standard error of mean (SEM) in each group with *p*-values and false discovery rate (FDR).

Metabolites (μM)	High RFI (n = 20)	Low RFI (n = 20)	*p*-value	FDR
Valine	12.0 ± 2.80	3.40 ± 0.79	0.001	0.037
Acetyl ornithine	0.61 ± 0.12	0.20 ± 0.03	0.001	0.019
Lysine	51.8 ± 11.7	18.6 ± 4.89	0.002	0.025
Histidine	25.1 ± 2.19	15.7 ± 2.25	0.002	0.019
Methylhistidine	1.10 ± 0.23	0.40 ± 0.08	0.002	0.015
Tryptophan	1.00 ± 0.21	0.40 ± 0.08	0.003	0.019
Proline	33.8 ± 5.94	16.1 ± 2.59	0.003	0.016
Citrulline	3.30 ± 0.75	1.20 ± 0.27	0.003	0.014
Ornithine	5.90 ± 0.94	3.00 ± 0.44	0.003	0.012
Arginine	15.5 ± 2.29	8.00 ± 1.18	0.003	0.011
Phenylalanine	4.20 ± 0.63	2.20 ± 0.33	0.004	0.013
Serine	9.30 ± 1.17	5.40 ± 0.68	0.005	0.015
Hexadecanoylcarnitine (C16)	0.04 ± 0.01	0.02 ± 0.00	0.006	0.017
Lactic acid	267 ± 66	104 ± 23.7	0.007	0.019
Methionine	2.50 ± 0.35	1.40 ± 0.20	0.01	0.025
Alanine	19.4 ± 7.30	5.20 ± 1.78	0.011	0.025
Total dimethylarginine	0.60 ± 0.06	0.40 ± 0.05	0.011	0.024
PC acyl-alkyl (ae) C40:6	0.03 ± 0.00	0.02 ± 0.00	0.013	0.027
Betaine	123 ± 19.50	80.8 ± 15.9	0.015	0.029
Carnosine	1.00 ± 0.19	0.50 ± 0.09	0.017	0.031
PC diacyl (aa) C36:6	0.03 ± 0.00	0.04 ± 0.00	0.017	0.030
Glutamine	4.12 ± 0.63	2.80 ± 0.53	0.018	0.030
SM C20:2	0.10 ± 0.01	0.07 ± 0.01	0.021	0.034
Pyruvic acid	29.7 ± 3.29	21.1 ± 2.13	0.023	0.035
SM C16:0	23.7 ± 1.65	19.5 ± 1.86	0.025	0.037
PC aa C38:6	0.10 ± 0.01	0.06 ± 0.01	0.032	0.046

(Continued on following page)

10.3389/fmolb.2023.1146069

TABLE 4 (*Continued*) List of milk metabolites with altered concentrations in the high vs. low RFI comparisons at late lactation stage. The metabolite concentrations were described in least square means (LSM) and corresponding standard error of mean (SEM) in each group with *p*-values and false discovery rate (FDR).

Metabolites (μM)	High RFI (n = 20)	Low RFI (n = 20)	*p*-value	FDR
Dodecanoylcarnitine (C12)	4.50 ± 0.32	5.40 ± 0.45	0.032	0.044
Choline	353 ± 26.2	276 ± 30.8	0.037	0.049
LysoPC a C18:2	1.80 ± 0.41	1.30 ± 0.35	0.044	0.056
Threonine	6.60 ± 1.51	3.60 ± 0.76	0.05	0.062
Spemidine	0.50 ± 0.07	0.30 ± 0.10	0.052	0.062
Carnitine (C0)	31.6 ± 3.60	21.4 ± 4.39	0.058	0.067
Hexadecadienylcarnitine (C16:2)	0.02 ± 0.00	0.02 ± 0.00	0.063	0.071
Glycine	45.5 ± 10.5	26.1 ± 5.51	0.071	0.077
PC ae C36:0	0.80 ± 0.05	0.60 ± 0.05	0.073	0.077
Creatinine	86.3 ± 3.79	93.8 ± 4.27	0.081	0.083
Hexenoylcarnitine (C6:1)	0.05 ± 0.00	0.06 ± 0.00	0.097	0.097

10.3389/fmolb.2023.1146069

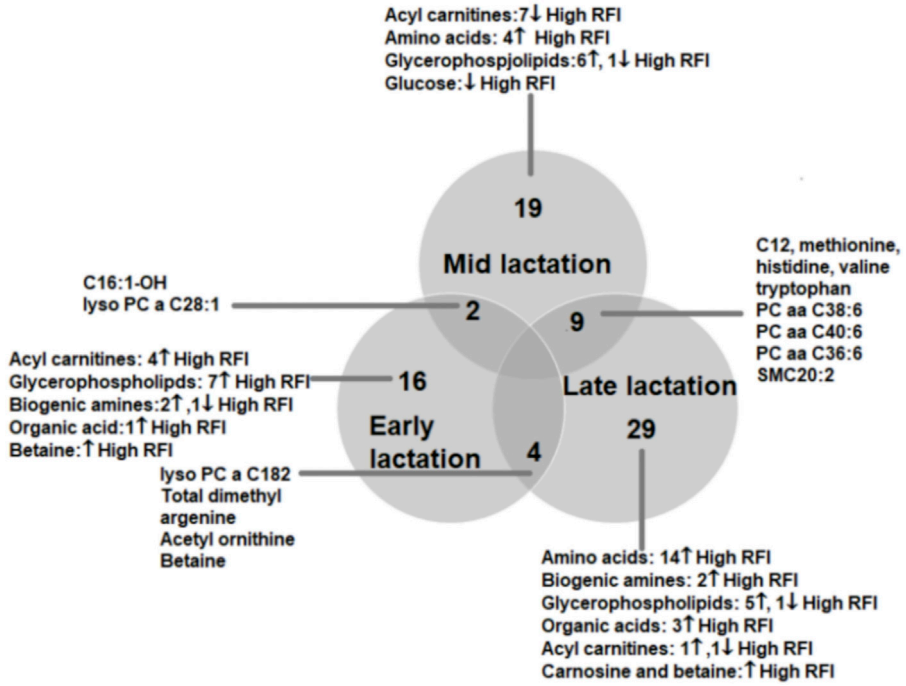

FIGURE 3
Venn diagram showing the number of metabolites altered between high and low RFI groups at early, mid and late lactation stages. The number of commonly altered metabolites between lactation stages are shown at the intersections of the circles representing the different lactation stages.

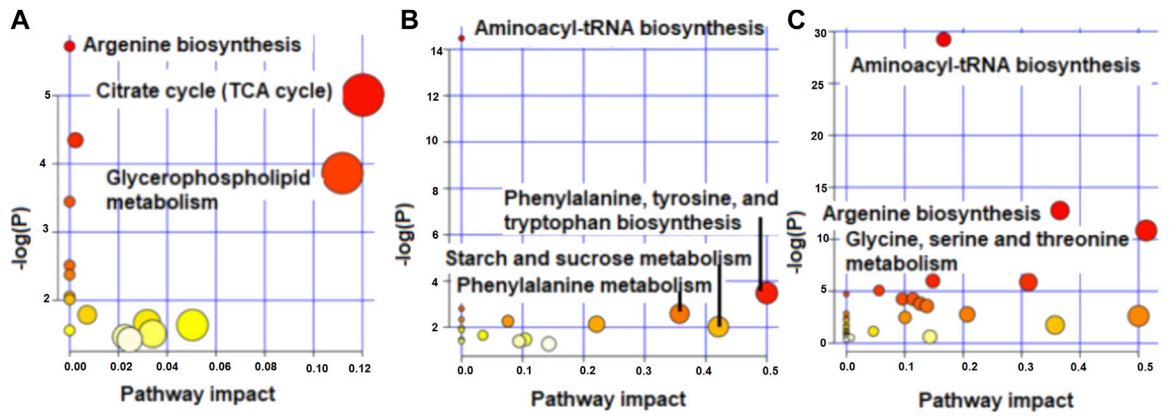

FIGURE 4
Metabolome view map showing enriched pathways for the metabolites that differed in concentration between high and low RFI groups at early **(A)**, mid **(B)** and late **(C)** stages of lactation.

Notably, acyl carnitines, glycerophospholipids and amino acids were predominantly different ($p < 0.05$) between RFI comparison groups (high vs. low). The concentrations of medium and long chain acyl carnitines (C10:2, C10:1, C10, C16:1-OH) were increased at early lactation stage in the high RFI group, however at the mid lactation stage the concentrations of short chain acyl carnitines (C3-OH, C5-M-DC, C6:1, C7-DC) were significantly decreased in high RFI cows. At the late lactation stage, the levels of a medium (C12) and long chain (C16) acyl carnitines were affected by the RFI grouping and C12 was decreased whereas C16 was increased in high RFI cows.

The comparison of glycerophospholipids (high vs. low RFI) at early lactation stage showed that lysophosphatidylcholines (lysoPC a C20:4, lysoPC a C18:1, lysoPC a C18:2, lysoPC a C16:1, lysoPC a C18:0 and lysoPC a C28:1) were significantly elevated in high RFI cows. Lysophosphatidylcholines are formed by hydrolysis of

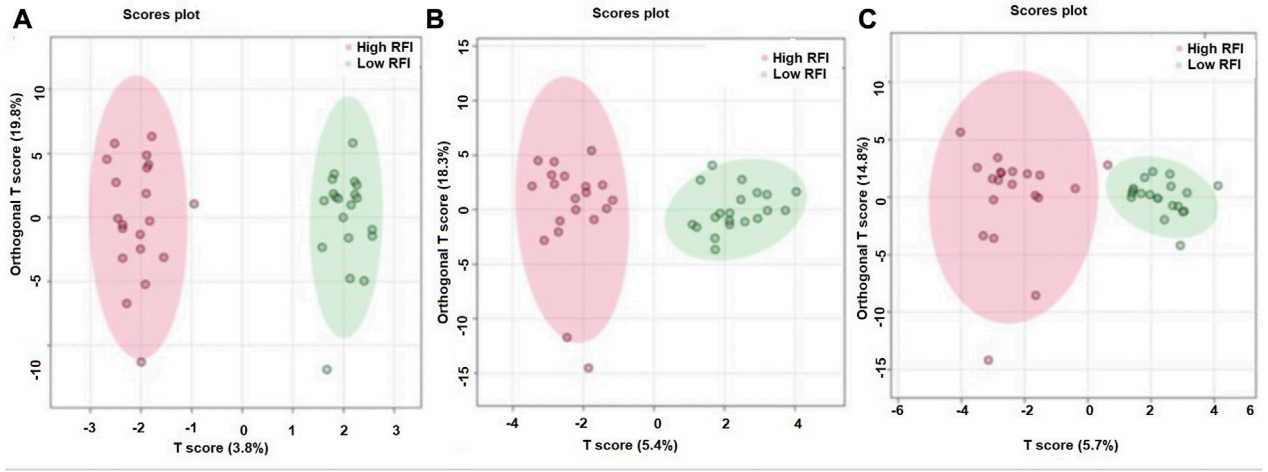

FIGURE 5
Orthogonal partial least squares discriminant analysis showing a clear separation between the least and most efficient cows at early **(A)**, mid **(B)** and late **(C)** lactation stages.

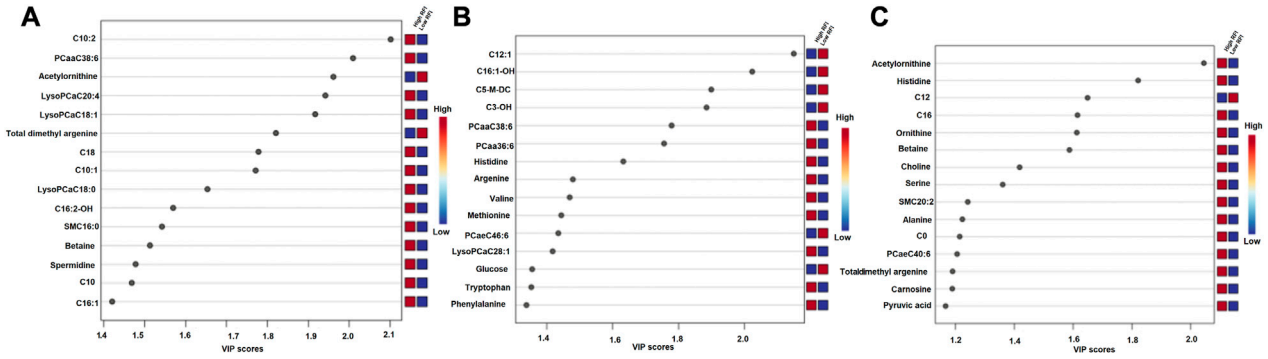

FIGURE 6
Metabolites ranked by variable importance in projection (VIP) at the early **(A)**, mid **(B)** and late **(C)** lactation stages. The VIP score plots indicate the top 15 metabolites that distinguished high and low RFI groups at each of the three time points.

phosphatidylcholines by lipoprotein-associated phospholipase A2. Interestingly, during mid lactation, phosphatidylcholines (PC aa C38:6, PC aa C32:2, PC aa C36:6 and PC ae C36:0) were elevated in high RFI cows. On the contrary, PC ae C40:6 was significantly decreased in high RFI cows. Among other species of glycerophospholipids, only lysoPC a C28:1 and SM C20:2 were significantly increased in high RFI cows at mid lactation stage. The increased ($p < 0.05$) level of PC aa C38:6 in high RFI cows persisted during the late lactation stage. The levels of PC ae C40:6 and PC aa C38:6 were elevated in high RFI cows whereas PC aa C36:6 decreased in high RFI cows at the late lactation stage. In addition, SM C16:0, SM C20:2 and lysoPC a C18:2 were significantly increased in high RFI cows.

The high and low RFI cows did not differ ($p > 0.05$) in any of the amino acids compared at the early stage of lactation. At the mid lactation stage, however, valine, tryptophan, methionine and histidine were significantly elevated in high RFI cows. Interestingly, the late lactation stage was characterized by significant elevation of amino acids: valine, lysine, histidine, methylhistidine, tryptophan, proline, citrulline, ornithine, arginine, phenylalanine, serine, methionine, alanine, glutamine, threonine and glycine. Valine, one of the branched chain amino acids, was markedly decreased in low RFI cows (Table 4). Among the biogenic amines, total dimethyl arginine and acetyl ornithine were significantly decreased in high RFI cows, whereas spermidine was significantly increased in the high RFI group at the early stage of lactation. Acetyl ornithine and total dimethylarginine were also significantly increased in high RFI cows at the late lactation stage. The comparison of organic acids (high vs. low RFI) at the early lactation stage revealed that the level of butyric acid was elevated in high RFI cows. In addition, fumaric and methyl malonic acid tended to increase in high RFI cows, while citric acid showed a tendency to increase in low RFI. Methyl malonic acid maintained a similar trend in mid lactation, where tendency of

TABLE 5 Top 5 metabolites (biomarkers) with corresponding AUC and CI at early, mid and late lactation stages. The correlation between the candidate biomarkers' concentration in milk and the RFI values is shown in Pearson correlation coefficient (r) and *p*-value.

Lactation stage	Metabolites	AUC	CI	r	*p*-value
Early lactation (50 DIM)	C10	0.81	0.67–0.93	0.29	0.070
	Acetylornithine	0.75	0.55–0.89	−0.41	0.009
	SM 16:1	0.75	0.57–0.90	0.38	0.020
	lysoPC a C16:1	0.74	0.57–0.88	0.15	0.350
	lysoPC a C18:1	0.74	0.56–0.88	0.37	0.020
Mid-lactation (150 DIM)	C12:1	0.81	0.64–0.93	−0.48	0.002
	Histidine	0.79	0.63–0.94	0.33	0.040
	Creatinine	0.78	0.61–0.91	0.05	0.740
	C3:1	0.77	0.62–0.91	0.01	0.970
	C16:1-OH	0.75	0.61–0.88	−0.40	0.010
Late lactation (240 DIM)	Phenylalanine	0.85	0.74–0.95	0.39	0.010
	Valine	0.81	0.67–0.93	0.43	0.006
	Methionine	0.79	0.64–0.92	0.39	0.010
	Arginine	0.79	0.64–0.92	0.44	0.005
	Acetylornithine	0.78	0.64–0.92	0.55	<0.001

10.3389/fmolb.2023.1146069

increase was observed in high RFI groups. At the late lactation stage, however, pyruvic and lactic acid significantly increased in high RFI cows (Table 4). The high RFI cows had consistently elevated levels of betaine at early and late lactation stages.

To understand the change in the types of metabolites affected by RFI grouping, we compared the significantly different metabolites between the lactation stages (early vs. mid, early vs. late and mid vs. late). The early vs. mid-lactation comparison showed that C16:1-OH, lysoPC a 28:1, SM C16:0, PC aa 38:6 and methyl malonic acid consistently differed between the RFI groups. In a comparison between early and late stages of lactation, the concentrations of lysoPC a C18:2, PC aa C38:6, SMC16:0, total dimethyl arginine, spermidine, acetylornithine and betaine were commonly altered while, C12, C16:1, methionine, histidine, arginine, phenylalanine, valine, tryptophan, PC aa C38:6, PC aa C36:6, PC ae C36:0, SMC20:2, SMC16:0 and creatinine were commonly different in the mid vs. late comparison (Figure 3). The mid and late lactation stage had more common metabolites than early and mid or -late lactation stage.

Enriched pathway shift with lactation stages

The enriched pathways ($p < 0.05$) for the metabolites that differed and tended to differ in concentration between high and low RFI cows at early, late and mid lactation are shown in Figure 4. Citrate cycle (TCA cycle) and glycerophospholipid metabolism had a pathway impact value higher than 0.1, which is the cutoff value for relevance (Figure 4A) at early lactation stage. Phenylalanine, tyrosine and tryptophan biosynthesis and phenylalanine metabolism were enriched pathways at mid lactation. Among the significant pathways, only phenylalanine metabolism and phenylalanine, tyrosine and tryptophan biosynthesis had a pathway impact factor greater than 0.1 (Figure 4B). At late lactation stage, aminoacyl-tRNA biosynthesis, argenine biosynthesis, glycine, serine and threonine metabolism were the top three pathways significantly ($p < 0.05$) enriched between high and low RFI groups (Figure 4C).

Multivariate analyses of milk metabolites during lactation

The supervised orthogonal partial least squares discriminant analysis (OPLS-DA) approach was used to explore the clustering of milk samples from high and low RFI cows at early (Figure 5A), mid (Figure 5B) and late (Figure 5C) lactations. The OPLS-DA score plot showed a clear separation of the high and low RFI cows at early ($Q^2 = 0.68$, $p < 0.001$; $R^2Y = 0.99$, $p = 0.008$), mid ($Q^2 = 0.65$, $p < 0.001$; $R^2Y = 0.98$, $p < 0.001$) and late ($Q^2 = 0.63$, $p < 0.001$; $R^2Y = 0.88$, $p < 0.001$) lactation. The variable importance in projection (VIP) analyses at early, mid and late lactation stages showed the top 15 metabolites that contributed to the separation of high and low RFI groups were shown in Figures 6A–C, respectively. The top 15 metabolites at all the three time points had VIP >1. The step wise linear regression analysis (metabolites significantly different between RFI groups) and VIP (metabolites with VIP >1) identified similar metabolites. Out of the top 15 metabolites (VIP) that contributed to the separation of high and low RFI groups, 12, 13, 14 metabolites were significantly different between RFI groups at early, mid and late lactation, respectively.

A ROC analyses was undertaken to identify the metabolites that could classify cows into high or low RFI categories. Candidate biomarkers were ranked based on the area under the curve (AUC) and the top five candidate biomarkers at each of the three stages of lactation are shown in Table 5. At the early stage of lactation, C10, acyl ornithine, SM C16:0, lysoPC a C16:1 and lysoPC a C18:1 were the top five candidate biomarkers with AUC values of 0.81, 0.75, 0.75, 0.74 and 0.74, respectively. Dodecenoylcarnitine (C12:1), histidine, creatinine, C3:1, C16:1OH were the top five metabolites that were able to distinguish cows in the high or low RFI categories. During the late stage of lactation, phenylalanine, valine, methionine, arginine, acetyl ornithine were the top 5 metabolites with AUC values of 0.85, 0.81, 0.79, 0.79 and 0.78, respectively (Table 5).

Correlation analyses were performed between the top five metabolites (ranked according to AUC values) and their corresponding RFI phenotypes at all the three stages of lactation. At the early stage of lactation, C10, SM C16:0, lysoPC a C18:1 were positively correlated ($p < 0.05$) with RFI phenotypes and acetyl-ornithine was negatively correlated ($p < 0.05$) with RFI. At the mid-lactation stage, out of the top five candidate biomarkers, C12:1 and C16:1-OH were negatively ($p < 0.05$) correlated with RFI phenotypes while, histidine had positive correlation ($p < 0.05$) with RFI. All the top five candidate biomarkers at the late stage of lactation are positively correlated ($p < 0.05$) with RFI phenotypes (Table 5).

Prediction of RFI phenotypes from milk metabolite profiles

A stepwise linear regression analysis was performed to identify milk metabolites that can predict individual RFI phenotypes at early, mid and late lactation stages. Out of the 118 metabolites identified and quantified at each stages of lactation, only metabolites that were significantly different and tended to differ between high and low RFI comparisons were used in the analysis. The analysis was performed on the metabolite concentration data after adjusting for significant fixed effects (parity, MY, HS, and AFC). At the early lactation stage, a total of 24 metabolites were fitted and the model picked 6 metabolites (lysoPC a C18:2, PC aa C40:1, lysoPC a C16:1, acetyl ornithine, citric acid and fumaric acid) as predictors of RFI phenotypes with high accuracy ($R^2 = 0.76$, adjusted $R^2 = 0.71$, root mean squares of error (RMSE) = 1.64). Leave-one-out cross validation R^2 (LOOCV R^2) of 0.65 was observed for the model. Among the 6 metabolites, fumaric acid and lysoPC a C18:2 explained 43% and 34% of the variation explained by the model, respectively. Similarly, at the mid lactation stage, the prediction model was fitted for 28 milk metabolites and the model picked 5 of them (C12.1, PC aa C36:6, C6:1, valine and C12) with relatively lower R^2 (Model $R^2 = 0.53$, adjusted $R^2 = 0.45$, RMSE = 2.2 and LOOCV $R^2 = 0.37$) compared to the early stage of lactation. A relatively lower prediction accuracy and higher root mean squares of error were observed at the mid lactation stage as compared to the early and late stages. At the late lactation,

37 metabolites were fitted in the model and ornithine, serine, PC ae C40:6, betaine, C0, PC ae 36:0, C6:1 and C16 predicted RFI with relatively higher accuracy (model R^2 = 0.77, adjusted R^2 = 0.71, RMSE = 1.73, LOOCV R^2 = 0.60).

Discussion

Lactation stage specific physiological changes in divergent RFI groups

The physiology of residual feed intake during lactation in dairy cows is affected by multi-dimensional factors. The magnitude of change in body reserve mobilization, drainage of nutrients from circulation towards milk synthesis and dry matter intake define the dynamics of physiological state during the lactation period. Taking these dynamics into account, we hypothesized that feed efficient cows may undergo unique physiological adjustments to cope with the metabolic challenges and maintain similar production level from less feed as compared to the feed inefficient cows. To this end, first we compared milk metabolite profiles between high and low RFI cows at the three time points (50, 150, 240 DIM) and traced the pathways enriched by the significantly different metabolite profiles during lactation. Furthermore, we tested the utilization of metabolite profiles which are components or by-products of regulatory networks to identify the feed efficiency level of the cows in the RFI ranking or predict individual RFI phenotypes.

Elevated acyl carnitines and lysophosphatidylcholines in high RFI cows

The comparison of milk metabolite profiles between high and low RFI cows at the early lactation stage revealed elevated concentrations of medium and long-chain acyl carnitines in high RFI cows. The result is in agreement with previous studies that reported increased plasma concentrations of medium and long chain acyl carnitines as an indication for intracellular energy metabolism pattern and metabolic dysfunction (Koves et al., 2008; Adams et al., 2009; Makrecka-Kuka et al., 2017). Carnitine plays an essential role in energy metabolism with the main function of transferring long-chain fatty acids to mitochondria for subsequent β-oxidation (Houten et al., 2016). Incomplete β-oxidation gives rise to even chain C4-C22 acylcarnitine species (Koves et al., 2008). The increase in concentration of milk acyl carnitines (C10:2, C10:1, C10, C16:1) in the least efficient cows is likely due to the incomplete fatty acid β-oxidation as early lactation is characterized by body fat mobilization to overcome the energy deficit. A study in model animals showed that raising plasma fatty acids induces increased biogenesis of mitochondria in skeletal muscle (Garcia-Roves et al., 2007) and lactating dairy cows divergent in genetic background for milk production had different mitochondrial DNA copy number in liver and mammary gland (Weikard and Kuehn, 2018). These results suggest that low RFI cows might increase their mitochondrial biogenesis in key energetically active tissues (mammary gland, liver and muscle) during early lactation to maximize the oxidation of body fat as compared to the high RFI cows. Conversely, it remains possible that the high RFI cows may have a mismatch between increased level of fat and mitochondrial copy number that may lead to increased levels of medium and long-chain acyl carnitines caused by incomplete β-oxidation.

The least efficient cows had increased milk concentration of glycerophospholipids, specifically lysophosphatidylcholines at the early stage of lactation. Lysophosphatidylcholines are formed by hydrolysis of phosphatidylcholines by lipoprotein-associated phospholipase A2 and have been identified as a group of proinflammatory lipids (Schmitz and Ruebsaamen, 2010). The overproduction of lysophosphatidylcholines can result from the overexpression or enhanced activity of enzymes such as lipoprotein-associated phospholipase A2 (Lp-PLA2) in circulation (Thompson et al., 2010). In hepatocytes, higher concentrations of lysophosphocholine disrupts mitochondrial integrity and enhances cytochrome C release (Hollie et al., 2014). The increased milk lysophosphatidylcholine (lysoPC a C20:4, lysoPC a C18:1, lysoPC a C18:2, lysoPC a C16:1, lysoPC a C18:0 and lysoPC a C28:1) concentration in the high RFI group might be due to increased level of lipoprotein-associated phospholipase A2. This may have caused disruption of mitochondrial integrity leading to compromised energy production in the high RFI group. Acyl carnitines and lysophosphatidylcholines are known to activate proinflammatory pathways in rodent models (Hung et al., 2012; Rutkowsky et al., 2014). The energy cost of activating the immune system has been reported to be 0.64 g of glucose/kg of metabolic body weight per hour in dairy cows (Kvidera et al., 2017). Therefore, the increased concentration of acyl carnitines and lysophosphatidylcholines in high RFI cows may have activated the immune system and caused comparatively higher energy loss.

Pathway enrichment analysis for the metabolites that differed ($p < 0.05$) in concentration between least and most efficient cows at the early stage of lactation revealed significant enrichment of TCA cycle and glycerophospholipid metabolism. This indicates that the difference between the least and most efficient lactating cows in energy efficiency at early lactation is likely related to the ATP production efficiency. Of note, mitochondria are responsible for producing over 90% of cellular ATP from acetyl CoA, which is generated upon digestion and catabolism of carbohydrates, protein and lipid derived from the diet and/or body reserves (Cantalapiedra-Hijar et al., 2018). Regulation of the TCA cycle occurs at the points that involve citrate synthase, isocitrate dehydrogenase, and alpha-ketoglutarate dehydrogenase (Cavalcanti et al., 2014). The increased concentration of citric acid in low RFI groups suggests a lower rate of energy production in low RFI cows as glycolysis is inhibited by increased citrate (Wiegand and Remington, 1986).

Elevated short-chain acyl carnitines and decreased amino acids in low RFI cows

At mid lactation stage short-chain acyl carnitines such as C3 and C5 were elevated in low RFI cows and the concentrations of valine, methionine, histidine and tryptophan were decreased ($p < 0.05$). The reciprocal regulation of short-chain acylcarnitines and valine observed in low RFI cows suggests that low RFI cows may supplement their energy source from valine catabolism compared with the high RFI cows. Amino acid catabolism is a source for

C3 and C5 species (Koves et al., 2008) and specifically, valine catabolism results in C3-acylcarnitine production (Newgard, 2012). The oxidation of branched-chain amino acids produces more energy than complete oxidation of glucose in the form of ATP (Monirujjaman and Ferdouse, 2014). The low RFI cows at the mid lactation stage may maintain a comparative energy efficiency by catabolizing amino acids for energy source and subsequently diluting amino acid concentration in milk. Contrary to the early lactation stage, low RFI cows at mid lactation had elevated long-chain acylcarnitines suggesting that low RFI cows oxidize body fat to a certain level as opposed to their high RFI counter parts that may have switched from mobilizing body fat for energy source. In addition, the concentration of methionine was concomitantly increased with the concentration of PC aa C38:6, PC aa C32:2, PC aa C36:6, PC ae C36:0 in high RFI cows and agrees with the finding that methionine activates phosphatidylcholine synthesis (Yao and Vance, 1988).

Compared to high RFI cows, the concentration of the methionine, histidine and tryptophan were decreased ($p < 0.05$) whereas phenylalanine and arginine tended to decrease in low RFI cows. Bifari and Nisoli (2017) reported that the effect of essential amino acids drastically changes when the animal is in catabolic or anabolic condition. In catabolic state, essential amino acids serve as energy substrates while, in anabolic condition they induce protein synthesis and cell growth. The decreased concentrations of these amino acids in milk from low RFI cows is likely due to catabolism that resulted in their subsequent depletion in milk. Notably, histidine, valine and methionine are reported to induce milk protein synthesis in mammary gland epithelial cells *via* the mTOR signalling pathway (Gao et al., 2015; Zhou et al., 2018). Protein production is a costly process and central to the cell physiology (Kafri et al., 2016). In line with this, Aoyagi et al. (1988) estimated the requirement of 7.52 ATPs per peptide synthesis in chicken. Thus, the elevated concentration of these amino acids in high RFI cows suggests that the energy demanding cellular process of protein synthesis or turnover is comparatively higher in high RFI cows. Conversely, the decreased concentration of valine, one of the three branched-chain amino acids, in the low RFI cows suggests that oxidation of amino acids as a fuel source may be taking place and this partly explains the comparative energy efficiency of lactating dairy cows.

Elevated concentrations of amino acids in high RFI cows at late lactation stage

Concentrations of valine, lysine, histidine, tryptophan, proline, citrulline, ornithine, argenine, phenylalanine, serine, methionine, alanine and glutamine were universally elevated in high RFI cows compared to the low RFI group at 240 DIM. In lactating dairy cows, the mammary gland may contribute 40%–45% of whole body protein flux (Lobley, 2003). Capuco et al. (2001) reported decrease in milk production and quantity of mammary gland epithelial cells by 23% and 17% between 90 and 240 DIM, respectively. The increase in the concentration of milk amino acids in the high RFI group at 240 DIM suggests that high RFI cows partition a higher amount of energy to maintain comparatively elevated levels of amino acid concentrations in milk. Richardson and Herd (2004) showed that 37% of the variation in RFI was explained by protein turnover and Cantalapiedra-Hijar et al. (2018) proposed lower energy metabolic rate that may be caused by decreased protein turnover for low RFI animals. The protein turnover in high RFI cows may be characterized by increased protein synthesis and decreased protein degradation, while the low RFI cows may be characterized by decreased protein synthesis and increased protein degradation. Furthermore, serum methylhistidine concentration is used as indicator of muscle breakdown in dairy cows (Houweling et al., 2012). Similarly, the increased concentration of methylhistidine in high RFI cows observed in our study may suggest increased mammary tissue regression in high RFI cows. Therefore, it is likely that at the late lactation stage the difference in feed efficiency levels at least partly accounted by the decreased protein turnover in low RFI cows.

In addition, the concentration of pyruvic acid was increased in the high RFI group compared to the low RFI cows suggesting lower uptake of pyruvate by mitochondria to be oxidized to acetylCoA as the energy source may have shifted to amino acid catabolism. Branched chain amino acids (BCAA) such as valine are oxidized in peripheral tissue (Monirujjaman and Ferdouse, 2014) and the catabolism of the BCAA in the mammary gland increases significantly during lactation (Manjarin et al., 2014). The proportion of mammary intracellular valine utilized for metabolism other than protein synthesis was 34% and this proportion appeared to remain unaffected by dietary AA regime, indicating that valine may participate considerably in metabolism. In the current study, the concentration of valine in milk from high RFI cows markedly exceeds the concentration in the low RFI groups (12.0 ± 2.8 vs. 3.4 ± 0.8) indicating that low RFI cows obtain more energy by catabolism of valine. The oxidation of BCCA produces more energy than complete oxidation of glucose in the form of ATP (Monirujjaman and Ferdouse, 2014) and this partly explains the comparative energy efficiency of most efficient cows.

Milk metabolite profiles as predictors of RFI

The result of ROC analysis revealed that decanoylcarnitine (AUC = 0.81) can distinguish high and low RFI cows and is positively correlated with RFI phenotypes at early lactation stage. This indicates that decanoylcarnitine (C10) can be used as a candidate biomarker of RFI with moderate utility and agrees with the finding that accumulation of medium-chain acylcarnitine fatty acid derivatives are markers of incomplete long-chain fatty acid oxidation (Adams et al., 2009). More interestingly, a set of six metabolites predicted individual RFI phenotypes with moderate accuracy and among the 6 metabolites TCA cycle intermediates (fumaric acid and citric acid) and lysoPC a C18:2 accounted 89% of the variation explained by the model. This complements the pathway enrichment analysis that revealed TCA cycle and glycerophopholipid metabolism as the most important pathways enriched at early lactation. At the mid lactation stage, dodecanoycarnitine (C12) was a promising candidate biomarker (AUC = 0.81) of feed efficiency, however, the panels of metabolites identified to predict individual RFI phenotypes had lower prediction potential indicating their more limited applicability. Ultimately, phenylalanine (AUC = 0.85) and valine (AUC = 0.81) were the top 2 candidate biomarkers at late lactation stage. The panels of metabolites identified to predict individual RFI phenotypes showed comparable prediction potential in early lactation. Overall, early

lactation is the optimum time period to predict RFI phenotypes from milk metabolite since this time point has higher prediction potential and provides individual RFI estimates earlier during the lactation period which can assist management decisions.

Conclusion

This study identified lactation stage specific metabolic differences between high and low RFI cows. We utilized these metabolic differences and identified candidate biomarkers that distinguish RFI categories and developed models that can be used to predict RFI phenotypes from panels of milk metabolite profiles. This result has potential for application to improve feed efficiency of dairy cows and reduce the carbon footprint of milk production.

Data availability statement

The original contributions presented in the study are included in the article/supplementary material, further inquiries can be directed to the corresponding author.

Ethics statement

The animal study was reviewed and approved by the University of Alberta Animal Policy and Welfare Committee for Livestock (Study ID: AUP00000170), and animals were cared for in accordance with the guidelines of the Canadian Council on Animal Care (2009).

Author contributions

DH: Conceptualization, supervision, investigation, methodology, data analyses, visualization, writing-original draft, reviewing and editing the manuscript; MH: Investigation and data analyses; GM: Data analyses, reviewing and editing the manuscript, PS: Conceptualization, reviewing and editing the manuscript; GP: Conceptualization, supervision, project administration, reviewing and editing the manuscript.

Funding

The project was funded by Alberta Agriculture and Forestry, Genome Canada and Alberta Milk.

Acknowledgments

The authors would like to thank University of Alberta Dairy Research and Technology Centre (DRTC) manager and staff for their help in the animal experiment part of the study. The LC-MS/MS analysis for milk samples was undertaken at The Metabolomics Innovation Centre (TMIC) at the University of Alberta.

Conflict of interest

The authors declare that the research was conducted in the absence of any commercial or financial relationships that could be construed as a potential conflict of interest.

Publisher's note

All claims expressed in this article are solely those of the authors and do not necessarily represent those of their affiliated organizations, or those of the publisher, the editors and the reviewers. Any product that may be evaluated in this article, or claim that may be made by its manufacturer, is not guaranteed or endorsed by the publisher.

References

Adams, S. H., Hoppel, C. L., Lok, K. H., Zhao, L., Wong, S. W., Minkler, P. E., et al. (2009). Plasma acylcarnitine profiles suggest incomplete long chain fatty acid beta oxidation and altered tricarboxylic acid cycle activity in type 2 diabetic African American women. *J. Nutr.* 139, 1073–1081. doi:10.3945/jn.108.103754

Aoyagi, Y., Tasaki, I., Okumura, J., and Muramatsu, T. (1988). Energy cost of whole-body protein synthesis measured *in vivo* in chicks. *Comp. Biochem. Physiol. A Comp. Physiol.* 91, 765–768. doi:10.1016/0300-9629(88)90962-0

Basarab, J. A., Beauchemin, K. A., Baron, V. S., Ominski, K. H., Guan, L. L., Miller, S. P., et al. (2013). Reducing GHG emissions through genetic improvement for feed efficiency: Effects on economically important traits and enteric methane production. *Animal* 7, 303–315. doi:10.1017/S1751731113000888

Berry, D. P., and Crowley, J. J. (2013). Cell biology symposium: Genetics of feed efficiency in dairy and beef cattle. *J. Anim. Sci.* 91, 1594–1613. doi:10.2527/jas.2012-5862

Bifari, F., and Nisoli, E. (2017). Branched-chain amino acids differently modulate catabolic and anabolic states in mammals: A pharmacological point of view. *Br. J. Pharmacol.* 174, 1366–1377. doi:10.1111/bph.13624

Canadian Council on Animal Care (2009). *Guidelines on the care and use of farm animals in research, teaching and testing*. Ottawa, Ontario, Canada: Canadian Council on Animal Care.

Cantalapiedra-Hijar, G., Abo-Ismail, M., Carstens, G. E., Guan, L. L., Hegarty, R., Kenny, D. A., et al. (2018). Review: Biological determinants of between-animal variation in feed efficiency of growing beef cattle. *Animal* 12, 321–335. doi:10.1017/S1751731118001489

Capuco, A. V., Wood, D. L., Baldwin, R., McLeod, K., and Paape, M. J. (2001). Mammary cell number, proliferation, and apoptosis during a bovine lactation: Relation to milk production and effect of bST. *J. Dairy Sci.* 84, 2177–2187. doi:10.3168/jds.S0022-0302(01)74664-4

Cavalcanti, J. H., Esteves-Ferreira, A. A., Quinhones, C. G., Pereira-Lima, I. A., Nunes-Nesi, A., Fernie, A. R., et al. (2014). Evolution and functional implications of the tricarboxylic acid cycle as revealed by phylogenetic analysis. *Genome Biol. Evol.* 6, 2830–2848. doi:10.1093/gbe/evu221

Gao, H., Hu, H., Zheng, N., and Wang, J. (2015). Leucine and histidine independently regulate milk protein synthesis in bovine mammary epithelial cells via mTOR signaling pathway. *J. Zhejiang Univ. Sci. B* 16, 560–572. doi:10.1631/jzus.B1400337

Garcia-Roves, P., Huss, J. M., Han, D. H., Hancock, C. R., Iglesias-Gutierrez, E., Chen, M., et al. (2007). Raising plasma fatty acid concentration induces increased biogenesis of mitochondria in skeletal muscle. *Proc. Natl. Acad. Sci. U. S. A.* 104, 10709–10713. doi:10.1073/pnas.0704024104

Hailemariam, D., Manafiazar, G., Basarab, J., Stothard, P., Miglior, F., Plastow, G., et al. (2021). Comparative analyses of enteric methane emissions, dry matter intake, and milk somatic cell count in different residual feed intake categories of dairy cows. *Can. J. Anim. Sci.* 101, 177–190. doi:10.1139/cjas-2019-0085

Hailemariam, D., Mandal, R., Saleem, F., Dunn, S. M., Wishart, D. S., and Ametaj, B. N. (2014). Identification of predictive biomarkers of disease state in transition dairy cows. *J. Dairy Sci.* 97, 2680–2693. doi:10.3168/jds.2013-6803

Hanigan, M. D., and Baldwin, R. L. (1994). A mechanistic model of mammary gland metabolism in the lactating cow. *Agric. Syst.* 45, 369–419. doi:10.1016/0308-521X(94)90132-Y

Hanigan, M. D., France, J., Mabjeesh, S. J., McNabb, W. C., and Bequette, B. J. (2009). High rates of mammary tissue protein turnover in lactating goats are energetically costly. *J. Nutr.* 139, 1118–1127. doi:10.3945/jn.108.103002

Herd, R. M., and Arthur, P. F. (2009). Physiological basis for residual feed intake. *J. Anim. Sci.* 87, E64–E71. doi:10.2527/jas.2008-1345

Hollie, N. I., Cash, J. G., Matlib, M. A., Wortman, M., Basford, J. E., Abplanalp, W., et al. (2014). Micromolar changes in lysophosphatidylcholine concentration cause minor effects on mitochondrial permeability but major alterations in function. *Biochim. Biophys. Acta.* 1841, 888–895. doi:10.1016/j.bbalip.2013.11.013

Houten, S. M., Violante, S., Ventura, F. V., and Wanders, R. J. (2016). The biochemistry and physiology of mitochondrial fatty acid β-Oxidation and its genetic disorders. *Annu. Rev. Physiol.* 78, 23–44. doi:10.1146/annurev-physiol-021115-105045

Houweling, M., van der Drift, S. G., Jorritsma, R., and Tielens, A. G. (2012). Technical note: Quantification of plasma 1- and 3-methylhistidine in dairy cows by high-performance liquid chromatography-tandem mass spectrometry. *J. Dairy Sci.* 95, 3125–3130. doi:10.3168/jds.2011-4769

Hung, N. D., Sok, D., and Kim, M. R. (2012). Prevention of 1-palmitoyl lysophosphatidylcholine-induced inflammation by polyunsaturated acyl lysophosphatidylcholine. *Inflamm. Res.* 61, 473–483. doi:10.1007/s00011-012-0434-x

Jewell, K. A., McCormick, C. A., Odt, C. L., Weimer, P. J., and Suen, G. (2015). Ruminal bacterial community composition in dairy cows is dynamic over the course of two lactations and correlates with feed efficiency. *Appl. Environ. Microbiol.* 81, 4697–4710. doi:10.1128/AEM.00720-15

Kafri, M., Metzl-Raz, E., Jona, G., and Barkai, N. (2016). The cost of protein production. *Cell Rep.* 14, 22–31. doi:10.1016/j.celrep.2015.12.015

Klein, M. S., Buttchereit, N., Miemczyk, S. P., Immervoll, A. K., Louis, C., Wiedemann, S., et al. (2011). NMR metabolomic analysis of dairy cows reveals milk glycerophosphocholine to phosphocholine ratio as prognostic biomarker for risk of ketosis. *J. Proteome Res.* 11, 1373–1381. doi:10.1021/pr201017n

Knight, C. H., France, J., and Beever, D. E. (1994). Nutrient metabolism and utilization in the mammary gland. *Livest. Prod. Sci.* 39, 129–137. doi:10.1016/0301-6226(94)90164-3

Koch, R. M., Swiger, L. A., Chambers, D., and Gregory, K. E. (1963). Efficiency of feed use in beef cattle. *J. Anim. Sci.* 22, 486–494. doi:10.2527/jas1963.222486x

Koves, T. R., Ussher, J. R., Noland, R. C., Slentz, D., Mosedale, M., Ilkayeva, O., et al. (2008). Mitochondrial overload and incomplete fatty acid oxidation contribute to skeletal muscle insulin resistance. *Cell Metab.* 7, 45–56. doi:10.1016/j.cmet.2007.10.013

Kuhn, M. (2005). Building predictive models in R using the caret package. *J. Stat. Softw.* 14, 981029. doi:10.18637/jss.v081.b02

Kvidera, S. K., Dickson, M. J., Abuajamieh, M., Snider, D. B., Sanz Fernandez, M. V., Johnson, J. S., et al. (2017). Intentionally induced intestinal barrier dysfunction causes inflammation, affects metabolism, and reduces productivity in lactating Holstein cows. *J. Dairy Sci.* 100, 4113–4127. doi:10.3168/jds.2016-12349

Li, P., Knabe, D. A., Kim, S. W., Lynch, C. J., Hutson, S. M., and Wu, G. (2009). Lactating porcine mammary tissue catabolizes branched-chain amino acids for glutamine and aspartate synthesis. *J. Nutr.* 139, 1502–1509. doi:10.3945/jn.109.105957

Lobley, G. E. (2003). Protein turnover—What does it mean for animal production? *Can. J. Anim. Sci.* 83, 327–340. doi:10.4141/a03-019

Makrecka-Kuka, M., Sevostjanovs, E., Vilks, K., Volska, K., Antone, U., Kuka, J., et al. (2017). Plasma acylcarnitine concentrations reflect the acylcarnitine profile in cardiac tissues. *Sci. Rep.* 7, 17528. doi:10.1038/s41598-017-17797-x

Manafiazar, G., McFadden, T., Goonewardene, L., Okine, E., Basarab, J., Li, P., et al. (2013). Prediction of residual feed intake for first-lactation dairy cows using orthogonal polynomial random regression. *J. Dairy Sci.* 96, 7991–8001. doi:10.3168/jds.2013-6560

Manjarin, R., Bequette, B. J., Wu, G., and Trottier, N. L. (2014). Linking our understanding of mammary gland metabolism to amino acid nutrition. *Amino Acids* 46, 2447–2462. doi:10.1007/s00726-014-1818-8

Monirujjaman, M., and Ferdouse, A. (2014). Metabolic and physiological roles of branched-chain amino acids. *Adv. Mol. Bio.* 2014, 1–6. doi:10.1155/2014/364976

Newgard, C. B. (2012). Interplay between lipids and branched-chain amino acids in development of insulin resistance. *Cell Metab.* 15, 606–614. doi:10.1016/j.cmet.2012.01.024

Potts, S. B., Boerman, J. P., Lock, A. L., Allen, M. S., and VandeHaar, M. J. (2017). Relationship between residual feed intake and digestibility for lactating Holstein cows fed high and low starch diets. *J. Dairy Sci.* 100, 265–278. doi:10.3168/jds.2016-11079

Rezaei, R., Wu, Z., Hou, Y., Bazer, F. W., and Wu, G. (2016). Amino acids and mammary gland development: Nutritional implications for milk production and neonatal growth. *J. Anim. Sci. Biotechnol.* 7, 20. doi:10.1186/s40104-016-0078-8

Richardson, E. C., and Herd, R. M. (2004). Biological basis for variation in residual feed intake in beef cattle. 2. Synthesis of results following divergent selection. *Aust. J. Exp. Agric.* 44, 431–440. doi:10.1071/EA02221

Rutkowsky, J. M., Knotts, T. A., Ono-Moore, K. D., McCoin, C. S., Huang, S., Schneider, D., et al. (2014). Acylcarnitines activate proinflammatory signaling pathways. *Am. J. Physiol. Endocrinol. Metab.* 306, E1378–E1387. doi:10.1152/ajpendo.00656.2013

Schmitz, G., and Ruebsaamen, K. (2010). Metabolism and atherogenic disease association of lysophosphatidylcholine. *Atherosclerosis* 208, 10–18. doi:10.1016/j.atherosclerosis.2009.05.029

Sun, H. Z., Shi, K., Wu, X. H., Xue, M. Y., Wei, Z. H., Liu, J. X., et al. (2017). Lactation-related metabolic mechanism investigated based on mammary gland metabolomics and 4 biofluids' metabolomics relationships in dairy cows. *BMC Genom* 18, 936. doi:10.1186/s12864-017-4314-1

Thompson, A., Gao, P., Orfei, L., Watson, S., Di Angelantonio, E., Kaptoge, S., et al. (2010). Lipoprotein-associated phospholipase A (2) and risk of coronary disease, stroke, and mortality: Collaborative analysis of 32 prospective studies. *Lancet* 375, 1536–1544. doi:10.1016/S0140-6736(10)60319-4

Tian, H., Zheng, N., Wang, W., Cheng, J., Li, S., Zhang, Y., et al. (2016). Integrated metabolomics study of the milk of heat-stressed lactating dairy cows. *Sci. Rep.* 6, 24208. doi:10.1038/srep24208

Weikard, R., and Kuehn, C. (2018). Different mitochondrial DNA copy number in liver and mammary gland of lactating cows with divergent genetic background for milk production. *Mol. Biol. Rep.* 45, 1209–1218. doi:10.1007/s11033-018-4273-x

Wiegand, G., and Remington, S. J. (1986). Citrate synthase: Structure, control, and mechanism. *Annu. Rev. Biophys. Biophys. Chem.* 15, 97–117. doi:10.1146/annurev.bb.15.060186.000525

Xia, J., Broadhurst, D. I., Wilson, M., and Wishart, D. S. (2013). Translational biomarker discovery in clinical metabolomics: An introductory tutorial. *Metabolomics* 9, 280–299. doi:10.1007/s11306-012-0482-9

Xiao, C. T., and Cant, J. P. (2005). Relationship between glucose transport and metabolism in isolated bovine mammary epithelial cells. *J. Dairy Sci.* 88, 2794–2805. doi:10.3168/jds.S0022-0302(05)72959-3

Yao, Z. M., and Vance, D. E. (1988). The active synthesis of phosphatidylcholine is required for very low density lipoprotein secretion from rat hepatocytes. *J. Biol. Chem.* 263, 2998–3004. doi:10.1016/s0021-9258(18)69166-5

Zhou, Y., Zhou, Z., Peng, J., and Loor, J. J. (2018). Methionine and valine activate the mammalian target of rapamycin complex 1 pathway through heterodimeric amino acid taste receptor (TAS1R1/TAS1R3) and intracellular Ca2+ in bovine mammary epithelial cells. *J. Dairy Sci.* 101, 11354–11363. doi:10.3168/jds.2018-14461

frontiers | Frontiers in Molecular Biosciences

TYPE Original Research
PUBLISHED 19 April 2023
DOI 10.3389/fmolb.2023.1171366

OPEN ACCESS

EDITED BY
Elda Dervishi,
University of Alberta, Canada

REVIEWED BY
Nagarjun Vijay,
Indian Institute of Science Education and Research, India
Yazhi Xing,
Shanghai Jiao Tong University, China

*CORRESPONDENCE
Hui Wang,
wangh681@nenu.edu.cn
Jiang Feng,
fengj@nenu.edu.cn

RECEIVED 22 February 2023
ACCEPTED 06 April 2023
PUBLISHED 19 April 2023

CITATION
Wang H, Sun R, Xu N, Wang X, Bao M, Li X, Li J, Lin A and Feng J (2023), Untargeted metabolomics of the cochleae from two laryngeally echolocating bats.
Front. Mol. Biosci. 10:1171366.
doi: 10.3389/fmolb.2023.1171366

Untargeted metabolomics of the cochleae from two laryngeally echolocating bats

Hui Wang[1]*, Ruyi Sun[1], Ningning Xu[1], Xue Wang[1], Mingyue Bao[1], Xin Li[1], Jiqian Li[2], Aiqing Lin[2] and Jiang Feng[1,2]*

[1]College of Life Science, Jilin Agricultural University, Changchun, China, [2]Jilin Provincial Key Laboratory of Animal Resource Conservation and Utilization, Northeast Normal University, Changchun, China

High-frequency hearing is regarded as one of the most functionally important traits in laryngeally echolocating bats. Abundant candidate hearing-related genes have been identified to be the important genetic bases underlying high-frequency hearing for laryngeally echolocating bats, however, extensive metabolites presented in the cochleae have not been studied. In this study, we identified 4,717 annotated metabolites in the cochleae of two typical laryngeally echolocating bats using the liquid chromatography–mass spectroscopy technology, metabolites classified as amino acids, peptides, and fatty acid esters were identified as the most abundant in the cochleae of these two echolocating bat species, *Rhinolophus sinicus* and *Vespertilio sinensis*. Furthermore, 357 metabolites were identified as significant differentially accumulated (adjusted *p*-value <0.05) in the cochleae of these two bat species with distinct echolocating dominant frequencies. Downstream KEGG enrichment analyses indicated that multiple biological processes, including signaling pathways, nervous system, and metabolic process, were putatively different in the cochleae of *R. sinicus* and *V. sinensis*. For the first time, this study investigated the extensive metabolites and associated biological pathways in the cochleae of two laryngeal echolocating bats and expanded our knowledge of the metabolic molecular bases underlying high-frequency hearing in the cochleae of echolocating bats.

KEYWORDS

bats, cochlea, echolocation, high-frequency hearing, untargeted metabolomics

1 Introduction

Echolocation is a remarkable and perceptive behavior that is well evolved in bats, which is usually used for orientation, obstacle avoidance, and hunting (Jones, 2005; Jones and Teeling, 2006). Although echolocation is found in several mammalian lineages (He et al., 2021), laryngeally echolocating bats are renowned for their sophisticated echolocation (Simmons et al., 1979; Jones and Teeling, 2006). High-frequency hearing is an important component of echolocation and is essential for echolocating bats to perceive ultrasonic signals (Wohlgemuth et al., 2016; Moss, 2018). The molecular bases underlying echolocation accompanied by high-frequency hearing have attracted increasing attentions (Cao et al., 2022).

The majority of echolocating bats are usually referred to as laryngeally echolocating bats who can emit ultrasonic vocalizations through their larynxes (Waters and Vollrath, 2003; Yovel et al., 2010), including constant-frequency (CF) bats and frequency-modulated (FM)

bats. Therefore, both CF and FM bats have been identified as laryngeally echolocating bats in the true sense of the term with high-frequency hearing. The realization of high-frequency hearing involves many organs and physiological processes, among them, the cochlea is a most important organ of the auditory system (Adams and Pedersen, 2013; Moss, 2018). It is a snail-shaped inner ear structure that plays important roles in sound perception, signal processing, and transmission to the brain (Davies et al., 2013; Moss, 2018). Previous studies have demonstrated that the cochleae of laryngeally echolocating bats have possessed special structural, physiological and genetic adaptations for detecting high-frequency acoustic signals (Ulanovsky and Moss, 2008; Schnitzler and Denzinger, 2011; Vater and Kössl, 2011; Davies et al., 2013).

Transcriptomic approaches have been usually used to uncover candidate genes and biological pathways underlying the genetic bases of adaptations for high-frequency hearing in echolocating bats (Dong et al., 2013; Wang et al., 2018; Ma et al., 2020). A study involving comparative inner ear transcriptomic analysis between *M. ricketti* (FM echolocating bat) and *Cynopterus sphinx* (non-echolocating bat) demonstrated that the genes upregulated in *Myotis ricketti* were particularly associated with cochlear morphogenesis, inner ear morphogenesis, and sensory perception of sound categories, which are consistent with the morphological and physiological differentiation of the inner ear between these two species (Dong et al., 2013). In addition, comparative cochlear transcriptomic analyses of four different bat species have demonstrated variations of gene expression among the bats and different nervous system activities during auditory perception in the cochlea particularly in CF bats (Wang et al., 2018). Besides, numerous efforts to identify high-frequency hearing-related genes have examined differences in coding sequences between echolocating and non-echolocating mammalian species including bats and even whales (Li et al., 2008; Liu et al., 2010; Davies et al., 2012; Wang et al., 2020; Liu et al., 2022). Genome-wide screening has also revealed that multiple hearing-related genes show molecular adaptation in lineages of echolocators (Parker et al., 2013; Zou and Zhang, 2015; Liu et al., 2018; Liu et al., 2022).

In recent years, an accumulating body of researches have indicated that abundant metabolites may be particularly important for specific phenotype (Keurentjes, 2009; Zampieri and Sauer, 2017; Han et al., 2021). Metabolomics is a new branch of "-omics" science in the postgenomic era that has high potential due to its close relationship with phenotype (Fraga-Corral et al., 2022). In addition to the hearing-related genes, cochlear metabolites may also play important roles in the realization of high-frequency hearing for echolocating bats (Meng et al., 2020; Wörheide et al., 2021). However, cochlear metabolites and associated metabolic pathways in laryngeally echolocating bats have been less clearly understood.

Therefore, in this study, we explored the utility of liquid chromatography–mass spectroscopy (LC-MS) to take an insight into the cochlear metabolites of two typical laryngeally echolocating bats, *R. sinicus* and *V. sinensis*. *R. sinicus*, belonging to the Rhinolophidae, is a typical CF bat species, whose dominant frequency is around 83.15 kHz (Xie et al., 2017; Wang et al., 2018). Meanwhile, *Vespertilio sinensis* is a typical FM bat and belongs to the Vespertilionidae, with a dominant frequency around 24.2 kHz (Fukui et al., 2004). For the first time, we here aim to detect the metabolites responsible for the cochlear function of laryngeally echolocating bats. We also aim to uncover the differences of metabolites and related biological processes in the cochleae between these two bat species. This study is expected to provide a new perspective for the studies of echolocation and high-frequency hearing in bats.

2 Materials and Methods

2.1 Sample collection

Six biological repeats for each bat species were included for the metabolomic analyses. Therefore, six adults of *R. sinicus* and *V. sinensis* were captured during July, respectively. To avoid any influence of sex-related differences, only females were selected for inclusion in the study. All individuals were euthanized by cervical dislocation, and a pair of cochleae from each individual were collected and immediately flash-frozen in liquid nitrogen in the field, before transfer to a −80°C freezer.

2.2 Metabolite extraction and sequencing sample preparation

Equal amounts of the cochlear samples from the two bat species (30 mg, n = 12) were transferred to a 2 ml centrifuge tube, supplemented with 600 µl of precooled 50% methanol (stored at −20°C) containing 2-amino-3-(2-chlorophenyl)-propionic acid (4 ppm), and vortexed for 1 min. Subsequently, the samples were precooled at −20°C for 2 min, supplemented with 100 mg of glass beads, and placed in a tissue grinder for 2 min at 60 Hz. Room temperature ultrasonic extraction was then applied for 15 min, followed by storage at −20°C for 30 min. After centrifugation at 13,000 g for 10 min at 4°C, the supernatant was transferred to a new tube. The extraction solution was vacuum-dried and resuspended in 50% methanol (vortexing for 30 s and ultrasonic extraction for 3 min), followed by storage at −20°C for 2 h. Finally, centrifugation was applied at 13,000 g for 10 min at 4°C, and the obtained supernatant was transferred into a detection bottle. Meanwhile, pooled quality control (QC) samples were prepared by mixing an equal volume of each extraction sample. All the samples were stored at −80°C prior to the LC-MS analysis. The experimental process mainly refers to the reagent supplies manual instruction and references (Zhou et al., 2012; Cao et al., 2020).

2.3 LC-MS-based metabolomic analysis

All samples were analyzed using an ACQUITY UPLC I-Class system (Waters Corporation, Milford, MA, USA) coupled with a VION IMS QTOF mass spectrometer (Waters Corporation, Milford, MA, United States) for metabolic profiling in both ESI positive and ESI negative ion modes. An ACQUITY UPLC BEH C18 column (1.8 µm, 2.1 × 100 mm) was employed in both positive and negative modes. Water and acetonitrile/methanol 2/3 (v/v), both containing 0.1% formic acid, were used as mobile phases A and B, respectively. The following linear gradient was applied: 0.01 min,

5% B; 4 min, 30% B; 8 min, 50% B; 10 min, 80% B; 14 min, 100% B; 15 min, 100% B; 15.1 min, 5% B; and 16 min, 5% B. The flow rate was 0.35 mL/min and the column temperature was maintained at 45°C. All samples were kept at 4°C during the analysis. The injection volume was 2 μL. The mass range was from m/z 100 to 1,200. The resolution was set at 70,000 for the full MS scans and 17,500 for the HCD MS/MS scans. The collision energy was set at 10, 20, and 40 eV. The mass spectrometer was operated as follows: spray voltage, 3,800 V (+) for the positive ion mode and 3,200 V (−) for the negative ion mode; sheath gas flow rate, 40 arbitrary units; auxiliary gas flow rate, 8 arbitrary units; capillary temperature, 320°C; probe heater temperature, 350°C; and S-lens RF level, 50. The QC samples (created by pooling all of the samples) were injected at regular intervals throughout the analytical run to provide a set of data from which repeatability could be assessed (Zhou et al., 2012; Cao et al., 2020).

2.4 Metabolomic data processing

The raw LC-MS data were processed using the software Progenesis QI V2.3 (Non-linear Dynamics, Newcastle, United Kingdom) for baseline filtering, peak identification, integrity, retention time correction, peak alignment, and normalization. The main parameters of 5 ppm precursor tolerance, 10 ppm product tolerance, and 5% product ion threshold were applied. Compound identification was based on the precise mass-to-charge ratio (m/z), secondary fragments, and isotopic distribution using the Human Metabolome Database (HMDB, http://www.hmdb.ca), The Kyoto Encyclopedia of Genes and Genomes (KEGG, http://www.kegg.com/), Lipidmaps (V2.3), Metlin, EMDB, PMDB, and custom-made databases to perform qualitative analysis. The extracted data were then further processed by removing any peaks with a missing value (ion intensity = 0) in more than 50% in groups, and by screening according to the qualitative results of the compound. Compounds with resulting scores below 36 points were also deemed to be inaccurate and removed (the full score is 60 and the pass mark is 36). A data matrix was combined from the positive ion and negative ion data. The matrix was imported into R to carry out principal component analysis (PCA) to observe the overall distribution among the samples and the stability of the whole analytical process. Orthogonal partial least-squares discriminant analysis (OPLS-DA) and partial least-squares discriminant analysis (PLS-DA) were used to distinguish the metabolites that differ between groups. To prevent overfitting, sevenfold cross-validation and 200 response permutation testing (RPT) were used to evaluate the quality of the model. Variable importance of projection (VIP) values obtained from the OPLS-DA model were used to rank the overall contribution of each variable to group discrimination. Two-tailed Student's t-test was further used to verify that the metabolites differing between groups were significant. Differential metabolites with VIP values greater than 1.0 and *p*-values less than 0.05 were selected.

2.5 Differentially accumulated metabolites (DAMs) identified and bioinformatic analysis

To reveal the differences between the cochleae of *R. sinicus* and *V. sinensis*, a series of criteria were used to identify the DAMs among annotated metabolites: VIP >1, |fold change| > 1.5, and adjusted *p*-value <0.05. Visualization of the DAMs in the two bat species was achieved by creating heatmaps and a volcano plot using the OmicShare tools (http://www.omicshare.com/tools), a free online platform for data analysis. Among the DAMs, the predominantly accumulated metabolites in the cochleae of *R. sinicus* and *V. sinensis* were submitted to the OmicShare tools (http://www.omicshare.com/tools) to identify the representative KEGG pathways for further elucidation of the functional properties.

3 Results

3.1 Global metabolites detected in the cochlea of two laryngeally echolocating bat species

To explore the global metabolites in the cochleae of the two laryngeally echolocating bats, *R. sinicus* and *V. sinensis*, untargeted metabolomic analyses were performed, which identified 4,717 annotated metabolites from 10,958 positive ion and negative ion features (Table 1; Supplementary Table S1). The overlapping total ion chromatograms (TIC) of positive mode and negative mode of all samples and the QC samples demonstrated that all samples obtained in the positive ion and negative ion modes had a good overlap, which indicated that this model was stable, reproducible, and consistent for all of the samples (Supplementary Figure S1).

3.2 Multivariate statistical analysis of sequencing samples

PCA was used to determine the sample separation and aggregation between *R. sinicus* and *V. sinensis* (Figure 1A). Each point on the PCA score graph represents a single sample. Aggregation of points indicates that the observed variables are highly similar, while discrete points represent significant differences in the observed variables. The PCA scores illustrated that PC1 and PC2 were responsible for 54.4% and 9.6% of the variation, respectively, indicating a clear separation between these two bat species. The results demonstrated that *R. sinicus* and *V. sinensis* had different cochlear metabolic characteristics. In addition, PLS-DA, which is a supervised discriminant profiling statistical method, was used to identify more specific differences between the groups (Figure 1B). Accordingly, higher values for PLS-DA model parameters denote greater reliability for the PLS-DA model. R2 of the PLS-DA model was 0.998 and Q2 was 0.967, which denoted greater reliability for the PLS-DA model. According to the PLS-DA model parameters, this model was reasonable for interpreting the differences between the two bat species. In addition, the OPLS-DA score plot demonstrated a clearer separation of *R. sinicus* and *V. sinensis* and the parameters were as follows: R2X = 0.774, R2Y = 0.998, and Q2 = 0.974, indicating that the current OPLS-DA model is more reliable and that consistent modeling and predictability were achieved (Figures 1C, D). Therefore, these data were used for subsequent analyses.

TABLE 1 Basic information of the cochlear metabolomics of the two echolocating bats.

Identification	Metabolites	Annotated metabolites	Super-class	Class	Sub-class
Positive ion	5,867	3,108	2,325	2,323	2,172
Negative ion	5,091	1,609	1,085	1,082	1,005
Total	10,958	4,717	3,410	3,405	3,177

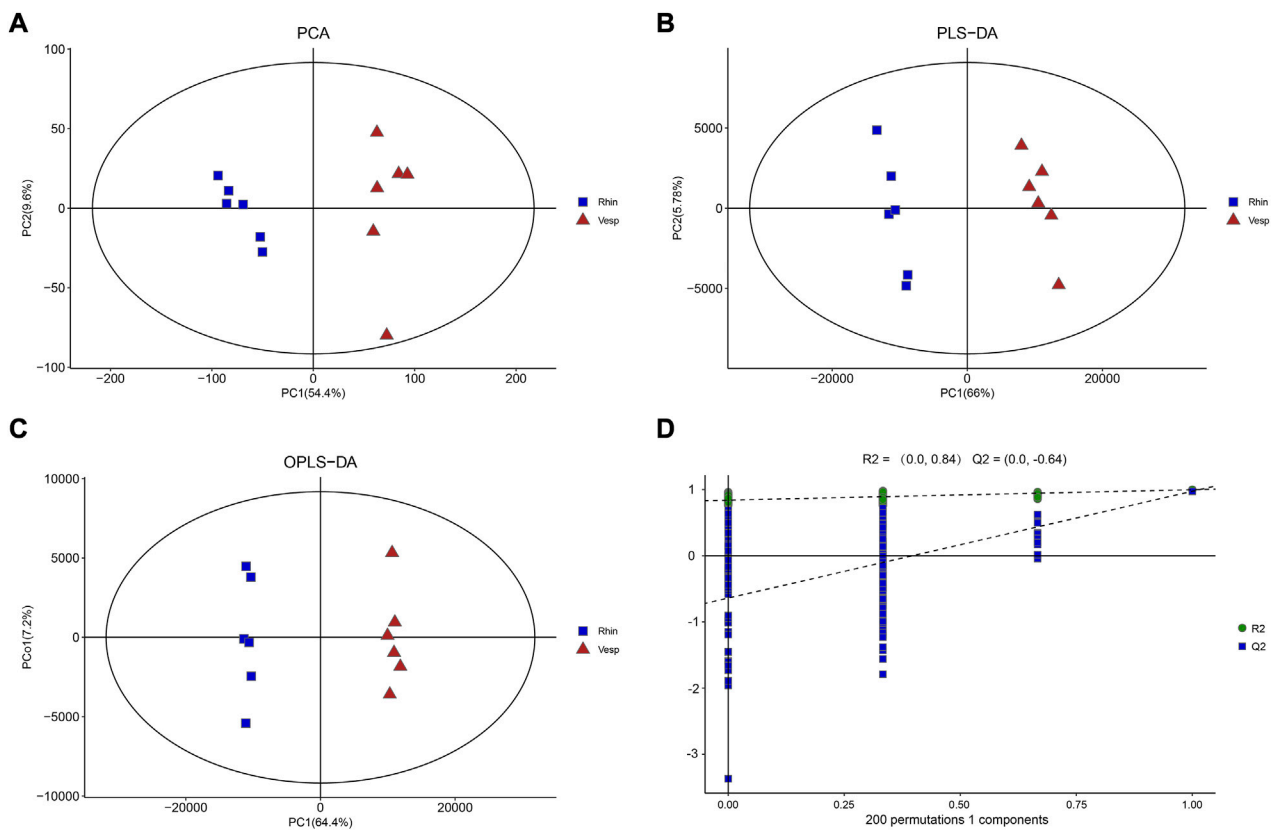

FIGURE 1
Results of multivariate analysis of cochlear samples from the *R. sinicus*, and *V. sinensis*. **(A)** PCA score plot, **(B)** OPLS-DA score plot, **(C)** PLS-DA score plot, **(D)** permutation plot. There is a clear separation of *R. sinicus*, and *V. sinensis*.

3.3 Classification of metabolites

In addition, heatmaps of the 4,717 annotated metabolites identified in the cochleae of the two echolocating bats are presented in Figure 2, which illustrates that metabolites varied greatly between *R. sinicus* and *V. sinensis* according to the total metabolites and both sets of metabolites detected based on positive ion and negative ion analyses.

Based on the annotations of the 4,717 metabolites, most metabolites were assigned to at least one metabolic category and various different types of metabolites were detected in the cochleae of the two echolocating bats (Supplementary Table S2). Among these 4,717 annotated metabolites, 3,410 metabolites, 3,405 metabolites, and 3,177 metabolites were identified to be Super-class, Class, and Sub-class metabolic categories (Figure 3; Supplementary Table S2). At the Super-class level, the three largest metabolic categories were Lipids and lipid-like molecules (1,987 metabolites), Organic acids and derivatives (446 metabolites), Organoheterocyclic compounds (315 metabolites) (Figure 3A). Similarly, metabolites detected at the Class and the Sub-class levels were illustrated by Figures 3B, C, respectively.

Various metabolic categories were identified for the metabolites detected in the cochleae of the two echolocating bats. Figure 4 has showed the KEGG classes of all identified metabolites, indicating that several metabolism related processes were the most abundant, including Amino acid metabolism, Lipid metabolism, and Carbohydrate

10.3389/fmolb.2023.1171366

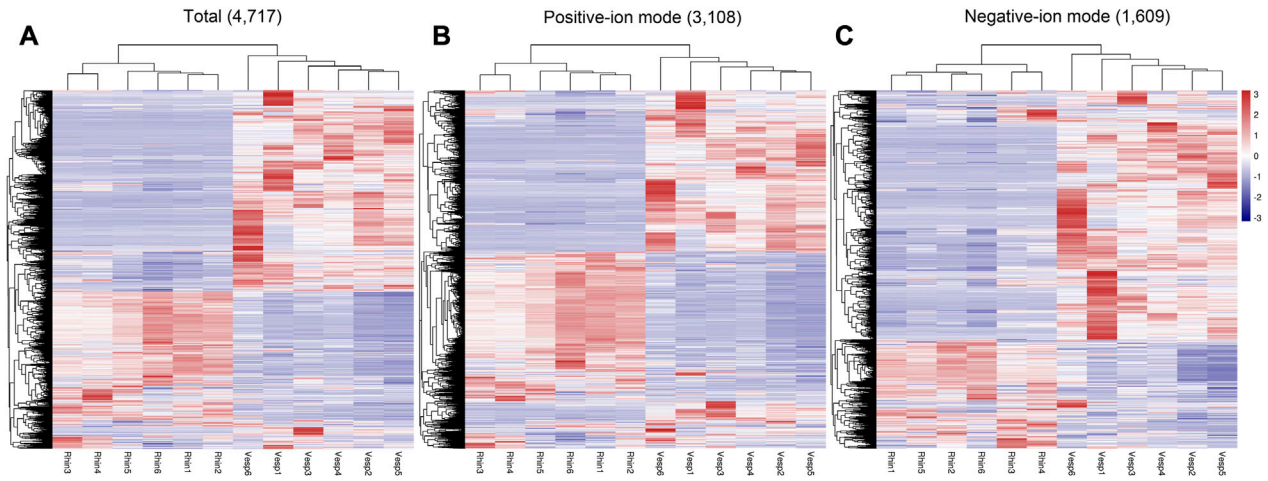

FIGURE 2
Heatmaps of the 4,717 annotated metabolites identified in the cochlea of *R. sinicus* and *V. sinensis*. **(A)** Total ions, **(B)** Positive ion mode, **(C)** Negative ion mode. Rhin and Vesp stand *R. sinicus* and *V. sinensis*, respectively, as also used elsewhere in this paper.

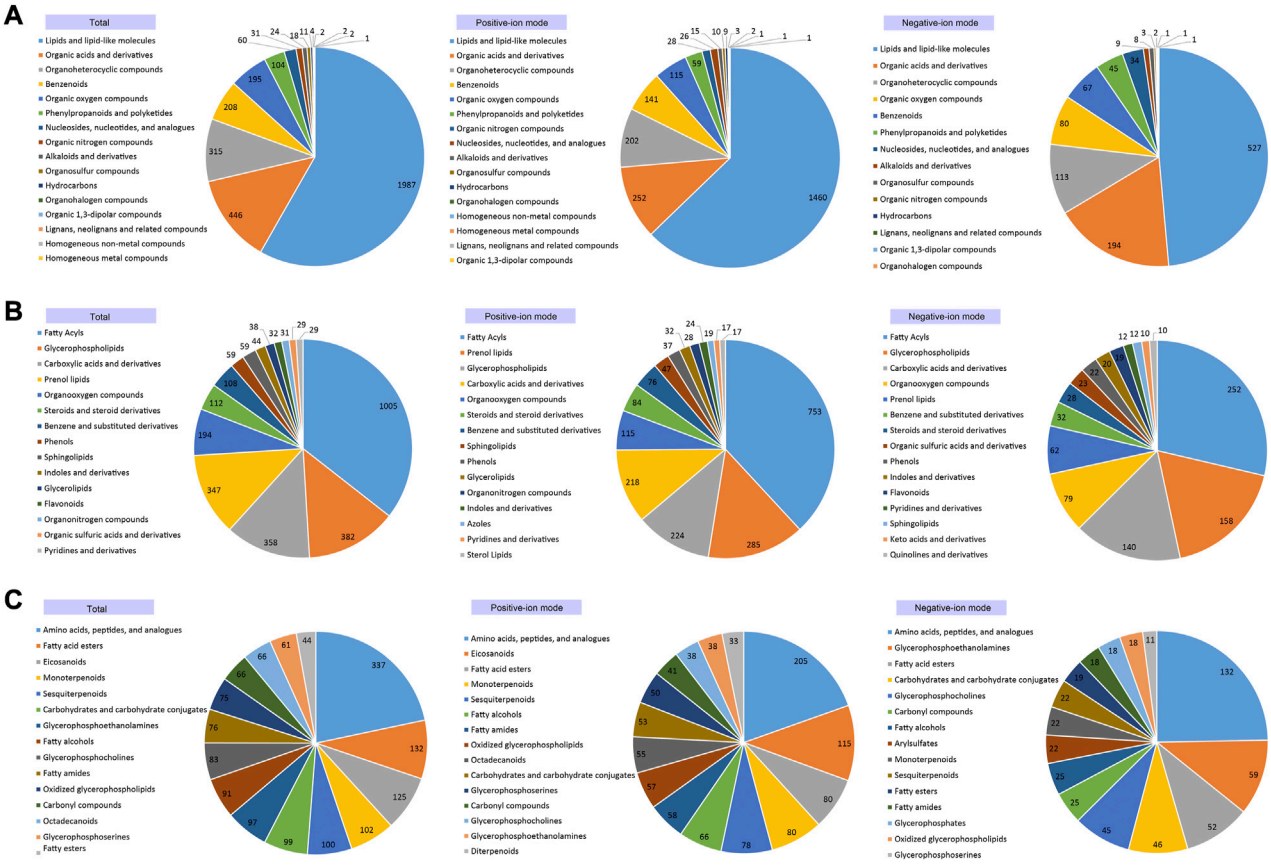

FIGURE 3
Annotated cochlear metabolites detected for Super-classification **(A)**, Classification **(B)** and Sub-classification **(C)**, respectively.

metabolism. Further analysis of the third hierarchical levels of KEGG pathways is listed in Supplementary Table S3. The top 5 largest KEGG pathways were Metabolic pathways (416), Arachidonic acid metabolism (46), Glycerophospholipid metabolism (39), Biosynthesis of amino acids (39), and ABC transporters (39).

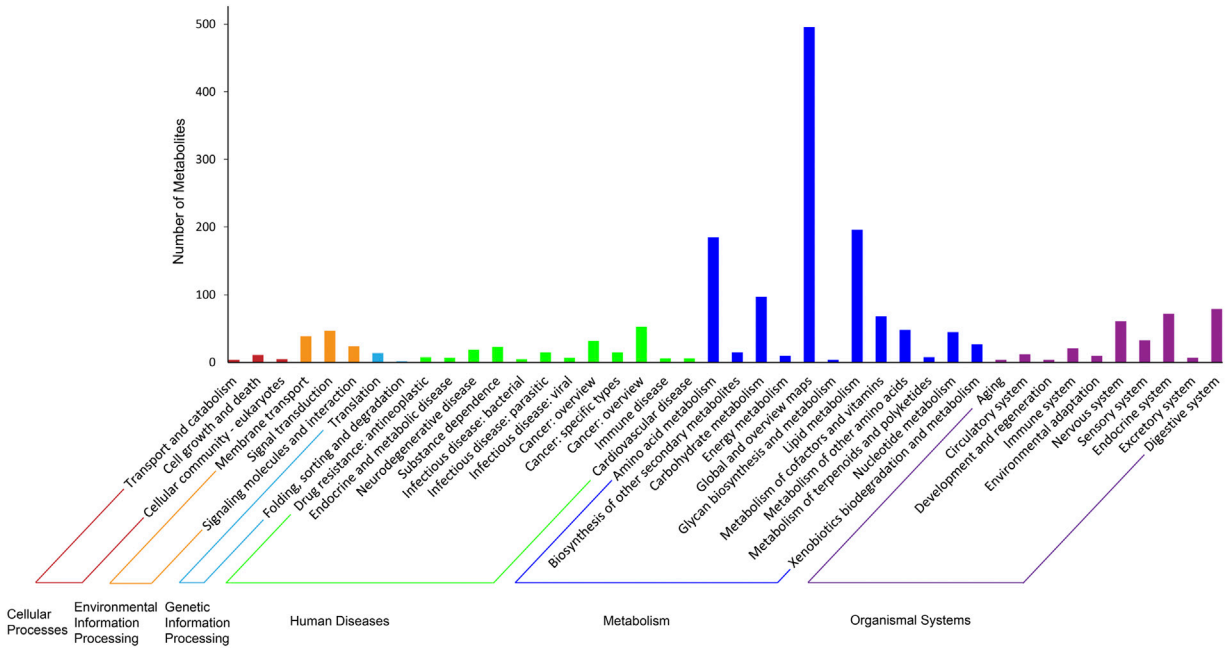

FIGURE 4
The KEGG categories of all identified metabolites.

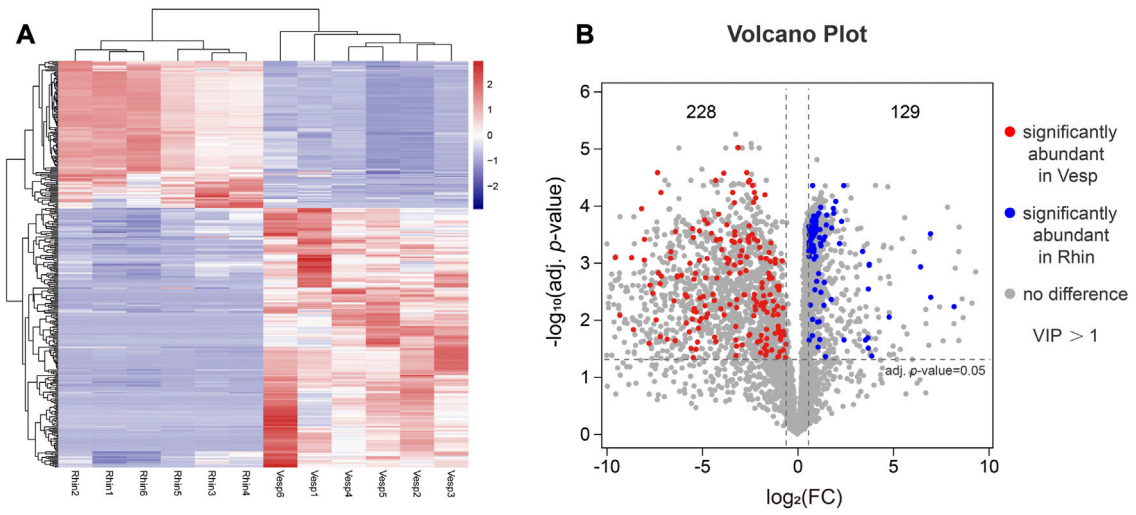

FIGURE 5
Visualization of DAMs present at significantly different levels in *R. sinicus* and *V. sinensis*. **(A)** Heatmaps of DAMs with the abundance levels in all cochlear samples. Red indicates an increase, blue indicates a decrease, rows indicate different metabolites, and columns indicate different samples. **(B)** Volcano plot of DAMs.

3.4 DAMs detected in the cochlea between *R. sinicus* and *V. sinensis*

Accordingly, 4,717 high-quality metabolites were used to screen the significant DAMs using the criteria referred to in the Materials and Methods. A total of 357 DAMs were identified to be significantly differentially accumulated (adjusted *p*-value <0.05) between *R. sinicus* and *V. sinensis*, including 129 and 228 metabolites significantly abundant in the cochleae of *R. sinicus* and *V. sinensis*, respectively. A heatmap was used to exhibit the 357 DAMs with different levels in the cochleae of *R. sinicus* and *V. sinensis* (Figure 5A), which suggested that significantly different metabolites were accumulated in the cochleae of the two bat species. A volcano plot indicated the results of analyzing the significance of

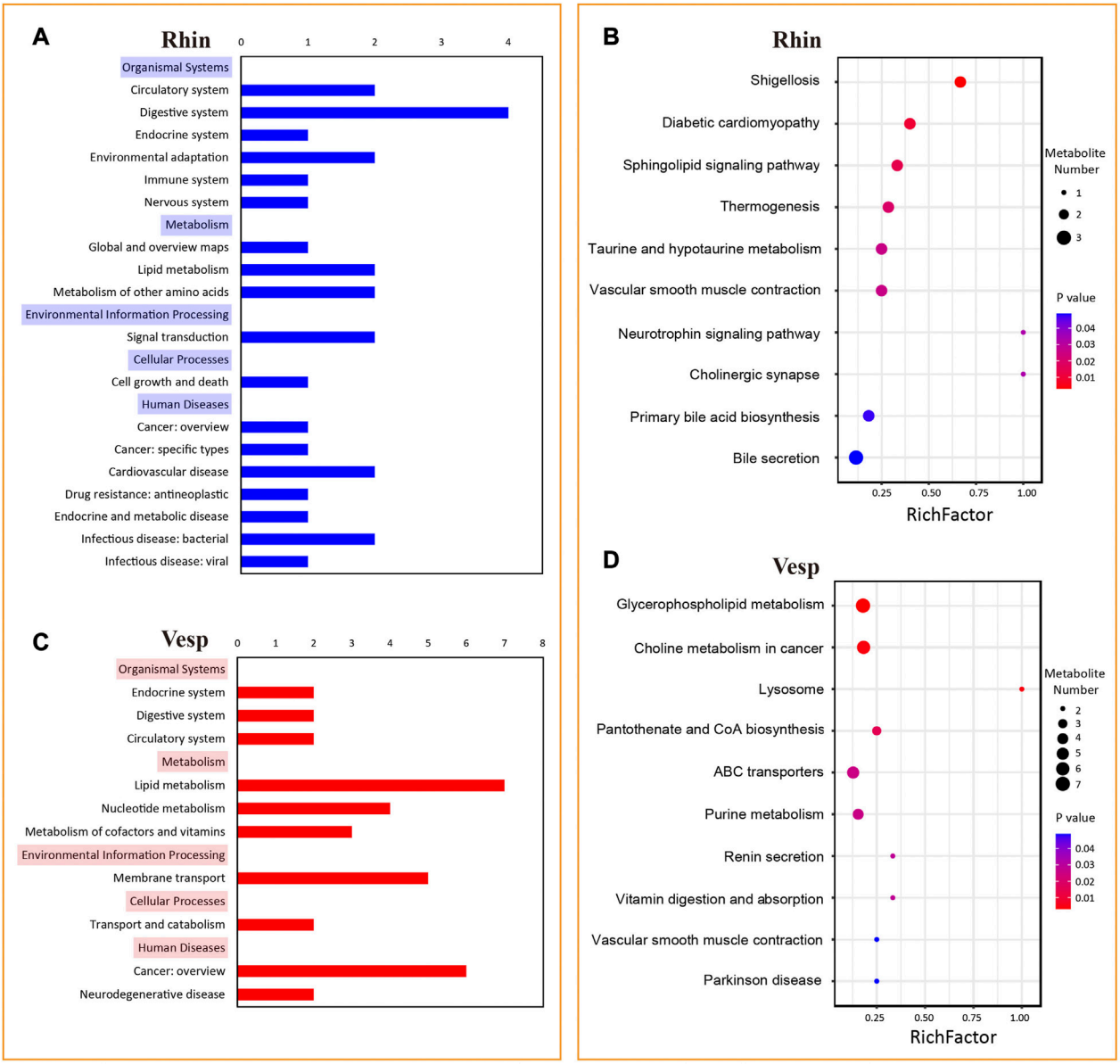

FIGURE 6
KEGG pathways significantly associated with 129 and 228 DAMs with significantly abundant levels in the cochleae of *R. sinicus* and *V. sinensis*, respectively. **(A)** and **(C)** KEGG A and B categories significantly associated with DAMs for *R. sinicus* and *V. sinensis*. **(B)** and **(D)** The top 10 KEGG pathways significantly associated with DAMs for *R. sinicus* and *V. sinensis*.

the DAMs between *R. sinicus* and *V. sinensis* (Figure 5B). Concretely, the DAMs were further assigned to the Super-class (Supplementary Figure S2), Class (Supplementary Figure S3), and Sub-class categories (Supplementary Figure S4) indicating variations of cochlear metabolites between *R. sinicus* and *V. sinensis*.

3.5 Differences of related biological processes between *R. sinicus* and *V. sinensis* revealed by DAMs

Numerous KEGG pathways were significantly associated with the DAMs from the *R. sinicus* versus *V. sinensis* comparison (Figure 6). In detail, 39 pathways were significantly associated with the DAMs predominantly accumulated in *R. sinicus*, while 10 pathways were for the DAMs predominantly accumulated in *V. sinensis*. According to the order of *p*-values, the top 10 pathways are represented in a bubble plot (Figures 6B, D), which indicates that different biological processes were activated in the cochleae of *R. sinicus* and *V. sinensis*. In particular, two nervous system-related pathways, Neurotrophin signaling pathway (ko04722) and Cholinergic synapse (ko04725), were significantly associated with the DAMs predominantly accumulated in *R. sinicus*, both of which are closely associated with the process of auditory perception. Several signal transduction-related pathways were also found to be important in the cochlea of *R. sinicus*, such as the MAPK

FIGURE 7
Network relationships of the KEGG pathways significantly associated with the significantly abundant metabolites in the cochlea of *R. sinicus* **(A)** and *V. sinensis* **(B)**, respectively. The size of the dot indicates the level of connectivity of a specific pathway interacting with others. Significantly enriched pathways are indicated by colored dots rather than gray ones. Dot and font colors are as follows: signal transduction-related pathways (red), metabolism-related pathways (orange), nervous system-related pathways (blue), immune system-related pathways (green), and others (purple).

signaling pathway (ko04010), ErbB signaling pathway (ko04012), Ras signaling pathway (ko04014), Rap1 signaling pathway (ko04015), and Calcium signaling pathway (ko04020).

Furthermore, network analysis for significantly enriched KEGG pathways was performed to obtain insights into the relationships of the metabolites differently accumulated in *R. sinicus* and *V. sinensis*. The network for *R. sinicus* as shown in Figure 7A indicated that the MAPK signaling pathway (ko04010) was the most important core pathway, which communicated with multiple other signaling pathways, such as the NF-kappa B signaling pathway (ko04064) and Calcium signaling pathway (ko04020). At the same time, it also connected with various biological systems, such as Nervous system, Immune system, and Endocrine system. Meanwhile, specific metabolism-related pathways were potentially more active in the cochlea of *V. sinensis*, as revealed by the network analysis of significantly enriched KEGG pathways (Figure 7B), including Glycerophospholipid metabolism (ko00564), Pantothenate and CoA biosynthesis (ko00770), and Purine metabolism (ko00230), which closely interacted with each other.

4 Discussion

Echolocating bats have attracted much attentions for their remarkable high-frequency hearing ability (Moss, 2018; Cao et al., 2022). However, there seems to be a lack of further understanding of the extensive metabolites in the key auditory organs. Among multiple omics approaches, metabolomics has gradually become the most direct and efficient method to explore complex biological traits (Fiehn, 2022). It is very necessary to identify the cochlear metabolites and to provide further scientific clues for understanding the molecular mechanisms of high-frequency hearing in echolocating bats. Therefore, untargeted metabolomics were performed here to obtain an insight into the

various metabolites and biological processes in the cochleae of echolocating bats for the first time, and also to reveal the differences of metabolites and related physiological processes in the cochleae of the two bat species.

The cochleae of *R. sinicus* and *V. sinensis* were characterized by abundant metabolites that reflect specific biochemical pathways involved in the process of auditory perception. Metabolites classified as amino acids, peptides, and analogues were the most abundant in the cochleae of echolocating bats, while similar abundance levels were also detected in the inner ear fluid of guinea pig (Fujita et al., 2015; Pirttilä et al., 2019). Besides, amino acid metabolites were also detected in the inner ear of mice (Ji et al., 2019). In addition to amino acids, various metabolites, including hydroxy acids, carbohydrates, alcohols and polyols, homogeneous non-metal compounds, carboxylic acids, fatty acids, and purines and purine derivatives were detected in the inner ear fluid of guinea pig cochlea by gas chromatography–mass spectrometry (GC-MS) (Fujita et al., 2015), which were also detected in the cochleae of the two echolocating bats in this study by LC-MS. However, 4,717 annotated metabolites were detected in the cochlea of bats, which was a greater number than the 77 kinds of metabolites detected in the inner ear fluid of guinea pig cochlea (Fujita et al., 2015). This is reasonable given that the cochlea contains more microscopic structures and more abundant cells than the inner ear fluid of the cochlea, so the metabolites in the cochlea could be more abundant than those only detected in the inner ear fluid of the cochlea. Besides, various metabolites across the major metabolic pathways in central carbon metabolism, including amino acids, nucleotides, cytosine, L-methionine, L-arginine, glutamate, xanthurenic acid, aspartate, phenylalanine, tyrosine, aromatic amino acids, adenosine, oxidized glutathione, methionine, and tryptophan, were detected in the inner ear of mice, which may be involved in responses to noise trauma (Ji et al., 2019); those metabolites were also identified in the cochlea of our two echolocating bat species, which may also constitute the molecular basis to response to noise stimulation, for bats were more usually expose to high intensity noise environment.

In addition, more abundant metabolites were found in the cochlea of laryngeally echolocating bats, which are involved in various aspects of the physiological function of the cochlea, including metabolic processes of amino acids, carbohydrates, lipids, cofactors and vitamins, and nucleotides, as well as the immune system, nervous system, sensory system, membrane transport, and signal transduction. Previous studies demonstrated that hearing acquisition relies on the functional maturation and appropriate organization of the cochlea that couples the transfer of signaling, ions, and nutrients (Kelly and Chen, 2009; Ceriani and Mammano, 2012). Therefore, metabolites detected in the cochleae of bats that participated in the pathways related to various signal transductions, the nervous system, membrane transport, and transport and catabolism, among others, potentially provide comprehensive references for future studies on cochlear function.

Significant metabolic differences were detected between the cochleae of *R. sinicus* and *V. sinensis*. Compared with the levels in *V. sinensis*, 129 metabolites were identified to be significantly abundant in the cochlea of *R. sinicus*. Multiple pathways were shown to be influenced by these metabolites, including those involving signal transduction, the nervous system, endocrine system, lipid metabolism, and environmental adaptation. This indicates that these biological processes were different and specific in the cochlea of *R. sinicus*. Neurotrophin signaling pathway (ko04722) and Cholinergic synapse (ko04725) were the two most important pathways, which may play important roles in the auditory perception in *R. sinicus*. Neurotrophins have been identified as a key factor in the maintenance of spiral ganglion health, playing important roles in the normal function of cochleae (Shew et al., 2021). Previous studies identified several key features of cholinergic synapses in the cochleae of mammals, especially the efferent cholinergic synaptic transmission in the vestibular periphery (Poppi et al., 2020). Our findings suggest that the metabolites participating in the neurotrophin signaling pathway and cholinergic synapses are potentially crucial metabolic bases for the process of auditory perception in *R. sinicus*. As a representative species of CF bats, *R. sinicus* possessed unique and high-frequency CF component in their echolocation calls compared with *V. sinensis*, this regarded as one of the possible reasons for the more abundant neurotrophin signaling pathway and cholinergic synapses in the cochleae of *R. sinicus*. Besides, CF bat have developed special cochlear adaptations, such as auditory fovea and neurons with extraordinarily sharp frequency tuning, these may consist of other potential reasons for the differences between *R. sinicus* and *V. sinensis* revealed by DAMs and related pathways. Besides, it has been reported that SK2 calcium-activated potassium channel is required for cholinergic function in mouse cochlear hair cells (Kong et al., 2008; Jordan et al., 2013) and also for the long-term maintenance of efferent synapses on-to mammalian cochlear hair cells (Murthy et al., 2009). A previous study demonstrated that the *SK2* gene, as one of the most important hearing-related genes, has undergone more rapid evolution in echolocating mammals than in non-echolocating mammals and may be involved in the high-frequency hearing of echolocating mammals (Wang et al., 2021). Therefore, adaptive evolutionary changes detected in the cochlea of *R. sinicus* may be revealed by analyses of both metabolites and genes, and even complex networks of interactions between them, which have adapted in the process of auditory perception.

Notably, compared with the findings in FM bat, different nervous system activities were also demonstrated in the cochlea of *R. sinicus* (CF bat), as revealed by the gene expression data obtained using RNA-Seq (Wang et al., 2018). Genes overexpressed in *R. sinicus* (CF bat) compared with the levels in *Taphozous melanopogon* (FM bat) were shown to be significantly associated with various nervous system components, such as Cholinergic synapse (ko04725), Glutamatergic synapse (ko04724), and Dopaminergic synapse (ko04728). Similarly, at the metabolic level here, two nervous system-related pathways, Cholinergic synapse (ko04725) and Neurotrophin signaling pathway (ko04722) were significantly associated with the DAMs predominantly accumulated in *R. sinicus*. The Cholinergic synapse (ko04725) was the same pathway that significantly enriched by overexpressed genes and high-accumulated metabolites detected in the cochleae of *R. sinicus*. Taken together, both expressed genes and metabolites detected in the cochlea of *R. sinicus* indicated that Cholinergic synapse (ko04725) is an important physiological basis underlying the auditory function. However, more studies are needed to conduct to verify if these clues were suitable for other CF bats.

In addition, the activity of multiple signal transduction pathways was also detected in the cochlea of *R. sinicus* compared with the findings for *V. sinensis*, which suggested more active signal transduction in the former. Importantly, the MAPK signaling pathway (ko04010) was identified as the most central signal

transduction pathway. Previously, metabolomic and bioinformatic analyses indicated that this is the major pathway in various types of hearing loss (Alagramam et al., 2014; Muurling and Stankovic, 2014; Liu et al., 2021). Numerous studies related to hearing damage have also shown that noise exposure immediately activates the cochlear MAPK signaling pathway, which plays important roles in maintaining normal physiological function of the cochlea (Maeda et al., 2013; Alagramam et al., 2014; Kurabi et al., 2017). For nocturnal echolocating bats, which are highly dependent on acoustic signals and are continually exposed to ultrasonic signals in daily life, the MAPK signaling pathway could be particularly important in regulating the development and survival of auditory hair cells. Compared with *V. sinensis* (around 24.2 kHz), *R. sinicus* (around 83.15 kHz) has developed a much higher- and constant-frequency component in its acoustic signals (Fukui et al., 2004; Xie et al., 2017; Wang et al., 2018), so the metabolites significantly accumulated in the MAPK signaling pathway may constitute an important auditory basis in the cochlea of *R. sinicus*. The molecular interactions of the MAPK signaling pathway and other signaling pathways play an important role in the survival of hair cells and the normal function of cochlea. Pathways such as the calcium signaling pathway play numerous fundamental roles in the inner ear (including in neurotransmitter release and synaptic transmission) (Ceriani and Mammano, 2012; Liu et al., 2021), along with multiple signaling pathways that interact with the MAPK signaling pathway in the cochlea of *R. sinicus*. Similarly, among the pathways significantly associated with the overexpressed genes detected in the cochlea of *R. sinicus* rather than in *T. melanopogon*, signal transduction pathways were almost the most represented, second only to nervous system pathways (Wang et al., 2018). Taken together, evidence from comparative cochlear transcriptomic and metabolomic analyses consistently indicated that signal transduction might be more active in the cochlea *R. sinicus* compared with FM bats.

More abundant metabolites in the cochlea of *V. sinensis* when compared with the levels in *R. sinicus* were significantly associated with metabolic pathways including Glycerophospholipid metabolism (ko00564), Pantothenate and CoA biosynthesis (ko00770), and Purine metabolism (ko00230), which have generally been demonstrated to be involved with exposure to noise. A recent animal experimental study on the brain of rats found that purine metabolism was markedly altered by acoustic trauma (He et al., 2017). Furthermore, in mice, purinergic signaling has been suggested to protect against noise trauma and contribute to cochlear adaptation to elevated sound levels (Muñoz et al., 1999; Housley et al., 2013). It was also identified that metabolites that showed a significant difference in accumulation between microtia and healthy ear cartilage were associated with Pantothenate and CoA biosynthesis, so these may have an association with the development of microtia ear cartilage (Yang and He, 2020). Finally, with regard to Glycerophospholipid metabolism, this has potential protective roles in the cochlea, which was reported to be significantly related to noise-induced hearing loss (Xie et al., 2021). Taken together, our results indicated that different metabolic processes presenting in the cochleae of *R. sinicus* and *V. sinensis*. The specific metabolic pathways identified in *V. sinensis* could be related to cochlear development and protective mechanisms in response to echolocation calls and echoes. Moreover, in this study, it should be noted that the *V. sinensis* individuals were collected from a large colony roosting under a bridge, containing about 10,000 individuals living together from early June to late September each year. These bats are thus exposed to high-intensity noise from their peers at night and from traffic in the day (Song et al., 2020). The specific metabolic pathways detected in the cochlea of *V. sinensis* could also be related to cochlear development and protective mechanisms in response to inhabiting a noisy environment. However, more evidences are needed in future to uncover the functions of these metabolic pathways in the cochlea of *V. sinensis*.

To better understand the molecular bases underlying high-frequency hearing of bats, our study provided an overview of the cochlear metabolites and associated biological processes of two typical laryngeally echolocating bat species. Our study takes new insights into the molecular mechanisms of auditory perception of echolocating bats. In consideration of the limitations of single omics, future work should focus on a comprehensively study to fully uncover the molecular mechanisms and key network relationships combing the transcriptome, proteome, and metabolome in echolocating bats. Unfortunately, no sufficient bat cochlear samples were left here for the experimental validation which needs to be further studied. Therefore, comparative cochlear metabolic and transcriptomic sequencing of more representative bat species from CF, FM and even non-echolocating bat groups will be further performed in future along with the experimental validations to reveal the genetic bases of high-frequency hearing and also the different molecular bases and biological mechanisms underlying the auditory processes of bats with distinct hearing traits.

Data availability statement

The datasets presented in this study can be found in the article/Supplementary Material.

Ethics statement

The animal study was reviewed and approved by Laboratory Animal Welfare and Ethics Committee of Jilin Agricultural University (approval code: 20210607001).

Author contributions

HW and JF designed the project. RS, NX, AL, and JL prepared the materials. XW, MB, and XL performed the experiments. HW analyzed the data and wrote the manuscript. All authors read and approved the final manuscript.

Funding

This research was funded by the National Natural Science Foundation of China (grant number 32001089 to HW and grant number 32071492 to JF).

Acknowledgments

We are grateful to the faculty and students of the Key Laboratory of Jilin Province for the conservation and utilization of animal resources for their invaluable assistance in the field. We thank Liwen Bianji (Edanz) (www.liwenbianji.cn) for editing the language of a draft of this manuscript.

Conflict of interest

The authors declare that the research was conducted in the absence of any commercial or financial relationships that could be construed as a potential conflict of interest.

Publisher's note

All claims expressed in this article are solely those of the authors and do not necessarily represent those of their affiliated organizations, or those of the publisher, the editors and the reviewers. Any product that may be evaluated in this article, or claim that may be made by its manufacturer, is not guaranteed or endorsed by the publisher.

Supplementary material

The Supplementary Material for this article can be found online at: https://www.frontiersin.org/articles/10.3389/fmolb.2023.1171366/full#supplementary-material

References

Adams, R. A., and Pedersen, S. C. (2013). *Bat evolution, ecology, and conservation*. New York: Springer.

Alagramam, K. N., Stepanyan, R., Jamesdaniel, S., Chen, D. H-C., and Davis, R. R. (2014). Noise exposure immediately activates cochlear mitogen-activated protein kinase signaling. *Noise Health* 16, 400–409. doi:10.4103/1463-1741.144418

Cao, M., Li, C., Liu, Y., Cai, K., Chen, L., Yuan, C., et al. (2020). Assessing urinary metabolomics in giant pandas using chromatography/mass spectrometry: Pregnancy-related changes in the metabolome. *Front. Endocrinol.* 11, 215. doi:10.3389/fendo.2020.00215

Cao, R., Li, J., and Koyabu, D. (2022). A bibliometric analysis of research trends in bat echolocation studies between 1970 and 2021. *Ecol. Inf.* 69, 101654. doi:10.1016/j.ecoinf.2022.101654

Ceriani, F., and Mammano, F. (2012). Calcium signaling in the cochlea–molecular mechanisms and physiopathological implications. *Cell Commun. Signal.* 10, 20–12. doi:10.1186/1478-811X-10-20

Davies, K., Cotton, J., Kirwan, J., Teeling, E., and Rossiter, S. (2012). Parallel signatures of sequence evolution among hearing genes in echolocating mammals: An emerging model of genetic convergence. *Heredity* 108, 480–489. doi:10.1038/hdy.2011.119

Davies, K. T., Maryanto, I., and Rossiter, S. J. (2013). Evolutionary origins of ultrasonic hearing and laryngeal echolocation in bats inferred from morphological analyses of the inner ear. *Front. Zool.* 10, 2–15. doi:10.1186/1742-9994-10-2

Dong, D., Lei, M., Liu, Y., and Zhang, S. (2013). Comparative inner ear transcriptome analysis between the Rickett's big-footed bats (*Myotis ricketti*) and the greater short-nosed fruit bats (*Cynopterus sphinx*). *BMC Genomics* 14, 916–1010. doi:10.1186/1471-2164-14-916

Fiehn, O. (2022). Metabolmics-the link between genotypes and phenotypes. *Plant Mol. bio.* 48, 155–171. doi:10.1023/a:1013713905833

Fraga-Corral, M., Carpena, M., Garcia-Oliveira, P., Pereira, A., Prieto, M., and Simal-Gandara, J. (2022). Analytical metabolomics and applications in health, environmental and food science. *Crit. Rev. Anal. Chem.* 52, 712–734. doi:10.1080/10408347.2020.1823811

Fujita, T., Yamashita, D., Irino, Y., Kitamoto, J., Fukuda, Y., Inokuchi, G., et al. (2015). Metabolomic profiling in inner ear fluid by gas chromatography/mass spectrometry in Guinea pig cochlea. *Neurosci. Lett.* 606, 188–193. doi:10.1016/j.neulet.2015.09.001

Fukui, D., Agetsuma, N., and Hill, D. A. (2004). Acoustic identification of eight species of bat (mammalia: Chiroptera) inhabiting forests of southern hokkaido, Japan: Potential for conservation monitoring. *Zool. Sci.* 21, 947–955. doi:10.2108/zsj.21.947

Han, S., Van-Treuren, W., Fischer, C. R., Merrill, B. D., DeFelice, B. C., Sanchez, J. M., et al. (2021). A metabolomics pipeline for the mechanistic interrogation of the gut microbiome. *Nature* 595, 415–420. doi:10.1038/s41586-021-03707-9

He, J., Zhu, Y., Aa, J., Smith, P. F., De-Ridder, D., Wang, G., et al. (2017). Brain metabolic changes in rats following acoustic trauma. *Front. Neurosci.* 11, 1–13. doi:10.3389/fnins.2017.00148

He, K., Liu, Q., Xu, D. M., Qi, F. Y., Bai, J., He, S. W., et al. (2021). Echolocation in soft-furred tree mice. *Science* 372, eaay1513. doi:10.1126/science.aay1513

Housley, G. D., Morton-Jones, R., Vlajkovic, S. M., Telang, R. S., Paramananthasivam, V., Tadros, S. F., et al. (2013). ATP-gated ion channels mediate adaptation to elevated sound levels. *P. Natl. Acad. Sci. U. S. A.* 110, 7494–7499. doi:10.1073/pnas.1222295110

Ji, L., Lee, H. J., Wan, G., Wang, G. P., Zhang, L., Sajjakulnukit, P., et al. (2019). Auditory metabolomics, an approach to identify acute molecular effects of noise trauma. *Sci. Rep.* 9, 9273–9279. doi:10.1038/s41598-019-45385-8

Jones, G. (2005). Echolocation. *Curr. Biol.* 15, R484–R488. doi:10.1016/j.cub.2005.06.051

Jones, G., and Teeling, E. C. (2006). The evolution of echolocation in bats. *Trends Ecol. Evol.* 21, 149–156. doi:10.1016/j.tree.2006.01.001

Jordan, P. M., Parks, X. X., Contini, D., and Holt, J. C. (2013). A review of synaptic mechanisms of vestibular efferent signaling in turtles: Extrapolation to efferent actions in mammals. *J. Vestibul. Res.* 23, 161–175. doi:10.3233/VES-130492

Kelly, M. C., and Chen, P. (2009). Development of form and function in the mammalian cochlea. *Curr. Opin. Neurobiol.* 19, 395–401. doi:10.1016/j.conb.2009.07.010

Keurentjes, J. J. (2009). Genetical metabolomics: Closing in on phenotypes. *Curr. Opin. Plant Biol.* 12, 223–230. doi:10.1016/j.pbi.2008.12.003

Kong, J. H., Adelman, J. P., and Fuchs, P. A. (2008). Expression of the SK2 calcium-activated potassium channel is required for cholinergic function in mouse cochlear hair cells. *J. Physiol.* 586, 5471–5485. doi:10.1113/jphysiol.2008.160077

Kurabi, A., Keithley, E. M., Housley, G. D., Ryan, A. F., and Wong, A. C-Y. (2017). Cellular mechanisms of noise-induced hearing loss. *Hear. Res.* 349, 129–137. doi:10.1016/j.heares.2016.11.013

Li, G., Wang, J., Rossiter, S. J., Jones, G., Cotton, J. A., and Zhang, S. (2008). The hearing gene *Prestin* reunites echolocating bats. *P. Natl. Acad. Sci. U. S. A.* 105, 13959–13964. doi:10.1073/pnas.0802097105

Liu, Y., Cotton, J. A., Shen, B., Han, X., Rossiter, S. J., and Zhang, S. (2010). Convergent sequence evolution between echolocating bats and dolphins. *Curr. Biol.* 20, R53–R54. doi:10.1016/j.cub.2009.11.058

Liu, Y., Wei, M., Mao, X., Chen, T., Lin, P., and Wang, W. (2021). Key signaling pathways regulate the development and survival of auditory hair cells. *Neural Plast.* 2021, 5522717–5522812. doi:10.1155/2021/5522717

Liu, Z., Chen, P., Xu, D. M., Qi, F. Y., Guo, Y. T., Liu, Q., et al. (2022). Molecular convergence and transgenic evidence suggest a single origin of laryngeal echolocation in bats. *Iscience* 25, 104114. doi:10.1016/j.isci.2022.104114

Liu, Z., Qi, F. Y., Xu, D. M., Zhou, X., and Shi, P. (2018). Genomic and functional evidence reveals molecular insights into the origin of echolocation in whales. *Sci. Adv.* 4, eaat8821. doi:10.1126/sciadv.aat8821

Ma, L., Sun, H., and Mao, X. (2020). Transcriptome sequencing of cochleae from constant-frequency and frequency-modulated echolocating bats. *Sci. Data* 7, 341–345. doi:10.1038/s41597-020-00686-w

Maeda, Y., Fukushima, K., Omichi, R., Kariya, S., and Nishizaki, K. (2013). Time courses of changes in phospho-and total-MAP kinases in the cochlea after intense noise exposure. *PloS One* 8, e58775. doi:10.1371/journal.pone.0058775

Meng, X., Li, G., Gu, L., Sun, Y., Li, Z., Liu, J., et al. (2020). Comparative metabolomic and transcriptome analysis reveal distinct flavonoid biosynthesis regulation between petals of white and purple phalaenopsis amabilis. *Phalaenopsis amabilis J. Plant Growth Regul.* 39, 823–840. doi:10.1007/s00344-019-10025-y

Moss, C. F. (2018). "Auditory mechanisms of echolocation in bats," in *Oxford research Encyclopedia of neuroscience*. Editor S. M. Sherman (Oxford University Press).

Muñoz, D. J., Thorne, P. R., and Housley, G. D. (1999). P2X receptor-mediated changes in cochlear potentials arising from exogenous adenosine 5′-triphosphate in endolymph. *Hear. Res.* 138, 56–64. doi:10.1016/s0378-5955(99)00151-3

Murthy, V., Maison, S. F., Taranda, J., Haque, N., Bond, C. T., Elgoyhen, A. B., et al. (2009). SK2 channels are required for function and long-term survival of efferent synapses on mammalian outer hair cells. *Mol. Cell. Neurosci.* 40, 39–49. doi:10.1016/j.mcn.2008.08.011

Muurling, T., and Stankovic, K. M. (2014). Metabolomic and network analysis of pharmacotherapies for sensorineural hearing loss. *Otol. Neurotol.* 35, 1–6. doi:10.1097/MAO.0000000000000254

Parker, J., Tsagkogeorga, G., Cotton, J. A., Liu, Y., Provero, P., Stupka, E., et al. (2013). Genome-wide signatures of convergent evolution in echolocating mammals. *Nature* 502, 228–231. doi:10.1038/nature12511

Pirttilä, K., Videhult-Pierre, P., Haglöf, J., Engskog, M., Hedeland, M., Laurell, G., et al. (2019). An LCMS-based untargeted metabolomics protocol for cochlear perilymph: Highlighting metabolic effects of hydrogen gas on the inner ear of noise exposed Guinea pigs. *Metabolomics* 15, 138–212. doi:10.1007/s11306-019-1595-1

Poppi, L. A., Holt, J. C., Lim, R., and Brichta, A. M. (2020). A review of efferent cholinergic synaptic transmission in the vestibular periphery and its functional implications. *J. Neurophysiol.* 123, 608–629. doi:10.1152/jn.00053.2019

Schnitzler, H. U., and Denzinger, A. (2011). Auditory fovea and Doppler shift compensation: Adaptations for flutter detection in echolocating bats using CF-FM signals. *J. Comp. Physiol. A* 197, 541–559. doi:10.1007/s00359-010-0569-6

Shew, M., Wichova, H., Warnecke, A., Lenarz, T., and Staecker, H. (2021). Evaluating neurotrophin signaling using microRNA perilymph profiling in cochlear implant patients with and without residual hearing. *Otol. Neurotol.* 42, e1125–e1133. doi:10.1097/MAO.0000000000003182

Simmons, J. A., Fenton, M. B., and O'Farrell, M. J. (1979). Echolocation and pursuit of prey by bats. *Science* 203, 16–21. doi:10.1126/science.758674

Song, S., Chang, Y., Wang, D., Jiang, T., Feng, J., and Lin, A. (2020). Chronic traffic noise increases food intake and alters gene expression associated with metabolism and disease in bats. *J. Appl. Ecol.* 57, 1915–1925. doi:10.1111/1365-2664.13710

Ulanovsky, N., and Moss, C. F. (2008). What the bat's voice tells the bat's brain. *P. Natl. Acad. Sci. U. S. A.* 105, 8491–8498. doi:10.1073/pnas.0703550105

Vater, M., and Kössl, M. (2011). Comparative aspects of cochlear functional organization in mammals. *Hear. Res.* 273, 89–99. doi:10.1016/j.heares.2010.05.018

Wang, H., Zhao, H., Chu, Y., Feng, J., and Sun, K. (2021). Assessing evidence for adaptive evolution in two hearing-related genes important for high-frequency hearing in echolocating mammals. *G3-Genes Genom. Genet.* 11, jkab069. doi:10.1093/g3journal/jkab069

Wang, H., Zhao, H., Huang, X., Sun, K., and Feng, J. (2018). Comparative cochlear transcriptomics of echolocating bats provides new insights into different nervous activities of CF bat species. *Sci. Rep.* 8, 15934–16012. doi:10.1038/s41598-018-34333-7

Wang, H., Zhao, H., Sun, K., Huang, X., Jin, L., and Feng, J. (2020). Evolutionary basis of high-frequency hearing in the cochleae of echolocators revealed by comparative genomics. *Genome Biol. Evol.* 12, 3740–3753. doi:10.1093/gbe/evz250

Waters, D. A., and Vollrath, C. (2003). Echolocation performance and call structure in the megachiropteran fruit-bat *Rousettus aegyptiacus*. *Acta Chiropterol* 5, 209–219.

Wohlgemuth, M. J., Luo, J., and Moss, C. F. (2016). Three-dimensional auditory localization in the echolocating bat. *Curr. Opin. Neurobiol.* 41, 78–86. doi:10.1016/j.conb.2016.08.002

Wörheide, M. A., Krumsiek, J., Kastenmüller, G., and Arnold, M. (2021). Multi-omics integration in biomedical research–A metabolomics-centric review. *Anal. Chim. Acta* 1141, 144–162. doi:10.1016/j.aca.2020.10.038

Xie, C., Niu, Y., Ping, J., Zhang, Q., Zhang, Z., Wang, Y., et al. (2021). Transcriptome-wide association study identifies novel susceptibility genes contributing to hearing impairment. *Res. Sq. Prepr.*, 1–19.

Xie, L., Sun, K., Jiang, T., Liu, S., Lu, G., Jin, L., et al. (2017). The effects of cultural drift on geographic variation in echolocation calls of the Chinese rufous horseshoe bat (*Rhinolophus sinicus*). *Ethology* 123, 532–541. doi:10.1111/eth.12627

Yang, J., and He, L. (2020). Mass spectrometric characterization of metabolites in ear cartilage: Congenital microtia and normal auricle. *Ann. Plas. Surg.* 85, 76–82. doi:10.1097/SAP.0000000000002127

Yovel, Y., Falk, B., Moss, C. F., and Ulanovsky, N. (2010). Optimal localization by pointing off axis. *Science* 327, 701–704. doi:10.1126/science.1183310

Zampieri, M., and Sauer, U. (2017). Metabolomics-driven understanding of genotype-phenotype relations in model organisms. *Curr. Opin. Syst. Biol.* 6, 28–36. doi:10.1016/j.coisb.2017.08.007

Zhou, B., Xiao, J. F., Tuli, L., and Ressom, H. W. (2012). LC-MS-based metabolomics. *Mol. Biosyst.* 8, 470–481. doi:10.1039/c1mb05350g

Zou, Z., and Zhang, J. (2015). No genome-wide protein sequence convergence for echolocation. *Mol. Biol. Evol.* 32, 1237–1241. doi:10.1093/molbev/msv014

frontiers | Frontiers in Molecular Biosciences

TYPE Original Research
PUBLISHED 13 July 2023
DOI 10.3389/fmolb.2023.1233586

OPEN ACCESS

EDITED BY
Elda Dervishi,
University of Alberta, Canada

REVIEWED BY
Paniz Jasbi,
Arizona State University, United States
Dhanasekaran Shanmugam,
National Chemical Laboratory (CSIR), India

*CORRESPONDENCE
Elżbieta Łopieńska-Biernat,
ela.lopienska@uwm.edu.pl

RECEIVED 02 June 2023
ACCEPTED 04 July 2023
PUBLISHED 13 July 2023

CITATION
Polak I, Stryiński R, Majewska M and Łopieńska-Biernat E (2023), Metabolomic analysis reveals a differential adaptation process of the larval stages of *Anisakis simplex* to the host environment. *Front. Mol. Biosci.* 10:1233586. doi: 10.3389/fmolb.2023.1233586

Metabolomic analysis reveals a differential adaptation process of the larval stages of *Anisakis simplex* to the host environment

Iwona Polak[1], Robert Stryiński[1], Marta Majewska[2] and Elżbieta Łopieńska-Biernat[1]*

[1]Department of Biochemistry, Faculty of Biology and Biotechnology, University of Warmia and Mazury in Olsztyn, Olsztyn, Poland, [2]Department of Human Physiology and Pathophysiology, School of Medicine, Collegium Medicum, University of Warmia and Mazury in Olsztyn, Olsztyn, Poland

Introduction: *Anisakis simplex* are parasitic nematodes that cause anisakiasis. The possibility of infection with this parasite is through consumption of raw or undercooked fish products. *A. simplex* infections are often misdiagnosed, especially in subclinical cases that do not present with typical symptoms such as urticaria, angioedema, and gastrointestinal allergy. The resulting allergic reactions range from rapid-onset and potentially fatal anaphylactic reactions to chronic, debilitating conditions. While there have been numerous published studies on the genomes and proteomes of *A. simplex*, less attention has been paid to the metabolomes. Metabolomics is concerned with the composition of metabolites in biological systems. Dynamic responses to endogenous and exogenous stimuli are particularly well suited for the study of holistic metabolic responses. In addition, metabolomics can be used to determine metabolic activity at different stages of development or during growth.

Materials and methods: In this study, we reveal for the first time the metabolomes of infectious stages (L3 and L4) of *A. simplex* using untargeted metabolomics by ultra-performance liquid chromatography-mass spectrometry.

Results: In the negative ionization mode (ESI-), we identified 172 different compounds, whereas in the positive ionization mode (ESI+), 186 metabolites were found. Statistical analysis showed that 60 metabolites were found in the ESI- mode with different concentration in each group, of which 21 were more enriched in the L3 larvae and 39 in the L4 stage of *A. simplex*. Comparison of the individual developmental stages in the ESI + mode also revealed a total of 60 differential metabolites, but 32 metabolites were more enriched in the L3 stage larvae, and 28 metabolites were more concentrated in the L4 stage.

Discussion: The metabolomics study revealed that the developmental stages of *A. simplex* differed in a number of metabolic pathways, including nicotinate and nicotinamide metabolism. In addition, molecules responsible for successful migration within their host, such as pyridoxine and prostaglandins (E1, E2, F1a) were present in the L4 stage. In contrast, metabolic pathways for amino acids, starch, and sucrose were mainly activated in the L3 stage. Our results provide new insights into the comparative metabolome profiles of two different developmental stages of *A. simplex*.

KEYWORDS

Anisakis simplex, larval development, metabolome, trehalose, fatty acids

1 Introduction

Anisakis simplex is one of the most important emerging parasitic nematodes in Europe, according to the Risk Management Ranking of Foodborne Parasites, prepared for recommendations by the Food and Agriculture Organization of the United Nations (FAO) and the World Health Organization (WHO) (Stryiński et al., 2020). The disease caused by the genus *Anisakis* is called anisakiasis and frequently described (Audicana et al., 2002; Aibinu et al., 2019). The life cycle of *A. simplex* is complex and involves four larval stages parasitizing several intermediate and paratenic hosts (fish, cephalopods, and crustaceans) and the adult stage parasitizing marine mammals (seals, dolphins, and whales). The first case of human infection by a species of the Anisakidae family occurred in the 1960s, when Van Thiel of the Institute of Tropical Medicine in Leiden, the Netherlands, identified patients who suffered severe abdominal pain after eating fish (van Thiel et al., 1960). Transmission of the parasite is clearly associated with the consumption of raw or undercooked fish. In particular, Japanese sushi and sashimi, Dutch salted or smoked herring, Nordic gravlax (dry, cured salmon), Hawaiian lomi-lomi (raw salmon), German rollmops (rolled fillet of marinated/pickled herring), South American cebiche, and Spanish boquerones en vinagre (pickled anchovies) are regular routes of infection (Audicana et al., 2002; Ivanovic et al., 2015). The ingestion of viable larvae might lead to gastrointestinal symptoms (abdominal pain, nausea, vomiting, diarrhea), which may be associated with mild to severe allergic reactions, and the clinical symptoms most often are such as rhinitis, urticaria, and, in worst cases, anaphylactic shock (Aibinu et al., 2019). Although, cooking (or freezing) is expected to kill the parasites, it might not decrease its allergenicity, because *A. simplex* allergens have high heat and frost resistance; and sensitization may occur after consumption (Audicana and Kennedy, 2008). It is estimated that the incidence of the disease is 0.32 cases per 100,000 individuals/year worldwide (Orpha.net, 2022). The globalization, development of diagnostic tools and better analytical methods, have led to significantly even more anisakiasis being reported. Before 2010, over 20,000 cases of anisakiasis were reported worldwide, with the highest prevalence (over 90%) in Japan (EFSA, 2010; Baird et al., 2014), where now 7,000 cases of the disease are reported annually (Yorimitsu et al., 2013; Suzuki et al., 2021). European countries where cases of anisakiasis have been reported include among others, Spain (Herrador et al., 2019), Italy (Guardone et al., 2018; Mattiucci et al., 2018), France (Yera et al., 2018), Croatia (Mladineo et al., 2015), and Poland (Kołodziejczyk et al., 2020). The ingested L3 larvae rarely develop to L4 stage in humans and consequently die, but both of these larval stages are considered dangerous to humans (Kagei and Isogaki, 1992; Sohn et al., 2015).

The infective L3 of parasitic nematodes require specific stimuli for resumption of development and completion of shedding of the outer cuticle; thus, CO_2 appears to be the most important stimulus for hatching or molting of *Anisakis* nematodes. In addition, temperature, pH, and pepsin are known to trigger the development of infectious L3 to adults *in vitro* (Iglesias et al., 2001, 2005). All these stimuli are thought to reflect the conditions that prevail *in vivo* when they reach the gastrointestinal tract of the definitive hosts, where they develop into adults. During this molting process, they adapt to the new environment of their hosts' digestive tracts and also exhibit pathogenicity toward their hosts. These differences may reflect metabolic adaptations of *A. simplex* larvae to the host switch from fish (L3) to mammals (L4), i.e., adaptations to a new habitat (Baird et al., 2014; Kuhn et al., 2016).

Metabolomics is a distinct 'omics' method that offers a more direct assessment of physiology compared to others. It responds promptly to nutrients, stress, and disease unlike transcriptomic or proteomic approaches. Given this advantage, metabolomics has gained considerable interest in various fields such as environmental toxicology, evolutionary biology and developmental studies, medical diagnosis and treatment responses as well as drug development (Vernocchi et al., 2016). Synthetic biologists also use metabolomic flux analyses for insights into the effect of genetic modifications on metabolic pathways and products. As it pertains directly to molecular response mechanisms resulting from genetic alterations or environmental changes at the ultimate level of biological systems' metabolism function regarding molecule abundance predictions offer better accuracy than gene expression or protein-level information provides (Liu et al., 2021). Similarly, parasitic nematode research increasingly relies on metabolomics techniques due to its immense potential applications in studying these organisms effectively. The gastrointestinal tract is a dynamic metabolic and immunologically active ecosystem, and its complete set of metabolites reflects both the enzymatic pathways of host and gut inhabitants and the complex network that connects them (Palevich et al., 2021, 2022; Whitman et al., 2021). The use of metabolomics is particularly suited to understanding nematode metabolism, including the identification of novel drug targets, differences between developmental stages, and mechanisms involved in host-parasite interactions (Jasmer et al., 2019; Molenaars et al., 2021).

A major problem with untargeted metabolomics in general is the lack of comprehensive measurements of the whole metabolome using a single technique because of its great complexity. As things stand, it is not possible to measure the entire metabolome of an organism in a single experiment. In addition to some known compounds, a large portion of the metabolome has not even been identified ("metabolic dark matter") (da Silva et al., 2015). Metabolomics is capable of providing a static snapshot of the current metabolic state. However, in most cases, it remains unclear how this state was reached, and which metabolic pathway was active (Salzer and Witting, 2021). With respect to parasitic nematodes, the field of metabolomics faces similar challenges to untargeted metabolomics in general, as its complex nature makes it difficult to obtain complete measurements of the entire metabolome using a single approach. Nevertheless, the use of metabolomics in the study of parasitic nematodes is a promising area that could provide important insights into their biology and pathogenesis.

Such studies on the metabolome of nematodes from the family Anisakidae are lacking. Therefore, to fill the described gap, it was decided to analyze and characterize the metabolome of *A. simplex*, a parasite of great public health importance. In the central part of this

work, we focused on the identification and characterization of the metabolites of *A. simplex* in two developmental stages to increase our knowledge of the biology of this organism and to find a way to understand how this parasite was able to adapt to different host environments by developing a unique metabolism.

2 Materials and methods

2.1 Parasites and *in vitro* culture

The study was performed on the L3 and L4 larval stages of *Anisakis simplex* Nematodes were collected from the Biobank platform implemented for the PARASITE project (www.parasite-project.eu) at Institute of Marine Research, Spanish National Research Council (IIM-CSIC), Vigo, Spain. The larval stages of *A. simplex* were isolated: L3 from hake (*Merluccius*) and L4 from striped dolphin (*Stenella coeruleoalba*). All used larvae were taxonomically identified using conventional PCR to amplify the ITS region and *Cox2* gene as described before by Levsen et al. (2018). Eight samples of L3 larvae (24 larvae in total) and four samples of L4 larvae (8 larvae in total) were preserved in −80°C until the time of next step of the analysis.

2.2 Samples preparation

Samples were thawed and add with 800 µL of 80% methanol. Then all samples were extracted at 4°C with ultrasound for 30 min, kept at −40°C for 1 h. After that, samples were vortexed for 30 s, and centrifuged at 12,000 rpm and 4°C for 15 min. Finally, 200 µL of supernatant and 5 µL of DL-o-chlorophenylalanine (140 µg/ml) was transferred to vial for LC-MS/MS analysis. Quality control (QC) samples were used to evaluate the methodology. The same amount of extract was obtained from each sample and mixed as QC samples. The QC samples (3 in total) were prepared using the same sample preparation procedure.

2.3 UPLC-TOF-MS/MS

The separation of compounds was performed by ultra-performance liquid chromatography coupled with tandem mass spectrometry using Ultimate 3000LC combined with Q Exactive MS (Thermo Fisher Scientific, Waltham, MA, United States) in both polarities (ESI −/+). The LC system was comprised of a Hyper gold C18 column (100 × 2.1 mm 1.9 µm) (Thermo Fisher Scientific, Waltham, MA, United States). The mobile phase was composed of solvent A (0.1% formic acid, 5% acetonitrile, HPLC-grade water) and solvent B (0.1% formic acid, acetonitrile) with a gradient elution (0–1.5 min, 0%–20% B; 1.5–9.5 min, 20%–100% B; 9.5–14.5 min, 100% B; 14.5–14.6 min, 100%–0% B; 14.6–18.0 min, 0% B). The flow rate of the mobile phase was 0.3 ml/min. The column temperature was maintained at 40°C, and the sample manager temperature was set at 4°C. Mass spectrometry parameters in ESI+ and ESI- mode are listed as follows: the sheath gas flow rate was set to 45 a. u. (arbitrary units), aux gas flow rate to 15 a. u., and sweep gas flow rate to 1 a. u., capillary temperature was 350°C, and probe heater temperature was 300°C. Electrospray ionization source was set to 3.0 kV in ESI+ and 3.2 kV in ESI-.

2.4 Data processing and analysis

The raw LC-MS/MS data were acquired and aligned using the Compound Discover (v. 3.0, Thermo Fisher Scientific, Waltham, MA, United States) based on the *m/z* value and the retention time (RT) of the ion signals. The spectral data were normalized, and auto scaled before statistical analysis. The data was introduced into the SIMCA-P software (version 14.1, Santorius, Goettingen, Germany) for multivariate analysis. A Principal Components Analysis (PCA) was first used as an unsupervised method for data visualization and outlier identification (Yeshi et al., 2020). Supervised regression modeling was performed on the data set by use of Partial Least Squares Discriminant Analysis (PLS-DA). The quality of the models was evaluated with the relevant R^2 and Q^2. The importance of each ion in the PLS-DA was evaluated by variable importance in the projection (VIP) score (Tambellini et al., 2013; Gao et al., 2016). The VIP score positively reflects the metabolite's influence on the classification, and metabolites with VIP >1 were considered important in the study.

The chemical structures and IDs for metabolites were identified according to Human Metabolome Database (Wishart et al., 2012), KEGG database (Kanehisa and Goto, 2000; Kanehisa et al., 2016), PubChem Compound ID database (Kim et al., 2022) and ChemSpider databse (https://www.chemspider.com/Default.aspx). When necessary, further identification was performed through comparisons of the retention times and MS/MS fragmentation patterns in other databases: Metabolite and Chemical Entity Database (METLIN) (Smith et al., 2005) or MassBank (https://massbank.eu/MassBank/) (Salek et al., 2013).

The metabolites showing different concentrations among two given groups (DMs) were filtered and confirmed by combining the results of the multivariate analysis (VIP values >1.0) and the results of univariate analyses: *t*-test (p-value ≤0.05) and fold-change (FC) method ($-1.5 \leqslant \mathrm{Log_2FC} \leqslant 1.5$) for both ESI modes. Data were visualized on volcano plots.

In multivariate analyses, the hierarchical clustering analysis (HCA) with Euclidean measured distance, and the average clustering algorithm was used to visualize the differences in the concentration of each statistically significant metabolites between groups in two different ESI modes. Subsequently, the metabolites assignment to the compounds groups and pathway enrichment analysis was performed using Metaboanalyst 5.0 (Xia et al., 2009; Pang et al., 2021). The enrichment overview was based on the KEGG database with *Caenorhabditis elegans* as a reference (Kanehisa and Goto, 2000; Kanehisa et al., 2016).

Furthermore, the distribution of common and unique metabolites identified in the two ESI modes was analyzed and visualized using the Venn Diagrams tool (https://bioinformatics.psb.ugent.be/webtools/Venn/).

3 Results

3.1 Metabolites identification and statistical analysis

The QC samples were used to demonstrate the stability of the LC-MS system. The QC samples run in positive and negative mode

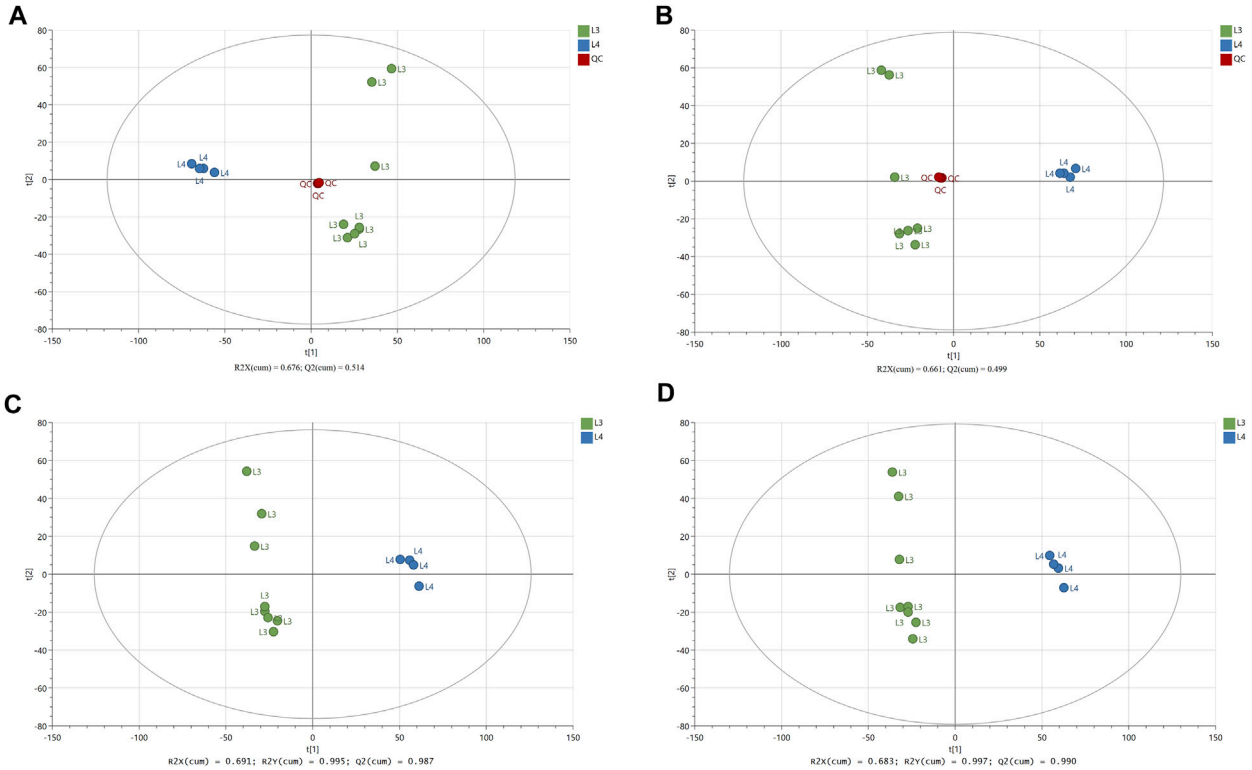

FIGURE 1
The results of multivariate data analysis. The score scatter plots of PCA model **(A, B)** comparing LC-MS/MS metabolomic profiles for the L3 and L4 developmental stages of *A. simplex* in negative and positive ionization mode (ESI−/+), respectively, and QC group. The score scatter plots of PLS-DA model **(C, D)** comparing LC-MS/MS metabolomic profiles for the L3 and L4 developmental stages of *A. simplex* in negative and positive ionization modes (ESI−/+), respectively. The R^2 and Q^2 values are indicated in the figures.

at regular intervals throughout the entire sequence. The ion features of the QC samples were used to calculate the relative standard deviation (RSD). The %RSD distribution for negative and positive modes is presented in Supplementary Figures S1A, B, respectively; an overwhelming majority of the RSD is less than 30%. The base peak intensity (BPI) chromatograms of the QC samples in ESI−/+ modes are presented in Supplementary Figures S1C, D. The normalization after alignment was also performed and the line plot (Supplementary Figures S1E, F) was used to evaluate the methodology. The *X* axis indicates the number of samples, the *Y* axis indicates the 95% confidence interval. The line plot demonstrated that the system is relatively stable during sample analysis. Due to all of that, the analysis procedure was robust and could be used for subsequent sample analysis.

To investigate the global metabolism variations, the PCA analysis was used to analyze all observations acquired in both ion modes. As show in PCA plot (Figures 1A, B), the QC samples were successfully separated from the tested samples and clustered together (QC, L3 and L4 developmental stages of *A. simplex*). The parameters R^2 and Q^2 confirmed the validity of the PCA model as follows: ESI- mode, R^2X = 0.676, Q^2 = 0.514; ESI + mode, R^2X = 0.661, Q^2 = 0.499 (Figures 1A, B). To eliminate any non-specific effects of the operative technique and confirm the presence of DMs, the PLS-DA was performed. The PLS-DA score scatter plots showed that there was significant separation between the L3 developmental stage group and the L4 developmental stage group in the ESI- and ESI + modes (Figures 1C, D). The values of the cumulative R^2 and Q^2 parameters confirmed the validity of the PLS-DA model: ESI- mode, R^2X = 0.691, R^2Y = 0.995, and Q^2 = 0.987; ESI + mode, R^2X = 0.683, R^2Y = 0.997, and Q^2 = 0.990 (Figures 1C, D). Additionally, the CV-ANOVA analysis assessing the reliability of the PLS-DA model was performed (Supplementary Figure S2). The *p*-value obtained for ESI- and ESI + modes was less than 0.05: 7.3415×10^{-6}, and 3.998×10^{-6}, respectively. The CV-score plots of the samples in ESI- and ESI + modes showed, as well, clear separation of the two analyzed groups with F factor = 77.64 and 91.61 for negative and positive ionization modes, respectively (Supplementary Figures S2A, B). According to the permutation test results, the PLS-DA model was proved to have good robustness without over fitting (Supplementary Figures S2C, D).

As a result of LC-MS/MS analysis, we identified a total of 3603 and 3877 compounds (Supplementary Tables S1, 2) in ESI- and ESI+, respectively. The peak intensities after normalization against QC samples (Supplementary Tables S3, 4) were further processed and the chemical structures and IDs for metabolites were identified (Supplementary Tables S5, 6). In the ESI- we identified 172 different compounds (Supplementary Table S5), when in ESI +, 186 metabolites were found (Supplementary Table S6). It was checked whether the identified compounds overlap and occur similarly in both used

10.3389/fmolb.2023.1233586

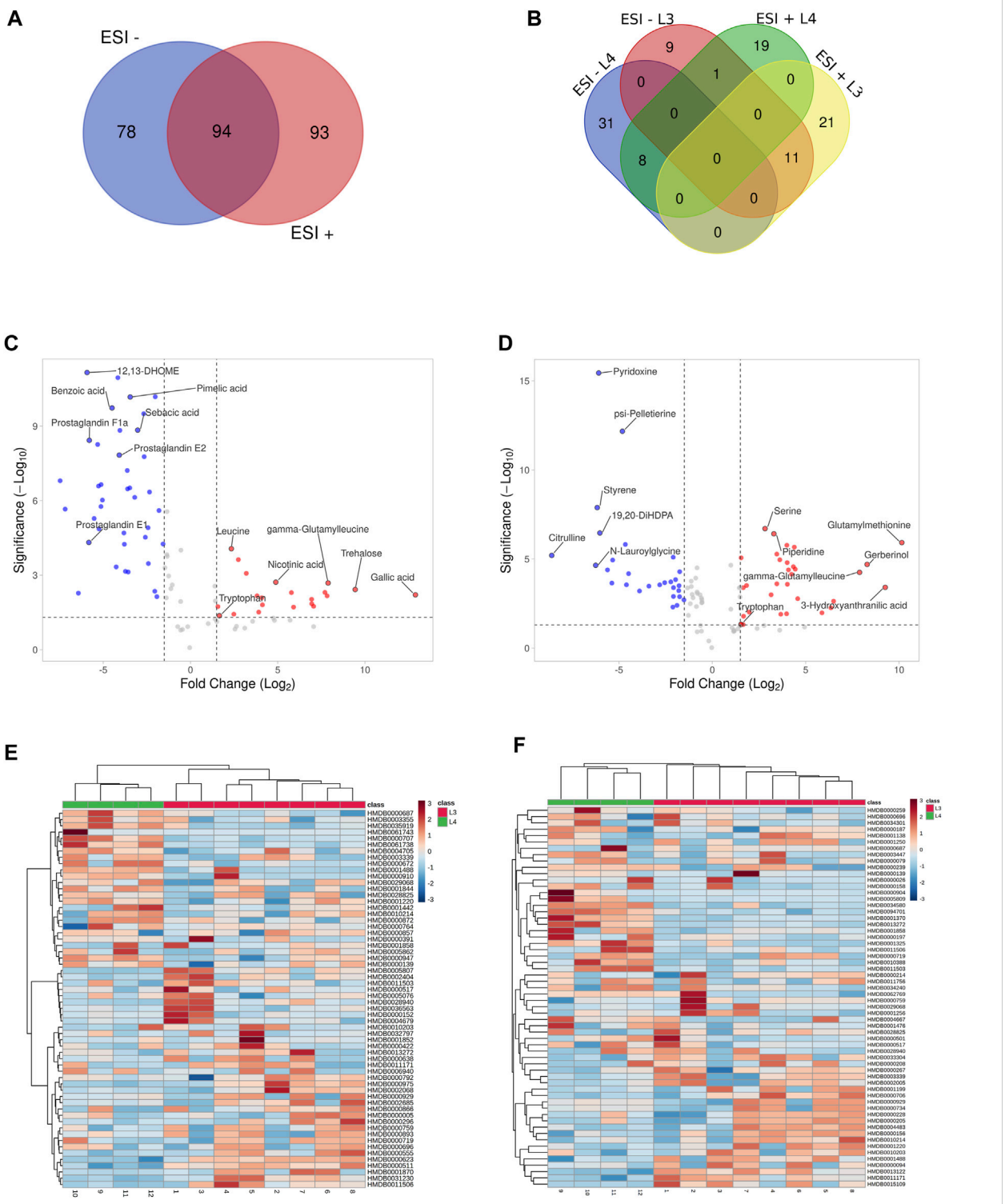

FIGURE 2
Visualization of statistically significant data results. Distribution of common and unique metabolites identified in the study between negative and positives ionization modes (ESI−/+) **(A)**. The metabolites IDs are listed in Supplementary Table S7. Distribution of common and unique metabolites for each of *A. simplex* developmental stage (L3 and L4) identified in the study in negative and positives ionization modes and (ESI−/+) **(B)**. The metabolites IDs are listed in Supplementary Table S10. Volcano plots of the untargeted metabolomics analysis in negative and positive ionization modes (ESI−/+), respectively **(C, D)**, of two developmental stages of *A. simplex*. The metabolites showing different concentrations among the given groups (DMs) were filtered and confirmed by combining the results of the multivariate analysis (VIP values >1.0) and the results of univariate analyses ($-1.5 \leqslant Log_2FC \leqslant 1.5$ in normalized ratios of L3 vs L4, p-value ≤0.05) for both ESI modes. Metabolites more enriched in the L3 stage are coloured in red, and in the L4 stage in blue. The metabolites IDs with calculated p-values, FC and VIP are listed in Supplementary Tables S8, 9. Hierarchical clustering analysis of the two sample groups (L3 and L4 stages of *A. simplex*) in negative (ESI-) and positive (ESI+) ionization modes, respectively **(E, F)**. The HCA shows discrimination between the samples groups and differential abundances of DMs in ESI- **(E)** and ESI+ **(F)**. The scale bars represent the normalized intensity of metabolites, where blue indicates a decrease/low and red an increase/high.

10.3389/fmolb.2023.1233586

TABLE 1 Metabolites of developmental stages of *A. simplex* (L3 and L4) identified in negative ionization mode (ESI-).

Hmdb ID	Compound name	Log_2(FC)	*p*-value	Stage with increased concentration
HMDB0005807	Gallic acid	12.89	0.006171	L3
HMDB0000005	2-Ketobutyric acid	2.49	0.037232	L3
HMDB0011171	gamma-Glutamylleucine	7.89	0.002065	L3
HMDB0003355	5-Aminopentanoic acid	2.75	0.000237	L3
HMDB0000687	Leucine	2.34	8.59E-05	L3
HMDB0003339	Glutamic acid	3.82	0.006789	L3
HMDB0000696	L-Methionine	4.13	0.015656	L3
HMDB0028825	Glutamylmethionine	4.09	0.008103	L3
HMDB0029068	Threonylphenylalanine	3.91	0.030709	L3
HMDB0001488	Nicotinic acid	4.89	0.001914	L3
HMDB0000975	Trehalose	9.44	0.003788	L3
HMDB0028940	Leucyl-Tryptophan	7.83	0.006797	L3
HMDB0000719	Homoserine	5.91	0.019309	L3
HMDB0002068	Erucic acid	1.57	0.018429	L3
HMDB0000929	Tryptophan	1.66	0.042818	L3
HMDB0000152	Gentisic acid	6.95	0.009357	L3
HMDB0000517	L-Arginine	7.06	0.017952	L3
HMDB0000296	Uridine	5.79	0.005042	L3
HMDB0000759	Glycylleucine	6.95	0.01415	L3
HMDB0000866	N-Acetyl-L-tyrosine	3.20	0.000844	L3
HMDB0002404	Alpha-Hydroxyhippuric acid	7.71	0.004941	L3
HMDB0000623	Dodecanedioic acid	-2.02	6.54E-11	L4
HMDB0036563	Valerenolic acid	-3.48	3.07E-07	L4
HMDB0000947	Undecanoic acid	-4.04	1.48E-09	L4
HMDB0001870	Benzoic acid	-4.49	1.85E-10	L4
HMDB0001220	Prostaglandin E2	-4.08	1.46E-08	L4
HMDB0000139	Glyceric acid	-3.62	6.09E-08	L4
HMDB0004679	8-HETE	-3.19	7.36E-07	L4
HMDB0000857	Pimelic acid	-3.45	6.7E-11	L4
HMDB0000792	Sebacic acid	-3.02	1.44E-09	L4
HMDB0002685	Prostaglandin F1a	-5.80	3.72E-09	L4
HMDB0000872	Tetradecanedioic acid	-4.16	1.11E-11	L4
HMDB0000511	Capric acid	-2.65	1.69E-08	L4
HMDB0000910	Tridecanoic acid	-1.80	2.49E-06	L4
HMDB0000555	3-Methyladipic acid	-5.32	5.45E-09	L4
HMDB0001858	p-Cresol	-5.12	2.25E-07	L4
HMDB0004705	12,13-DHOME	-5.92	6.92E-12	L4
HMDB0035919	Corchorifatty acid F	-5.27	2.57E-07	L4

(Continued on following page)

TABLE 1 (*Continued*) Metabolites of developmental stages of *A. simplex* (L3 and L4) identified in negative ionization mode (ESI-).

Hmdb ID	Compound name	Log_2(FC)	*p*-value	Stage with increased concentration
HMDB0031230	2-Ethylhexanoic acid	-2.68	3.15E-10	L4
HMDB0061743	Perfluoroundecanoic acid	-7.47	1.57E-07	L4
HMDB0000707	4-Hydroxyphenylpyruvic acid	-5.13	1.72E-06	L4
HMDB0000672	Hexadecanedioic acid	-5.04	9.47E-07	L4
HMDB0005076	13,14-Dihydro PGF-1a	-3.81	1.99E-05	L4
HMDB0000764	Hydrocinnamic acid	-7.18	2.19E-06	L4
HMDB0013272	N-Lauroylglycine	-5.52	5.22E-06	L4
HMDB0000893	Suberic acid	-2.34	4.47E-07	L4
HMDB0061738	Perfluorodecanoic acid	-5.24	1.37E-05	L4
HMDB0000638	Dodecanoic acid	-1.57	5.55E-05	L4
HMDB0001852	Retinoic acid	-3.79	5.68E-05	L4
HMDB0001442	Prostaglandin E1	-5.82	4.8E-05	L4
HMDB0010203	13-HOTE	-2.43	1.23E-05	L4
HMDB0000391	7-Ketodeoxycholic acid	-3.60	3.35E-07	L4
HMDB0010214	19,20-DiHDPA	-3.57	0.000744	L4
HMDB0032797	Jasmonic acid	-4.26	0.000464	L4
HMDB0001844	Methylsuccinic acid	-2.58	2.97E-05	L4
HMDB0011503	LysoPE (16:0/0:0)	-2.41	0.00034	L4
HMDB0006940	9(S)-HPODE	-3.73	0.000702	L4
HMDB0000422	2-Methylglutaric acid	-2.04	0.004432	L4
HMDB0011506	LysoPE (18:1 (9Z)/0:0)	-1.92	0.007341	L4
HMDB0005862	2-Methylguanosine	-6.42	0.005289	L4

polarization modes (Figure 2A). Analysis showed that 94 metabolites are common for both ESI modes (Supplementary Table S6).

These data were further processed, and several filters were next applied to obtain the final list of DMs among the given groups: a) $-1.5 \leqslant Log_2FC \leqslant 1.5$ in normalized ratios (L3 vs L4), b) *t*-test (*p*-value ≤0.05), c) VIP >1.0. Afterwards, the significantly changed metabolites between the two groups were filtered out and listed in Supplementary Tables S8, 9. Statistical analysis showed that in ESI- mode was 60 DMs, of which 21 were more detected in the L3 larvae and 39 in the L4 stage of *A. simplex* (Supplementary Table S8). Comparison of the individual developmental stages in ESI + mode revealed, as well, a total of 60 DMs, however with 32 metabolites more enriched in the L3 stage larvae and 28 metabolites more enriched in the L4 stage (Supplementary Table S9). The distribution of common and unique metabolites identified in the two ESI modes specific for each developmental stage was also analyzed and visualized with the use of Venn diagram (Figure 2B, Supplementary Table S10). It was found that there are 11 common metabolites between the ESI −/+ modes for the L3 stage (L-arginine, tryptophan, threonylphenylalanine, homoserine, leucyl-tryptophan, glutamylmethionine, gamma-glutamylleucine, glutamic acid, L-methionine, leucine, and glycylleucine), and eight for the L4 stage (13-HOTE, LysoPE (18:1 (9Z)/0:0), prostaglandin E2, N-lauroylglycine, glyceric acid, LysoPE (16:0/0:0), p-cresol, and 19,20-DiHDPA) (Figure 2B, Supplementary Table S10). The volcano plot representations of DMs are shown in Figures 2C, D. Among the DMs more enriched for L3 stage larvae, found in ESI-, we identified gallic acid and trehalose, as those with the highest fold change. Moreover, in the group of metabolites more enriched in L3 we found, e.g., nicotinic acid, leucine, tryptophan or gamma-glutamylleucine (Figure 2C; Table 1). In the studied polarization (ESI-), such compounds as pimelic acid, sebacic acid, benzoic acid, or prostaglandins E1, E2, F1a were found in increased concentration in L4 larvae compared to L3 (Figure 2C; Table 1). The analysis of the *A. simplex* metabolome in ESI + mode showed higher concentration in L3 compared to L4 of such metabolites as: glutamylmethionine, serine, piperidine or 3-hydroxyanthranilic acid (Figure 2D; Table 2). Moreover, in ESI + mode, increased amounts of e.g., pyridoxine, psi-pelletierine, styrene, citrulline or N-laurolylglicine were observed in L4 larvae in relation to the L3 stage (Figure 2D; Table 2). The HCA was used to visualize the differences in the concentration of each

TABLE 2 Metabolites of developmental stages of *A. simplex* (L3 and L4) identified in positive ionization mode (ESI+).

Hmdb ID	Compound name	Log_2(FC)	*p*-value	Stage with increased concentration
HMDB0094701	N-Acetylproline	1.83	0.00030629	L3
HMDB0000687	Leucine	1.54	0.00000855	L3
HMDB0000696	L-Methionine	3.15	0.00101515	L3
HMDB0033304	Gerberinol	8.29	0.00002015	L3
HMDB0034301	Piperidine	3.30	0.00000038	L3
HMDB0003339	Glutamic acid	4.44	0.00003730	L3
HMDB0000517	L-Arginine	6.49	0.00234735	L3
HMDB0000267	Pyroglutamic acid	3.99	0.00000169	L3
HMDB0000156	Malic acid	4.08	0.00004064	L3
HMDB0000719	Homoserine	3.45	0.00000530	L3
HMDB0011171	gamma-Glutamylleucine	7.88	0.00005651	L3
HMDB0001476	3-Hydroxyanthranilic acid	9.26	0.00039118	L3
HMDB0028825	Glutamylmethionine	10.15	0.00000120	L3
HMDB0001138	N-Acetyl-L-glutamic acid	3.46	0.00024656	L3
HMDB0000929	Tryptophan	1.54	0.04665395	L3
HMDB0000734	Indoleacrylic acid	1.54	0.04653269	L3
HMDB0028940	Leucyl-Tryptophan	3.98	0.01189554	L3
HMDB0000187	Serine	2.82	0.00000020	L3
HMDB0001325	N6,N6,N6-Trimethyl-L-lysine	1.65	0.04833034	L3
HMDB0000228	Phenol	4.01	0.00001597	L3
HMDB0001250	N-Acetylarylamine	3.62	0.00001107	L3
HMDB0001199	N2-Succinyl-L-ornithine	4.57	0.00169112	L3
HMDB0000026	Ureidopropionic acid	4.39	0.00000215	L3
HMDB0000205	Phenylpyruvic acid	4.34	0.00002708	L3
HMDB0000759	Glycylleucine	6.35	0.00550864	L3
HMDB0011756	N-Acetylleucine	3.67	0.01260170	L3
HMDB0013122	LysoPC(P-18:0/0:0)	1.66	0.00040691	L3
HMDB0000158	L-Tyrosine	4.24	0.00007212	L3
HMDB0000214	Ornithine	1.67	0.01629332	L3
HMDB0003447	Tryptophol	1.98	0.00949214	L3
HMDB0029068	Threonylphenylalanine	5.87	0.01050157	L3
HMDB0000706	Aspartylphenylalanine	4.02	0.00026174	L3
HMDB0062769	Epsilon-caprolactam	-1.75	0.00005150	L4
HMDB0034580	psi-Pelletierine	-4.81	0.00000000	L4
HMDB0000239	Pyridoxine	-6.08	0.00000000	L4
HMDB0010214	19,20-DiHDPA	-6.02	0.00000035	L4
HMDB0034240	Styrene	-6.16	0.00000001	L4
HMDB0001858	p-Cresol	-4.65	0.00000152	L4

(Continued on following page)

TABLE 2 (*Continued*) Metabolites of developmental stages of *A. simplex* (L3 and L4) identified in positive ionization mode (ESI+).

Hmdb ID	Compound name	Log_2(FC)	*p*-value	Stage with increased concentration
HMDB0002005	Methionine sulfoxide	-2.09	0.00000794	L4
HMDB0000904	Citrulline	-8.60	0.00000631	L4
HMDB0001370	Diaminopimelic acid	-5.33	0.00001148	L4
HMDB0013272	N-Lauroylglycine	-6.24	0.00002255	L4
HMDB0001220	Prostaglandin E2	-2.08	0.00126021	L4
HMDB0010203	13-HOTE	-2.81	0.00028251	L4
HMDB0001256	Spermine	-1.78	0.00031453	L4
HMDB0005809	Eugenol	-5.61	0.00004089	L4
HMDB0004667	13-HODE	-4.48	0.00006656	L4
HMDB0000197	Indoleacetic acid	-2.55	0.00021292	L4
HMDB0004483	Estrone glucuronide	-5.38	0.00022515	L4
HMDB0010388	LysoPC(18:3 (9Z,12Z,15Z)/0:0)	-4.60	0.00028059	L4
HMDB0000139	Glyceric acid	-1.52	0.00197458	L4
HMDB0000259	Serotonin	-3.90	0.00062622	L4
HMDB0000079	Dihydrothymine	-3.39	0.00033464	L4
HMDB0001488	Nicotinic acid	-1.97	0.00014390	L4
HMDB0000094	Citric acid	-2.22	0.00019260	L4
HMDB0000501	7-Ketocholesterol	-1.89	0.00398334	L4
HMDB0011503	LysoPE (16:0/0:0)	-1.80	0.00059878	L4
HMDB0000208	Oxoglutaric acid	-2.08	0.00040543	L4
HMDB0011506	LysoPE (18:1 (9Z)/0:0)	-2.11	0.00499579	L4
HMDB0015109	Edetic Acid	-1.75	0.00130870	L4

statistically significant metabolite between L3 and L4 developmental stages of *A. simplex* in two different ESI modes (Figures 2E,F). An overview on the DMs concentrations from all samples can be observed and clear clustering and grouping trend between L3 and L4 developmental stages of *A. simplex* is showed.

3.2 Metabolite classes and enriched pathways

The DMs identified in ESI- and ESI+ (60 in each mode) were assigned to different metabolite classes/groups (Supplementary Tables S11, 12). The highest number of metabolites identified in ESI- mode were categorized into the fatty acyls (e.g., prostaglandin E2, prostaglandin E1, prostaglandin F1a, 8-HETE, 13-HOTE), organic acids (e.g., sebacic acid, pimelic acid, suberic acid, methylsuccinic acid), and benzenoids (p-cresol, benzoic acid, alpha-hydroxyhippuric acid) (Figure 3A, Supplementary Table S11). Of 60 DMs identified in ESI + mode, 23 of them were organic acids (e.g., ureidopropionic acid, citric acid, L-malic acid), nine were organoheterocyclic compounds (dihydrothymine, indoleacetic acid, pyridoxine, serotonin, pyroglutamic acid, indoleacrylic acid, nicotinic acid, tryptophanol, piperidine), 10 were fatty acyls and benzenoids, and four were glycerophospholipids (e.g., LysoPC(18:3 (9Z,12Z, 15Z)); LysoPE (16:0/0:0); LysoPE (18:1 (9Z)/0:0); LysoPC(P-18:0)) (Figure 3B, Supplementary Table S12).

Based on the DMs identified in both developmental stages of *A. simplex* in ESI−/+ ionization modes, the metabolic pathways were mapped, and enrichment analysis was performed (*p*-value ≤0.05) (Figures 3C, D; Supplementary Tables S13, 14). In negative ionization mode (ESI-) the highest number of identified DMs were products of ubiquinone and other terpenoid-quinone biosynthesis (KEGG 00130), followed by phenylalanine, tyrosine and tryptophan biosynthesis (KEGG 00400), fatty acid biosynthesis (KEGG 00061), valine, leucine and isoleucine biosynthesis and degradation (KEGG 00290, 00280), tyrosine metabolism (KEGG 00350), starch and sucrose metabolism (KEGG 00500), and nicotinate and nicotinamide metabolism (KEGG 00760) (Kanehisa and Goto, 2000; Kanehisa et al., 2016). Mapping and enrichment analysis of pathways for identified DMs in positive ionization mode (ESI+) against known pathways in KEGG database, showed that highest number of DMs were products of lysine degradation (KEGG 00310), and nicotinate and nicotinamide metabolism (KEGG 00760) (Kanehisa and Goto, 2000; Kanehisa et al., 2016).

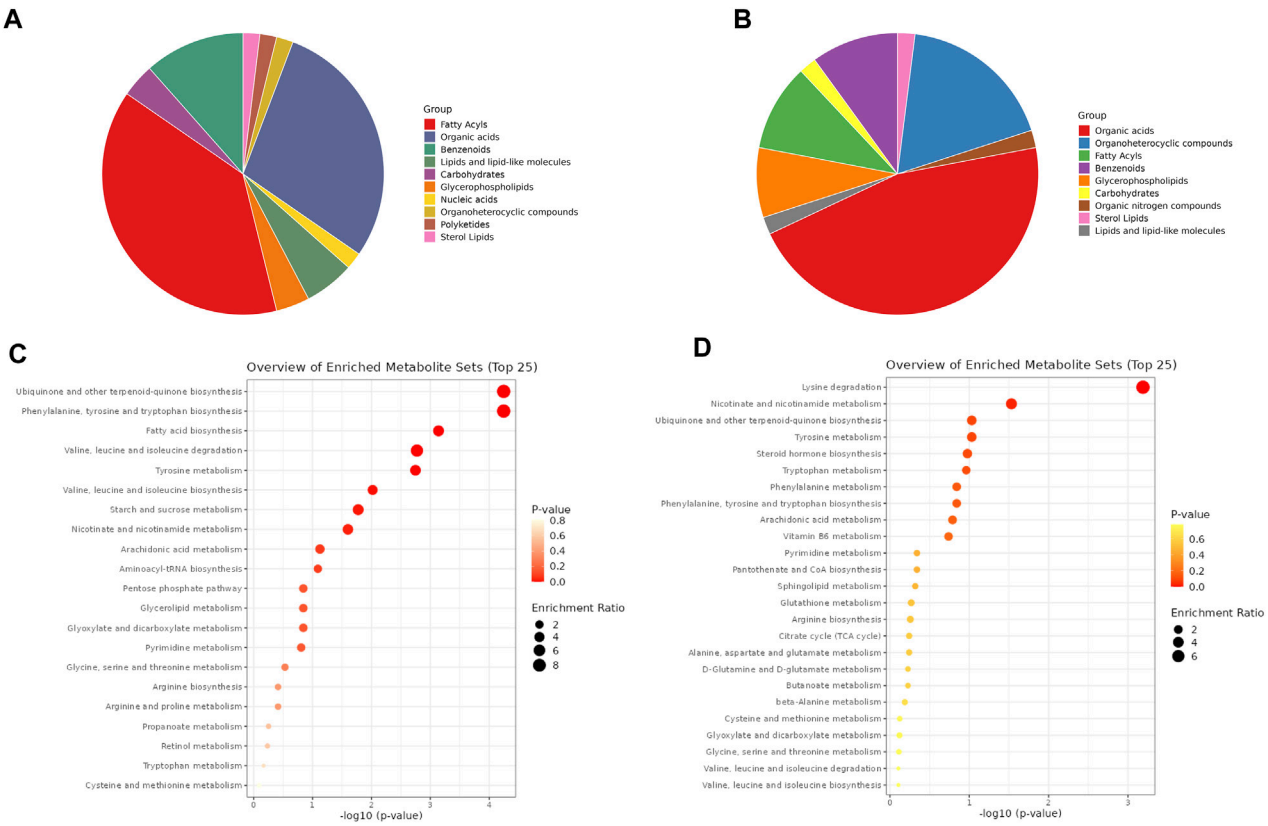

FIGURE 3
Metabolite classes and enriched pathways. Distribution of DMs by different metabolite classes identified in negative and positive ionization modes, respectively **(A, B)**. The metabolites names assigned to different classes are listed in Supplementary Tables S11, 12. Dot plots of pathway enrichment analysis of DMs identified in negative and positive ionization modes, respectively **(C, D)**. The scale bars represent *p*-value and enrichment ratio. The pathways names with calculated *p*-value are listed in Supplementary Tables S13, 14.

4 Discussion

One of the most recent additions to the *Caenorhabditis elegans* toolbox is metabolomics and lipidomics, which allow new and deeper investigations of nematode metabolism. Combining a genetically defensible model organism such as *C. elegans* with the functional evaluation of metabolomics and/or lipidomics holds great promise for expanding our knowledge of metabolism and metabolic regulation (Salzer and Witting, 2021). While there are numerous published studies on the genomes (Mattiucci et al., 2016; Coghlan et al., 2019; Łopieńska-Biernat et al., 2019), transcriptomes (Cavallero et al., 2018; Kim et al., 2018; Llorens et al., 2018; Łopieńska-Biernat et al., 2018; Cavallero et al., 2020), and proteomes (Stryiński et al., 2019; Stryiński et al., 2022; Polak et al., 2020; Mierzejewski et al., 2021; Kochanowski et al., 2022) of *A. simplex*, less attention has been paid to its metabolome. Metabolic changes between L3 and L4 larval stages of *A. simplex* have been studied previously, however in a narrow range, e.g., of one metabolic pathway (Łopieńska-Biernat et al., 2008; Łopieńska-Biernat et al., 2018; Łopieńska-Biernat et al., 2019), and almost nothing is known about the complement of an intermediate or end product of metabolism in *Anisakis* nematodes, especially in the stages found in humans (L3 and L4).

In the first stage of infection the larvae are invading the host intestinal tissues and establishing in the gastrointestinal tract of the host. Such tissue migration requires larvae to adapt to constantly changing external environments, in terms of temperature, oxygen supply, redox potential and host immune reactions (Huang et al., 2020; Yeshi et al., 2020). In this metabolomic study, we observed substantial differences in the composition and abundance of trehalose, nicotinic acid, prostaglandins, and acyl acids, likely associated with key biological functions, including energy metabolism and nicotinate and nicotinamide metabolism during the parasite's growth and development. Alterations in metabolomic profiles are likely reflected in the adaptation of *A. simplex* nematode to changing environments within the host (poikilotherm and homeotherm organisms). Nevertheless, comparative analyses of levels of metabolites in the L3 and L4 of these two larval stages led to the identification of groups of molecules with putative roles in mechanisms of parasite pathogenicity.

Our results revealed that specific to L3 are nicotinic acid and branched-chain and aromatic amino acids (BCAA). The recent metabolomics studies showed that BCAA are positively related to longevity common to Dauer in *C. elegans* and *Haemonhus contortus* during mitochondrial biogenesis in ensheathment eggs (Palevich

et al., 2022). In this study, BCAA were only identified in L3 stage, which like a Dauer stage, uses endogenous energy sources. Starvation-induced stress may invoke a series of regulations of metabolic pathways (Fuchs et al., 2010; Łopieńska-Biernat et al., 2019). In this study, some pathways, including fatty acid metabolism, nicotinate/nicotinamide metabolism, terpenoid backbone biosynthesis were only identified in L3 stage.

Fatty acids serve as energy storage and structural components in biomembranes. The main chemical composition of the cuticular lipids in *A. simplex* from Atlantic cod (*Godus morhua*) was recognized as three fatty acids, 15 triacylglycerols, five sterols and 12 sphingolipids (Mika et al., 2010) what is consisted with our current results. Moreover, we have identified fatty acyls and glycerophospholipids in L4 stage larvae.

Terpenoids are the precursor in the production of steroids and sterols. Therefore, the constant activity of the terpenoid backbone biosynthesis pathway is important for the regulation of steroids metabolism, as they regulate a variety of developmental and biological processes (molting, larval development, and innate immunity) (Hernández-Bello et al., 2011). The ubiquinone/terpenoid quinone biosynthesis (energy metabolism) involved in biosynthesis of other secondary metabolites, and metabolism of cofactors (nicotinate/nicotinamide metabolism) and vitamins is specific to two larval stages. Based on current results and previous studies, energy metabolism of *A. simplex* is based on carbohydrates metabolism, where L3 larvae is metabolizing trehalose, and L4 larvae glycogen (Łopieńska-Biernat et al., 2006, Łopieńska-Biernat et al., 2007; Łopieńska-Biernat et al., 2008; Łopieńska-Biernat et al., 2018; Łopieńska-Biernat et al., 2019). However, based on the current results we can suppose that L4 larvae energy metabolism is also related to fatty acids (Ma et al., 2019). This could be an adaptation due to different host environments and usage of energy sources.

In addition, we have identified significant amounts of the prostaglandin PGE2 in L4 larvae of *A. simplex*, which helps larvae successfully migrate into their host and acts as a mediator of host immunity. These molecules mediate and have an immunosuppressive effect on T cells (Tebbey and Buttke, 1990). Genes of the prostaglandin synthesis cascade (Fitzpatrick, 2004), including cyclooxygenase (WormBase ParaSite ASIM_0001219401), alpha-tubulin N-acetyltransferaseare (WormBase ParaSite ASIM_0001506401), and phospholipase A2 (WormBase ParaSite ASIM_0001246201) are present in the genome of the nematode studied (Coghlan et al., 2019), demonstrating that *A. simplex* larvae can synthesize prostaglandins. Moreover, studies on *Trichuris suis* may provide insight into the mechanisms by which the worm suppresses inflammatory host responses, with one active component identified as prostaglandin PGE2 (Laan et al., 2017).

Lipidome analysis of *Schistosoma mansoni* has detected eicosanoids, signaling molecules made by the enzymatic or non-enzymatic oxidation of polyunsaturated fatty acids, that promote a Th2 response (Shepherd et al., 2015; Whitman et al., 2021). Metabolites analysis in this study specific to L4 stage also revealed eicosanoids. However, studies show that some helminth-derived small molecules have distinct immunomodulatory components, suggesting that further studies are needed at this host-pathogen interface (Shepherd et al., 2015; Whitman et al., 2021).

Our metabolomics study showed that *A. simplex* induced metabolic changes in a variety of metabolic pathways in both larval stages, including amino acid metabolism, phospholipid metabolism, energy metabolism, nicotinate/nicotinamide metabolism and ubiquinone/terpenoid quinone biosynthesis. In addition, several stage-specific metabolites were identified, providing potential clues for understanding the molecular mechanisms of this parasite biology: its pathogenicity and adaptation to the host environment.

By undertaking the first small-scale analysis of the metabolome molecules present in the L3 and L4 of *A. simplex* that are putatively involved in the host environment, we provide here a ready-to-use molecular groundwork for in-depth studies of the biological pathways specifically involved in parasite growth and development. Further studies under experimental, controlled *in vitro* conditions, as well as between other developmental stages of the life cycle, are needed to reliably assess the role of these molecules in the pathogenesis of anisakiasis. A snapshot of the metabolic status in specific age of the larvae and/or tissues of larval stages of *A. simplex* could provide new information on the expression of target metabolites potentially involved in host invasion. Furthermore, 13C flux experiments can provide adequate information on the route of formation of key metabolites.

Gastrointestinal nematodes strategy mediated through the carbohydrates and lipid metabolites and employed for the manipulation of the host immune response towards successful propagation and parasitism, opens a wide perspective that should be compounded by the contemporary use of multi-omics approaches.

Data availability statement

The raw data generated for this study can be found in the EMBL-EBI MetaboLights database (www.ebi.ac.uk/metabolights/MTBLS6458) with the identifier MTBLS6458.

Author contributions

Conceptualization: RS and EŁ-B. Methodology: IP and RS. Formal analysis: IP. Data curation: RS. Software: RS. Writing—original draft preparation: IP, RS, and EŁ-B. Writing—review and editing: RS, MM, and EŁ-B. All authors contributed to the article and approved the submitted version.

Funding

This work was supported by National Science Centre of Poland, grant no. 2020/37/N/NZ9/03312.

Acknowledgments

We thank PARASITE Biobank at the Institute of Marine Research (IIM-CSIC), Vigo, Spain for providing the L4 larvae of *Anisakis simplex* used in this study.

Conflict of interest

The authors declare that the research was conducted in the absence of any commercial or financial relationships that could be construed as a potential conflict of interest.

Publisher's note

All claims expressed in this article are solely those of the authors and do not necessarily represent those of their affiliated organizations, or those of the publisher, the editors and the reviewers. Any product that may be evaluated in this article, or claim that may be made by its manufacturer, is not guaranteed or endorsed by the publisher.

Supplementary material

The Supplementary Material for this article can be found online at: https://www.frontiersin.org/articles/10.3389/fmolb.2023.1233586/full#supplementary-material

References

Aibinu, I. E., Smooker, P. M., and Lopata, A. L. (2019). Anisakis nematodes in fish and shellfish-from infection to allergies. *Int. J. Parasitol. Parasites Wildl.* 9, 384–393. doi:10.1016/j.ijppaw.2019.04.007

Audicana, M. T., and Kennedy, M. W. (2008). Anisakis simplex: From obscure infectious worm to inducer of immune hypersensitivity. *Clin. Microbiol. Rev.* 21, 360–379. doi:10.1128/CMR.00012-07

Audicana, M. T., Ansotegui, I. J., de Corres, L. F., and Kennedy, M. W. (2002). Anisakis simplex: Dangerous — Dead and alive? *Trends Parasitol.* 18, 20–25. doi:10.1016/S1471-4922(01)02152-3

Baird, F. J., Gasser, R. B., Jabbar, A., and Lopata, A. L. (2014). Foodborne anisakiasis and allergy. *Mol. Cell Probes* 28, 167–174. doi:10.1016/j.mcp.2014.02.003

Cavallero, S., Lombardo, F., Su, X., Salvemini, M., Cantacessi, C., and D'Amelio, S. (2018). Tissue-specific transcriptomes of Anisakis simplex (sensu stricto) and Anisakis pegreffii reveal potential molecular mechanisms involved in pathogenicity. *Parasit. Vectors* 11, 31. doi:10.1186/S13071-017-2585-7

Cavallero, S., Lombardo, F., Salvemini, M., Pizzarelli, A., Cantacessi, C., and D'Amelio, S. (2020). Comparative transcriptomics reveals clues for differences in pathogenicity between hysterothylacium aduncum, Anisakis simplex sensu stricto and Anisakis pegreffii. *Genes (Basel)* 11, 321. doi:10.3390/genes11030321

Coghlan, A., Tyagi, R., Cotton, J. A., Holroyd, N., Rosa, B. A., Tsai, I. J., et al. (2019). Comparative genomics of the major parasitic worms. *Nat. Genet.* 51, 163–174. doi:10.1038/s41588-018-0262-1

da Silva, R. R., Dorrestein, P. C., and Quinn, R. A. (2015). Illuminating the dark matter in metabolomics. *Proc. Natl. Acad. Sci.* 112, 12549–12550. doi:10.1073/pnas.1516878112

EFSA (2010). Scientific Opinion on risk assessment of parasites in fishery products. *EFSA J.* 8, 1543. doi:10.2903/j.efsa.2010.1543

Fitzpatrick, F. (2004). Cyclooxygenase enzymes: Regulation and function. *Curr. Pharm. Des.* 10, 577–588. doi:10.2174/1381612043453144

Fuchs, S., Bundy, J. G., Davies, S. K., Viney, J. M., Swire, J. S., and Leroi, A. M. (2010). A metabolic signature of long life in *Caenorhabditis elegans*. *BMC Biol.* 8, 14. doi:10.1186/1741-7007-8-14

Gao, X., Zhang, W., Wang, Y., Pedram, P., Cahill, F., Zhai, G., et al. (2016). Serum metabolic biomarkers distinguish metabolically healthy peripherally obese from unhealthy centrally obese individuals. *Nutr. Metab. (Lond)* 13, 33. doi:10.1186/s12986-016-0095-9

Guardone, L., Armani, A., Nucera, D., Costanzo, F., Mattiucci, S., and Bruschi, F. (2018). Human anisakiasis in Italy: A retrospective epidemiological study over two decades. *Parasite* 25, 41. doi:10.1051/parasite/2018034

Hernández-Bello, R., Ramirez-Nieto, R., Muñiz-Hernández, S., Nava-Castro, K., Pavón, L., Sánchez-Acosta, A. G., et al. (2011). Sex steroids effects on the molting process of the helminth human parasite *Trichinella spiralis*. *J. Biomed. Biotechnol.* 2011, 625380–625410. doi:10.1155/2011/625380

Herrador, Z., Daschner, Á., Perteguer, M. J., and Benito, A. (2019). Epidemiological scenario of anisakidosis in Spain based on associated hospitalizations: The tip of the iceberg. *Clin. Infect. Dis.* 69, 69–76. doi:10.1093/cid/ciy853

Huang, Y., Wu, Q., Zhao, L., Xiong, C., Xu, Y., Dong, X., et al. (2020). UHPLC-MS-Based metabolomics analysis reveals the process of schistosomiasis in mice. *Front. Microbiol.* 11, 1517. doi:10.3389/fmicb.2020.01517

Iglesias, L., Valero, A., Benitez, R., and Adroher, F. J. (2001). *In vitro* cultivation of Anisakis simplex: Pepsin increases survival and moulting from fourth larval to adult stage. *Parasitology* 123, 285–291. doi:10.1017/S0031182001008423

Iglesias, L., Malagón, D., Valero, A., Benítez, R., and Javier Adroher, F. (2005). CO2-fixing enzymes during moulting from third larval to fourth larval stage of Anisakis simplex and Hysterothylacium aduncum (Nematoda: Anisakidae). *Parasitol. Res.* 96, 212–215. doi:10.1007/s00436-005-1342-6

Ivanovic, J., Baltic, M. Z., Boskovic, M., Kilibarda, N., Dokmanovic, M., Markovic, R., et al. (2015). Anisakis infection and allergy in humans. *Procedia Food Sci.* 5, 101–104. doi:10.1016/j.profoo.2015.09.028

Jasmer, D. P., Rosa, B. A., Tyagi, R., and Mitreva, M. (2019). Omics driven understanding of the intestines of parasitic nematodes. *Front. Genet.* 10, 652. doi:10.3389/fgene.2019.00652

Kagei, N., and Isogaki, H. (1992). A case of abdominal syndrome caused by the presence of a large number of Anisakis larvae. *Int. J. Parasitol.* 22, 251–253. doi:10.1016/0020-7519(92)90111-W

Kanehisa, M., and Goto, S. (2000). Kegg: Kyoto encyclopedia of genes and genomes. *Nucleic Acids Res.* 28, 27–30. doi:10.1093/nar/28.1.27

Kanehisa, M., Sato, Y., Kawashima, M., Furumichi, M., and Tanabe, M. (2016). KEGG as a reference resource for gene and protein annotation. *Nucleic Acids Res.* 44, D457–D462. doi:10.1093/nar/gkv1070

Kim, J. H., Kim, J. O., Jeon, C. H., Nam, U. H., Subramaniyam, S., Yoo, S. I., et al. (2018). Comparative transcriptome analyses of the third and fourth stage larvae of Anisakis simplex (Nematoda: Anisakidae). *Mol. Biochem. Parasitol.* 226, 24–33. doi:10.1016/j.molbiopara.2018.10.002

Kim, S., Cheng, T., He, S., Thiessen, P. A., Li, Q., Gindulyte, A., et al. (2022). PubChem protein, gene, pathway, and taxonomy data collections: Bridging biology and chemistry through target-centric views of PubChem data. *J. Mol. Biol.* 434, 167514. doi:10.1016/j.jmb.2022.167514

Kochanowski, M., Dąbrowska, J., Różycki, M., Sroka, J., Karamon, J., Bełcik, A., et al. (2022). Proteomic profiling and in silico characterization of the secretome of Anisakis simplex sensu stricto L3 larvae. *Pathogens* 11, 246. doi:10.3390/pathogens11020246

Kołodziejczyk, L., Szostakowska, B., Sobecka, E., Szczucki, K., and Stankiewicz, K. (2020). First case of human anisakiasis in Poland. *Parasitol. Int.* 76, 102073. doi:10.1016/j.parint.2020.102073

Kuhn, T., Cunze, S., Kochmann, J., and Klimpel, S. (2016). Environmental variables and definitive host distribution: A habitat suitability modelling for endohelminth parasites in the marine realm. *Sci. Rep.* 6, 30246. doi:10.1038/srep30246

Laan, L. C., Williams, A. R., Stavenhagen, K., Giera, M., Kooij, G., Vlasakov, I., et al. (2017). The whipworm (*Trichuris suis*) secretes prostaglandin E2 to suppress proinflammatory properties in human dendritic cells. *FASEB J.* 31, 719–731. doi:10.1096/fj.201600841R

Levsen, A., Svanevik, C. S., Cipriani, P., Mattiucci, S., Gay, M., Hastie, L. C., et al. (2018). A survey of zoonotic nematodes of commercial key fish species from major European fishing grounds—introducing the FP7 PARASITE exposure assessment study. *Fish. Res.* 202, 4–21. doi:10.1016/j.fishres.2017.09.009

Liu, R., Bao, Z.-X., Zhao, P.-J., and Li, G.-H. (2021). Advances in the study of metabolomics and metabolites in some species interactions. *Molecules* 26, 3311. doi:10.3390/molecules26113311

Llorens, C., Arcos, S. C., Robertson, L., Ramos, R., Futami, R., Soriano, B., et al. (2018). Functional insights into the infective larval stage of Anisakis simplex s.s., Anisakis pegreffii and their hybrids based on gene expression patterns. *BMC Genomics* 19, 592. doi:10.1186/s12864-018-4970-9

Łopieńska-Biernat, E., Żółtowska, K., and Rokicki, J. (2006). The content of carbohydrates in larval stages of Anisakis simplex (Nematoda, Anisakidae). *Helminthologia* 43, 125–129. doi:10.2478/s11687-006-0024-y

Łopieńska-Biernat, E., Żółtowska, K., and Rokicki, J. (2007). Trehalose catabolism enzymes in L3 and L4 larvae of Anisakis simplex. *J. Parasitol.* 93, 1291–1294. doi:10.1645/GE-906.1

Łopieńska-Biernat, E., Żółtowska, K., and Rokicki, J. (2008). Glycogen catabolism enzymes and protein fractions in the third and fourth larval stages of *Anisakis simplex*. *J. Helminthol.* 82, 45–51. doi:10.1017/S0022149X0787355X

Łopieńska-Biernat, E., Molcan, T., Paukszto, Ł., Jastrzębski, J. P., and Myszczyński, K. (2018). Modelling studies determing the mode of action of anthelmintics inhibiting *in vitro* trehalose-6-phosphate phosphatase (TPP) of Anisakis simplex s.l. *Exp. Parasitol.* 184, 46–56. doi:10.1016/j.exppara.2017.11.006

Łopieńska-Biernat, E., Stryiński, R., Dmitryjuk, M., and Wasilewska, B. (2019). Infective larvae of Anisakis simplex (Nematoda) accumulate trehalose and glycogen in response to starvation and temperature stress. *Biol. Open* 8, bio040014. doi:10.1242/bio.040014

Ma, G., Wang, T., Korhonen, P. K., Young, N. D., Nie, S., Ang, C.-S., et al. (2019). Dafachronic acid promotes larval development in *Haemonchus contortus* by modulating dauer signalling and lipid metabolism. *PLoS Pathog.* 15, e1007960. doi:10.1371/journal.ppat.1007960

Mattiucci, S., Acerra, V., Paoletti, M., Cipriani, P., Levsen, A., Webb, S. C., et al. (2016). No more time to stay 'single' in the detection of *Anisakis pegreffii, A. simplex* (s. S.) and hybridization events between them: A multi-marker nuclear genotyping approach *Parasitology* 143, 998–1011. doi:10.1017/S0031182016000330

Mattiucci, S., Cipriani, P., Levsen, A., Paoletti, M., and Nascetti, G. (2018). Molecular epidemiology of Anisakis and anisakiasis: An ecological and evolutionary road map. *Adv. Parasitol.* 99, 93–263. doi:10.1016/bs.apar.2017.12.001

Mierzejewski, K., Stryiński, R., Łopieńska-Biernat, E., Mateos, J., Bogacka, I., and Carrera, M. (2021). A complex proteomic response of the parasitic nematode Anisakis simplex s.s. to *Escherichia coli* lipopolysaccharide. *Mol. Cell. Proteomics* 20, 100166. doi:10.1016/j.mcpro.2021.100166

Mika, A., Gołębiowski, M., Szafranek, J., Rokicki, J., and Stepnowski, P. (2010). Identification of lipids in the cuticle of the parasitic nematode Anisakis simplex and the somatic tissues of the Atlantic cod *Gadus morhua*. *Exp. Parasitol.* 124, 334–340. doi:10.1016/j.exppara.2009.11.013

Mladineo, I., Popović, M., Drmić-Hofman, I., and Poljak, V. (2015). A case report of Anisakis pegreffii (Nematoda, Anisakidae) identified from archival paraffin sections of a Croatian patient. *BMC Infect. Dis.* 16, 42. doi:10.1186/s12879-016-1401-x

Molenaars, M., Schomakers, B. V., Elfrink, H. L., Gao, A. W., Vervaart, M. A. T., Pras-Raves, M. L., et al. (2021). Metabolomics and lipidomics in *Caenorhabditis elegans* using a single-sample preparation. *Dis. Model Mech.* 14, dmm047746. doi:10.1242/dmm.047746

Orpha.net (2022). *Prevalence of rare diseases: Bibliographic data, orphanet report series, rare diseases collection, january 2022, number 1: Diseases listed in alphabetical order*. Available at: https://www.orpha.net/orphacom/cahiers/docs/GB/Prevalence_of_rare_diseases_by_alphabetical_list.pdf.

Palevich, N., Maclean, P. H., Subbaraj, A. K., and Cao, M. (2021). A multimodal metabolomics approach to elucidate the trigger components of rumen fluid for larval exsheathment in a model gastrointestinal parasitic nematode, *Haemonchus contortus*. *bioRxiv*, 1–44. doi:10.1101/2021.01.10.426113

Palevich, N., Maclean, P. H., Candy, P. M., Taylor, W., Mladineo, I., and Cao, M. (2022). Untargeted multimodal metabolomics investigation of the *Haemonchus contortus* exsheathment secretome. *Cells* 11, 2525. doi:10.3390/cells11162525

Pang, Z., Chong, J., Zhou, G., de Lima Morais, D. A., Chang, L., Barrette, M., et al. (2021). MetaboAnalyst 5.0: Narrowing the gap between raw spectra and functional insights. *Nucleic Acids Res.* 49, W388–W396. doi:10.1093/nar/gkab382

Polak, I., Łopieńska-Biernat, E., Stryiński, R., Mateos, J., and Carrera, M. (2020). Comparative proteomics analysis of Anisakis simplex s.s.—evaluation of the response of invasive larvae to ivermectin. *Genes (Basel)* 11, 710. doi:10.3390/genes11060710

Salek, R. M., Steinbeck, C., Viant, M. R., Goodacre, R., and Dunn, W. B. (2013). The role of reporting standards for metabolite annotation and identification in metabolomic studies. *Gigascience* 2, 13. doi:10.1186/2047-217X-2-13

Salzer, L., and Witting, M. (2021). Quo vadis *Caenorhabditis elegans* metabolomics—a review of current methods and applications to explore metabolism in the nematode. *Metabolites* 11, 284. doi:10.3390/metabo11050284

Shepherd, C., Navarro, S., Wangchuk, P., Wilson, D., Daly, N. L., and Loukas, A. (2015). Identifying the immunomodulatory components of helminths. *Parasite Immunol.* 37, 293–303. doi:10.1111/pim.12192

Smith, C. A., Maille, G. O., Want, E. J., Qin, C., Trauger, S. A., Brandon, T. R., et al. (2005). Metlin: A metabolite mass spectral database. *Ther. Drug Monit.* 27, 747–751. doi:10.1097/01.ftd.0000179845.53213.39

Sohn, W.-M., Na, B.-K., Kim, T. H., and Park, T.-J. (2015). Anisakiasis: Report of 15 gastric cases caused by Anisakis type I larvae and a brief review of Korean anisakiasis cases. *Korean J. Parasitol.* 53, 465–470. doi:10.3347/kjp.2015.53.4.465

Stryiński, R., Mateos, J., Pascual, S., González, Á. F., Gallardo, J. M., Łopieńska-Biernat, E., et al. (2019). Proteome profiling of L3 and L4 Anisakis simplex development stages by TMT-based quantitative proteomics. *J. Proteomics* 201, 1–11. doi:10.1016/j.jprot.2019.04.006

Stryiński, R., Łopieńska-Biernat, E., and Carrera, M. (2020). Proteomic insights into the biology of the most important Foodborne parasites in Europe. *Foods* 9, 1403. doi:10.3390/foods9101403

Stryiński, R., Mateos, J., Carrera, M., Jastrzębski, J. P., Bogacka, I., and Łopieńska-Biernat, E. (2022). Tandem mass tagging (TMT) reveals tissue-specific proteome of L4 larvae of Anisakis simplex s. s.: Enzymes of energy and/or carbohydrate metabolism as potential drug targets in anisakiasis. *Int. J. Mol. Sci.* 23, 4336. doi:10.3390/ijms23084336

Suzuki, J., Murata, R., and Kodo, Y. (2021). Current status of anisakiasis and *Anisakis* larvae in tokyo, Japan. *Food Saf.* 9, 89–100. doi:10.14252/foodsafetyfscj.D-21-00004

Tambellini, N., Zaremberg, V., Turner, R., and Weljie, A. (2013). Evaluation of extraction protocols for simultaneous polar and non-polar yeast metabolite analysis using multivariate projection methods. *Metabolites* 3, 592–605. doi:10.3390/metabo3030592

Tebbey, P. W., and Buttke, T. M. (1990). Molecular basis for the immunosuppressive action of stearic acid on T cells. *Immunology* 70, 379–384.

van Thiel, P., Kuipers, F. C., and Roskam, R. T. (1960). A nematode parasitic to herring, causing acute abdominal syndromes in man. *Trop. Geogr. Med.* 12, 97–113.

Vernocchi, P., Del Chierico, F., and Putignani, L. (2016). Gut microbiota profiling: Metabolomics based approach to unravel compounds affecting human health. *Front. Microbiol.* 7, 1144. doi:10.3389/fmicb.2016.01144

Whitman, J. D., Sakanari, J. A., and Mitreva, M. (2021). Areas of metabolomic exploration for helminth infections. *ACS Infect. Dis.* 7, 206–214. doi:10.1021/acsinfecdis.0c00658

Wishart, D. S., Jewison, T., Guo, A. C., Wilson, M., Knox, C., Liu, Y., et al. (2012). HMDB 3.0—the human metabolome database in 2013. *Nucleic Acids Res.* 41, D801–D807. doi:10.1093/nar/gks1065

Xia, J., Psychogios, N., Young, N., and Wishart, D. S. (2009). MetaboAnalyst: A web server for metabolomic data analysis and interpretation. *Nucleic Acids Res.* 37, W652–W660. doi:10.1093/nar/gkp356

Yera, H., Fréalle, É., Dutoit, E., and Dupouy-Camet, J. (2018). A national retrospective survey of anisakidosis in France (2010-2014): Decreasing incidence, female predominance, and emerging allergic potential. *Parasite* 25, 23. doi:10.1051/parasite/2018016

Yeshi, K., Creek, D. J., Anderson, D., Ritmejerytė, E., Becker, L., Loukas, A., et al. (2020). Metabolomes and lipidomes of the infective stages of the gastrointestinal nematodes, nippostrongylus brasiliensis and Trichuris muris. *Metabolites* 10, 446. doi:10.3390/metabo10110446

Yorimitsu, N., Hiraoka, A., Utsunomiya, H., Imai, Y., Tatsukawa, H., Tazuya, N., et al. (2013). Colonic intussusception caused by anisakiasis: A case report and review of the literature. *Intern. Med.* 52, 223–226. doi:10.2169/internalmedicine.52.8629

frontiers | Frontiers in Animal Science

TYPE Original Research
PUBLISHED 08 November 2023
DOI 10.3389/fanim.2023.1241033

OPEN ACCESS

EDITED BY
Elda Dervishi,
University of Alberta, Canada

REVIEWED BY
Mariana Carriquiry,
Universidad de la República, Uruguay
Marcos Colazo,
University of Alberta, Canada

*CORRESPONDENCE
J. Lannett Edwards
jedwards@utk.edu
Sarah E. Moorey
smoorey5@utk.edu

†PRESENT ADDRESS
Jessica L. Klabnik,
Department of Clinical Sciences, College of Veterinary Medicine, Auburn University, Auburn, AL, United States

RECEIVED 15 June 2023
ACCEPTED 19 October 2023
PUBLISHED 08 November 2023

CITATION
Pollock AB, Moorey SE, Hessock EA, Klabnik JL, Payton RR, Schrick FN, Campagna SR and Edwards JL (2023) Relationship between higher estrus-associated temperatures and the bovine preovulatory follicular fluid metabolome. *Front. Anim. Sci.* 4:1241033. doi: 10.3389/fanim.2023.1241033

Relationship between higher estrus-associated temperatures and the bovine preovulatory follicular fluid metabolome

Abigayle B. Pollock[1], Sarah E. Moorey[1*], Emma A. Hessock[1], Jessica L. Klabnik[1†], Rebecca R. Payton[1], F. Neal Schrick[1], Shawn R. Campagna[2] and J. Lannett Edwards[1*]

[1]Department of Animal Science, The University of Tennessee Institute of Agriculture and AgResearch, Knoxville, TN, United States, [2]Department of Chemistry, University of Tennessee Knoxville, Knoxville, TN, United States

Introduction: A higher estrus-associated temperature (HEAT) is a hallmark feature in sexually active females; however, its functional importance is unclear. Our objective was to examine the relationship between HEAT and the preovulatory follicular fluid metabolome. It was hypothesized that HEAT is functionally important as it affects fertility-related components in the preovulatory follicle.

Methods: Estrus was synchronized in non-lactating Jersey cows. A Thermochron iButton temperature data logger was affixed to blank controlled internal drug release (CIDR) devices and intravaginally inserted after CIDR device removal. The follicular fluid was aspirated 14.9 h + 3.3 h after an animal first stood to be mounted. Regression models were performed using metabolite abundance and HEAT variables. Best-fit models were determined using backward manual selection ($p < 0.05$).

Results: A total of 86 metabolites were identified in cow follicular fluid samples. The vaginal temperature at first mount and when it was expressed as a change from baseline was positively related to the abundance of four metabolites (i.e., taurine, *sn*-glycerol 3-phosphate, glycine, and cysteine) and negatively related to one metabolite (i.e., serine). The vaginal temperature at the first standing mount was related to the differential abundance of two metabolites (i.e., jasmonate and *N*-carbamoyl-L-aspartate). Three metabolites were related to the maximum vaginal temperature (i.e., *N*-carbamoyl-L-aspartate, uracil, and glycodeoxycholate). When expressed as a change from baseline, the maximum vaginal temperature was related to the differential abundances of uracil, uric acid, and 6-phospho-D-gluconate. The time taken to reach maximum vaginal temperature was related to *N*-carbamoyl-L-aspartate, glycodeoxycholate, jasmonate, and tricarballylic acid. Pertaining to the combination of HEAT and its duration, the area under the curve associated with the time between the first increase in vaginal temperature and the maximum vaginal temperature was related to 6-phospho-D-gluconate, sulfolactate, guanidoacetic acid, and aspartate. The area under the curve associated with the time between the initial vaginal temperature increase and up to 10 h after a cow first stood to be mounted or

when a cow's temperature returned to baseline was related to the differential abundances of uracil, *sn*-glycerol 3-phosphate, methionine sulfoxide, and taurodeoxycholate.

Discussion: Our findings support the notion that HEAT is related to changes in the preovulatory follicular fluid metabolites involved in energy metabolism, thermoregulation, and oxidative stress management.

KEYWORDS

estrus, vaginal temperature, HEAT, metabolome, follicular fluid, preovulatory follicle, bovine

1 Introduction

Although the basis of fertility in cattle is multifaceted, events occurring at or around estrus are essential for reproductive success. Estrus signifies the major endocrine transition in which the preovulatory follicle prepares for ovulation. To this end, the estradiol-induced gonadotropin-releasing hormone (GnRH)—luteinizing hormone (LH) surge (Stumpf et al., 1991) sets the stage for ovulation 24 h to 30 h thereafter (Malhi et al., 2005; Saumande and Humblot, 2005; Ginther et al., 2013). The mural granulosa undergoes luteinization (i.e., the beginnings of corpus luteum formation) and the oocyte contained within the preovulatory follicle undergoes meiotic resumption and progression to metaphase II (Smith et al., 1994; Duggavathi and Murphy, 2009).

Increasing estradiol levels during the follicular phase of the estrous cycle underlie much of the behavioral changes leading up to and during estrus (Lyimo et al., 2000). Female cattle approaching estrus become restless, may walk up to four times more than those not exhibiting estrus, and interact with others forming sexually active groups (Kiddy, 1977; Diskin and Sreenan, 2000; Sveberg et al., 2013). Other secondary signs of estrus activity include, but are not limited to, chin-resting, head butting, and vulva sniffing (Kerbrat and Disenhaus, 2004). The most definitive sign of estrus, however, is the willingness of a female to stand to be mounted by another cow. Interestingly, several studies report a positive relationship between the level of activity in an estrual female and the probability of pregnancy outcome (López-Gatius et al., 2005; Madureira et al., 2015; Madureira et al., 2019; Tippenhauer et al., 2023).

Increased body temperature is another hallmark feature of estrus-active females, even under thermoneutral environmental conditions (Piccione et al., 2003; Sakatani et al., 2016). Higher estrus-associated temperatures (HEAT) may range from 0.3°C to 1.3°C or greater above the baseline (Redden et al., 1993; Kyle et al., 1998; Piccione et al., 2003; Fisher et al., 2008; Suthar et al., 2011; Randi et al., 2018). An estrus-related increase in body temperature is short in duration (5 h to 18 h; Redden et al., 1993; Kyle et al., 1998; Sakatani et al., 2016); it typically occurs around the LH surge and persists for several hours thereafter (Fisher et al., 2008; Miura et al., 2017). In addition to being an informative indicator of estrus (Redden et al., 1993; Sakatani et al., 2016), varying levels of HEAT may be functionally relevant.

In support of HEAT's functional impact on fertility important events specific to the cumulus–oocyte complex, an acute, but short episode of exposure at 41°C for 4 h to 6 h *in vitro*, induces germinal vesicle breakdown earlier than in thermoneutral controls (Edwards et al., 2005; Hooper et al., 2015) without compromising embryo development after fertilization (Rowinski et al., 2021). In terms of impacts on other preovulatory follicle components, two transcripts (i.e., calreticulin and serpin family F member 2) in granulosa cells have been shown by others to potentiate ovulation (Tsafriri et al., 1989; Tokuhiro et al., 2015). These transcripts were upregulated by varying degrees of hyperthermia occurring after a pharmacologically induced LH surge (Klabnik et al., 2022). Calreticulin can enhance the binding of bradykinin to its receptor (reviewed in Bedard et al., 2005). Interestingly, higher bradykinin levels were noted in the preovulatory follicular fluid of the same cows exhibiting varying levels of hyperthermia, from which the granulosa samples (Klabnik et al., 2022) were collected (Rispoli et al., 2019). Bradykinin has been shown to potentiate follicular rupture in other species (Yoshimura et al., 1988; Hellberg et al., 1991).

Follicular fluid provides the necessary substrates for follicle growth and progression, oocyte developmental competence, and subsequent embryo viability (Leroy et al., 2011; Sirard, 2011). The differences in follicular fluid metabolome profiles have recently been associated with fertility, follicle maturity, or follicle progression after the onset of estrus (Read et al., 2021; Read et al., 2022; Hessock et al., 2023). Although changes in milk, serum, and urine metabolome profiles have been noted in cattle experiencing elevated body temperature resulting from chronic heat stress (Liao et al., 2018; Yue et al., 2020), it remains unclear whether an acute episode of HEAT is associated with changes in the follicular fluid metabolome of the preovulatory follicle. Thus, the objective of this study was to examine the relationship between HEAT and the preovulatory follicular fluid metabolome.

2 Materials and methods

2.1 Animals and synchronization protocol

Animal use during this study occurred during the month of May. Institutional animal care and use approval at the University of Tennessee, Knoxville, TN, USA, was obtained before the onset of this study. Non-lactating Jersey cows located at a University of Tennessee AgResearch and Education Center grazed the same fescue-based pasture and were provided *ad libitum* access to minerals (Burkmann Nutrition; Danville, KY, USA). Cows ranged in age from 2.5 years to 7.7 years (5.1 years ± 1.4 years), weighed between 365.6 kg and 585.1 kg (508.3 kg ± 61.6 kg), and had a body condition score ranging from 2.5 to 3.5 (3.1 ± 0.4). Toward the synchronization of a first wave dominant–preovulatory follicle (Figure 1), GnRH was administered (Cystorelin®; 100 μg; i.m.; Boehringer Ingelheim; Ingelheim am Rhein, Germany) and a controlled internal drug release (CIDR) device was placed intravaginally (1.38 g progesterone; Eazi-Breed CIDR; Zoetis Animal Health, Kalamazoo, MI, USA). Nine days later, the CIDR device was removed and prostaglandin $F_{2\alpha}$ ($PGF_{2\alpha}$; 12.5 mg of dinoprost tromethamine/mL Lutalyse® HighCon; Zoetis Animal Health, Kalamazoo, MI, USA) was administered. GnRH was administered 48 hours after $PGF_{2\alpha}$ (when progesterone levels were < 1 ng/mL; Supplementary Figure 1) and a new CIDR device was inserted. $PGF_{2\alpha}$ was administered 7 days later, after CIDR device removal. The cattle were visually monitored for behavioral signs of estrus; this took place every 4 h after $PGF_{2\alpha}$ administration and continued until a cow displayed estrus activity (~ 31 h after $PGF_{2\alpha}$). Thereafter, cows were continually monitored by a team of individuals trained in the visual observation of estrus activity. The onset of estrus was defined as the first time a cow was observed to stand to be mounted by another. Of the 16 cows used for this study, 14 exhibited estrus (87.5%).

2.2 Vaginal and ambient temperature data

Cows' vaginal temperature was recorded using a Thermochron iButton™ 1922L data logger (Embedded Data Systems, Lawrenceburg, KY, USA) affixed to a blank CIDR device (i.e., containing no progesterone) consistent with the method described by Burdick et al. (2012). Cows' vaginal temperature was recorded every 3 min (0.5°C resolution), beginning 12 h after $PGF_{2\alpha}$ administration and continuing until iButton removal, which occurred immediately before preovulatory follicle aspiration. During the time when estrus expression was induced, the ambient temperature and humidity were recorded onsite (hourly) using the HOBO U23 Pro v2 data logger (Onset Computer Corporation, Bourne, MA, USA). Data for the ambient temperature and humidity from the start of the pre-synchronization protocol to $PGF_{2\alpha}$ administration to induce estrus were collected at a local meteorological station and averaged every 2 h. The temperature humidity index (THI) was calculated in accordance with the method described by Abbott et al. (2018).

2.3 Ovarian ultrasound and follicular fluid aspiration

The largest follicle diameter (> 7 mm) was recorded at GnRH, $PGF_{2\alpha}$, first mount, and follicle aspiration using an IBEX EVO® II ultrasound and eL7 linear probe (E.I. Medical Imaging, Loveland, CO, USA; Figure 1). The neat follicular fluid was successfully collected from the preovulatory follicles of 13 out of the 14 estrus cows through ultrasound-guided transvaginal aspiration (18-g needle; Rispoli et al., 2019; Hessock et al., 2023) using a Samsung HM70A ultrasound and CFA-9 convex probe 14.9 h± 3.3 h after a cow was first observed to stand to be mounted by another cow.

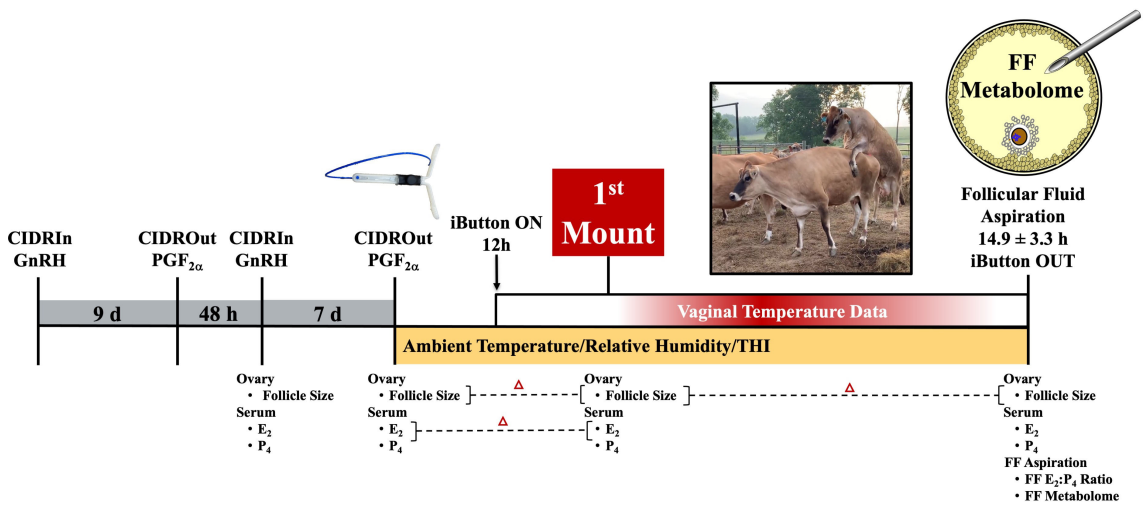

FIGURE 1
Study schematic depicting synchronization scheme and data collected at each of the different time points relative to when follicle aspiration occurred. GnRH, gonadotropin-releasing hormone; CIDR, controlled internal drug release; $PGF_{2\alpha}$, prostaglandin $F_{2\alpha}$; E_2, estradiol; P_4, progesterone; FF, follicular fluid.

2.4 Serum and follicular fluid hormone assays

The blood samples were collected from the coccygeal vein/artery (Figure 1) and processed in accordance with Hessock et al. (2023). Serum estradiol (E_2) was evaluated using a radioimmunoassay (Kirby et al., 1997), with intra- and inter-assay coefficients of variation (CVs) of 3.6% and 6.7%, respectively. The sensitivity of the serum estradiol assay was 1.03 pg/mL. The follicular fluid E_2 was analyzed using the DetectX® Serum 17β-Estradiol ELISA Kit (Arbor Assays, Ann Arbor, MI, USA; the sensitivity was 2.21 pg/mL). The intra- and inter-assay CVs for the follicular fluid E_2 were 1.7% and 7.3%, respectively. The serum and follicular fluid progesterone (P_4) concentrations were measured using ImmuChem™ Double Antibody Radioimmunoassay Kit (MP Biomedicals, LLC, Orangeburg, NY, USA). The intra- and inter-assay CVs for serum P_4 were 8.0% and 4.2%, respectively; whereas the follicular fluid progesterone intra- and inter-assay CVs were 4.4% and 5.7%, respectively. The sensitivity of the progesterone assays was 0.11 ng/mL.

2.5 HEAT data—pertinent variables of interest

Vaginal temperature, recorded every 3 min, was averaged every 30 min. The HEAT variables of interest are defined in Table 1 and highlighted in Figure 2. A baseline temperature was calculated for each cow. The baseline temperature was defined as the average vaginal temperature of those recorded between the first temperature, which was taken 12 h after $PGF_{2\alpha}$, and those recorded over the next 20 h. An increase in vaginal temperature related to HEAT was defined as the first time when the vaginal temperature was 0.3°C higher than baseline, with the increase persisting for 3 h or more (Clapper et al., 1990). Cow vaginal temperature when first observed to stand to be mounted by another cow was noted as first mount. The maximum HEAT vaginal temperature was denoted as *VT*max. Both the first mount and *VT*max temperature, when expressed as a change from baseline, were also considered. The time to *VT*max was the number of hours from the first mount to *VT*max. The area under the different portions of the HEAT curves (AUC_1: time when vaginal temperature first increased to *V*max; AUC_2: time when the vaginal temperature first increased up to 10 h after estrus onset or when the vaginal temperature returned to baseline) was calculated for each cow, in accordance with Pruessner et al. (2003), using the trapezoid formula with the baseline temperature as a lower limit.

2.6 Metabolome profiling of follicular fluid

Ultra-high-performance liquid chromatography–high resolution mass spectrometry (UHPLC-HRMS) was performed at the University of Tennessee Knoxville Biological and Small Molecule Mass Spectrometry Core Facility [Research Resource Identifier (RRID):SCR_021368], as previously described by Horn et al. (2022). In brief, metabolites were extracted from 50 µL of each follicular fluid sample (n = 13) with a solution of 20: 40: 40 water/methanol/acetonitrile with 0.1 M formic acid. The metabolites were then separated on a Synergi Hydro RP, 2.5 µm, 100 mm × 2.0 mm column (Phenomenex, Torrance, CA, USA). The solvents for the mobile phase to elute metabolites were (A) 97: 3 methanol to water with 11 mM tributylamine and 15 mM acetic acid and (B) 100% methanol. The solvent gradient from 0 min to 5 min was (A) 100% and (B) 0%; from 5 min to 13 min, it was (A) 80% and (B) 20%; from 13 min to 15.5 min, it was (A) 45% and (B) 55%; from

TABLE 1 Higher estrus-associated temperature (HEAT) variables of interest.

HEAT variables	Definition	Range	Mean	SEM
Baseline[1]	Average vaginal temperature of those recorded between the first temperature, which was taken 12 h after $PGF_{2\alpha}$, and those recorded over the next 20 h	38.0°C to 38.8°C	38.4	0.05
First mount	Cow vaginal temperature when first observed to stand to be mounted by another cow	38.1°C to 39.1°C	38.6	0.1
Change (baseline to first mount)	Change in vaginal temperature: first mount minus the baseline	−0.5°C to 0.5°C	0.1	0.07
VT_{Max}	Maximum HEAT vaginal temperature	38.5°C to 40.1°C	39.3	0.1
Change (baseline to VT_{Max})	Change in vaginal temperature: VT_{Max} minus the baseline	0.2°C to 1.5°C	0.8	0.1
Time to VT_{Max}	Number of hours from first mount to VT_{Max}	0.5 h to 6.0 h	3.0	0.7
AUC_1	Area under the curve: time when vaginal temperature first increased* to VT_{Max}	4.5 to 147.1	45.8	12.0
AUC_2	Area under the curve: time when vaginal temperature first increased up to 10 h after estrus onset or when vaginal temperature returned to baseline	53.8 to 209.9	127.9	11.6

[1]Data used to calculate the HEAT variables of interest but were not used as an independent variable in the statistical analysis.
*The time when the vaginal temperature increased was defined as the first time when the vaginal temperature was 0.3°C higher than the baseline temperature, with this increased temperature observed for 3 or more hours thereafter (Clapper et al., 1990).

10.3389/fanim.2023.1241033

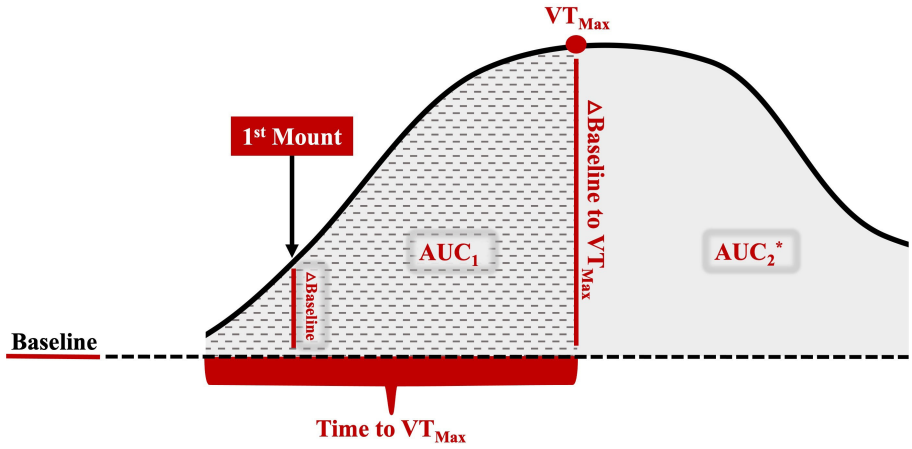

FIGURE 2
Representative image of the different HEAT variables of interest used to examine the relationship between HEAT and the preovulatory follicular fluid metabolome. The baseline is the average vaginal temperature of those recorded between the first temperature, which was taken 12 h after $PGF_{2\alpha}$, and those recorded over the next 20 h, which was well before HEAT-related increases. A HEAT-related vaginal temperature increase was defined as the time that the vaginal temperature was 0.3°C higher than the baseline, with this increased temperature observed for 3 or more hours thereafter (Clapper et al., 1990). First mount: the vaginal temperature when the cow was first observed to stand to be mounted by another cow; △ baseline to 1M: the vaginal temperature at first mount minus the baseline; VT_{Max}: the maximum HEAT vaginal temperature; △ baseline to VT_{Max}: the maximum vaginal temperature minus the baseline; time to VT_{Max}: hours from first mount to VT_{Max}; AUC_1: area under the curve—time when the vaginal temperature first increased to VT_{Max}; AUC_2: area under the curve—time when the vaginal temperature first increased up to 10 h after estrus onset or when the vaginal temperature returned to the baseline; △=change; *AUC_2 includes AUC_1 area and remaining solid gray shaded area.

15.5 min to19 min, it was (A) 5% and (B) 95%; and from 19 min to 25 min, it was (A) 100% and (B) 0%, with a flow rate of 0.2 µL per min. The mass spectrometry was performed using an Exactive™ Plus Orbitrap™ mass spectrometer (Thermo Fisher Scientific, Waltham, MA, USA) fitted with an electrospray ionization probe operating in negative mode. The scan range was 72000 m/z to 1,000 m/z, with a resolution of 140,000 and an acquisition gain control of 3×10^6 (Greene et al., 2020).

The files generated by HRMS in the Xcalibur® (RAW) format were converted to an open-source mzML format (msconvert; ProteoWizard package) and then processed using the Metabolomic Analysis and Visualization Engine (MAVEN; mzroll software, Princeton University) for an untargeted analysis of the full-scan LC-MS data. A group algorithm for non-linear retention time alignment was used to pick peaks, integrate intensities, and visualize extracted ion chromatograms. The metabolites were identified based on peak shape, signal-to-noise ratio, and retention time. The MAVEN preprocessed peak data were used for further statistical analysis.

2.7 Statistical analyses

The analyses were conducted using R Studio (version 2023.3.0.386; RStudio Team 2020, Boston, MA, USA). Data were checked for normality using the Shapiro–Wilk test and log-transformed when necessary. The outliers identified using the interquartile range (IQR) method were removed. Supplementary Table 1 denotes the metabolites that were log-transformed or had outliers removed for statistical analyses. To examine the relationship between the different features of HEAT (independent variable of interest, e.g., VT_{Max} and other HEAT variables defined and listed in Table 1) with metabolite abundance (dependent variable), hierarchical linear regression models were performed using a backward stepwise approach to derive the best-fit models for each metabolite. The cow and other related independent variables used to derive the best-fit models were utilized as covariates [i.e., variables that may affect response variables but were not of direct interest in our study; these included cow age, weight, body condition score (BCS), proestrus length, serum estradiol and progesterone, follicular fluid E_2-to-P_4 ratio, follicle size, and THI]. The covariates were included in the model only if they were deemed significant in an initial simple linear regression ($p < 0.1$). The final models included the HEAT variables of interest (significant if p-value ≤ 0.05) and the covariates significant at a p-value < 0.05.

3 Results

3.1 Proestrus length, follicle size, and ambient conditions

The time from $PGF_{2\alpha}$ to the first observed standing mount (i.e., proestrus length) was 43.1 h ± 8.4 h (range 31.1 h–63.9 h). The preovulatory follicle size at aspiration was 16.2 mm ± 1.3 mm (range 12.9 mm–18.5 mm). At the time of follicle aspiration, serum progesterone and estradiol were 0.13 ng/mL ± 0.02 ng/mL (range 0.1 ng/mL–0.37 ng/mL) and 4.42 pg/mL ± 0.74 pg/mL (range 1.03 pg/mL–9.14 pg/mL), respectively. The ambient temperature, relative humidity, and the THI from the start of the pre-synchronization protocol through to the time of the final

follicular fluid aspiration are shown in Figure 3. The estrus-associated vaginal temperature curves for each individual cow (n = 13) are shown in Figure 4.

3.2 Preovulatory follicular fluid metabolites

Eighty-six metabolites were identified in the preovulatory follicular fluid aspirates collected 14.9 h ± 3.3 h after the onset of estrus (Supplementary Table 1). Identified metabolites primarily included amino acids, glucose metabolism and tricarboxylic acid (TCA) cycle derivatives, and nucleosides. The abundances of 17 out of 86 metabolites (19.8%) were related to different aspects of HEAT.

3.3 Follicular fluid metabolites related to HEAT

The vaginal temperature at first standing mount, when expressed as a change from baseline, was associated with the differential abundance of five metabolites. Four of the five metabolites had a positive relationship with the vaginal temperature change from baseline to first mount (i.e., taurine, *sn*-glycerol 3-phosphate, glycine, and cysteine), and one metabolite, serine, had a negative relationship (Figure 5; Supplementary Table 2). The vaginal temperature at first standing mount was related to the differential abundance of two metabolites. Jasmonate was negatively related to it, and *N*-carbamoyl-L-aspartate was positively related to it (Figure 6; Supplementary Table 3).

The abundances of three follicular fluid metabolites at 14.9 h ± 3.3 h after the onset of estrus were related to VT_{Max}: *N*-carbamoyl-L-aspartate was positively related to it, whereas uracil and glycodeoxycholate were negatively related to it (Figure 7; Supplementary Table 4). When VT_{Max} was expressed as a change from baseline, uric acid and 6-phospho-D-gluconate were positively related to it, whereas uracil was negatively related to it (Figure 8; Supplementary Table 5).

To examine the relationship between HEAT duration and the preovulatory follicular fluid metabolome, time to VT_{Max} was used as an independent variable. Time to VT_{Max} was positively associated with the abundance of *N*-carbamoyl-L-aspartate but negatively related to the abundances of glycodeoxycholate, jasmonate, and tricarballylic acid (Figure 9; Supplementary Table 6).

Combining HEAT level with duration, AUC_1 and AUC_2 were tested as independent variables of interest. Sulfolactate, 6-phospho-D-gluconate, and aspartate levels were positively related to AUC_1, whereas guanidoacetic acid abundance was negatively related to AUC_1 (Figure 10; Supplementary Table 7). In contrast, AUC_2 was positively associated with the abundance of methionine sulfoxide, taurodeoxycholate, and *sn*-glycerol 3-phosphate but negatively related to uracil abundance (Figure 11; Supplementary Table 8).

3.4 Metabolites relating to multiple HEAT variables

Of the 17 metabolites (35.3%) significantly related to different aspects of HEAT, 6 were related to two or more HEAT variables (Figure 12). Uracil and *N*-carbamoyl-L-aspartate were related to three HEAT variables (uracil: $VT_{Max,}$ vaginal temperature change from baseline to VT_{Max}, and AUC2; *N*-carbamoyl-L-aspartate: first mount, VT_{Max}, and time to VT_{Max}; Figure 12). The abundances of jasmonate, glycodeoxycholate, 6-phospho-D-gluconate, and *sn*-glycerol 3-phosphate were related to two HEAT variables (Figure 12). Jasmonate was related to both vaginal temperature at first standing mount and time to VT_{Max}. Glycodeoxycholate was related to both VT_{Max} and time to $VT_{Max.}$ Neither AUC_1 nor AUC_2 were related to any common differentially abundant metabolites; however, 6-phospho-D-gluconate was differentially abundant in analyses of AUC_1 and temperature change from baseline to VT_{Max}, while *sn*-glycerol 3-phosphate abundance was related to AUC_2 and temperature change from baseline to first standing mount (Figure 12).

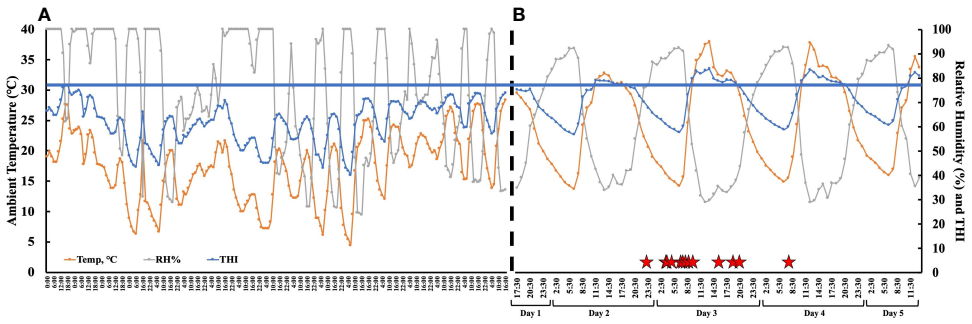

FIGURE 3
(A) The ambient temperature, relative humidity, and temperature humidity index (THI) collected from a local meteorological station from the start of pre-synchronization protocol to the $PGF_{2\alpha}$ administration to induce estrus. The weather data were averaged every 2 hours. The black dotted line represents the end of the meteorological data and the beginning of the hourly onsite environmental data. **(B)** The hourly ambient temperature, relative humidity, and temperature humidity index (THI) from $PGF_{2\alpha}$ administration to induce estrus (day 1—17:30) to after final follicle aspiration (day 5—11:30). The red stars denote the time each animal first stood to be mounted. The blue line represents the THI threshold (77) for non-lactating dairy cattle (Ouellet et al., 2021). The THI was calculated as per Abbott et al. (2018).

10.3389/fanim.2023.1241033

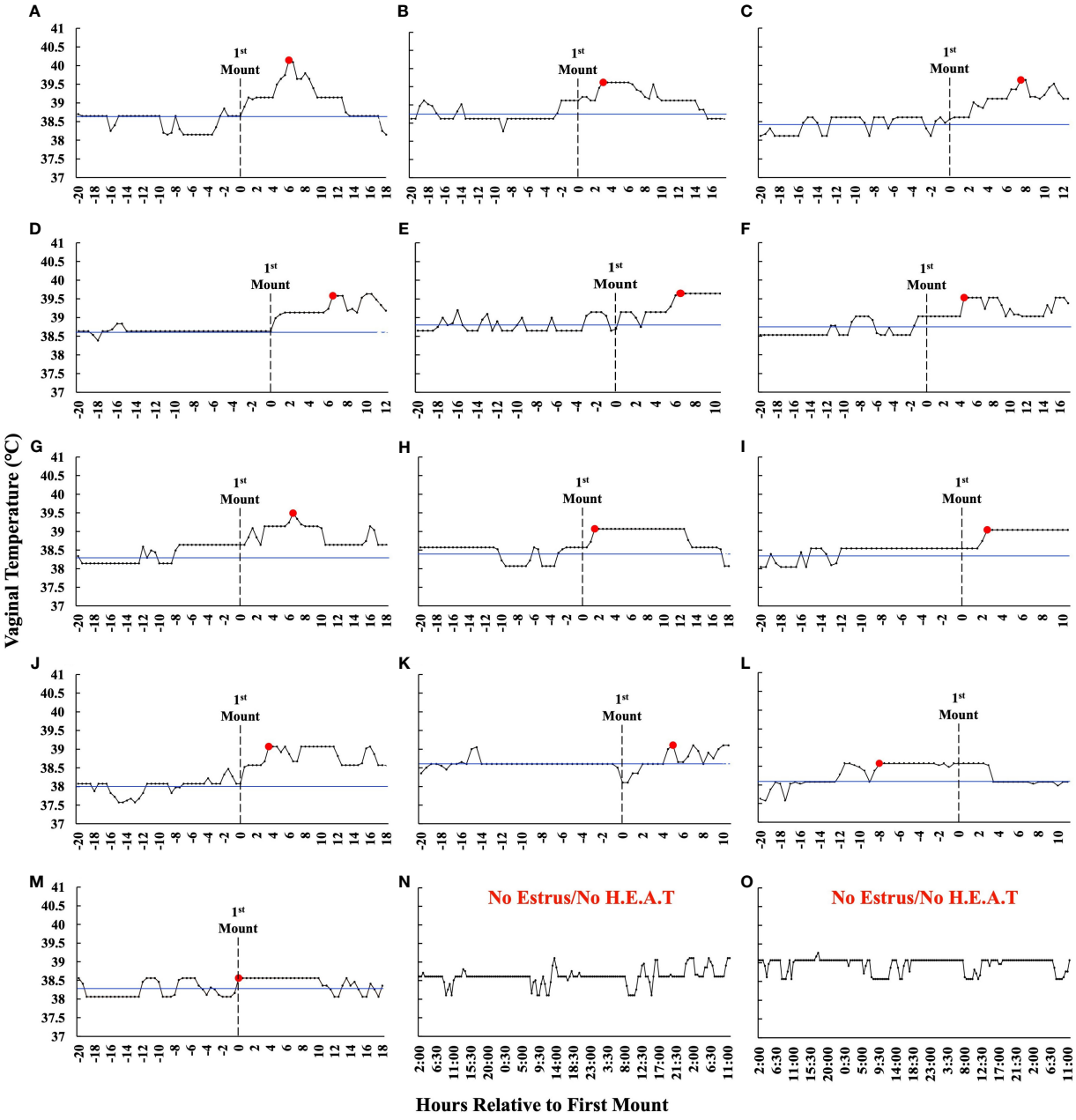

FIGURE 4
(A–M) Estrus-associated vaginal temperatures for the 13 estrus cows whereby follicular fluid was collected from the preovulatory follicle are presented relative to the time that they first stood to be mounted (hour 0) in order of greatest **(A)** to least **(M)** VT_{Max}. The blue line represents an individual animal's baseline temperature, which was calculated by averaging the vaginal temperature of those recorded between the first temperature, which was taken 12 h after $PGF_{2\alpha}$, and those over the next 20 h. The red dot depicts VT_{Max}, and the dotted line represents the first time an animal stood to be mounted. The graphs have been truncated for clarity and depict only the first 20 h before estrus and through preovulatory follicle aspiration. **(N, O)** Representative vaginal temperature graphs of the cows that did not exhibit estrus and did not exhibit a higher estrus-associated vaginal temperature. These animals were not included in the analysis and are displayed for reference only. Data are not shown for the one cow where follicular fluid was not successfully collected.

4 Discussion

The novel findings described in this study highlight the relationship of varying levels of HEAT with the abundance of multiple metabolites in the preovulatory follicle fluid (19.8% of 86 total) ~ 14 h after the onset of estrus. Interestingly, the majority of affected metabolites were positively related to HEAT (11/17; 65%). This finding is especially interesting because intra-follicular changes in the preovulatory follicle in the final hours leading up to the LH surge are important for promoting oocyte competence for embryo development (Atkins et al., 2013; Jinks et al., 2013) and impacting cumulus–oocyte complex metabolism (Read et al., 2021; Moorey

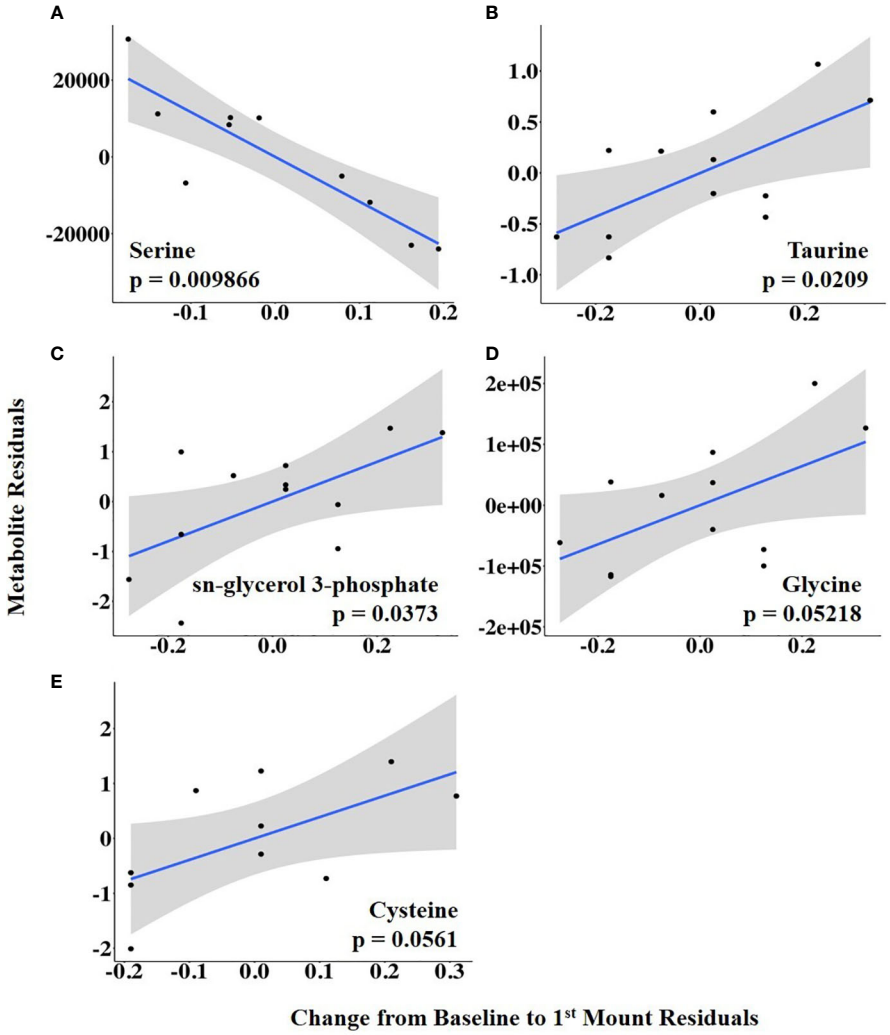

FIGURE 5
(A–E) Partial regression plots for the final model for each metabolite related to the change in vaginal temperature from the baseline to first mount. The plots depict the relationship between the vaginal temperature change from the baseline to first mount and metabolite abundance while adjusting for additional variables included in the final model.

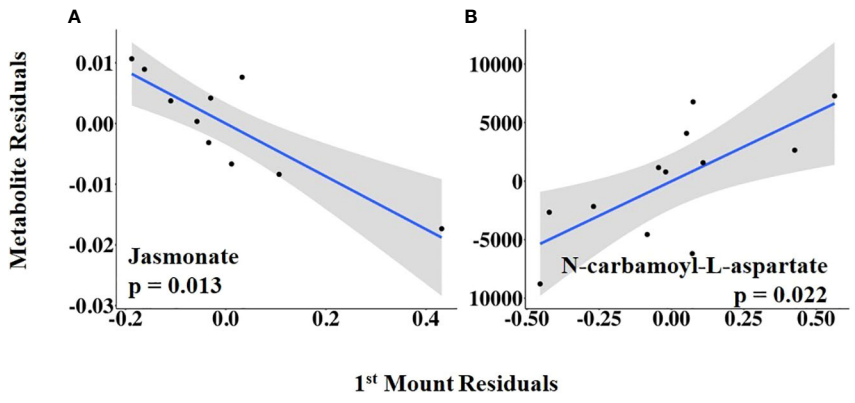

FIGURE 6
(A, B) Partial regression plots for the final model for each metabolite related to the vaginal temperature at first standing mount. The plots depict the relationship between vaginal temperature at first standing mount and metabolite abundance while adjusting for the additional variables included in the final model.

10.3389/fanim.2023.1241033

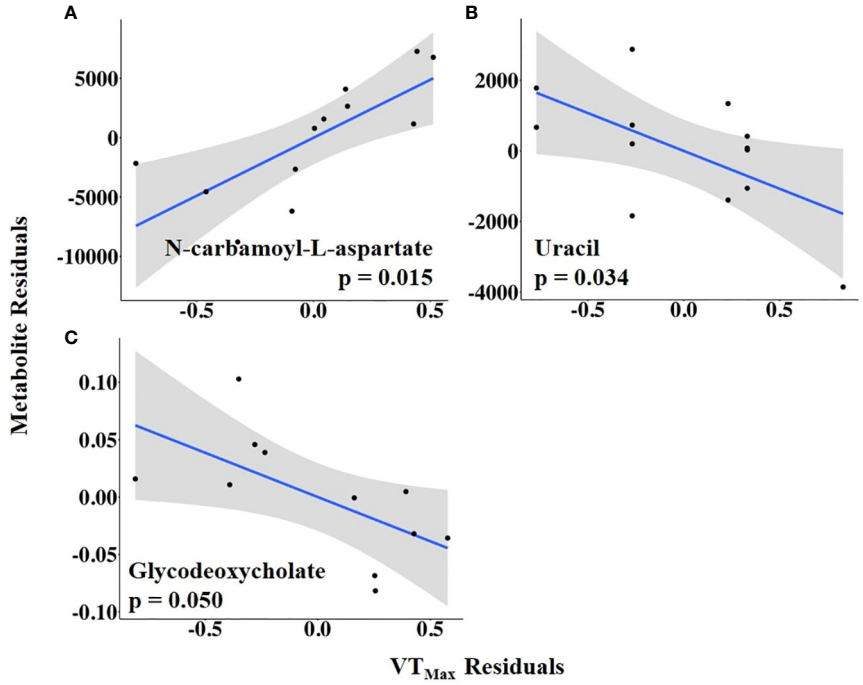

FIGURE 7
(A–C) Partial regression plots for the final model for each metabolite related to maximum vaginal temperature (VT_{Max}). The plots depict the relationship between VT_{Max} and metabolite abundance while adjusting for additional variables included in the final model.

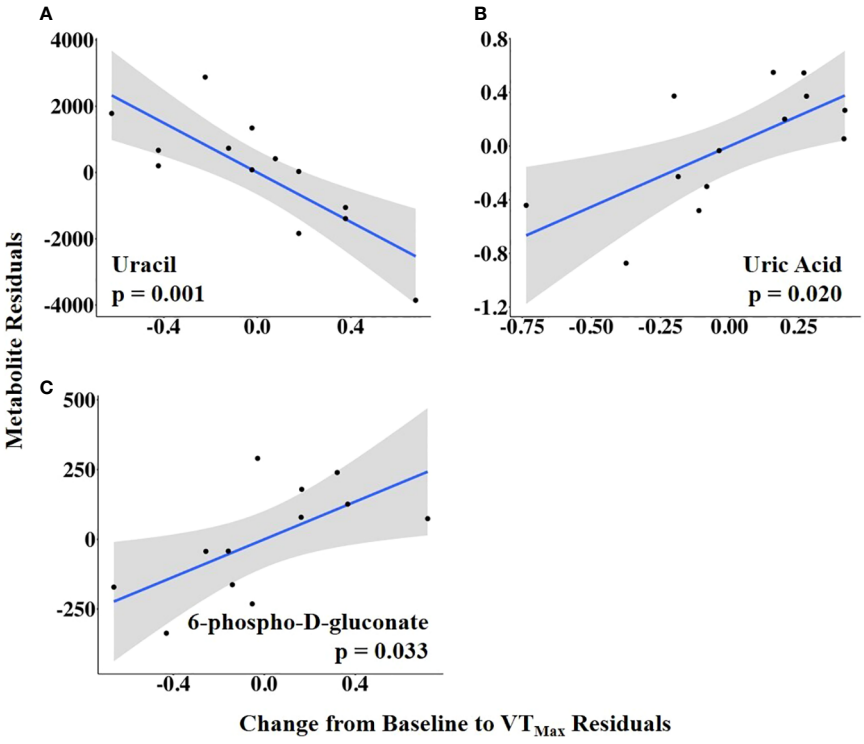

FIGURE 8
(A–C) Partial regression plots for the final model for each metabolite related to the vaginal temperature change from the baseline to the maximum vaginal temperature (VT_{Max}). The plots depict the relationship between vaginal temperature change from the baseline to VT_{Max} and metabolite abundance while adjusting for additional variables included in the final model.

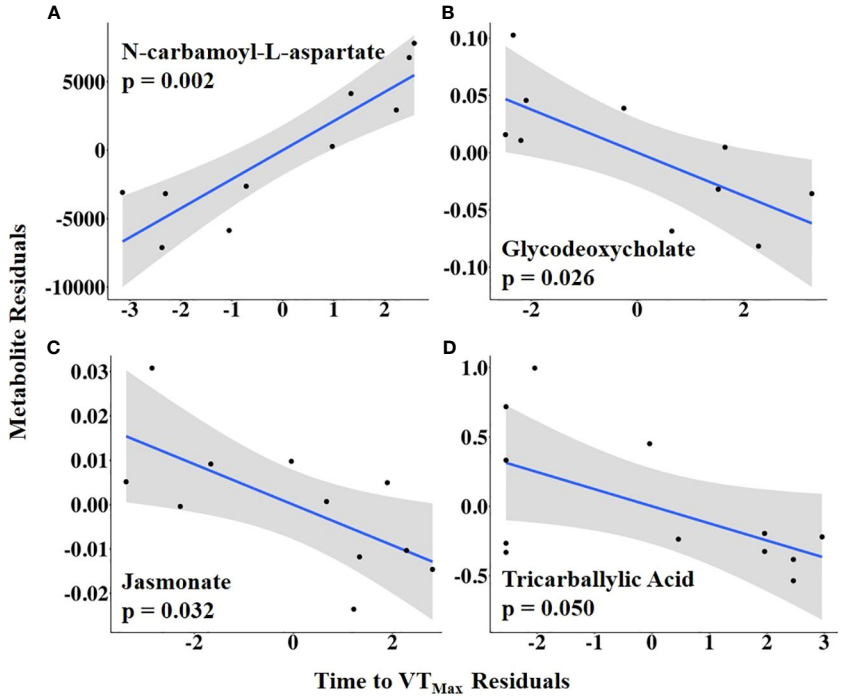

FIGURE 9
(A–D) Partial regression plots for the final model for each metabolite related to time from first temperature increase to maximum vaginal temperature (VT_{Max}). The plots depict the relationship between the time from the first temperature increase to VT_{Max} and metabolite abundance while adjusting for additional variables included in the final model.

et al., 2022; Read et al., 2022) in addition to affecting subsequent luteal function (Perry et al., 2005) and pregnancy outcome (Lamb et al., 2001; Perry et al., 2005; Atkins et al., 2013).

Regardless of species, sex, or reproductive status, heightened levels of activity for as few as 45 min to 1 hour increase body temperature (Murray and Yeates, 1967; Vajrabukka and Thwaites, 1984; Gleeson, 1998). Estrus-induced or not, resultant increases in body temperature are likely a by-product of increased metabolic activity, increased blood flow, and or muscle strain due to elevated activity (Gleeson, 1998). Higher estrus-associated temperatures in our study fell within a range reported by others (Lewis and Newman, 1984; Redden et al., 1993; Kyle et al., 1998; Fisher et al., 2008), with one cow exceeding 40°C. Although the THI during the final week of our study approached the upper limit of thermoneutral conditions (77 THI for non-lactating Holsteins; Ouellet et al., 2021), the varying levels of HEAT likely reflect those attributable to changes in estrus activity. Increases in vaginal temperature were most notable after a cow first stood to be mounted, which is not surprising when using non-lactating Jersey cows, as they are more thermotolerant (Seath and Miller, 1947; Harris et al., 1960; Muller and Botha, 1993; Lim et al., 2021). In addition, the calculated baseline body temperature for each individual cow fell within the range of normal body temperatures for cattle not experiencing heat stress (Gaalaas, 1945). It is also important to note that estrus onset occurred in the majority of cows when the ambient conditions were thermoneutral.

Although instances of chronic elevations in body temperature because of disease or heat stress are detrimental to reproductive success, short-term acute increases in temperature may in fact be beneficial. At the cellular level, Hoshino (2018) demonstrated that increased oocyte intracellular temperature during maturation may be an indicator of oocyte quality and developmental competence. Fallon (1962) reported rectal temperatures ranging from 98.8°F to 105°F in dairy cows undergoing artificial insemination (AI) the morning (a.m.) after estrus was first observed the preceding afternoon (p.m.). In this otherwise synchronized set of females, cows with rectal temperatures ranging from 101.7°F to 105.0°F had higher fertility (73.5%) than those with lower rectal temperatures (98.8°F to 101.6°F). Fallon speculated that cows with a lower rectal temperature may have been out of estrus or were too close to ovulation when AI was performed. However, because the pregnancy outcomes (60.2%) in the cows with a lower rectal temperature were similar to those in other reported cow groupings observed in estrus and bred at different times, it is also plausible that HEAT was functionally relevant and impactful. The positive benefits of elevated body temperature are not limited to dairy cattle. Recently, our laboratory reported that a higher rectal temperature at AI in beef cattle subjected to a fixed-time AI protocol was related to a higher likelihood of pregnancy (Liles et al., 2022).

Nonetheless, for HEAT-related changes to be related to estrus activity, Laitano et al. (2010) reported that whole-body heat stress-induced oxidative stress in humans. When hyperthermia was

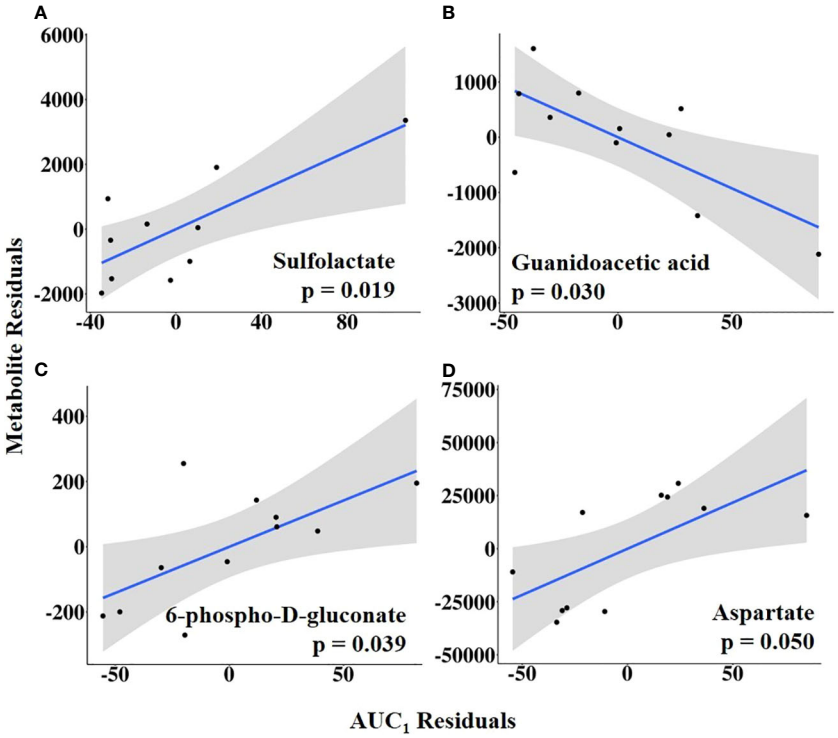

FIGURE 10
(A–D) Partial regression plots for the final model for each metabolite related to the area under the curve from the first increase to the maximum vaginal temperature (AUC_1). The plots depict the relationship between AUC_1 and metabolite abundance while adjusting for additional variables included in the final model.

combined with moderate-intensity exercise, however, a parallel increase in antioxidant defense compensated for hyperthermia-induced oxidative stress. Laitano et al. (2010) further speculated that elevated body temperature in combination with exercise likely enhances antioxidant defense by avoiding redox imbalance, thereby preventing cellular damage. Antioxidants are essential components within mammals, as they maintain oxidative homeostasis within the body (Mulla et al., 2018). Glutathione, an important antioxidant, is a major component of animal cells (Wu et al., 2004) and has properties that have been deemed essential to successful reproduction through maintaining reactive oxygen species levels (ROS; De Matos et al., 1997; Edwards et al., 2001; Zuelke et al., 2003).

Pertaining to our study, HEAT was positively related to different glutathione precursors (cysteine and glycine). Interestingly, cysteine alleviates the negative consequences of prolonged exposure of bovine oocytes to elevated temperature through the stimulation of glutathione production (De Matos et al., 1996; Luberda, 2005; Nabenishi et al., 2012). Glutathione levels fluctuate throughout the estrous cycle, with the highest concentrations at or around meiotic maturation (Sutovsky and Schatten, 1997; Brad et al., 2003; Zuelke et al., 2003). Not only is glutathione involved in events related to meiotic maturation and subsequent development, but its levels have also been linked to thermal responses. When a glutathione inhibitor was administered, the thermotolerance of various cell types decreased (Mitchell et al., 1983; Russo et al., 1984; Harris et al., 1991). Given that cold stress depletes glutathione levels and the inhibition of glutathione results in decreased thermotolerance, metabolite abundance changes associated with HEATs are more likely the result of a combination of activity-induced elevations in temperature.

Serine was the only metabolite that had a negative association with vaginal temperature at the onset of estrus when expressed as a change from the baseline. This metabolite is a non-essential amino acid that serves as a precursor for numerous molecules, including glutathione, taurine, and cysteine (Kalhan and Hanson, 2012). Turathum et al. (2021) suggested that oxidative stress is managed during oocyte maturation through the utilization of serine for glutathione synthesis within the developing oocyte. In mice, serine uptake within the oocyte reaches its maximum during the latter stages of metaphase I and then rapidly decreases once the oocyte reaches metaphase II (Zhang et al., 2020). Given its role in mediating ROS accumulation in the maturing oocyte and that elevated temperatures are known to promote ROS production, in retrospect, it is not surprising that HEAT may be negatively related to serine abundance in the follicular fluid of the preovulatory follicle.

The increased bioavailability of other metabolites highlights other potential HEAT-related consequences on intrafollicular metabolism important to support oocyte maturation and maintain oxidative balance. The amino acid taurine was positively associated with the vaginal temperature at estrus onset when

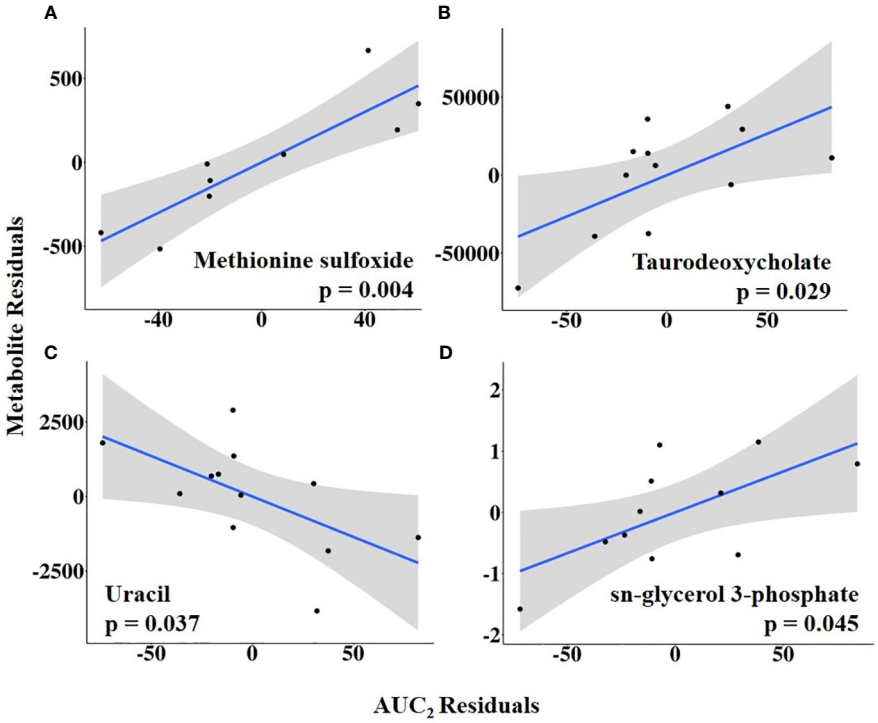

FIGURE 11
(A–D) Partial regression plots for the final model for each metabolite related to area under the curve from the first temperature increase to 10 h post-estrus onset, or the completion of the temperature curve (AUC_2). The plots depict the relationship between AUC_2 and metabolite abundance while adjusting for additional variables included in the final model.

expressed as a change from the baseline. Taurine is present in many mammalian tissues and is involved in numerous cellular functions. Specifically, it is a cytoprotective molecule with antioxidant properties that is also thought to be involved in the thermoregulatory process (Schaffer and Kim, 2018; Page et al., 2019). Toward this end, when humans engaged in intense exercise, the oral administration of taurine resulted in increased exercise endurance and temperature regulation in hotter environments (Page et al., 2019). While the impacts of taurine supplementation before the LH surge and during oocyte maturation are not clear, it is interesting to note that taurine positively impacts bovine embryo development under thermoneutral conditions (Dumoulin et al., 1992; Takahashi and Kanagawa, 1998).

The generation of heat is a natural and normal byproduct of cellular function and processes (Holtzclaw, 2001). In our study, during times of elevated body temperature, three pyrimidines (i.e., cytidine, uridine, and uracil) that have been implicated to play a role in body temperature increases (Cradock et al., 1986; Peters et al., 1987b) were detected in preovulatory follicular fluid. One of these metabolites (uracil) was HEAT-related. Notably, the administration of uracil's precursor, uridine, has been shown to induce hyperthermia in rabbits, mice, and humans (Cradock et al., 1986; Peters et al., 1987b). Because uridine's effect on body temperature is delayed, it has been postulated that uridine's catabolites may be responsible for the induction of hyperthermia (Peters et al., 1987a; Peters et al., 1987b). The administration of uracil to rabbits increased their body temperature by 0.3°C (Peters et al., 1987b). The uracil levels in the follicular fluid collected ~ 14 h after estrus onset were negatively related to the vaginal temperature at first mount when expressed as change from the baseline, maximum vaginal temperature change from the baseline (VT_{Max}), and AUC_2, representing a combination of temperature increase and duration. These findings, while still unclear, are the first that we are aware of that associate pyrimidine metabolites with HEAT.

In instances of HEAT, it is not surprising for thermoregulatory and other processes to be impacted as the body strives for homeostasis during bouts of hyperthermia (reviewed by Godyń et al., 2019). The change in vaginal temperature at VT_{Max} was also positively related to follicular fluid uric acid levels. Although the significance of these findings in estrus-active females remains unclear, it is interesting to note that increases in exercise intensity in both horses and humans increase plasma uric acid levels (Green and Fraser, 1988; Räsänen et al., 1996). In humans, uric acid may in certain instances act as an antioxidant through its reduction of exercise-induced oxidative stress (Waring et al., 2003).

Regardless of related or contributive factors, the consequences of elevated body temperature are largely systemic in nature (Finch, 1986; Hahn, 1999). Whether HEAT-related differences in metabolite abundance in the follicular fluid of the preovulatory follicle ~14 h after estrus onset are reflective of changes occurring in the circulation or altered function of cells comprising the preovulatory follicle (i.e., granulosa and or cumulus–oocyte complex) remains unclear. Toward having a potential impact or a putative role, granulosa cells, which are contributors to follicular

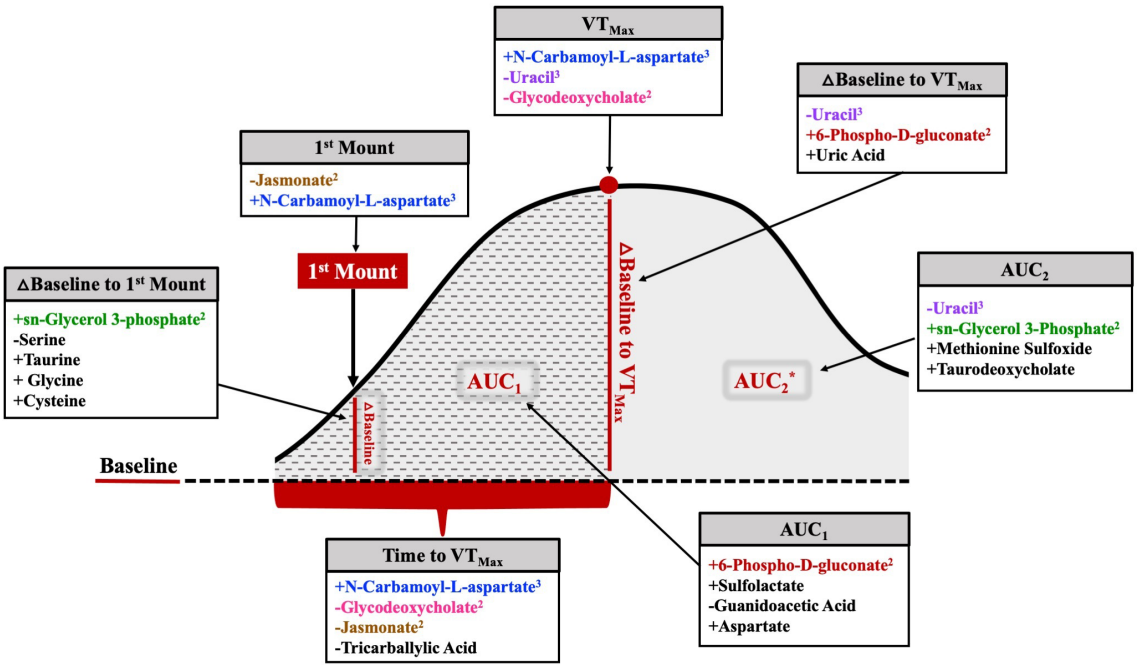

FIGURE 12
Comprehensive figure depicting metabolites related to each HEAT variable of interest. The metabolites listed in color were related to at least one other temperature variable. The metabolites listed in black were solely related to a specific temperature variable. Positive or negative relationships between metabolite abundance and each variable are depicted by the symbol preceding the metabolite name. Superscript following metabolite name denotes the number of HEAT variables to which the metabolite was significantly related. △=change; *AUC_2 includes AUC_1 area and remaining solid gray shaded area.

fluid components, have been shown to increase metabolism and amino acid production approximately 6 h after the LH surge (Gilbert et al., 2011).

To our knowledge, this is the first study to investigate the relationship between estrus-induced changes in body temperature and preovulatory follicular fluid metabolites. The significant outcomes related to temperature changes at or around the time of estrus onset are suggestive of a functional relevance of HEAT in driving the preparatory mechanisms involved in thermoregulation, energy metabolism, and oxidative stress management, and, in turn, possibly impacting oocyte competence and other preovulatory follicle components.

Although outside the scope of this study, it is interesting to note that the best-fit models derived to assess the impact of different aspects of HEAT on follicular fluid metabolomes included, in some instances, covariates related to estradiol and follicle size (see Supplementary Tables 4–6). We are only aware of one other study examining follicular fluid metabolomics in estrual cattle (Hessock et al., 2023), but its authors did not relate their findings to hormone levels or follicle size. In non-estrual cows, metabolites in preovulatory follicular fluid have been reported (Bender et al., 2010; Read et al., 2021; Read et al., 2022). Although estradiol concentration and follicle diameter have been found to be related to a number of follicular fluid metabolites (Read et al., 2021; Read et al., 2022), these findings do not overlap with those in this study. This is not entirely unexpected due to the dynamic changes occurring in the follicle around estrus and the inherent impact of those changes on systemic hormones.

Data availability statement

The original contributions presented in the study are included in the article/Supplementary Material. Further inquiries can be directed to the corresponding authors.

Ethics statement

The animal study was approved by Institutional Animal Care and Use Committee at the University of Tennessee, Knoxville. The study was conducted in accordance with the local legislation and institutional requirements.

Author contributions

Conception and design of study: JE, SM, and FS. Investigation/methodology: AP, EH, JE, SM, JK, RP, FS, and SC. Data and statistical analyses: AP, SM, JE, and RP. Writing—original draft, review, and editing: AP, JE, and SM. Review and editing: RP, EH, JK, FS, and SC. All authors contributed to the article and approved the submitted version.

Funding

This project was supported by Agriculture and Food Research Initiative (competitive grant no. 2022-67015-36374) (project director: JE) from the USDA National Institute of Food and Agriculture, USDA Multistate project NE2227, and The University of Tennessee AgResearch, and the Department of Animal Science.

Acknowledgments

We would like to thank The University of Tennessee Middle Tennessee AgResearch and Education Center (MTREC) for providing the animals and for its assistance with conducting the study (Kevin Thompson, Wes Gilliam, David Johnson, Nolan Rinks, and other MTREC staff). We are also thankful for the research support provided by Zoetis (Drs. Fernando DiCroce and Richard Wallace). In addition, we greatly appreciate Courtney Christopher, Hector Castro, and Sara Howard for processing the UHPLC-HRMS metabolomics data. Appreciation is also extended to Megan Mills, Jake Watts, Claire Hunkler, Samantha Roberts, Casey Read, Pablo Fioravanti, and Ian Batey for their assistance with sample collection or data analysis. We would also like to thank Michael O'Neil, Julia Zhu, and Josh Price at The University of Tennessee, Knoxville Office of Integrated Technologies-Research Computing Support, for their advice on statistical analysis and figure preparation.

Conflict of interest

The authors declare that the research was conducted in the absence of any commercial or financial relationships that could be construed as a potential conflict of interest.

Publisher's note

Supplementary material

The Supplementary Material for this article can be found online at: https://www.frontiersin.org/articles/10.3389/fanim.2023.1241033/full#supplementary-material

References

Abbott, C. R., Saxton, A. M., Rispoli, L. A., Payton, R. R., Pohler, K. G., Schrick, F. N., et al. (2018). An in *vivo* model to assess the thermoregulatory response of lactating Holsteins to an acute heat stress event occurring after a pharmacologically-induced LH surge. *J. Therm. Biol.* 78, 247–256. doi: 10.1016/j.jtherbio.2018.10.003

Atkins, J. A., Smith, M. F., Macneil, M. D., Jinks, E. M., Abreu, F. M., Alexander, L. J., et al. (2013). Pregnancy establishment and maintenance in cattle. *J. Anim. Sci.* 91, 722–733. doi: 10.2527/jas.2012-5368

Bedard, K., Szabo, E., Michalak, M., and Opas, M. (2005). Cellular functions of endoplasmic reticulum chaperones calreticulin, calnexin, and ERp57. *Int. Rev. Cytol.* 245, 91–121. doi: 10.1016/s0074-7696(05)45004-4

Bender, K., Walsh, S., Evans, A. C., Fair, T., and Brennan, L. (2010). Metabolite concentrations in follicular fluid may explain differences in fertility between heifers and lactating cows. *Reproduction* 139 (6), 1047–1055. doi: 10.1530/REP-10-0068

Brad, A., Bormann, C., Swain, J., Durkin, R., Johnson, A., Clifford, A., et al. (2003). Glutathione and adenosine triphosphate content of in *vivo* and in *vitro* matured porcine oocytes. *Mol. Reprod. Dev.* 64, 492–498. doi: 10.1002/mrd.10254

Burdick, N., Carroll, J., Dailey, J., Randel, R., Falkenberg, S., and Schmidt, T. (2012). Development of a self-contained, indwelling vaginal temperature probe for use in cattle research. *J. Therm. Biol.* 37, 339–343. doi: 10.1016/j.jtherbio.2011.10.007

Clapper, J., Ottobre, J., Ottobre, A., and Zartman, D. (1990). Estrual rise in body temperature in the bovine I. Temporal relationships with serum patterns of reproductive hormones. *Anim. Reprod. Sci.* 23, 89–98. doi: 10.1016/0378-4320(90)90051-G

Cradock, J., Vishnuvajjala, B., Chin, T., Hochstein, H., and Ackerman, S. (1986). Uridine-induced hyperthermia in the rabbit. *J. Pharm. Pharmacol.* 38, 226–229. doi: 10.1111/j.2042-7158.1986.tb04552.x

De Matos, D., Furnus, C., Moses, D., Martinez, A., and Matkovic, M. (1996). Stimulation of glutathione synthesis of in *vitro* matured bovine oocytes and its effect on embryo development and freezability. *Mol. Reprod. Dev.* 45, 451–457. doi: 10.1002/(SICI)1098-2795(199612)45:4<451::AID-MRD7>3.0.CO;2-Q

De Matos, D. G., Furnus, C. C., and Moses, D. F. (1997). Glutathione synthesis during in *vitro* maturation of bovine oocytes: role of cumulus cells. *Biol. Reprod.* 57, 1420–1425. doi: 10.1095/biolreprod57.6.1420

Diskin, M. G., and Sreenan, J. M. (2000). Expression and detection of oestrus in cattle. *Reprod. Nutr. Dev.* 40, 481–491. doi: 10.1051/rnd:2000112

Duggavathi, R., and Murphy, B. D. (2009). Ovulation signals. *Science* 324, 890–891. doi: 10.1126/science.1174130

Dumoulin, J., Evers, J., Bras, M., Pieters, M., and Geraedts, J. (1992). Positive effect of taurine on preimplantation development of mouse embryos. *vitro. Reprod.* 94, 373–380. doi: 10.1530/jrf.0.0940373

Edwards, J., King, W., Kawarsky, S., and Ealy, A. (2001). Responsiveness of early embryos to environmental insults: potential protective roles of HSP70 and glutathione. *Theriogenology* 55, 209–223. doi: 10.1016/s0093-691x(00)00455-6

Edwards, J., Saxton, A., Lawrence, J., Payton, R., and Dunlap, J. (2005). Exposure to a physiologically relevant elevated temperature hastens in *vitro* maturation in bovine oocytes. *J. Dairy Sci.* 88, 4326–4333. doi: 10.3168/jds.s0022-0302(05)73119-2

Fallon, G. (1962). Body temperature and fertilization in the cow. *J. Reprod. Fertil.* 3, 116–123. doi: 10.1530/jrf.0.0030116

Finch, V. A. (1986). Body temperature in beef cattle: Its control and relevance to production in the tropics. *J. Anim. Sci.* 62, 531–542. doi: 10.2527/jas1986.622531x

Fisher, A., Morton, R., Dempsey, J., Henshall, J., and Hill, J. (2008). Evaluation of a new approach for the estimation of the time of the LH surge in dairy cows using vaginal temperature and electrodeless conductivity measurements. *Theriogenology* 70, 1065–1074. doi: 10.1016/j.theriogenology.2008.06.023

Gaalaas, R. (1945). Effect of atmospheric temperature on body temperature and respiration rate of Jersey cattle. *J. Dairy Sci.* 28, 555–563. doi: 10.3168/jds.S0022-0302(45)95208-8

Gilbert, I., Robert, C., Dieleman, S., Blondin, P., and Sirard, M. (2011). Transcriptional effect of the LH surge in bovine granulosa cells during the peri-ovulation period. *Reproduction* 141, 193–205. doi: 10.1530/rep-10-0381

Ginther, O. J., Pinaffi, F. L. V., Khan, F. A., Duarte, L. F., and Beg, M. A. (2013). Follicular-phase concentrations of progesterone, estradiol-17β, LH, FSH, and a PGF2α metabolite and daily clustering of prolactin pulses, based on hourly blood sampling and hourly detection of ovulation in heifers. *Theriogenology* 79, 918–928. doi: 10.1016/j.theriogenology.2012.12.015

Gleeson, M. (1998). Temperature regulation during exercise. *Int. J. Sports Med.* 19, S96–S99. doi: 10.1055/s-2007-971967

Godyń, D., Herbut, P., and Angrecka, S. (2019). Measurements of peripheral and deep body temperature in cattle – A review. *J. Therm. Biol.* 79, 42–49. doi: 10.1016/j.jtherbio.2018.11.011

Green, H. J., and Fraser, I. (1988). Differential effects of exercise intensity on serum uric acid concentration. *Med. Sci. Sports Exerc.* 20, 55–59. doi: 10.1249/00005768-198802000-00008

Greene, E., Cauble, R., Dhamad, A. E., Kidd, M. T., Kong, B., Howard, S. M., et al. (2020). Muscle metabolome profiles in woody breast-(un) affected broilers: effects of quantum blue phytase-enriched diet. *Front. Vet. Sci.* 7. doi: 10.3389/fvets.2020.00458

Hahn, G. L. (1999). Dynamic responses of cattle to thermal heat loads. *J. Anim. Sci.* 77, 10–20. doi: 10.2527/1997.77suppl_210x

Harris, C., Juchau, M. R., and Mirkes, P. E. (1991). Role of glutathione and Hsp 70 in the acquisition of thermotolerance in postimplantation rat embryos. *Teratology* 43, 229–239. doi: 10.1002/tera.1420430307

Harris, D., Shrode, R., Rupel, I., and Leighton, R. (1960). A study of solar radiation as related to physiological and production responses of lactating Holstein and Jersey cows. *J. Dairy Sci.* 43, 1255–1262. doi: 10.3168/jds.S0022-0302(60)90312-X

Hellberg, P., Larson, L., Olofsson, J., Hedin, L., and Brännström, M. (1991). Stimulatory effects of bradykinin on the ovulatory process in the in *vitro*-perfused rat ovary. *Biol. Reprod.* 44, 269–274. doi: 10.1095/biolreprod44.2.269

Hessock, E. A., Edwards, J. L., Schrick, F. N., Payton, R. R., Campagna, S. R., Pollock, A. B., et al. (2023). Metabolite abundance in bovine preovulatory follicular fluid is influenced by follicle developmental progression post estrous onset in cattle. *Front. Cell Dev. Biol.* 11. doi: 10.3389/fcell.2023.1156060

Holtzclaw, B. J. (2001). Circadian rhythmicity and homeostatic stability in thermoregulation. *Biol. Res. Nurs.* 2, 221–235. doi: 10.1177/109980040100200402

Hooper, L. M., Payton, R. R., Rispoli, L. A., Saxton, A. M., and Edwards, J. L. (2015). Impact of heat stress on germinal vesicle breakdown and lipolytic changes during in *vitro* maturation of bovine oocytes. *J. Repod. Dev.* 61, 459–464. doi: 10.1262/jrd.2014-168

Horn, E. J., Read, C. C., Edwards, J. L., Schrick, F. N., Rhinehart, J. D., Payton, R. R., et al. (2022). Preovulatory follicular fluid and serum metabolome profiles in lactating beef cows with thin, moderate, and obese body condition. *J. Anim. Sci.* 100, skac152. doi: 10.1093/jas/skac152

Hoshino, Y. (2018). Updating the markers for oocyte quality evaluation: intracellular temperature as a new index. *Reprod. Med. Biol.* 17, 434–441. doi: 10.1002/rmb2.12245

Jinks, E. M., Smith, M. F., Atkins, J. A., Pohler, K. G., Perry, G. A., Macneil, M. D., et al. (2013). Preovulatory estradiol and the establishment and maintenance of pregnancy in suckled beef cows. *J. Anim. Sci.* 91, 1176–1185. doi: 10.2527/jas.2012-5611

Kalhan, S. C., and Hanson, R. W. (2012). Resurgence of serine: an often neglected but indispensable amino Acid. *J. Biol. Chem.* 287, 19786–19791. doi: 10.1074/jbc.R112.357194

Kerbrat, S., and Disenhaus, C. (2004). A proposition for an updated behavioural characterisation of the oestrus period in dairy cows. *Appl. Anim. Behav. Sci.* 87, 223–238. doi: 10.1016/j.applanim.2003.12.001

Kiddy, C. A. (1977). Variation in physical activity as an indication of estrus in dairy cows. *J. Dairy Sci.* 60, 235–243. doi: 10.3168/jds.s0022-0302(77)83859-9

Kirby, C. J., Smith, M. F., Keisler, D. H., and Lucy, M. C. (1997). Follicular function in lactating dairy cows treated with sustained-release bovine somatotropin. *J. Dairy Sci.* 80, 273–285. doi: 10.3168/jds.s0022-0302(97)75935-6

Klabnik, J. L., Christenson, L. K., Gunewardena, S. S., Pohler, K. G., Rispoli, L. A., Payton, R. R., et al. (2022). Heat-induced increases in body temperature in lactating dairy cows: impact on the cumulus and granulosa cell transcriptome of the periovulatory follicle. *J. Anim. Sci.* 100, skac121. doi: 10.1093/jas/skac121

Kyle, B. L., Kennedy, A. D., and Small, J. A. (1998). Measurement of vaginal temperature by radiotelemetry for the prediction of estrus in beef cows. *Theriogenology* 49, 1437–1449. doi: 10.1016/S0093-691X(98)00090-9

Laitano, O., Kalsi, K. K., Pook, M., Oliveira, A. R., and González-Alonso, J. (2010). Separate and combined effects of heat stress and exercise on circulatory markers of oxidative stress in euhydrated humans. *Eur. J. Appl. Physiol.* 110, 953–960. doi: 10.1007/s00421-010-1577-5

Lamb, G. C., Stevenson, J. S., Kesler, D. J., Garverick, H. A., Brown, D. R., and Salfen, B. E. (2001). Inclusion of an intravaginal progesterone insert plus GnRH and prostaglandin F2α for ovulation control in postpartum suckled beef cows. *J. Anim. Sci.* 79, 2253–2259. doi: 10.2527/2001.7992253x

Leroy, J., Rizos, D., Sturmey, R., Bossaert, P., Gutierrez-Adan, A., Van Hoeck, V., et al. (2011). Intrafollicular conditions as a major link between maternal metabolism and oocyte quality: a focus on dairy cow fertility. *Reprod. Fertil. Dev.* 24, 1–12. doi: 10.1071/rd11901

Lewis, G. S., and Newman, S. K. (1984). Changes throughout estrous cycles of variables that might indicate estrus in dairy cows. *J. Dairy Sci.* 67, 146–152. doi: 10.3168/jds.S0022-0302(84)81278-3

Liao, Y., Hu, R., Wang, Z., Peng, Q., Dong, X., Zhang, X., et al. (2018). Metabolomics profiling of serum and urine in three beef cattle breeds revealed different levels of tolerance to heat stress. *J. Agric. Food Chem.* 66, 6926–6935. doi: 10.1021/acs.jafc.8b01794

Liles, H. L., Schneider, L. G., Pohler, K. G., Oliveira Filho, R. V., Schrick, F. N., Payton, R. R., et al. (2022). Positive relationship of rectal temperature at fixed timed artificial insemination on pregnancy outcomes in beef cattle. *J. Anim. Sci.* 100, skac100. doi: 10.1093/jas/skac100

Lim, D. H., Kim, T. I., Park, S. M., Ki, K. S., and Kim, Y. (2021). Evaluation of heat stress responses in Holstein and Jersey cows by analyzing physiological characteristics and milk production in Korea. *J. Anim. Sci. Technol.* 63, 872. doi: 10.5187/jast.2021.e62

López-Gatius, F., Santolaria, P., Mundet, I., and Yániz, J. (2005). Walking activity at estrus and subsequent fertility in dairy cows. *Theriogenology* 63, 1419–1429. doi: 10.1016/j.theriogenology.2004.07.007

Luberda, Z. (2005). The role of glutathione in mammalian gametes. *Reprod. Biol.* 5, 5–17.

Lyimo, Z., Nielen, M., Ouweltjes, W., Kruip, T., and Van Eerdenburg, F. (2000). Relationship among estradiol, cortisol and intensity of estrous behavior in dairy cattle. *Theriogenology* 53, 1783–1795. doi: 10.1016/s0093-691x(00)00314-9

Madureira, A. M. L., Polsky, L. B., Burnett, T. A., Silper, B. F., Soriano, S., Sica, A. F., et al. (2019). Intensity of estrus following an estradiol-progesterone-based ovulation synchronization protocol influences fertility outcomes. *J. Dairy Sci.* 102, 3598–3608. doi: 10.3168/jds.2018-15129

Madureira, A. M. L., Silper, B. F., Burnett, T. A., Polsky, L., Cruppe, L. H., Veira, D. M., et al. (2015). Factors affecting expression of estrus measured by activity monitors and conception risk of lactating dairy cows. *J. Dairy Sci.* 98, 7003–7014. doi: 10.3168/jds.2015-9672

Malhi, P. S., Adams, G. P., and Singh, J. (2005). Bovine model for the study of reproductive aging in women: follicular, luteal, and endocrine characteristics. *Biol. Reprod.* 73, 45–53. doi: 10.1095/biolreprod.104.038745

Mitchell, J. B., Russo, A., Kinsella, T. J., and Glatstein, E. (1983). Glutathione elevation during thermotolerance induction and thermosensitization by glutathione depletion. *Cancer Res.* 43, 987–991.

Miura, R., Yoshioka, K., Miyamoto, T., Nogami, H., Okada, H., and Itoh, T. (2017). Estrous detection by monitoring ventral tail base surface temperature using a wearable wireless sensor in cattle. *Anim. Reprod. Sci.* 180, 50–57. doi: 10.1016/j.anireprosci.2017.03.002

Moorey, S. E., Hessock, E. A., and Edwards, J. L. (2022). Preovulatory follicle contributions to oocyte competence in cattle: importance of the ever-evolving intrafollicular environment leading up to the luteinizing hormone surge. *J. Anim. Sci.* 100, skac153. doi: 10.1093/jas/skac153

Mulla, A. A., Fazari, A., Elkhouly, M., and Moghaddam, N. (2018). Role of antioxidants in female fertility. *Open J. Obstet. Gynecol.* 8, 85–91. doi: 10.4236/ojog.2018.82011

Muller, C., and Botha, J. (1993). Effect of summer climatic conditions on different heat tolerance indicators in primiparous Friesian and Jersey cows. *S. Afr. J. Anim. Sci.* 23, 98–103.

Murray, D. M., and Yeates, N. T. M. (1967). Walking trials with cattle II. A comparison of bulls, steers and heifers. *J. Agric. Sci.* 69, 71–78. doi: 10.1017/S0021859600016476

Nabenishi, H., Ohta, H., Nishimoto, T., Morita, T., Ashizawa, K., and Tsuzuki, Y. (2012). The effects of cysteine addition during in *vitro* maturation on the developmental competence, ROS, GSH and apoptosis level of bovine oocytes exposed to heat stress. *Zygote* 20, 249–259. doi: 10.1017/S0967199411000220

Ouellet, V., Toledo, I. M., Dado-Senn, B., Dahl, G. E., and Laporta, J. (2021). Critical temperature-humidity index thresholds for dry cows in a subtropical climate. *Front. Anim. Sci.* 2. doi: 10.3389/fanim.2021.706636

Page, L. K., Jeffries, O., and Waldron, M. (2019). Acute taurine supplementation enhances thermoregulation and endurance cycling performance in the heat. *Eur. J. Sport Sci.* 19, 1101–1109. doi: 10.1080/17461391.2019.1578417

Perry, G. A., Smith, M. F., Lucy, M. C., Green, J. A., Parks, T. E., Macneil, M. D., et al. (2005). Relationship between follicle size at insemination and pregnancy success. *Proc. Natl. Acad. Sci. U.S.A.* 102, 5268–5273. doi: 10.1073/pnas.0501700102

Peters, G. J., Van Groeningen, C. J., Laurensse, E., Kraal, I., Leyva, A., Lankelma, J., et al. (1987b). Effect of pyrimidine nucleosides on body temperatures of man and rabbit in relation to pharmacokinetic data. *Pharm. Res.* 4, 113–119. doi: 10.1023/a:1016410817898

Peters, G., Van Groeningen, C., Laurensse, E., Lankelma, J., Leyva, A., and Pinedo, H. (1987a). Uridine-induced hypothermia in mice and rats in relation to plasma and tissue levels of uridine and its metabolites. *Cancer Chemother. Pharmacol.* 20, 101–108. doi: 10.1007/BF00253962

Piccione, G., Caola, G., and Refinetti, R. (2003). Daily and estrous rhythmicity of body temperature in domestic cattle. *BMC Physiol.* 3, 7. doi: 10.1186/1472-6793-3-7

Pruessner, J. C., Kirschbaum, C., Meinlschmid, G., and Hellhammer, D. H. (2003). Two formulas for computation of the area under the curve represent measures of total hormone concentration versus time-dependent change. *Psychoneuroendocrinology* 28, 916–931. doi: 10.1016/s0306-4530(02)00108-7

Randi, F., Mcdonald, M., Duffy, P., Kelly, A. K., and Lonergan, P. (2018). The relationship between external auditory canal temperature and onset of estrus and ovulation in beef heifers. *Theriogenology* 110, 175–181. doi: 10.1016/j.theriogenology.2018.01.001

Räsänen, L. A., Wiitanen, P. A., Lilius, E. M., Hyyppä, S., and Pösö, A. R. (1996). Accumulation of uric acid in plasma after repeated bouts of exercise in the horse. *Comp. Biochem. Physiol. B Biochem. Mol. Biol.* 114, 139–144. doi: 10.1016/0305-0491(96)00022-3

Read, C. C., Edwards, L., Schrick, N., Rhinehart, J. D., Payton, R. R., Campagna, S. R., et al. (2021). Correlation between pre-ovulatory follicle diameter and follicular fluid metabolome profiles in lactating beef cows. *Metabolites* 11, 623. doi: 10.3390/metabo11090623

Read, C. C., Edwards, J. L., Schrick, F. N., Rhinehart, J. D., Payton, R. R., Campagna, S. R., et al. (2022). Preovulatory serum estradiol concentration is positively associated with oocyte ATP and follicular fluid metabolite abundance in lactating beef cattle. *J. Anim. Sci.* 100, skac136. doi: 10.1093/jas/skac136

Redden, K. D., Kennedy, A. D., Ingalls, J. R., and Gilson, T. L. (1993). Detection of estrus by radiotelemetric monitoring of vaginal and ear skin temperature and pedometer measurements of activity. *J. Dairy Sci.* 76, 713–721. doi: 10.3168/jds.S0022-0302(93)77394-

Rispoli, L. A., Edwards, J. L., Pohler, K. G., Russell, S., Somiari, R. I., Payton, R. R., et al. (2019). Heat-induced hyperthermia impacts the follicular fluid proteome of the periovulatory follicle in lactating dairy cows. *PloS One* 14, e0227095. doi: 10.1371/journal.pone.0227095

Rowinski, J. R., Rispoli, L. A., Payton, R. R., Schneider, L. G., Schrick, F. N., Mclean, K. J., et al. (2021). Impact of an acute heat shock during in *vitro* maturation on interleukin 6 and its associated receptor component transcripts in bovine cumulus-oocyte complexes. *Anim. Reprod.* 17, e20200221. doi: 10.1590/1984-3143-ar2020-0221

Russo, A., Mitchell, J., and Mcpherson, S. (1984). The effects of glutathione depletion on thermotolerance and heat stress protein synthesis. *Br. J. Cancer* 49, 753–758. doi: 10.1038/bjc.1984.118

Sakatani, M., Takahashi, M., and Takenouchi, N. (2016). The efficiency of vaginal temperature measurement for detection of estrus in Japanese Black cows. *J. Repod. Dev.* 62, 201–207. doi: 10.1262/jrd.2015-095

Saumande, J., and Humblot, P. (2005). The variability in the interval between estrus and ovulation in cattle and its determinants. *Anim. Reprod. Sci.* 85, 171–182. doi: 10.1016/j.anireprosci.2003.09.009

Schaffer, S., and Kim, H. W. (2018). Effects and mechanisms of taurine as a therapeutic agent. *Biolmol. Ther.* 26, 225. doi: 10.4062/biomolther.2017.251

Seath, D., and Miller, G. (1947). Heat tolerance comparisons between Jersey and Holstein cows. *J. Anim. Sci.* 6, 24–34. doi: 10.2527/jas1947.6124

Sirard, M. A. (2011). Follicle environment and quality of in *vitro* matured oocytes. *J. Assist. Reprod. Genet.* 28, 483–488. doi: 10.1007/s10815-011-9554-4

Smith, M. F., Mcintush, E. W., and Smith, G. W. (1994). Mechanisms associated with corpus luteum development. *J. Anim. Sci.* 72, 1857–1872. doi: 10.2527/1994.7271857x

Stumpf, T. T., Wolfe, M. W., Day, M. L., Stotts, J. A., Wolfe, P. L., Kittok, R. J., et al. (1991). Effect of 17β-estradiol on the preovulatory surge of LH in the bovine female. *Theriogenology* 36, 201–207. doi: 10.1016/0093-691X(91)90379-R

Suthar, V., Burfeind, O., Patel, J., Dhami, A., and Heuwieser, W. (2011). Body temperature around induced estrus in dairy cows. *J. Dairy Sci.* 94, 2368–2373. doi: 10.3168/jds.2010-3858

Sutovsky, P., and Schatten, G. (1997). Depletion of glutathione during bovine oocyte maturation reversibly blocks the decondensation of the male pronucleus and pronuclear apposition during fertilization. *Biol. Reprod.* 56, 1503–1512. doi: 10.1095/biolreprod56.6.1503

Sveberg, G., Refsdal, A., Erhard, H., Kommisrud, E., Aldrin, M., Tvete, I., et al. (2013). Sexually active groups in cattle—a novel estrus sign. *J. Dairy Sci.* 96, 4375–4386. doi: 10.3168/jds.2012-6407

Takahashi, Y., and Kanagawa, H. (1998). Effects of glutamine, glycine and taurine on the development of in *vitro* fertilized bovine zygotes in a chemically defined medium. *J. Vet. Med.* 60, 433–437. doi: 10.1292/jvms.60.433

Tippenhauer, C., Plenio, J., Heuwieser, W., and Borchardt, S. (2023). Association of activity and subsequent fertility of dairy cows after spontaneous estrus or timed artificial insemination. *J. Dairy Sci.* 106, 4291–4305. doi: 10.3168/jds.2022-22057

Tokuhiro, K., Satouh, Y., Nozawa, K., Isotani, A., Fujihara, Y., Hirashima, Y., et al. (2015). Calreticulin is required for development of the cumulus oocyte complex and female fertility. *Sci. Rep.* 5, 1–10. doi: 10.1038/srep14254

Tsafriri, A., Bicsak, T. A., Cajander, S. B., Ny, T., and Hsueh, A. J. W. (1989). Suppression of ovulation rate by antibodies to tissue-type plasminogen activator and α2-antiplasmin. *Endocrinology* 124, 415–421. doi: 10.1210/endo-124-1-415

Turathum, B., Gao, E., and Chian, R. (2021). The function of cumulus cells in oocyte growth and maturation and in subsequent ovulation and fertilization. *Cells* 10, 2292. doi: 10.3390/cells10092292

Vajrabukka, C., and Thwaites, C. (1984). The relative influences of exercise and coat-type on the thermoregulatory responses of cattle. *Int. J. Biometeorol.* 28, 9–15. doi: 10.1007/BF02193509

Waring, W., Convery, A., Mishra, V., Shenkin, A., Webb, D. J., and Maxwell, S. (2003). Uric acid reduces exercise-induced oxidative stress in healthy adults. *Clin. Sci.* 105, 425–430. doi: 10.1042/CS20030149

Wu, G., Lupton, J. R., Turner, N. D., Fang, Y. Z., and Yang, S. (2004). Glutathione metabolism and its implications for health. *J. Nutr.* 134, 489–492. doi: 10.1093/jn/134.3.489

Yoshimura, Y., Espey, L., Hosoi, Y., Adachi, T., Atlas, S., Ghodgaonkar, R., et al. (1988). The effects of bradykinin on ovulation and prostaglandin production by the perfused rabbit ovary. *Endocrinology* 122, 2540–2546. doi: 10.1210/endo-122-6-2540

Yue, S., Ding, S., Zhou, J., Yang, C., Hu, X., Zhao, X., et al. (2020). Metabolomics approach explore diagnostic biomarkers and metabolic changes in heat-stressed dairy cows. *Animals* 10, 1741. doi: 10.3390/ani10101741

Zhang, H., Mcclatchie, T., and Baltz, J. M. (2020). L-Serine transport in growing and maturing mouse oocytes. *J. Cell. Physiol.* 235, 8585–8600. doi: 10.1002/jcp.29702

Zuelke, K. A., Jeffay, S. C., Zucker, R. M., and Perreault, S. D. (2003). Glutathione (GSH) concentrations vary with the cell cycle in maturing hamster oocytes, zygotes, and pre-implantation stage embryos. *Mol. Reprod. Dev.* 64, 106–112. doi: 10.1002/mrd.10214

frontiers | Frontiers in Molecular Biosciences

TYPE Original Research
PUBLISHED 21 May 2024
DOI 10.3389/fmolb.2024.1364637

OPEN ACCESS

EDITED BY
Dagnachew Hailemariam,
University of Alberta, Canada

REVIEWED BY
Shawn R. Campagna,
The University of Tennessee, United States
Vinod Kumar Narayana,
The University of Melbourne, Australia
Elda Dervishi,
University of Alberta, Canada

*CORRESPONDENCE
Karla A. Vasco,
karlitavasco87@gmail.com
Shannon D. Manning,
mannin71@msu.edu

†PRESENT ADDRESSES
Karla A. Vasco,
Michigan Department of Health and Human Services, MI, United States;
Zoe A. Hansen,
Department of Plant Pathology, University of Minnesota, Minneapolis, MN, United States

RECEIVED 02 January 2024
ACCEPTED 29 April 2024
PUBLISHED 21 May 2024

CITATION
Vasco KA, Hansen ZA, Schilmiller AL, Bowcutt B, Carbonell SL, Ruegg PL, Quinn RA, Zhang L and Manning SD (2024), Untargeted metabolomics and metagenomics reveal signatures for intramammary ceftiofur treatment and lactation stage in the cattle hindgut.
Front. Mol. Biosci. 11:1364637.
doi: 10.3389/fmolb.2024.1364637

Untargeted metabolomics and metagenomics reveal signatures for intramammary ceftiofur treatment and lactation stage in the cattle hindgut

Karla A. Vasco[1*†], Zoe A. Hansen[1†], Anthony L. Schilmiller[2], Bailey Bowcutt[1], Samantha L. Carbonell[1], Pamela L. Ruegg[3], Robert A. Quinn[4], Lixin Zhang[1,5] and Shannon D. Manning[1*]

[1]Department of Microbiology, Genetics and Immunology, Michigan State University, East Lansing, MI, United States, [2]Research Technology Support Facility, Mass Spectrometry and Metabolomics Core, Michigan State University, East Lansing, MI, United States, [3]Department of Large Animal and Clinical Sciences, Michigan State University, East Lansing, MI, United States, [4]Department of Biochemistry and Molecular Biology, Michigan State University, East Lansing, MI, United States, [5]Department of Epidemiology and Biostatistics, Michigan State University, East Lansing, MI, United States

The gut microbiota in cattle is essential for protein, energy, and vitamin production and hence, microbiota perturbations can affect cattle performance. This study evaluated the effect of intramammary (IMM) ceftiofur treatment and lactation stage on the functional gut microbiome and metabolome. Forty dairy cows were enrolled at dry-off. Half received IMM ceftiofur and a non-antibiotic teat sealant containing bismuth subnitrate (cases), while the other half received the teat sealant (controls). Fecal samples were collected before treatment at dry off, during the dry period (weeks 1 and 5) and the first week after calving (week 9). Shotgun metagenomic sequencing was applied to predict microbial metabolic pathways whereas untargeted metabolomics was used identify polar and nonpolar metabolites. Compared to controls, long-term changes were observed in the cows given ceftiofur, including a lower abundance of microbial pathways linked to energy production, amino acid biosynthesis, and other vital molecules. The metabolome of treated cows had elevated levels of stachyose, phosphatidylethanolamine diacylglycerol (PE-DAG), and inosine a week after the IMM ceftiofur application, indicating alterations in microbial fermentation, lipid metabolism, energy, and cellular signaling. Differences were also observed by sampling, with cows in late lactation having more diverse metabolic pathways and a unique metabolome containing higher levels of histamine and histamine-producing bacteria. These data illustrate how IMM ceftiofur treatment can alter the functionality of the hindgut metabolome and microbiome. Understanding how antibiotics and lactation stages, which are each characterized by unique diets and physiology, impact the function of resident microbes is critical to define normal gut function in dairy cattle.

KEYWORDS

metabolomics, gut microbiome, antibiotic use, ceftiofur, metagenomics

1 Introduction

The gut microbiota of ruminants produces proteins, vitamins, and ~75% of the energy necessary for the host through an obligatory symbiotic relationship (Bergman, 1990). Rumen microorganisms ferment the plant biomass to generate energy in the form of volatile fatty acids (VFAs) (Bergman, 1990) and convert nitrogen-containing compounds into protein (Bach et al., 2005). Thus, prior studies have sought to determine the relationship between the microbiome composition of cattle and animal production and methane emissions (reviewed by (O'Hara et al., 2020)). Most notably, microbial communities of the gastrointestinal tract were shown to influence the quality and yield of milk production, affecting key components such as fat, protein, and lactose content (Jami et al., 2014; Xu et al., 2017; Buitenhuis et al., 2019; Wu et al., 2021). Consequently, shifts in the microbiome and metabolome can potentially alter milk composition and affect cow health. Although antibiotics are known to cause perturbations in the gut microbiome, little is known about the specific effects of intramammary (IMM) antibiotic treatment on the function of the fecal microbiome in dairy cows.

β-lactam antibiotics such as ceftiofur, a third-generation cephalosporin, are often used in dairy cattle for the treatment of mastitis or dry cow therapy (Hallberg et al., 2006; Campos et al., 2021). When cephalosporins are applied intramammarily, they are mainly excreted through the urine and udder (Wilson and Gilbert, 1986; Rule et al., 1998; Ray et al., 2014). Yet, ~13% of the IMM-administered ceftiofur dose in lactating cows, which includes two doses of 125 mg per quarter given 12 h apart, is detectable in the feces 5–6 days post-treatment (European Agency for the Evaluation of Medicinal Products, 2002). When administered subcutaneously to Holstein steers, ceftiofur active metabolites were shown to alter the microbiota composition of the gut (Foster et al., 2019) due to activity against both Gram-negative and Gram-positive bacteria. Our previous study of Holstein cows given IMM ceftiofur treatment at dry-off also showed an altered abundance of specific taxa in the short and long-term, although no effect was observed on microbiota diversity (Vasco et al., 2023). Specifically, we observed a higher abundance of Actinobacteria and Bacteroidetes and lower abundance of Proteobacteria and Firmicutes in the cows given IMM antibiotics at dry off *versus* untreated cattle over a 9-week period. It is therefore possible that these taxa play an important role in the function of the gut microbiota during antibiotic therapy.

To examine the function of microbial communities, metagenomic approaches have been applied that enable the prediction of microbial metabolic capacity based on the detection of genes encoding enzymes and mapping them onto metabolic pathways (Beghini et al., 2021). The characterization of metabolites from host, dietary, and microbiome sources can also provide a better understanding of the functional interactions between the microbiome and environment. Untargeted metabolomics, for instance, uses liquid chromatography–tandem mass spectrometry (LC–MS/MS) to simultaneously detect multiple compounds based on their retention time and spectral fragmentation patterns (MS/MS) (Rakusanova et al., 2023). Metabolomics of the rumen content of dairy cows has improved understanding of diet-related metabolism while defining how it is influenced by the introduction of grain into the diet (Saleem et al., 2012) and identifying differences between fecal and rumen metabolites (Malheiros et al., 2021). Furthermore, integrated 'omics approaches such as metagenomics, metatranscriptomics, and metabolomics, have been used to characterize the functional microbiome in the rumen to identify microbial features linked to feed efficiency (Xue et al., 2022).

Since we demonstrated that IMM ceftiofur treatment of dairy cattle impacted the fecal microbiota and antibiotic-resistant bacterial populations when compared to cows without treatment (Vasco et al., 2023), we sought to characterize the function of the hindgut microbiome and metabolome in the same dairy cows. To identify short- and long-term changes due to antibiotic therapy, samples were taken a day prior to dry-off and ceftiofur treatment and again at 1 and 9 weeks later as described (Vasco et al., 2023). These time points correspond to three different stages of lactation and include late lactation (day -1), dry-off (week 1), and the periparturient period (week 9).

The different stages of lactation differ with respect to the diet given to the cows but also their physiology as outlined by the National Research Council (National Research Council, 2001). Indeed, cows in late lactation require a maintenance diet containing high levels of metabolizable protein and energy. During the dry period when cows are not producing milk, however, the mammary gland and udder tissue will involute and regenerate before the next lactation. The dry period lasts about 60 days prior to calving. As opposed to lactation, cows require lower quantities of metabolizable energy in their diet during the dry period. Comparatively, early lactation lasts approximately 30 days post-calving and represents the start of the lactation period. Higher levels of energy, calcium, and metabolizable protein are required for fresh cows when compared to dry cows to compensate for the energy imbalance induced by milk production and low dry-matter intake (National Research Council, 2001). This energy deficit generally persists through the 60th day of lactation, after which the cows shift to a net positive energy state. Since dietary changes are also linked to alterations in the gut microbiota in dairy cattle (Lin et al., 2023), we applied multi-omics approaches to identify interactions between the microbiome and metabolites present in fecal samples from ceftiofur-treated and ceftiofur-untreated dairy cows during different stages of lactation. The findings of this study enhance understanding of the effects that both ceftiofur treatment and lactation stage have on the function of the gut microbiome.

2 Materials and methods

2.1 Study population and epidemiological data

Forty Holstein cows were enrolled at the start of the dry-off period in June-November of 2019 at the Michigan State University (MSU) Dairy Cattle Teaching and Research Center as described (Vasco et al., 2023). After the last milking, twenty cows (cases) received a single IMM infusion containing 500 mg of ceftiofur hydrochloride (CHCL; SpectramastDC®; Zoetis Animal Health) along with a non-antibiotic teat sealant with bismuth subnitrate (Orbeseal®; Zoetis Animal Health) in each teat (n = 4; total of 2 g of CHCL). Cows in the control group (n = 20) received only the IMM teat sealant. All cows had a somatic cell count (SCC)

TABLE 1 Diet rations fed to dairy cows at four different lactation stages.

Ration component	Maintenance	Early dry	Close-up	Fresh
As-Fed (kg)	48.77	32.58	19.89	31.35
DM Fed (kg)	24.04	12.98	12.74	15.89
Corn grain ground fine (DM fed kg)	4.31	0	0	2.27
Corn gluten feed dry (DM fed kg)	1.81	0	0	0.45
Soybean Hulls Pellet (DM fed kg)	2.04	0	0	0
Soybean meal 475 solvent (DM fed kg)	1.13	0.95	2.72	1.36
Cottonseed Fuzzy (DM fed kg)	1.36	0	0	0
MSU Corn silage (DM fed kg)	4.08	4.08	3.8	5.58
MSU Haylage (DM fed kg)	4.08	4.04	0	2.72
CFE MSU dairy base (DM fed kg)	0.45	0.27	0.32	0.36
MSU Long bunk BMR CS (DM fed kg)	3.63	0	0	0
MSU fresh high supplement (DM fed kg)	1.13	0	0	1.07
MSU Purchased Alfalfa Hay (DM fed kg)	0	0	0	2.09
CFE MSU PreFresh DE (DM fed kg)	0	0	0.45	0
MSU Low K Grass Hay (DM fed kg)	0	0	4.76	0
SoyChlor (DM fed kg)	0	0	0.69	0
MSU grasslage (DM fed kg)	0	2.72	0	0
MSU Straw (DM fed kg)	0	0.91	0	0
Grass Pasture 16 CP 55 NDF 7 LNDF (DM fed kg)	0	0	0	0
QLF Ignite Dry Cow 25 (tub) (DM fed kg)	0	0	0	0

DM, dry matter; NDF, neutral detergent fiber; LNDF, Lignin as a percent of the NDF; CP, crude protein; CS, corn silage; BMR, brown midrib.

of <150,000 cells/mL at the most recent Dairy Herd Improvement Association test and none received antibiotics in the prior 90 days of lactation. The study protocol was approved by the Institutional Animal Care and Use Committee at MSU (IACUC number ROTO201800166) prior to sampling.

To avoid a parity effect, controls were matched to the ceftiofur-treated cows based on parity as well as monthly milk production. Diet regimens were formulated using Spartan Dairy 3™ software per guidelines outlined in the Nutrient Requirements of Dairy Cattle report (National Research Council, 2001). Based on the dietary information extracted from farm records, different diets were given to the cows in accordance with their production demands across the sampling period (Table 1); the matched treated and control cows were given the same diets within each lactation stage. Near the end of lactation, which corresponded to a day prior to the IMM treatment (day -1), cows received the maintenance diet containing 14% more metabolizable energy and 2.5 times more metabolizable protein (g) than is provided in the dry-off diet (weeks 1 through 5) (Supplementary Table S1). At week 9, animals were given a diet for fresh cows consisting of 64% of dry matter intake when compared to lactating cows, but with transitioning levels of energy and protein that were 15% and 64% higher than during dry-off, respectively.

Animals in all phases received corn silage, soybean meal with 47.5% crude protein, CFE MSU dairy base, and haylage. It was only during the lactation and fresh periods that the ration included corn (ground fine and fed dry) as well as MSU fresh high supplement to increase the energy density and provide essential nutrients such as calcium, magnesium, potassium, and niacin to prevent metabolic disorders that can occur during the transition into lactation. Comparatively, soybean hull pellets, cottonseed, and long bulk brown midrib (BMR) corn silage (CS) were exclusively given to cows in late lactation, while alfalfa hay was only provided to fresh cows. Although grass silage, MSU straw, grass pasture, and ignite supplement (Quality Liquid Feeds®, WI, Unites States) were given to all animals, they were only provided during the dry period in small quantities. The ignite supplement contains 25% protein, fat, trace minerals, and vitamins A, D, and E (https://onealsfarmandgarden.com/products/tub-qlf-ignite-30).

2.2 Sample collection and processing

Fecal samples were collected from all cows at four time points corresponding to the different stages of lactation (Figure 1). These stages included late lactation (day -1), dry-off (weeks 1 and 5), and the periparturient period (week 9). Along with physiological differences, the dietary needs of the animals and feed formulations differ across the three lactation stages. Samples were collected before ceftiofur administration at the end of lactation when

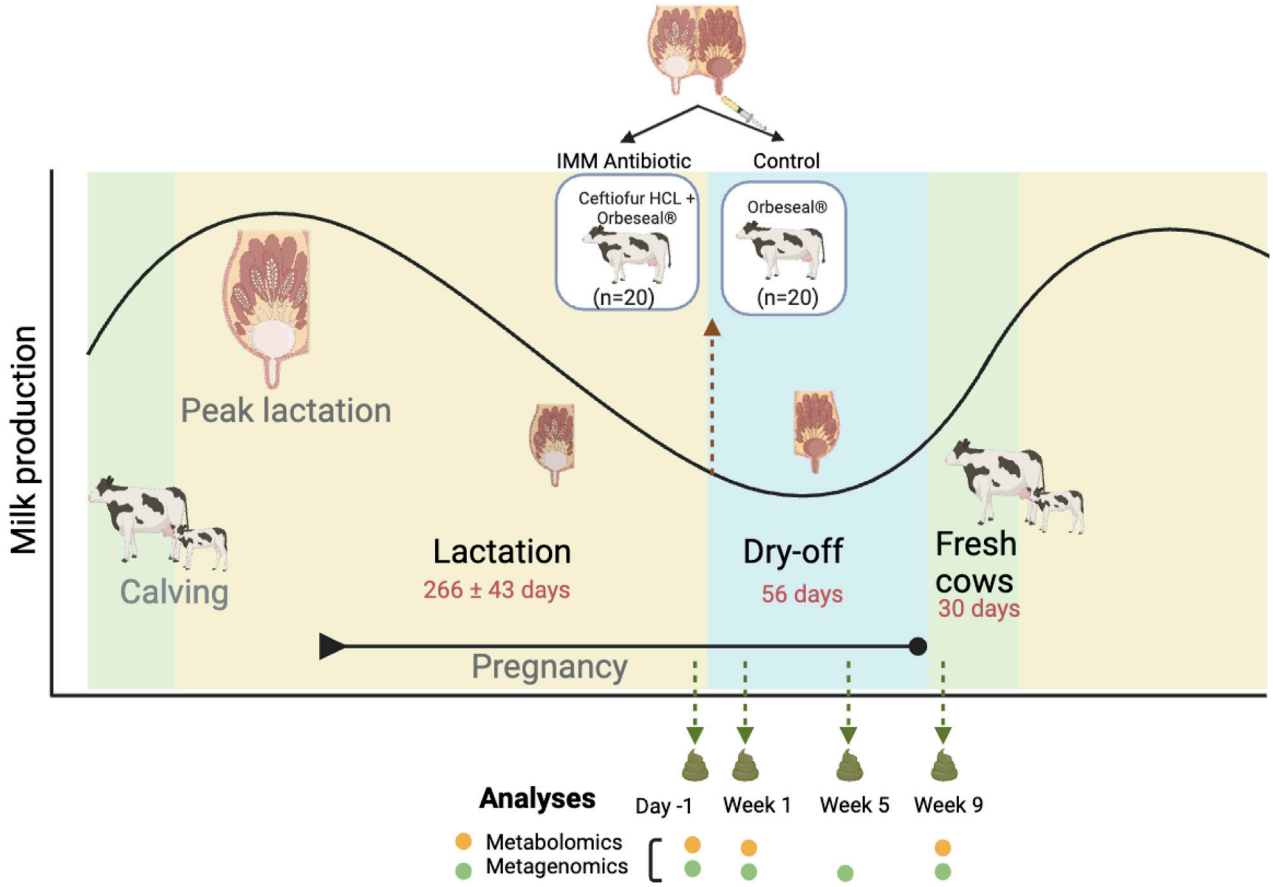

FIGURE 1
Diagram illustrating the animal treatment schedule and sample collections across the stages of lactation. The fecal sampling regimen coincided with three key lactation stages. These include: 1) the end of lactation (1 day before the initiation of dry cow therapy with intramammary (IMM) ceftiofur, or Day -1); 2) after dry cow therapy during the dry-off period (Weeks 1 and 5); and 3) 9 weeks after treatment at the end of the dry-off period and beginning of the fresh phase (Week 9). The black line demonstrates the fluctuations in milk production across each stage.

the cows received a maintenance diet (day -1) as well as after dry-off (week 1; week 5) when they were given an early dry diet. The final sample was collected during or just prior to calving (week 9) when the cows were given the fresh formulation. One cow could not be sampled at week 9 due to birthing by cesarean section that required antibiotics treatment, leaving 79 samples for analysis from the 9-week sampling point and 159 samples in all. As indicated previously (Vasco et al., 2023), the fecal samples were collected via the rectum using clean obstetric sleeves and transported in a cooler to MSU in sterilized sampling bags for processing.

Each sample was homogenized by hand and aliquots containing 0.25 g of feces and 0.25 g of feces in 750 µL of 190 Proof ethanol were stored for metabolite and DNA extractions, respectively. All fecal aliquots were flash frozen with liquid nitrogen for 1 min and were stored at −80°C until further processing. The 119 samples collected at the day -1, week 1, and week 9 samplings were used for both untargeted metabolomics and metagenomic sequencing, while metagenomic sequencing data were also available for the 40 samples collected at week 5 through our prior study (Vasco et al., 2023). Since we previously observed similar microbiota diversity and composition in the samples collected at weeks 1 and 5, metabolomics was not applied to the week 5 (dry-off) samples.

2.3 Metagenomics analyses

2.3.1 Metagenomic sequencing

Fecal samples were centrifuged for 5 min at 16,000 rpm at 4°C to remove the supernatant and the pellets were washed twice with 1 mL of 1× PBS as described (Vasco et al., 2023). DNA was extracted with the DNeasy PowerSoil Pro Kit (Qiagen, Germantown, MD, United States) using the manufacturer's protocol followed by an additional wash step using the C5 solution to improve quality. Samples with an average dsDNA concentration of 1,277.3 ng (±310.5 ng) as measured using a Qubit, were sent to CosmosID (Rockville, MD, United States) for metagenomic next-generation sequencing (mNGS). The Nextera™ XT DNA Library Preparation Kit (Illumina, San Diego, CA, United States) was used on all samples and sequencing was performed using the Illumina HiSeq X platform (2 × 150 bp).

2.3.2 Microbiome characterization

Metagenomic analyses to characterize the gut microbiota and resistome in the same cows were described previously (Vasco et al., 2023). Briefly, removal of bovine DNA and adapter sequences was performed and the microbiome and resistome composition were

analyzed with MetaPhlan4 (Blanco-Miguez et al., 2023) and Resistome Gene Identifier (Alcock et al., 2020), respectively. The software KMA was used to identify plasmids, virulence genes and viruses using the databases PLSDB (Schmartz et al., 2022), VFDB (Chen et al., 2005), and Virus-Host (Mihara et al., 2016). Abundance scores were determined based on genome equivalents and the number of reads to calculate the relative abundance of taxa and genes.

An evaluation of the function of the cattle microbiome was performed using the HUMAnN 3.0 pipeline (Beghini et al., 2021), which allows for the identification of metabolic pathways with their microbial species-level contributions. The following databases were used: ChocoPhlAn 3 (Beghini et al., 2021) for taxonomic identification, UniRef90 (Steinegger and Söding, 2018) for enzyme commission number screening, and MetaCyc v24.0 (Caspi et al., 2020) for the assignation of pathways. First, paired-raw sequences were processed with Trimommatic v.0.39 (Bolger et al., 2014) to remove low-quality reads and adapters used for Illumina sequencing. Burrows-Wheeler Aligner v.0.7.15 (Li, 2013) and SAMtools v.1.4.1 (Danecek et al., 2021) removed bovine DNA reads [*Bos taurus*, ARS-UCD1.2 (Rosen et al., 2020)]. Trimmed non-host paired FASTQ reads were merged with the UNIX command 'cat'. Merged reads were used as input for HUMAnN 3.0 and the resulting pathway abundances, reported as reads-per-kilobase (RPK), were normalized as the relative abundance per sample. A joined matrix containing the pathway relative abundances for all samples was generated with the command "humann_join_tables", whereas pathways of interest were depicted with the "humann_barplot" function while stratifying the pathway contributions by bacterial taxa (https://github.com/biobakery/humann).

2.4 Extraction of metabolites from cattle feces

Metabolite extractions were performed on all 119 fecal samples collected at day -1 (n = 40), week 1 (n = 40), and week 9 (n = 39). Internal standard solutions were prepared for quality control and normalization including: 1) labeled short-chain fatty acids (SCFAs) (10 µM each of [^{13}C]sodium formate, [$^{13}C_2$]sodium acetate, [$^{13}C_3$] sodium propionate, and [$^{13}C_4$]sodium butyrate) in 50:50 (v/v) methanol/water; 2)) [$^{13}C_{16}$]palmitic acid (10 µM in 100% isopropanol); 3) phenylalanine-d_7 (10 µM in 50:50 methanol/water); 4) succinic acid-d_4 (10 µM in 50:50 methanol/water); and 5) labeled bile acids (10 µM each of glycocholic acid-d_4 and glycoursodeoxycholic acid-d_4 in 50:50 methanol/water). A total of 20 mg of feces was weighed under sterile conditions and 350 µL of ice-cold methanol containing 0.1% butylated hydroxytoluene (BHT) was added. The sample was homogenized and incubated on ice for 10 min. For feces sedimentation, 10 µL of each standard was mixed into the samples, agitated for 30 s, and centrifuged at 10,000 × rpm at 4°C for 10 min. The supernatant was pipette-transferred to a sterile microcentrifuge tube on ice, while ice-cold HPLC-grade isopropanol (200 µL) was added to the pellet, homogenized for 30 s, and centrifuged at 10,000 × rpm and 4°C for 10 min. Finally, the isopropanol supernatant was combined with the initial extract and 100 µL aliquots of the mixed extracts were stored into glass vials inserted in 2-mL amber glass autosampler vials sealed with 9 mm screw septum caps. Metabolite extracts were preserved at −80°C until analyzed.

2.5 Metabolomics analyses

2.5.1 Untargeted metabolomics

Polar and nonpolar positive metabolites, which are a group of metabolites that carry a net positive charge, were analyzed through LC-MS/MS in a Thermo Scientific Vanquish™ Ultra High-Performance Liquid Chromatography (UHPLC) coupled to a Q Exactive™ Hybrid Quadrupole-Orbitrap™ mass spectrometer (MS). Metabolites with a net negative charge were not evaluated in this study. Along with the samples (n = 119), three blanks and pools were included at the beginning of each run (polar and nonpolar) and for every 20 samples. The Xcalibur™ software (ThermoFisher Scientific™, United States) was used for method setup and data acquisition.

The analysis of polar and nonpolar metabolites was conducted using distinct chromatographic conditions tailored to the properties of each metabolite class. Nonpolar metabolites were detected with reversed-phase chromatography using 10 µL of each sample injected with a column Waters Acquity Ethylene Bridged Hybrid (BEH)-C18 UPLC (2.1 × 100 mm) at 60°C. A 0.4 mL/min flow rate was used for a gradient analysis that consisted of 98% mobile phase A (water plus 0.1% formic acid) and 2% mobile phase B (acetonitrile plus 0.1% formic acid) for 1 min. Mobile phase B was ramped to 100% at minute 8 and was held for 2 min. Lastly, mobile phase B was returned to 2% at 10.01 min and held at that concentration for two more minutes.

By contrast, polar metabolites were detected through hydrophilic interaction liquid chromatography (HILIC). A Waters BEH-Amide UPLC column (2.1 × 100 mm) held at 60°C was used to inject 10 µL of sample. The gradient analysis was carried out at a rate of 0.4 mL/min starting with 100% mobile phase B (10 mM ammonium formate/10 mM ammonium hydroxide in 95:5 acetonitrile/water (v/v)) and 0% mobile phase A (10 mM ammonium formate/10 mM ammonium hydroxide in water) for 1 min. Mobile phase B was ramped to 40% at minute 8 and held at this concentration for 2 min. Mobile phase B was returned to 100% at minute 10.01 and held at this concentration for 2 min.

Data were acquired using a data-dependent MS/MS method with electrospray ionization in positive mode and capillary voltage of 3.5 kV, transfer capillary temperature at 262.5°C, sheath gas at 50, auxiliary gas at 12.5, probe heater at 425°C, and S-lens RF level at 50. Survey scans were acquired at 35,000 resolution, automatic gain control (AGC) target of 1E6, maximum inject time 100 m, and m/z range 100–1,500. The top 5 ions were selected for MS/MS with a resolution setting of 17,500, AGC target of 1E5, minimum AGC of 5E3, maximum inject time 50 m, isolation window of 1.5, fixed first mass at m/z 50, dynamic exclusion setting of 3 s and stepped normalized collision energy settings of 20, 40 and 60.

2.5.2 Mass-spectrometry (MS) data processing

Raw files (.RAW) for each sample were transformed to mzXML format with the Global Natural Product Social Molecular Networking (GNPS) conversion software. MS data processing was performed using MZmine v2.53 (Pluskal et al., 2010) while

analyzing the polar and nonpolar files separately. Instead of using standards for comparison, we determined the noise levels for MS1 and MS2 (centroided spectrum type) using the blanks and pools. First, mzXML files were imported to MZmine for mass detection at the levels MS1 and MS2 using a noise level of 4E04 for MS1 and 3.5E03 for MS2, which was set based on visual analyses of chromatograms from the pools and blanks. Chromatograms were built with the ADAP (Automated Data Analysis Pipeline) (Myers et al., 2017) module using a scan retention time of 1.00–10.00 min for MS level 1, minimum group size in number of scans equal to 4, group intensity threshold of 4.0E4, minimum highest intensity of 5.0E4, and scan to scan accuracy of 0.002 m/z or 10.00 ppm.

Chromatograms were smoothed using the Savitzky Golay algorithm with a filter width of 5 and deconvoluted with local minimum feature resolver. The deconvolution settings included MS/MS scan pairing with a retention time tolerance of 0.15 absolute min and MS1 to MS2 precursor tolerance of 0.002 Da. Additionally, the deconvolution algorithm was set up with a chromatographic threshold of 83.3999%, minimum search range RT/Mobility (absolute) of 0.05, minimum relative height of 0.0%, minimum absolute height of 5.0E4, min ratio of peak top/edge 1.80, and peak duration range (min/mobility) 0.00–1.51. Isotopes were grouped with a m/z tolerance of 0.0015 m/z or 3.0 ppm, a retention time tolerance of 0.05 absolute mins, and a maximum charge of 2 while choosing the most intense representative isotopes.

Next, an aligned feature list containing data from all samples was generated with module join aligner using a tolerance of 0.0015 m/z or 5.0 ppm, weight for m/z of 3, retention time (RT) tolerance of 0.1 absolute min, and weight for RT of 1. Gaps in the aligned list were filled with the module peak finder using an intensity tolerance of 20%, an m/z tolerance of 0.002 m/z or 10.0 ppm, and a retention time tolerance of 0.05 absolute min. Duplicate peaks generated during gap filling were removed at a m/z tolerance of 8.0E-4 m/z or 1.5 ppm and an RT tolerance of 0.035 absolute (min). To identify only those features present in at least three samples, the module "feature list rows filter" was used with at least 3 peaks in a row, keeping only peaks with MS2 scan, and resetting the peak number ID. Finally, the feature list was exported for analyses in GNPS for the Feature-Based Molecular Networking (FBMN) workflow using filter rows only with MS2. The exported files consisted of a feature quantification table (.CSV format) and an MS/MS spectral summary file (.MGF format) with a list of MS/MS spectra associated with the LC-MS/MS ion features.

2.5.3 Metabolite classification

The FBMN workflow in GNPS was used (Wang et al., 2016; Nothias et al., 2020) after importing the MGF file and feature quantification table generated in MZmine as well as the metadata containing the sample attributes. Precursor ion mass and fragment ion mass tolerances were set at 0.02 Da. Default settings were used for the advanced options except for minimum matched fragment ions for networks and library search min matched peaks, which were set at 4. All the spectra with IDs were downloaded; library ID and the network component index were recorded for each metabolite and are referred to as "cluster" for the downstream analyses. Molecular networks were visualized in GNPS to identify metabolite components and clusters of interest.

2.5.4 Metabolome data analyses

The R package Phyloseq v.1.38 was used to analyze metabolomics diversity and composition (McMurdie and Holmes, 2013). A Phyloseq object was generated by merging metadata with the feature table containing cluster intensities, and the cluster identifications, which included three levels: network component, library ID and cluster numbers. The R package decontam v.1.14 (Davis et al., 2018) was used to remove contaminant clusters associated with the standards based on a combined method that uses the Fisher's exact test. This method concatenates the probabilities of a cluster being present in a sample based on the amount of feces used for the metabolite extraction and the prevalence of a given cluster in controls versus the samples. Although the standards were present in the blanks and assessed separately, they were excluded from the final analysis. Lastly, cluster intensities were normalized to their relative abundances per sample.

2.5.5 Metabolome diversity analyses

The alpha diversity was calculated using the Shannon index and the number of observed features. The paired, one-tailed Wilcoxon signed-rank test was used to compare alpha diversity between groups and time points, whereas the Friedman's test was used to compare the indexes by animal over time since it accounts for repeated measures. Differences in beta-diversity or metabolome composition, were evaluated based on Bray-Curtis dissimilarity distances that were mapped with Principal Coordinate Analyses (PCoA) using the R packages Vegan v.2.5-7 (Dixon, 2003) and ggplot2 v.3.3.5 (Wickham, 2011). The mean compositions, represented by the centroid of each group of samples in the PCoA, were compared with permutational multivariate analysis of variance (PERMANOVA) with 999 permutations, while dispersion was compared with PERMDISP (Anderson, 2006).

2.6 Statistical analyses

2.6.1 Detecting significantly different features between groups

To detect significantly different features between the treatment groups and stages of lactation (time points), the following were used: 1) Linear Discriminant Analysis (LDA) Effect Size (LEfSe) (Segata et al., 2011); 2) Analysis of compositions of microbiomes with bias correction (ANCOM-BC) (Lin and Peddada, 2020); and 3) Microbiome Multivariable Associations with Linear Models (MaAsLin2) (Mallick et al., 2021), as suggested in a prior study (Nearing et al., 2022). LEfSe analysis was performed on normalized log2 abundances, focusing solely on features that passed a significance threshold in the Kruskal-Wallis test (p-value ≤0.05). ANCOM-BC analysis was conducted to detect differences between groups applying the Holm method for p-value adjustment. This analysis included only features present in at least 90% of samples, setting a convergence tolerance of 1e-05 and limiting the analysis to 100 iterations to minimize type I error rates. MaAsLin2 was utilized to identify associations with the group as a fixed effect, requiring a minimum feature prevalence of 90% and employing z-score standardization for data normalization. Because case and control cows were paired and shared the same environment, timing since treatment, parity, and diet, other covariates (random effects) were not included when using any of these analytical methods. Significantly

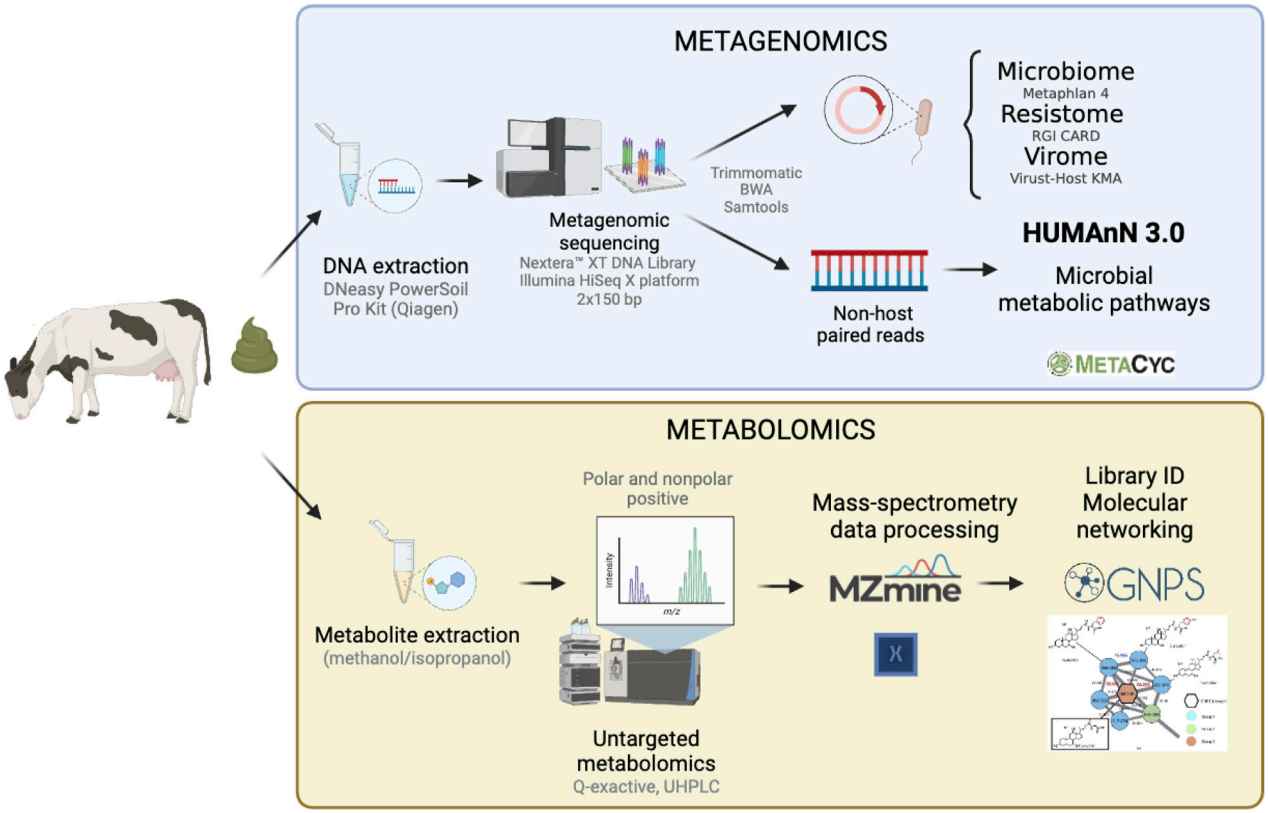

FIGURE 2
Summary of the methodology applied to analyze the functional gut microbiome of dairy cattle. Metagenomic sequencing (top panel) was used to characterize the microbial metabolic pathways, while metabolomics (bottom panel) was used to examine the metabolome composition among fecal samples collected from 40 dairy cows.

different features (adjusted p-value ≤0.05) were noted if they were detected using at least two of the three methods. Pairwise comparisons were made between treatment groups at each time point as well as between stages of lactation. Random Forest (RF) with 5,000 decision trees was used to estimate the out-of-bag (OOB) error rate that allows for correctly classifying the sample groups based on the metabolite composition. RF was also used to predict features (clusters and components) based on the discriminatory levels between sample groups ranked by their mean decrease accuracy (MDA).

2.6.2 Multi-omics analyses

Associations between the fecal microbiome and metabolome were examined by correlating the relative abundances of known metabolites (by library ID) with microbial taxa at the phylum and species levels and for antimicrobial resistance genes (ARGs), virulence genes, and microbial metabolic pathways across samples. Spearman correlations were calculated with the R package Hmisc (https://cran.r-project.org/web/packages/Hmisc/index.html); coefficients (ρ) >0.75 with p-values < 0.01 were filtered to construct networks with Gephi v.0.9.2 (Bastian et al., 2009).

To characterize patterns of change in the abundance of microbial and metabolic features, hierarchical clustering was performed using the R package stats v4.1.2 (https://www.r-project.org/). Only those features that differed significantly between lactation stages using two of the three analytical methods (LefSe, ANCOM-BC and MaAsLin2) were included in this analysis. First, a distance matrix was constructed with the Euclidean metric using the fold-change (FC) relative to each feature average per sample. The FC was calculated by computing the mean abundance of each feature across samples, and by dividing the abundance of a feature from a given sample by their corresponding mean. The distance matrix was used for hierarchical clustering with the Ward method (ward.D) and the resulting tree was cut into 30 clusters. The optimal number of clusters was identified with the NbClust v3.0.1 package (Charrad et al., 2014), which resulted in five clusters; however, a finer analysis of each branch was biologically more meaningful. Boxplots of each hierarchical clustering group were constructed to visualize the patterns of change between stages of lactation. Experimental and analytical methods are summarized in Figure 2.

3 Results

3.1 Untargeted metabolomics reveals a diverse metabolite composition

Analysis of mass-spectra identified twice the amount of nonpolar (n = 11,007) metabolite clusters than polar (n = 5,390)

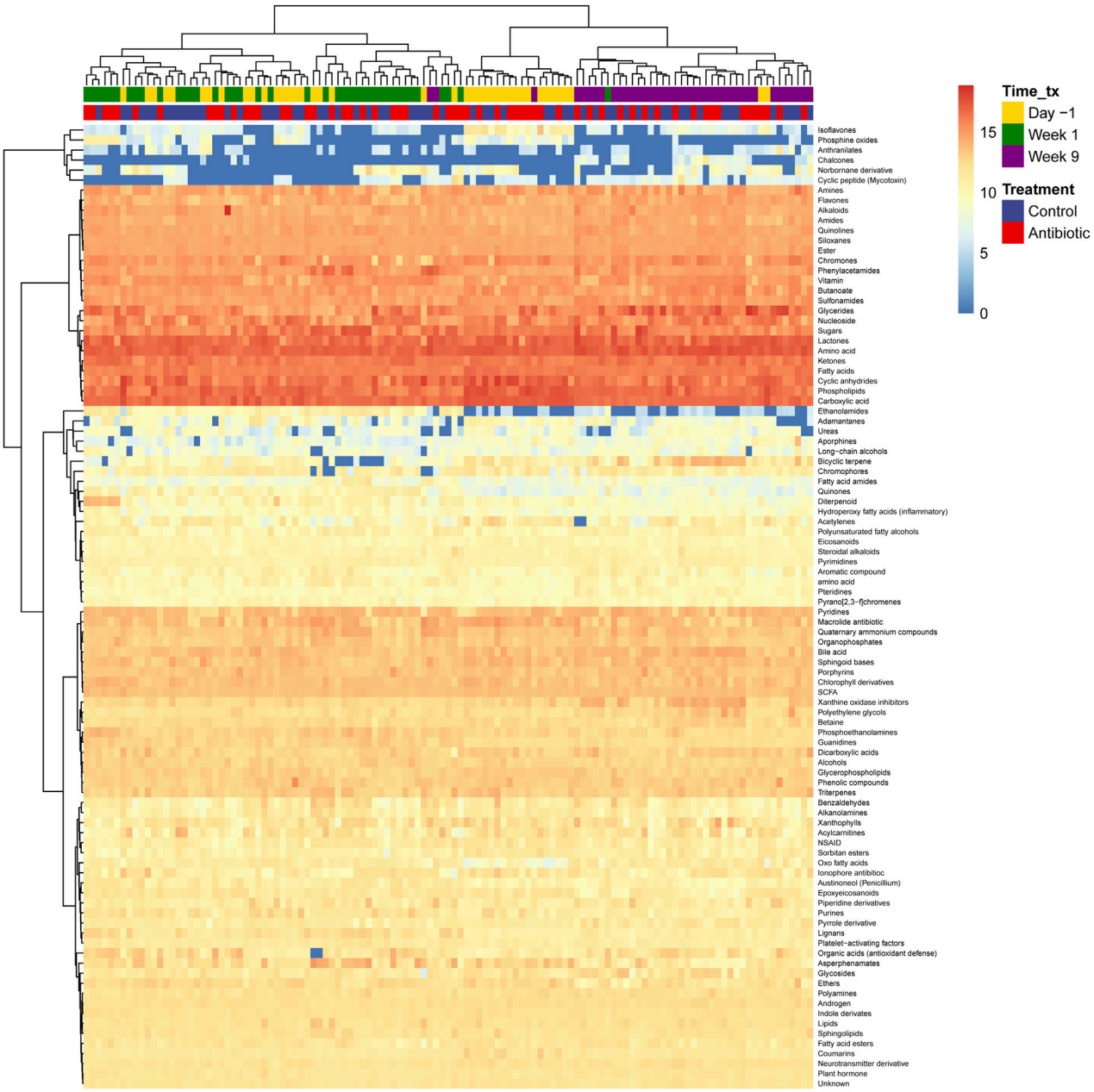

FIGURE 3
Fecal metabolome of dairy cows. The hierarchical clustering method Ward D2 was used to cluster rows (metabolites) and columns (samples) and only metabolites with library identification were included and aggregated at the class level. The color scale represents the logarithm (log) 10 of the relative abundance, with orange representing the most abundant metabolites and blue representing the least. Columns correspond to the samples, in which the time of collection (time_Tx) and IMM ceftiofur treatment status (Treatment) are indicated.

clusters. Likewise, molecular networks aggregating metabolites based on their MS^2 spectral similarity resulted in 1,122 nonpolar and 658 polar components (Supplementary Figure S1A). Network components connect clusters (nodes) that are structurally related via edges representing a modified cosine score that is calculated based on ions that differ by the mass difference (Supplementary Figure S1B). Only a small fraction of clusters had annotations based on library matches, corresponding to 2.48% of the total metabolites (polar, n = 135; nonpolar, n = 270), of which 68 were found with both polar and nonpolar modes.

In the metabolite clusters with library matches, various classes of metabolites were observed in all samples (Figure 3). These included amino acids, lactones, carboxylic acids, cyclic anhydrides, phospholipids, glycerides, ketones, sugars, fatty acids, nucleosides, chromones, vitamins, and butanoate derivatives. Additionally, several highly abundant metabolites including guanosine, benzofuran-2-one, phthalic anhydride, phosphocholine, monoelaidin, anzacyclotridecan-2-one, cytidine, glycan lacto-N-biose, glycan lacto-N-biose, hexanedioic acid, propanoic acid, octadecenoic acid, and others, were found in all samples. A

comprehensive list of the relative abundance of each metabolite and class detected is shown in Supplementary Table S2. Importantly, known metabolites categorized at the class level clustered together based on the stage of lactation but not the ceftiofur treatment status. The samples collected during the fresh period were most similar to each other.

3.2 Microbial metabolic pathways highlight the importance of essential molecule biosynthesis

Among the 159 samples, 262 metabolic pathways were identified that were assigned to bacterial taxa representing 797 pathways with different bacterial contributions. Only nine bacterial genera, however, were assigned to the pathways and included: *Bifidobacterium* (n = 75 pathways), *Clostridium* (n = 4), *Escherichia* (n = 25), *Methanobrevibacter* (n = 18), *Olsenella* (n = 2), *Ruminococcaceae* unclassified (n = 26), *Sarcina* (n = 12), *Turicibacter* (n = 12), other (n = 262), and unclassified (n = 200). On average, 93% of the reads were classified as unmapped and 6% as unintegrated for microbial metabolic pathways.

At the class level the most abundant microbial pathways were associated with the biosynthesis of amino acids, nucleoside and nucleotides, carbohydrates, and vitamins (Supplementary Figure S2). Aminoacyl-tRNA charging, fermentation and glycolysis pathways were also highly abundant in all samples. Pathways associated with the biosynthesis of fatty acid/lipids, cell structures, aromatic compounds, pentose phosphate and secondary metabolites were also common but were found in lower abundance. Similarly, pathways linked to the degradation of nucleoside/nucleotides as well as carbohydrates, carboxylates, and amine polyamines were commonly found (Supplementary Table S3). The abundance of microbial metabolic pathways varied between phases, with late lactation predominantly displaying elevated levels for most pathways. Nonetheless, no distinct clustering at the class level was evident among the lactation stages or by treatment status (Supplementary Figure S2).

3.3 Fluctuations in alpha diversity were observed across the sampling period

The within-sample diversity was measured by comparing the number of observed features and the Shannon index for the metabolomes and metagenomes among samples collected from the same time point, between two time points, and over the entire sampling period while accounting for repeated measures. For the number of nonpolar metabolites, considerable fluctuations in alpha diversity were detected over time (ANOVA, *nonpolar*: p = 0.001). The number of polar metabolites, however, displayed a more consistent number of clusters (*Observed*, ANOVA, p = 0.288) but with varying evenness (*Shannon*, ANOVA, p = 0.005) (Figures 4A,D). A significantly greater number of nonpolar metabolites was detected during lactation (day -1) relative to the dry-off period (week 1) (t-test: $p < 0.0001$), though no difference was observed relative to the fresh period (t-test, p = 0.086). Fresh cows exhibited a similar number of metabolites as when they were dry (t-test, polar: p = 0.71, nonpolar: 0.98) but with lower evenness for polar (*Shannon*, t-test, p = 0.0028) and nonpolar (*Shannon*, t-test, nonpolar: p = 0.0025) metabolites (Figures 4B,E). Although the metabolite richness was similar between fresh and lactating cows, the Shannon index showed lower diversity in the fresh phase denoting a transition like the one detected for diet composition. No differences were observed between polar and nonpolar metabolites when comparing the ceftiofur-treated and control cattle at any of the time points.

For the metabolic pathway predications, fluctuations in alpha diversity were also observed across samplings (ANOVA, $p < 0.0001$) (Figures 4C,F). Interestingly, the alpha diversity was more similar between the dry and fresh cows than between fresh and lactating cows despite the similarity in diet. Compared to cows in the dry and fresh periods, cows in late lactation had a significantly greater quantity and diversity of microbial metabolic pathways (t-test, $p < 0.0001$). Stratifying by treatment status did not result in significant differences in alpha diversity between the groups, except that the number of metabolic pathways at week 5 was significantly higher in control cows as compared to the cows given IMM ceftiofur at dry off (t-test, $p < 0.001$). Because samples from week 5 were not analyzed with untargeted metabolomics, however, we could not compare between treatment groups at this time point. Nonetheless, no long-term effects in the number of metabolites were observed at week 9 (fresh cows).

3.4 Beta diversity of the metabolome and microbial pathways varies across samplings, whereas the effects of ceftiofur treatment manifest several weeks post-treatment

Bray-Curtis dissimilarity distances showed significant differences between samplings for polar and nonpolar metabolome composition comprising all metabolite clusters (PERMANOVA, $p < 0.001$) (Figure 5A). Although the microbial pathways had overlapping composition between dry and fresh cows (PERMANOVA, $p > 0.3$), the lactating cows showed a significantly higher dispersion in the PCoA compared to the samples from dry and fresh cows (PERMDISP, F = 53.32, p = 1.34e-11) as well as a different average composition (PERMANOVA, F = 63.69, p = 0.001) (Figure 5B). Despite the metabolome composition differences associated with the sampling period, the microbial metabolic pathways were similar in the dry and fresh phases. Furthermore, cows treated with IMM ceftiofur had an identical mean metabolite composition as the controls (PERMANOVA, $p > 0.38$) even though differences in the composition of the microbial pathways were observed in weeks 5 (PERMANOVA, F = 4.25, p = 0.007) and 9 (PERMANOVA, F = 2.67, p = 0.045).

3.5 Differences in the metabolome were observed between ceftiofur-treated and control cows at specific time points

After comparing the abundance of a total of 16,589 metabolite clusters, 3,753 metabolite components, and 797 microbial-metabolic

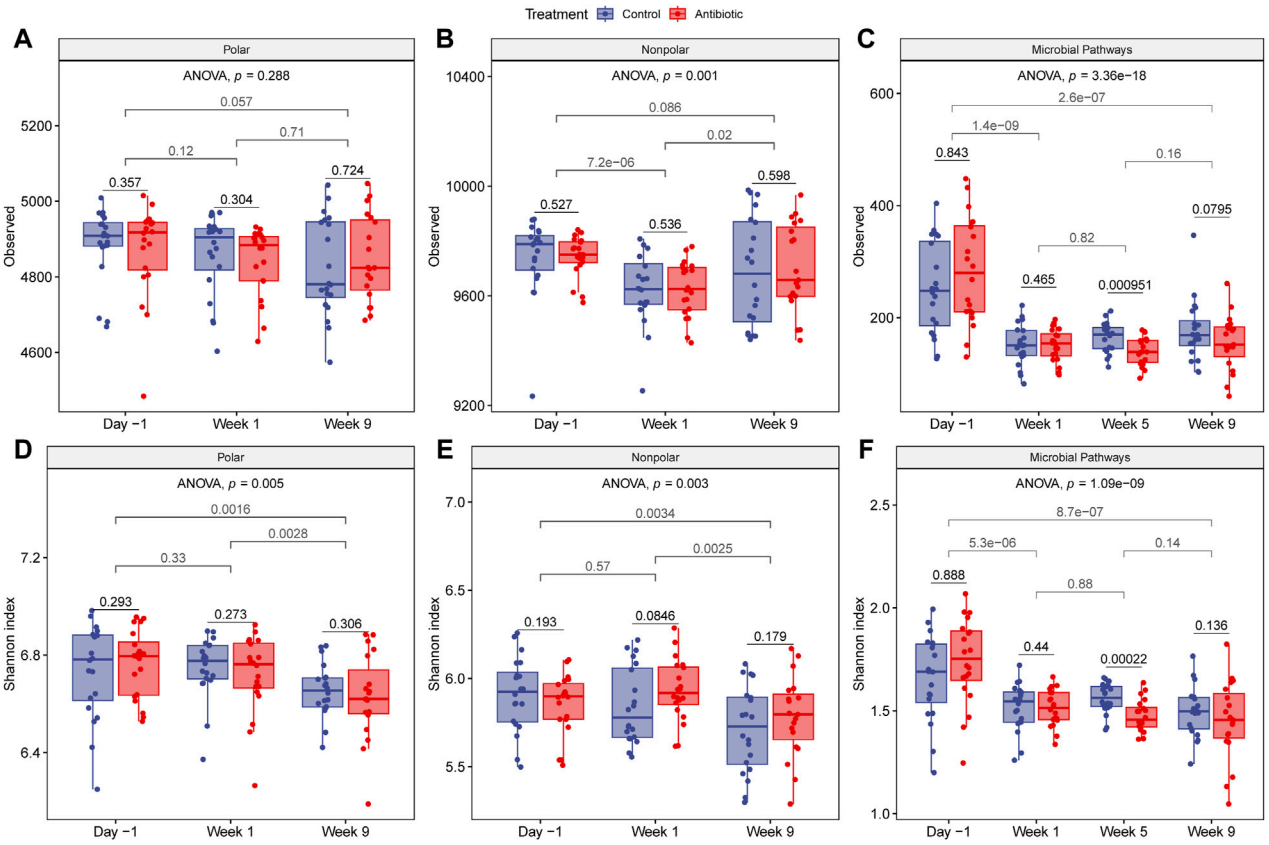

FIGURE 4
Alpha diversity of metabolites and microbial pathways. The top three panels show the number of observed features for **(A)** polar, **(B)** nonpolar, and **(C)** microbial metabolic pathways, while the bottom panels represent the Shannon index, for **(D)** polar, **(E)** nonpolar, and **(F)** microbial metabolic pathways, respectively. *p*-values were calculated with one-sided and paired *t*-test to compare treatment groups within a sampling point (black) or between time points regardless of treatment (gray). Each boxplot shows the median, lower, and upper quartiles with the whiskers representing extreme values in the distribution. Friedman's test, which accounts for repeated measures, indicates significant fluctuations in alpha diversity over time.

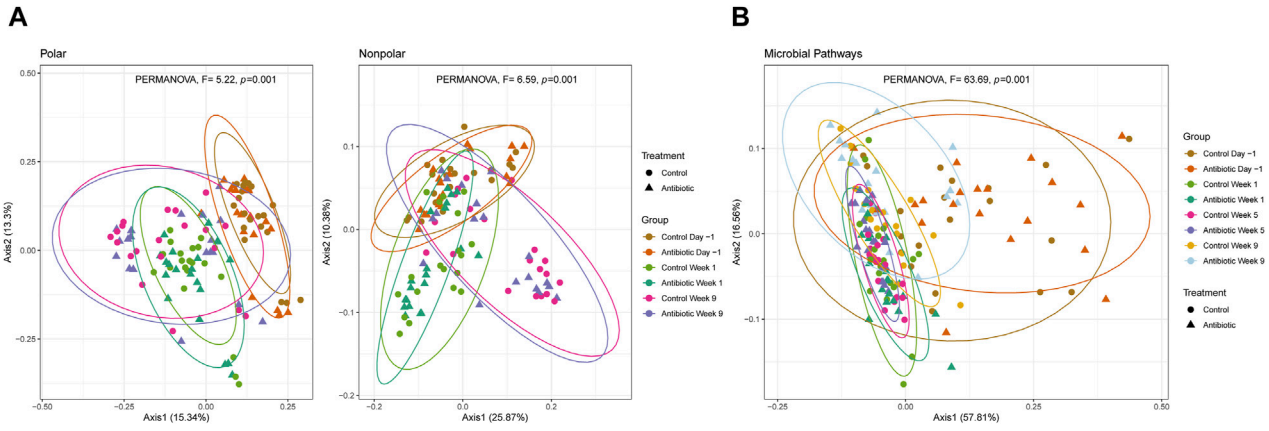

FIGURE 5
Beta diversity of **(A)** polar and nonpolar metabolites; and **(B)** microbial pathways. PCoA of the Bray-Curtis dissimilarity is clustered by treatment and sampling point (ellipses contain at least 90% of the samples in a group). Control animals are indicated by circles, whereas the ceftiofur-treated animals are indicated by triangles within each plot.

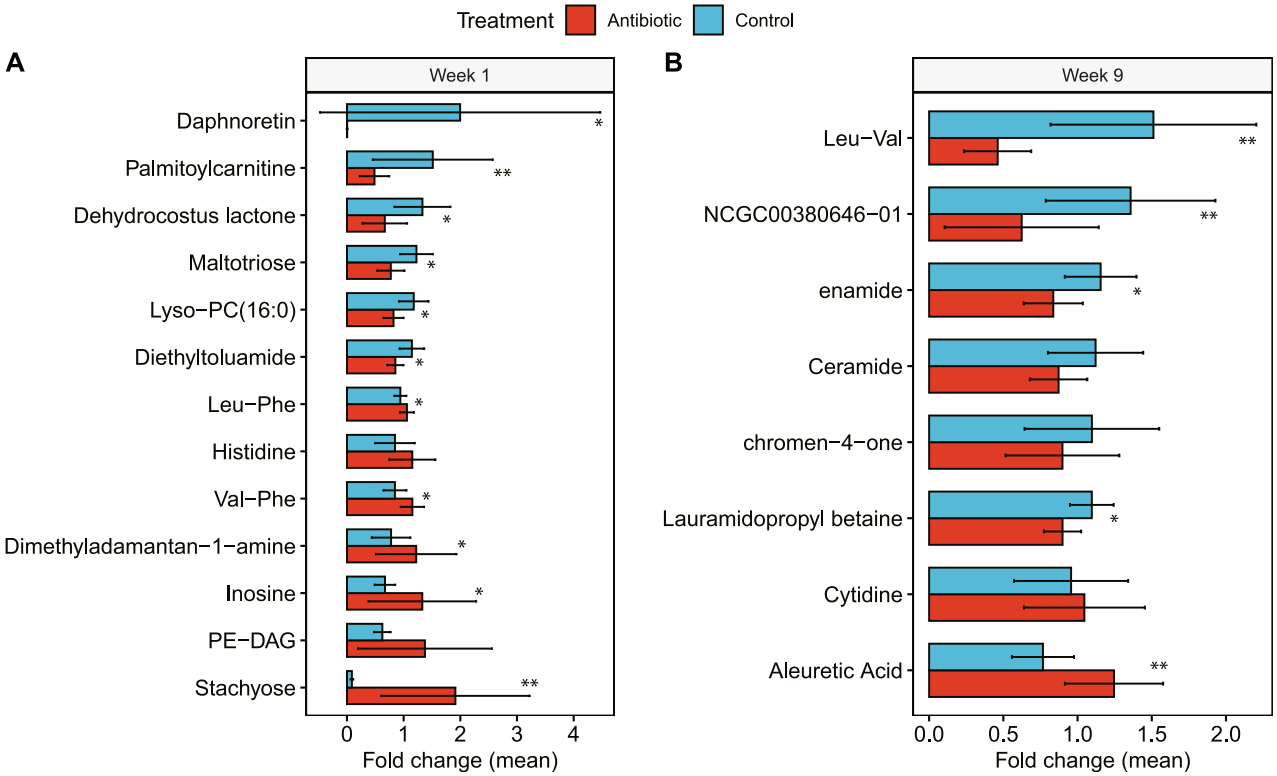

FIGURE 6
Hindgut metabolites identified in dairy cows with IMM ceftiofur (antibiotic) treatment relative to the control group. Differences in the relative abundance of each metabolite are shown at **(A)** 1 week after treatment (Week 1) and **(B)** 9 weeks after treatment (Week 9). The bars in the figure represent the mean fold change along with the corresponding confidence interval. One-tailed Wilcoxon signed-rank test was used to compare the relative abundance and significance (*p*-value) is shown as **≤0.01, or *≤0.05. NCGC00380646-01 represents (E)-5-(4-methoxy-5-methyl-6-oxopyran-2-yl)-3-methylhex-4-enoic acid.

pathways, only one metabolite cluster was significantly different between controls and cows treated with IMM ceftiofur 1 week after the treatment. This cluster corresponds to the nonpolar-positive metabolite cluster #6574 with a parent mass of 245.07 m/z, and a consensus retention time of 1.08 min (Supplementary Figure S3). This cluster is not identifiable and was not part of a network component, thereby limiting our understanding of its occurrence in the ceftiofur-treated animals. Similarly, RF could not correctly classify the metabolomic composition by treatment group at any time point; the OOB estimate of error rate was >55% when groups were compared based on metabolite or microbial-pathway composition at each time point.

Comparing groups with RF when considering only metabolite clusters with a library ID, which excluded unknown metabolites, the classifier error between treatment groups was reduced. Specifically, the OOB was 30% at day -1, 25% at week 1, and 18% at week 9. The primary identifiable metabolites that influenced the classification with RF varied across the time points. A week after drying off, for instance, inosine and palmitoylcarnitine were higher and lower, respectively, in cows treated with IMM ceftiofur (Mean decrease accuracy (MDA): 10.43, 7.83) than controls (Figure 6A). At week 9, the most important classifier was Leu-Val, followed by (E)-5-(4-methoxy-5-methyl-6-oxopyran-2-yl)-3-methylhex-4-enoic acid, which was higher in the controls relative to the antibiotic-treated cows (MDA: 14.31) (Figure 6B). By contrast, aleuretic acid (MDA: 7.49) was higher in the antibiotic-treated cows at week 9 compared to the controls.

3.6 Predicted microbial functions differed between ceftiofur-treated and control cows at specific time points

In the microbial metabolic pathway analysis, we identified nuanced distinctions among treatment groups. During the first week, for example, only seven microbial metabolic pathways exhibited disparities between cows treated with ceftiofur and the control group. These differences included an elevated presence of thiamine phosphate pathways by yeasts, as well as reduced levels of biosynthesis of cis-vaccenate and the degradation of punine ribonucleosides, D-fructuronate, and 4-deoxy-L-threo-hex-4enopyranuronate in the ceftiofur-treated cows.

At week 5, 17 microbial pathways were significantly less abundant in the cows treated with ceftiofur than the control cows; these included pathways involved in the biosynthesis of amino acids (i.e., L-ornithine, L-isoleucine, L-lysin, L-threonine, L-methionine), peptidoglycan, glycogen, isoprene, preQ0, chorismate, and coenzyme A, as well as in the degradation of L-arginine (Figure 7A). The unintegrated pathways of

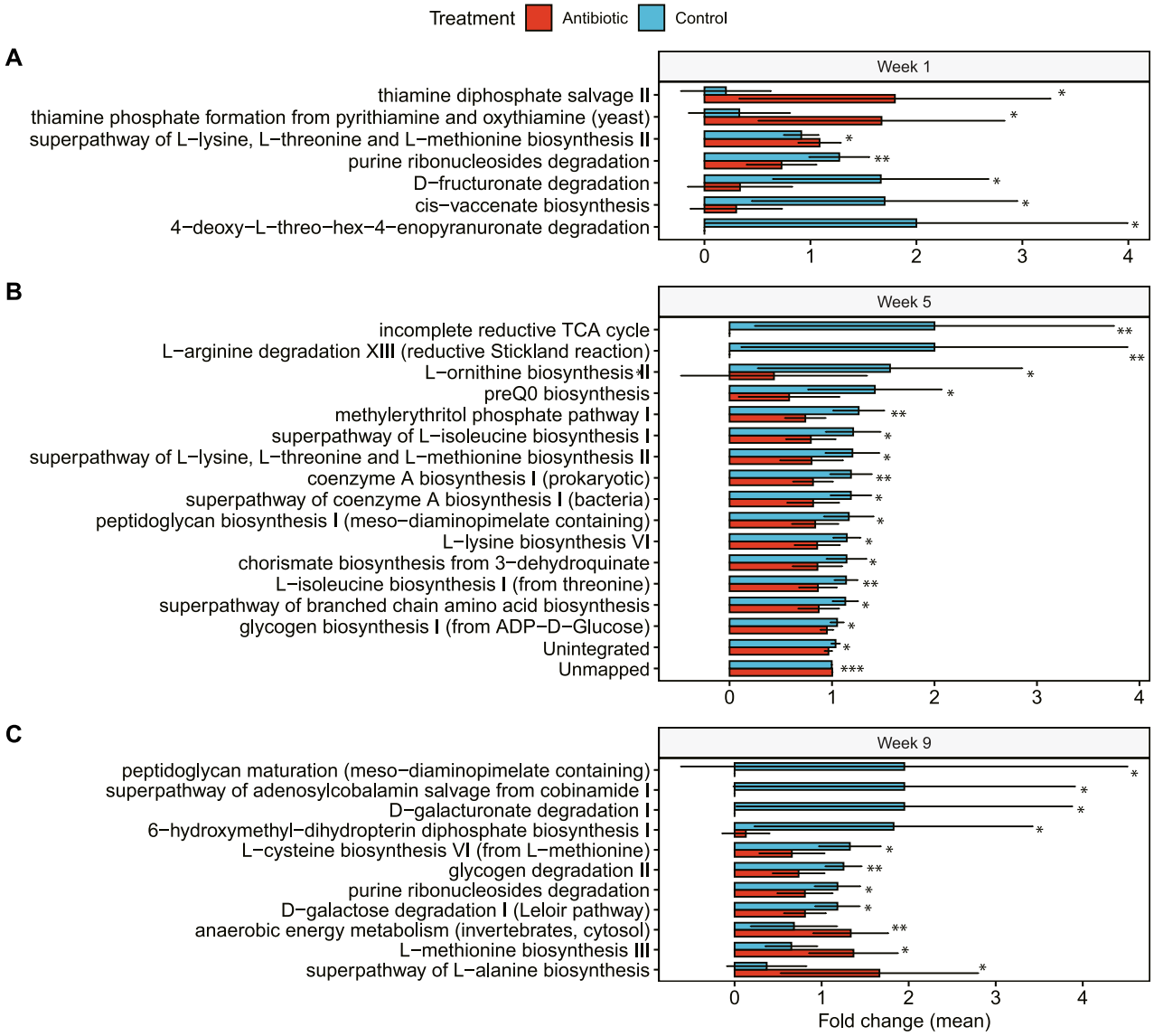

FIGURE 7
Differentially abundant microbial pathways in cows treated with IMM ceftiofur (antibiotic) compared to the control group. Differences in the relative abundance of each microbial pathway are shown at: **(A)** 1 week after IMM treatment (Week 1); **(B)** 5 weeks after treatment (Week 5); and **(C)** 9 weeks after treatment (Week 9). The bars in the figure represent the mean fold change along with the corresponding confidence interval. One-tailed Wilcoxon signed-rank test was used to compare the relative abundance and significance (*p*-value) is shown as **≤0.01, or *≤0.05.

Ruminococcaceae bacterium P7 and methylerythritol phosphate pathway I, however, were significantly lower in ceftiofur-treated cows. During week 5, several pathways were primarily identified in control cows but were absent in those given ceftiofur (Figure 7B). These pathways include L-arginine degradation XIII (controls, n = 5), the incomplete reductive TCA cycle (controls, n = 5), and L-ornithine biosynthesis II (controls, n = 6; ceftiofur, n = 1).

At week 9 (fresh phase), eleven microbial pathways explained differences between treatments using RF (Figure 7C). The most important differentially abundant pathways among the ceftiofur-treated cows included those related to peptidoglycan maturation, degradation of D-galacturonate, glycogen, purines, D-galactose, and the biosynthesis of 6-hydroxymethy-dihydropterin diphosphate and L-cysteine. Mirroring the observations from week 5, three microbial pathways were exclusive to controls (n = 4) at week 9, while another pathway was detected in just one ceftiofur-treated cow and seven controls. Curiously, a higher abundance of pathways related to anaerobic energy metabolism, and the biosynthesis of L-methionine and L-alanine were identified in cows treated with ceftiofur compared to the controls.

3.7 Differences in metabolites and microbial pathways were detected across samplings regardless of treatment status

The OOB error was 1.68% across the samplings, as the metabolomes of two fresh cows were misclassified as lactating

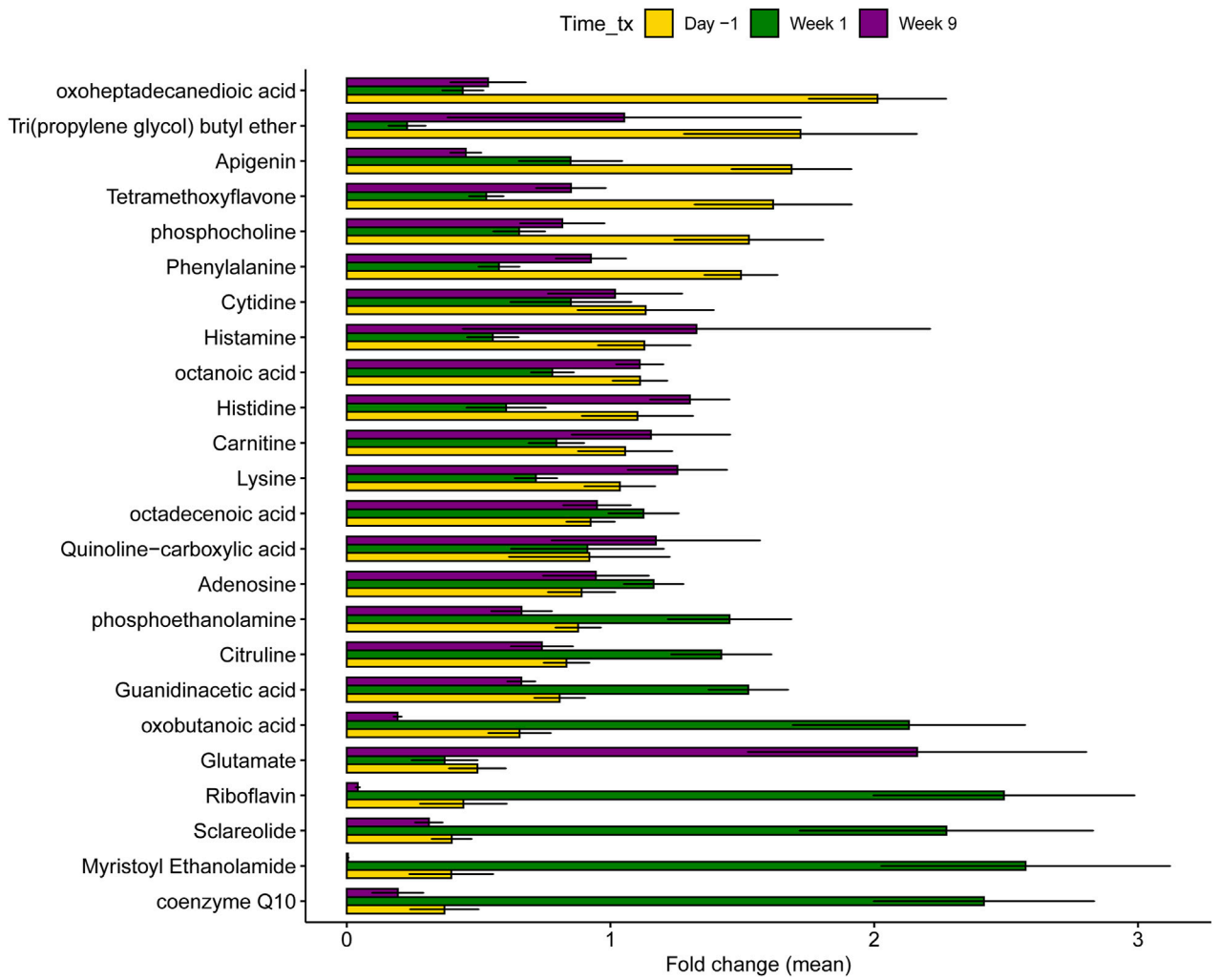

FIGURE 8
Differentially abundant metabolites across the three samplings in all 40 dairy cows regardless of treatment status. Each sampling corresponds to different stages of lactation. Day -1 corresponds to late lactation, Week 1 to dry off, and Week 9 to fresh cows. Data from all animals was combined and not stratified by treatment status. The bars in the figure represent the mean fold change along with the corresponding confidence interval.

cows. Hierarchical clustering of the 50 most important metabolite components identified with RF showed a transitional composition in fresh cows between the lactation stages (Supplementary Figure S4). Only four of these 50 components had clusters with library identification representing long-chain fatty acids, which were more abundant in the dry-off period (week 1), and amino acids that were increased during lactation (Supplementary Figure S5).

Differential abundance tests also identified 9,850 features that differed between samplings, corresponding to 46.59% of the total features (metabolites and microbial pathways) (Supplementary Figure S6). Dry and fresh cows showed a lower number of different features (53.88% of the total) than lactating and dry and cows (64.64%) or lactating and fresh cows (66.9%). In particular, the dry and fresh cows only differed in a few microbial pathways, whereas approximately one-third of the microbial metabolic pathways had varying abundances during lactation as compared to the other stages.

Among the top 25 most important metabolites classified by RF with library matches (Figure 8), cows in late lactation had a greater abundance of oxoheptadecanedioic acid, tri(propylene glycol) butyl ether, apigenin tetramethoxyflavone, phosphocholine, and phenylalanine compared to dry and fresh cows. Conversely, dry cows had higher concentrations of coenzyme Q10, myristoyl ethanolamide, riboflavin, harmol, oxobutanoic acid, guanidineacetic acid, citrulline, and phosphoethanolamide. Fresh cows demonstrated increased abundance of glutamate, histidine, and lysine, alongside histamine, which was elevated in both fresh and lactating cows compared to dry cows. Similarly, an evaluation of the top 25 microbial metabolic pathways showed that multiple pathways were significantly higher in lactating cows compared to those cows in the other stages (Figure 9). Pathways involved in the biosynthesis of nucleotides, amino acids, cell wall and glycolysis are among the most abundant. Intriguingly, during dry-off (week 5), higher levels of 2-oxobutanoate degradation I pathways were detected.

Notably, the top 8 most important pathways that predicted the sampling period through RF corresponded to three categories: 1) cell division, 2) amino acid biosynthesis, and 3) carbohydrate

10.3389/fmolb.2024.1364637

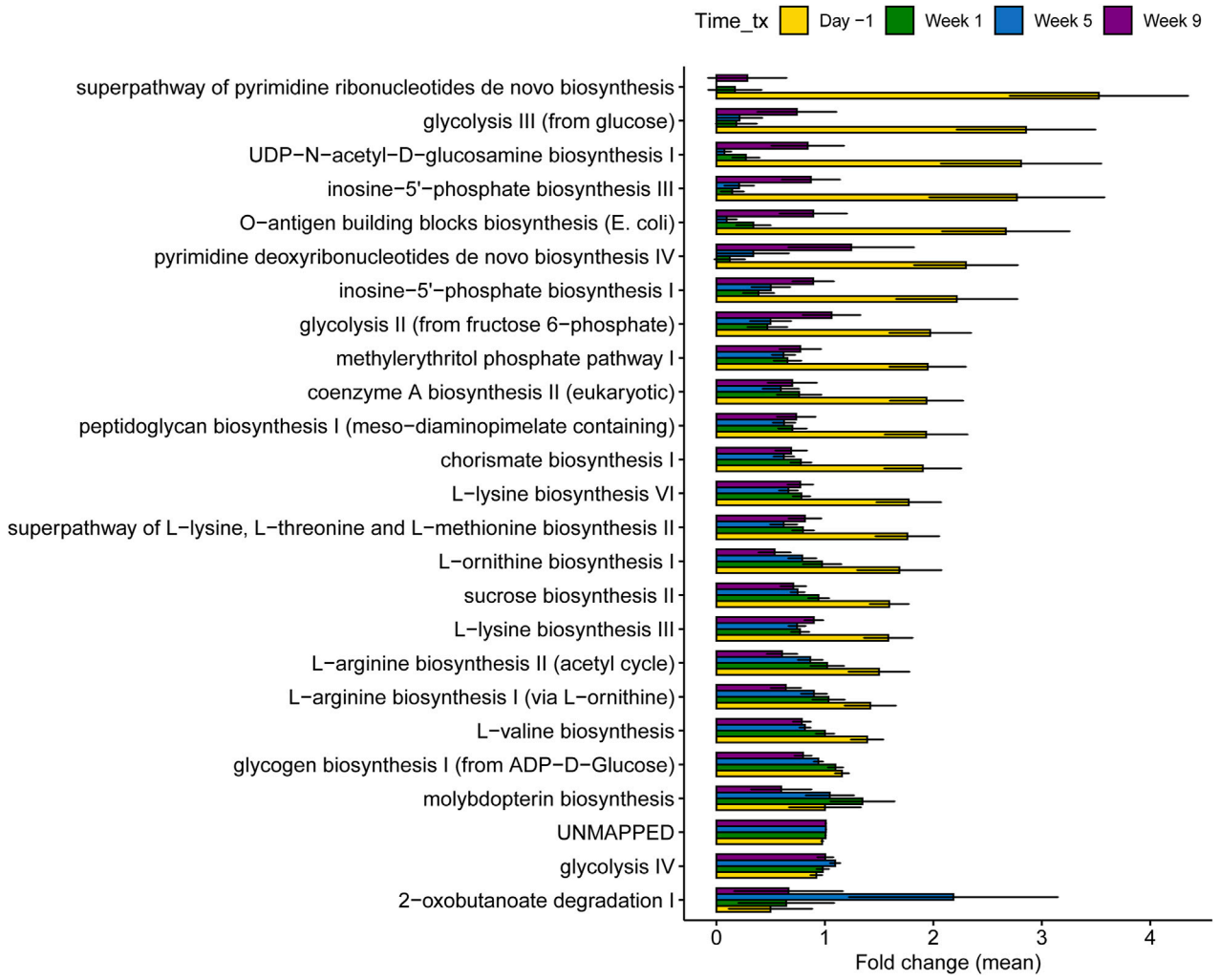

FIGURE 9
Differentially abundant microbial pathways across samplings in 40 dairy cows regardless of treatment status. The different samplings are shown and correspond to the different stages of lactation. Day -1 represents late lactation, while Week 1 and Week 9 represent the dry-off and fresh periods, respectively. The bars in the figure represent the mean fold change along with the corresponding confidence interval.

biosynthesis. These pathways were significantly higher during lactation, particularly those related to cell division that were mostly absent during the dry-off period. Cell-division pathways included inosine-5′-phosphate biosynthesis III, pyrimidine deoxyribonucleotides *de novo* biosynthesis IV, UDP-N-acetyl-D-glucosamine biosynthesis I, and O-antigen building blocks biosynthesis (*E. coli*), which were assigned to *Bifidobacterium*, *Turicibacter*, *Olsenella*, and *Escherichia coli* (Supplementary Figure S7). The three main pathways related to amino acid biosynthesis involved the superpathway of L-lysine, L-lysine biosynthesis VI, L-valine biosynthesis, and L-threonine and L-methionine biosynthesis II (Supplementary Figure S8). During lactation, these amino acid biosynthesis pathways were mainly assigned to *Bifidobacterium* spp. No taxa could be assigned to these pathways in the samples collected during the dry and fresh periods. Finally, carbohydrate biosynthesis pathways included glycogen biosynthesis I (from ADP-D-Glucose), sucrose biosynthesis II, and horismite biosynthesis I (Supplementary Figure S9). Although *Sarcina* was the main taxa assigned to glycogen and sucrose biosynthesis during the dry-off and fresh periods, *Bifidobacterium* was mainly associated with carbohydrate biosynthesis during lactation.

3.8 Multi-omics analysis identifies correlations between the microbiome and metabolome

Positive Spearman's correlations among metabolites, microbial pathways, microbial species, viruses, and antimicrobial resistance genes were analyzed. Potential functional relationships between metabolites and microbial species included uncultured Firmicutes and Bacteroidetes species with triacylglycerol (TAG); *Clostridium* with N,N,N-trimethyllysine, N,N-dimethyldodecylamine N-oxide and myristamidopropyl betaine; Proteobacteria and *Blautia* with histamine; monolinolenin, beauvericin [+NH4+], and neobavaisoflavone, with *Campylobacter*, Ruminococcaceae uncultured bacteria (GGB3236), and bacteriophages from

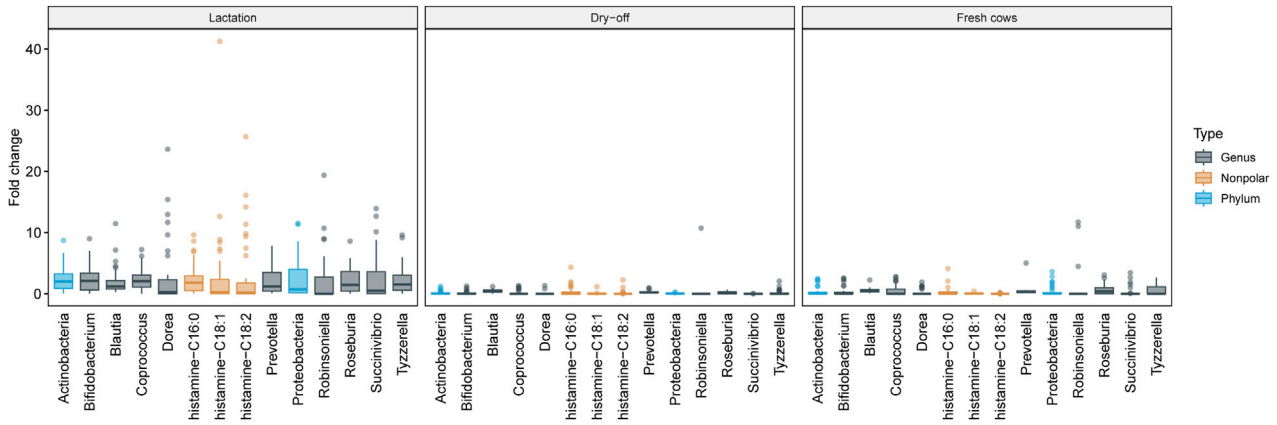

FIGURE 10
Metagenome and metabolome patterns by sampling period. This figure shows the variation in metagenome feature abundance at the genus and phylum levels as well as metabolome feature abundance across the sampling period. The samplings correspond to the Lactation (left panel), Dry-off (middle panel), and Fresh (right panel) periods. Emphasis is placed on features that are dominant in one sampling but nearly absent in others. These patterns were discerned using Hierarchical Clustering with the Ward D2 method. The *Y*-axis details the fold-change, compared to the average feature abundance across all samples. Boxplots encapsulate the median and interquartiles with whiskers indicating extreme values and marked outliers also presented.

enterobacteria (Vectrevirus Vec3); 2′-deoxyadenosine with Gammaproteobacterial; 1,2-Diheptadecanoyl-sn-glycero-3-phosphocholine with uncultured Bacteroidetes. Fruchterman Reingold networks show other correlations between the microbiome and polar metabolites (Supplementary Figure S10) as well as nonpolar metabolites (Supplementary Figure S11).

3.9 Metabolome and microbiome patterns changed across the sampling period

To better explore the functional associations of differentially abundant features, hierarchical clustering was performed with only those known metabolic clusters that differed significantly between samplings using LefSe, MaAsLin2 and ANCOM-BC. A tree was constructed based on a distance matrix highlighting the fold-change of metabolites and metagenomic features that differed significantly (n = 684). One relevant group showed concomitant higher levels of Actinobacteria, Proteobacteria, and histamine during lactation (Figure 10). This finding suggests a role of these taxa in the production of pro-inflammatory compounds such as histamine, which was also observed in the correlation networks.

Fresh cows showed higher levels of urate and nonpolar plant-derived compounds, which was likely due to a diet rich in alfalfa hay that was provided to the animals during this phase. Other clusters also showed patterns with lower contrast across the stages of lactation, with the most relevant HC groups displayed in Supplementary Figure S12. For instance, higher quantities of amino acids and dipeptides were detected with the polar mode on samples from lactation, which was related to a higher abundance of bacterial amino acid synthesis pathways mentioned priorly (Supplementary Figure S8). Not surprisingly, higher levels of androstane were also detected in fresh cows, which are expected to have peak levels of estrogens at this time (Supplementary Figure S13).

4 Discussion

In this study, we sought to identify changes in the gut metabolome of dairy cows due to IMM treatment with ceftiofur applied at dry-off over a 9-week period. Although IMM ceftiofur treatment impacted the abundance of specific metabolites, substantial alterations in the overall metabolome composition were not observed and could be attributed to low levels of ceftiofur metabolites in the cattle gut. Indeed, ceftiofur metabolites were not detected in the feces of IMM-treated cows 1-week after treatment. This was an anticipated finding as a prior study of steers treated subcutaneously found the total concentration of ceftiofur equivalents to be negligible in the gastrointestinal tract after 96 h (Foster et al., 2019). Another study showed that ceftiofur excretion began as early as 24 h after intramuscular administration, but most residues were detected in the urine (60%–80%) (Brown et al., 1991). Therefore, the lack of detection of ceftiofur metabolites in our samples post-treatment likely contributed to fewer functional alterations in the gut. Regardless, several metabolites were detected in greater abundance in the ceftiofur-treated *versus* -untreated cows along with an uncharacterized metabolite, which was found exclusively in the treated cows 1-week after treatment. This metabolite could represent a constituent of Spectramast® DC, which also contains microcrystalline wax, oleoyl oilyoxyglyceride, and cottonseed oil as well. Additional studies are needed for verification.

Among the metabolites present in greater abundance in the ceftiofur-treated cows was stachyose, an oligosaccharide of plant origin that is resistant to host enzymatic digestion (Zheng et al., 2000). Its presence suggests potential disruptions in gut bacteria responsible for its fermentation. Additionally, the enhanced levels of PE-DAG and inosine detected in the ceftiofur-treated cows suggest variation in microbial metabolism of lipids, energy, and cellular signaling, while lower concentrations of anti-inflammatory compounds, daphnoretin and dehydrocostus lactone (He et al.,

2002; Chen et al., 2020), were discerned. Diminished fatty acid oxidation processes, as reflected by the reduced levels of palmitoylcarnitine, phospholipids, and trisaccharide maltrotiose in the ceftiofur-treated cows, also suggest differences in digestive processes compared to the controls.

Microbial metabolic pathways were also modified following IMM ceftiofur treatment. While the impact was not immediately observable in these pathways 1-week after treatment, discernible functional alterations were detected by week 5. Indeed, the diminished abundance of numerous microbial metabolic pathways at week 5 suggests a curtailed metabolic potential of the bovine microbiome in response to ceftiofur treatment. Notable among these were decreased utilization and biosynthesis of certain amino acids encompassing L-arginine, L-ornithine, L-isoleucine, L-lysine, L-threonine, and L-methionine. Furthermore, the capacity to produce precursor molecules and the synthesis of crucial biochemicals such as sterols, carotenoids, chlorophylls, fatty acids, cholesterol, among others, was decreased in the ceftiofur-treated group. Since the metagenomic analysis did not invariably elucidate the activity of the gene-encoded enzymes present in fecal samples in the first week post-treatment, the application of metatranscriptomics could be used in future studies to provide clarification.

Importantly, ceftiofur treatment had no short-term or persistent effects on metabolome diversity in the cow gut over the 9-week sampling period. Although this result is consistent with our findings showing no difference in microbiome diversity in the same cohort of cows (Vasco et al., 2023), the ceftiofur-treated microbiome showed a reduced propensity for energy production. Evidence for this observation is provided by the observed downturn in the biosynthesis of glycogen and coenzyme A. By the ninth week, however, multiple pathways associated with *Bifidobacterium* were more abundant in ceftiofur-treated cows. For example, L-methionine and L-alanine, which are prominently involved in anaerobic energy metabolism and the biosynthesis of amino acids, are associated with the genus *Bifidobacterium*, a member of the phylum Actinobacteria that was significantly more abundant in ceftiofur-treated cows previously (Vasco et al., 2023). Despite these observations, a decline in sugar degradation (such as D-galactose, purine ribonucleosides, glycogen, D-galacturonate) and a reduction in the production of vitamin B12 and peptidoglycan maturation were observed in the ninth week following ceftiofur treatment. These findings highlight the complex and multilayered response of the bovine gut microbiome to IMM ceftiofur treatment.

While we did not collect milk samples for evaluation in this study, it is worth noting that treatment-associated modifications in the gut microbiome and metabolome could potentially impact milk quality. The presence of *Bifidobacterium*, for example, has been linked to higher milk-fat yields (Jami et al., 2014), while genus *Prevotella* (phylum Bacteroidetes) has been connected to metabolic pathways integral to protein and fat content in milk as well as the production of volatile fatty acids (Wu et al., 2021). Despite these associations, the primary determinants of milk composition are specific to each herd's diet (Albonico et al., 2020) and to a lesser extent, the interplay between genetic makeup and the composition of rumen bacteria (Buitenhuis et al., 2019). It is important to recognize that even though IMM ceftiofur may exert specific effects on the fecal metabolome and the functionality of the microbiome, the judicious application of antibiotic therapy during the dry-off period is essential for preventing mastitis. This condition not only impairs milk production but also has adverse consequences on the welfare of the animal (Ruegg, 2017). We did not assess the efficacy of IMM ceftiofur in preventing IMM infections herein, nor did we investigate whether IMM infections induce inflammation and independently perturb the gut microbiota.

Moreover, our analysis demonstrated that the overall metabolome and related microbial metabolic pathways varied across the sampling period. Each stage of lactation, which is characterized by unique physiology and diets, had a distinct metabolome and functional microbiome, highlighting the collective role that these factors play in metabolome variation regardless of ceftiofur treatment. Even though the individual impact of these factors could not be explored based on our study design, prior studies have shown that diet impacts the fecal metabolome and microbiome composition in cows (Zhang et al., 2018; Hagey et al., 2019; Liu et al., 2020; Vasco et al., 2021). For instance, increasing grain-forage ratios have been linked to a higher abundance of Proteobacteria and a lower abundance of Bacteroidetes in feces (Zhang et al., 2018; Liu et al., 2020). Moreover, diets with >30% grain given to cows in early lactation significantly changed the ruminal metabolome, increasing the abundance of short-chain fatty acids as well as toxins, inflammatory compounds, putrescine, methylamines, and ethanolamine (Saleem et al., 2012). Herein, cows in late lactation (day -1) received the highest amount of grain in the diet, constituting about 39% of the dry matter intake vs 26% in fresh cows (week 9) and 7% in dry cows (week 1). It is therefore likely that different feed ingredients will have distinct effects on the metabolome and microbial activity in the bovine gastrointestinal tract.

Comparatively, those cows sampled during late lactation also had enhanced diversity of microbial pathways and metabolites. Phenylalanine, for instance, is an essential amino acid, and had higher levels during late lactation. This finding suggests increased protein intake or metabolism in cows on the maintenance diet compared to the diets used during other stages of lactation (Reitelseder et al., 2020). It also aligns with the diet formulation containing higher levels of crude protein compared to those administered in the early dry and fresh phases. Similarly, compounds like phosphocholine and carnitine are involved in lipid metabolism and energy production; hence, the higher levels observed during late lactation may reflect differences in energy substrate utilization compared to dry and fresh phases. Higher levels of dry matter, fat, net energy, non-fiber carbohydrates, starch and vitamin A were also provided during lactation that could have differentially impacted community function and require further examination.

During late lactation when a higher abundance of Actinobacteria and Proteobacteria was observed, greater levels of histamine were also found. Microbial-origin gut histamine, which is linked to grain-rich diets, has been associated with inflammatory responses, such as laminitis (Garner et al., 2002), and inflammatory reactions in the bovine lung (Barcik et al., 2019). Furthermore, increased levels of histamine in the gut can

lead to symptoms such as increased vascular permeability, edema, and the recruitment of inflammatory cells (Ashina et al., 2015). These outcomes can result in the translocation of bacteria, toxins, and other molecules across the intestinal barrier, potentially contributing to inflammatory processes and other gut issues.

During the dry-off period, cows are typically transitioned to a diet primarily composed of forage with a lower percentage of grain (Dancy et al., 2019), which could impact the metabolic response. For example, propionic acid is a volatile fatty acid produced during rumen fermentation of carbohydrates, and its higher levels may reflect increased fermentation of forage-based diets, particularly grasslage (Ribeiro et al., 2009). Compounds like citrulline, guanidinacetic acid, oxobutanoic acid, riboflavin, myristoyl ethanolamide, and coenzyme Q10 are involved in energy metabolism, amino acid metabolism, and cellular processes, and their levels may be influenced by metabolic shifts. Similarly, during dry off, cows also exhibited a higher abundance of the 2-oxobutanoate degradation I pathway, which plays a role in the breakdown of specific amino acids and contributes to energy production and the generation of key metabolic intermediates. Since dry-off is associated with changes in hormone levels, particularly the decline in lactation-related hormones such as prolactin (Ollier et al., 2013), hormonal fluctuations can also impact metabolic pathways and the production or utilization of certain compounds.

A higher diversity of microbial pathways, as was observed during late lactation, has also been associated with enteric infection in monogastrics in a case-control clinical study performed by our group (Hansen et al., 2024). Despite the similarity in diet and the metabolome between the fresh and lactating cows, the microbial metabolic pathway diversity and composition were significantly different. Hence, it is essential to emphasize the marked disparity in dry matter intake and metabolic status between fresh and lactating cows, particularly when distinguishing between negative and positive energy balances. During early lactation, cows typically experience a negative energy balance, whereas those in late lactation transition to a positive energy balance (Butler and Smith, 1989). In fact, the pathway profiles of fresh cows were like those observed in the dry phase suggesting a slow adaptation to a high grain diet. Although it only took a week on a forage-based diet at dry-off to identify changes in the functional gut microbiome, this was accompanied by lower levels of histamine-producing bacteria compared to the lactation stage. Since the core microbiome composition is unique to each farm due to factors that include housing, breed, and age (Hagey et al., 2019; Furman et al., 2020), changes in the diet are the most impactful on the cattle metabolome and microbial diversity. Although manipulation of the functional microbiome through dietary changes is plausible, functional changes can take longer to develop in a new environment as was observed herein. Nonetheless, it is important to note that we did not control for diet or other factors when making comparisons across sampling periods and hence, these relationships require validation in future studies.

Similar to findings from other metabolomic studies (da Silva et al., 2015; Peisl et al., 2018), many of the metabolites and microbial-metabolic pathways were unknown and could not be classified. Despite this limitation, biologically important compounds and metabolic pathways enabled the interpretation of some associations that were observed between the microbiome and metabolome. Future studies, however, should include GC/MS to promote the identification of short-chain fatty acids (SCFAs) since they have been linked to health outcomes in humans (Tan et al., 2014) and production in cattle (Bionaz et al., 2020). Moreover, associations between metagenome, metabolome and milk production could guide improvements in diet formulations, health, and probiotic development. Serum metabolome analyses could also help identify relationships between microbiome functionality and host factors such as hormonal levels (i.e., estrogens, cortisol, progesterone, prolactin), or metabolic disorders in cattle. Neither SCFAs or serum metabolites were evaluated in our study nor was the application of fecal proteomics, which could be used to define markers of immunity and inflammation that are indicative of specific host responses. These analyses as well as the use of metatranscriptomics and metaproteomics combined with targeted metabolomics should be performed in the future to better characterize the functional microbiome (Van Den Bossche et al., 2021).

5 Conclusion

IMM ceftiofur treatment of dairy cattle at dry-off resulted in alterations to the microbial metabolic pathways and fecal metabolites associated with lower biosynthesis of amino acids and energy a week after its application. Nevertheless, these alterations were not as pronounced as those observed with dietary changes and physiological shifts linked to lactation stage. Indeed, each stage of lactation was characterized by a distinct metabolome composition that was related to feed ration and physiology regardless of treatment status. During lactation, a higher level of microbial activity, particularly amino acid biosynthesis, was observed as compared to dry and fresh cows; however, histamine-producing bacteria were more abundant during late lactation. Together, these data highlight how integrative analyses of metagenomics and untargeted metabolomics data can be used to define the metabolite-microbe interactions in the cattle gut. Understanding the role of the gut environment in the microbial profile is critical to identify factors related to cow health in dairy farms.

Data availability statement

The paired-end metagenome raw reads used in this study are deposited in the NCBI repository, BioProject PRJNA825520 (Biosamples SAMN27520269 to SAMN27520427). FBMN data processed through GNPS is available online for polar and nonpolar metabolites (https://gnps.ucsd.edu/ProteoSAFe/status.jsp?task=d4a761f0a6be422c8b89db9408f57b0d and https://gnps.ucsd.edu/ProteoSAFe/status.jsp?task=1d6f7e95d2f04f96a94fede8c195702d, respectively). Additional analyses that support our conclusions are available in the GitHub repository (https://github.com/karla-vasco/metabolome_microbiome_cattle).

Ethics statement

The animal studies were approved by the Institutional Animal Care and Use Committee at Michigan State University (IACUC number ROTO201800166). The studies were conducted in accordance with the local legislation and institutional requirements. The collection of information and samples was authorized by the Michigan State University (MSU) Dairy Cattle Teaching & Research Center, as confirmed through written informed consent.

Author contributions

KV: Conceptualization, Data curation, Formal Analysis, Investigation, Methodology, Supervision, Validation, Visualization, Writing–original draft, Writing–review and editing. ZH: Formal Analysis, Methodology, Writing–review and editing. AS: Conceptualization, Methodology, Supervision, Writing–review and editing. BB: Methodology, Writing–review and editing. SC: Methodology, Writing–review and editing. PR: Funding acquisition, Project administration, Supervision, Writing–review and editing. RQ: Conceptualization, Methodology, Resources, Supervision, Writing–review and editing. LZ: Conceptualization, Funding acquisition, Methodology, Project administration, Resources, Supervision, Writing–review and editing. SM: Conceptualization, Funding acquisition, Investigation, Project administration, Resources, Supervision, Validation, Writing–review and editing.

Funding

The author(s) declare that financial support was received for the research, authorship, and/or publication of this article. This study was funded by the U.S. Department of Agriculture (USDA), grant number 2019-67017-29112. USDA did not participate in the study design or data analyses associated with this project. Additional support was provided by the Michigan Sequencing and Academic Partnerships for Public Health Innovation and Response (MI-SAPPHIRE) initiative at the Michigan Department of Health and Human Services via the Centers for Disease Control and Prevention through the Epidemiology and Laboratory Capacity for Prevention and Control of Emerging Infectious Diseases Enhancing Detection Expansion program (6NU50CK000510-02-07) as well as the Michigan State University (MSU) Foundation and AgBioResearch (SDM). Student support for KV was provided by the Department of Microbiology, Genetics, and Immunology at MSU through the Thomas S. Whittam award, and the MSU College of Natural Sciences.

Acknowledgments

We thank Bo Norby, Ronald Erskine, and the late Lorraine Sordillo-Gandy for their instrumental contributions to the original study's conception and design along with the team at the MSU Dairy Cattle Teaching and Research Center for assistance with planning and data collection. We thank Rebekah Sloup, Carmen Garcia, Jose Rodrigues, Jaimie Strickland, Jennifer Brown, Jeffery Gandy, Robert West, and Aspen Robak for assistance with field and laboratory work. We appreciate the assistance provided by Doug Guzior and Christian Martin in the metabolomics analyses and thank Daniel Jones at the Mass Spectrometry and Metabolomics Core at MSU for the fecal metabolite extraction protocol.

Conflict of interest

The authors declare that the research was conducted in the absence of any commercial or financial relationships that could be construed as a potential conflict of interest.

The author(s) declared that they were an editorial board member of Frontiers, at the time of submission. This had no impact on the peer review process and the final decision.

Publisher's note

Supplementary material

The Supplementary Material for this article can be found online at: https://www.frontiersin.org/articles/10.3389/fmolb.2024.1364637/full#supplementary-material

References

Albonico, F., Barelli, C. I., Albanese, D., Manica, M. I., Partel, E., Rosso, F., et al. (2020). Raw milk and fecal microbiota of commercial Alpine dairy cows varies with herd, fat content and diet. *PLoS One* 15, e0237262. doi:10.1371/journal.pone.0237262

Alcock, B. P., Raphenya, A. R., Lau, T. T. Y., Tsang, K. K., Bouchard, M., Edalatmand, A., et al. (2020). CARD 2020: antibiotic resistome surveillance with the comprehensive antibiotic resistance database. *Nucleic Acids Res.* 48, D517–D525. doi:10.1093/nar/gkz935

Anderson, M. J. (2006). Distance-based tests for homogeneity of multivariate dispersions. *Biometrics* 62, 245–253. doi:10.1111/j.1541-0420.2005.00440.x

Ashina, K., Tsubosaka, Y., Nakamura, T., Omori, K., Kobayashi, K., Hori, M., et al. (2015). Histamine induces vascular hyperpermeability by increasing blood flow and endothelial barrier disruption *in vivo*. *PLoS One* 10, e0132367. doi:10.1371/journal.pone.0132367

Bach, A., Calsamiglia, S., and Stern, M. D. (2005). Nitrogen metabolism in the rumen. *J. Dairy Sci.* 88, E9–E21. doi:10.3168/jds.S0022-0302(05)73133-7

Barcik, W., Pugin, B., Brescó, M. S., Westermann, P., Rinaldi, A., Groeger, D., et al. (2019). Bacterial secretion of histamine within the gut influences immune responses within the lung. *Allergy* 74, 899–909. doi:10.1111/all.13709

Bastian, M., Heymann, S., and Jacomy, M. (2009). Gephi: an open source software for exploring and manipulating networks. Available at: https://gephi.org/publications/gephi-bastian-feb09.pdf.

Beghini, F., McIver, L. J., Blanco-Míguez, A., Dubois, L., Asnicar, F., Maharjan, S., et al. (2021). Integrating taxonomic, functional, and strain-level profiling of diverse microbial communities with bioBakery 3. *Elife* 10, e65088. doi:10.7554/eLife.65088

Bergman, E. N. (1990). Energy contributions of volatile fatty acids from the gastrointestinal tract in various species. *Physiol. Rev.* 70, 567–590. doi:10.1152/physrev.1990.70.2.567

Bionaz, M., Vargas-Bello-Pérez, E., and Busato, S. (2020). Advances in fatty acids nutrition in dairy cows: from gut to cells and effects on performance. *J. Anim. Sci. Biotechnol.* 11, 110. doi:10.1186/s40104-020-00512-8

Blanco-Miguez, A., Beghini, F., Cumbo, F., McIver, L. J., Thompson, K. N., Zolfo, M., et al. (2023). Extending and improving metagenomic taxonomic profiling with uncharacterized species using MetaPhlAn 4. *Nat. Biotechnol.* 41, 1633–1644. doi:10.1038/s41587-023-01688-w

Bolger, A. M., Lohse, M., and Usadel, B. (2014). Trimmomatic: a flexible trimmer for Illumina sequence data. *Bioinformatics* 30, 2114–2120. doi:10.1093/bioinformatics/btu170

Brown, S. A., Jaglan, P. S., and Banting, A. (1991). Ceftiofur sodium: disposition, protein-binding, metabolism, and residue depletion profile in various species. *Acta Veterinaria Scand. Suppl. Den.* 87, 97–99. doi:10.5555/19922272369

Buitenhuis, B., Lassen, J., Noel, S. J., Plichta, D. R., Sørensen, P., Difford, G. F., et al. (2019). Impact of the rumen microbiome on milk fatty acid composition of Holstein cattle. *Genet. Sel.* 51, 23–28. doi:10.1186/s12711-019-0464-8

Butler, W. R., and Smith, R. D. (1989). Interrelationships between energy balance and postpartum reproductive function in dairy cattle. *J. Dairy Sci.* 72, 767–783. doi:10.3168/jds.S0022-0302(89)79169-4

Campos, J. L. de, Kates, A., Steinberger, A., Sethi, A., Suen, G., Shutske, J., et al. (2021). Quantification of antimicrobial usage in adult cows and preweaned calves on 40 large Wisconsin dairy farms using dose-based and mass-based metrics. *J. Dairy Sci.* 104, 4727–4745. doi:10.3168/jds.2020-19315

Caspi, R., Billington, R., Keseler, I. M., Kothari, A., Krummenacker, M., Midford, P. E., et al. (2020). The MetaCyc database of metabolic pathways and enzymes - a 2019 update. *Nucleic Acids Res.* 48, D445–D453. doi:10.1093/nar/gkz862

Charrad, M., Ghazzali, N., Boiteau, V., and Niknafs, A. (2014). NbClust: an R package for determining the relevant number of clusters in a data set. *J. Stat. Softw.* 61, 1–36. doi:10.18637/jss.v061.i06

Chen, L., Yang, J., Yu, J., Yao, Z., Sun, L., Shen, Y., et al. (2005). VFDB: a reference database for bacterial virulence factors. *Nucleic Acids Res.* 33, D325–D328. doi:10.1093/nar/gki008

Chen, Y., Li, R., Wang, Z., Hou, X., Wang, C., Ai, Y., et al. (2020). Dehydrocostus lactone inhibits NLRP3 inflammasome activation by blocking ASC oligomerization and prevents LPS-mediated inflammation *in vivo*. *Cell Immunol.* 349, 104046. doi:10.1016/j.cellimm.2020.104046

Dancy, K. M., Ribeiro, E. S., and DeVries, T. J. (2019). Effect of dietary transition at dry off on the behavior and physiology of dairy cows. *J. Dairy Sci.* 102, 4387–4402. doi:10.3168/jds.2018-15718

Danecek, P., Bonfield, J. K., Liddle, J., Marshall, J., Ohan, V., Pollard, M. O., et al. (2021). Twelve years of SAMtools and BCFtools. *Gigascience* 10, giab008. doi:10.1093/gigascience/giab008

da Silva, R. R., Dorrestein, P. C., and Quinn, R. A. (2015). Illuminating the dark matter in metabolomics. *Proc. Natl. Acad. Sci. U. S. A.* 112, 12549–12550. doi:10.1073/pnas.1516878112

Davis, N. M., Proctor, D. M., Holmes, S. P., Relman, D. A., and Callahan, B. J. (2018). Simple statistical identification and removal of contaminant sequences in marker-gene and metagenomics data. *Microbiome* 6, 226. doi:10.1186/s40168-018-0605-2

Dixon, P. (2003). VEGAN, a package of R functions for community ecology. *J. Veg. Sci.* 14, 927–930. doi:10.1111/j.1654-1103.2003.tb02228.x

European Agency for the Evaluation of Medicinal Products (2002). "Ceftiofur, modification of MRLs for bovine species," in *Summary report veterinary medicines and infections. London, United Kingdom*. Available at: https://www.ema.europa.eu/en/documents/mrl-report/ceftiofur-modification-mrls-bovine-species-summary-report-3-committee-veterinary-medicinal-products_en.pdf (Accessed November 19, 2023).

Foster, D. M., Jacob, M. E., Farmer, K. A., Callahan, B. J., Theriot, C. M., Kathariou, S., et al. (2019). Ceftiofur formulation differentially affects the intestinal drug concentration, resistance of fecal *Escherichia coli*, and the microbiome of steers. *PLoS One* 14, e0223378. doi:10.1371/journal.pone.0223378

Furman, O., Shenhav, L., Sasson, G., Kokou, F., Honig, H., Jacoby, S., et al. (2020). Stochasticity constrained by deterministic effects of diet and age drive rumen microbiome assembly dynamics. *Nat. Commun.* 11, 1904. doi:10.1038/s41467-020-15652-8

Garner, M. R., Flint, J. F., and Russell, J. B. (2002). *Allisonella histaminiformans* gen. nov., sp. nov.: a novel bacterium that produces histamine, utilizes histidine as its sole energy source, and could play a role in bovine and equine laminitis. *Syst. Appl. Microbiol.* 25, 498–506. doi:10.1078/07232020260517625

Hagey, J. V., Bhatnagar, S., Heguy, J. M., Karle, B. M., Price, P. L., Meyer, D., et al. (2019). Fecal microbial communities in a large representative cohort of California dairy cows. *Front. Microbiol.* 10, 1093. doi:10.3389/fmicb.2019.01093

Hallberg, J. W., Wachowski, M., Moseley, W. M., Dame, K. J., Meyer, J., and Wood, S. L. (2006). Efficacy of intramammary infusion of ceftiofur hydrochloride at drying off for treatment and prevention of bovine mastitis during the nonlactating period. *Vet. Ther.* 7, 35–42.

Hansen, Z. A., Schilmiller, A., Guzior, D., Vasco, K. A., Rudrik, J. T., Quinn, R., et al. (2024). Shifts in the functional capacity and metabolite composition of the gut microbiome during recovery from enteric infection. *Front Cell Infect Microbiol* 14. doi:10.3389/fcimb.2024.1359576

He, W., Cik, M., Appendino, G., Puyvelde, L. V., Leysen, J. E., and Kimpe, N.De (2002). Daphnane-type diterpene orthoesters and their biological activities. *Mini-Rev Med. Chem.* 2, 185–200. doi:10.2174/1389557024605492

Jami, E., White, B. A., and Mizrahi, I. (2014). Potential role of the bovine rumen microbiome in modulating milk composition and feed efficiency. *PLoS One* 9, e85423. doi:10.1371/JOURNAL.PONE.0085423

Li, H. (2013) *Aligning sequence reads, clone sequences and assembly contigs with BWA-MEM*. Available at: https://arxiv.org/abs/1303.3997.

Lin, H., and Peddada, S. D. (2020). Analysis of compositions of microbiomes with bias correction. *Nat. Commun.* 11, 3514. doi:10.1038/s41467-020-17041-7

Lin, L., Lai, Z., Zhang, J., Zhu, W., and Mao, S. (2023). The gastrointestinal microbiome in dairy cattle is constrained by the deterministic driver of the region and the modified effect of diet. *Microbiome* 11, 10. doi:10.1186/s40168-022-01453-2

Liu, J., Liu, F., Cai, W., Jia, C., Bai, Y., He, Y., et al. (2020). Diet-induced changes in bacterial communities in the jejunum and their associations with bile acids in Angus beef cattle. *Anim. Microbiome* 2, 33. doi:10.1186/s42523-020-00051-7

Malheiros, J. M., Correia, B. S. B., Ceribeli, C., Cardoso, D. R., Colnago, L. A., Junior, S. B., et al. (2021). Comparative untargeted metabolome analysis of ruminal fluid and feces of Nelore steers (*Bos indicus*). *Sci. Rep.* 11, 12752. doi:10.1038/s41598-021-92179-y

Mallick, H., Rahnavard, A., McIver, L. J., Ma, S., Zhang, Y., Nguyen, L. H., et al. (2021). Multivariable association discovery in population-scale meta-omics studies. *PLoS Comput. Biol.* 17, e1009442. doi:10.1371/journal.pcbi.1009442

McMurdie, P. J., and Holmes, S. (2013). phyloseq: an R package for reproducible interactive analysis and graphics of microbiome census data. *PLoS One* 8, e61217. doi:10.1371/journal.pone.0061217

Mihara, T., Nishimura, Y., Shimizu, Y., Nishiyama, H., Yoshikawa, G., Uehara, H., et al. (2016). Linking virus genomes with host taxonomy. *Viruses* 8, 66. doi:10.3390/v8030066

Myers, O. D., Sumner, S. J., Li, S., Barnes, S., and Du, X. (2017). One step forward for reducing false positive and false negative compound identifications from mass spectrometry metabolomics data: new algorithms for constructing extracted ion chromatograms and detecting chromatographic peaks. *Anal. Chem.* 89, 8696–8703. doi:10.1021/acs.analchem.7b00947

National Research Council (2001) *Subcommittee on dairy cattle nutrition, committee on animal nutrition, board on agriculture and natural resources. Nutrient requirements of dairy cattle. 7th rev. Ed.* Washington, DC: National Academy Press. Available at: https://profsite.um.ac.ir/~kalidari/software/NRC/HELP/NRC%202001.pdf.

Nearing, J. T., Douglas, G. M., Hayes, M. G., MacDonald, J., Desai, D. K., Allward, N., et al. (2022). Microbiome differential abundance methods produce different results across 38 datasets. *Nat. Commun.* 13, 342. doi:10.1038/s41467-022-28034-z

Nothias, L.-F., Petras, D., Schmid, R., Dührkop, K., Rainer, J., Sarvepalli, A., et al. (2020). Feature-based molecular networking in the GNPS analysis environment. *Nat. Methods* 17, 905–908. doi:10.1038/s41592-020-0933-6

O'Hara, E., Neves, A. L. A., Song, Y., and Guan, L. L. (2020). The role of the gut microbiome in cattle production and health: driver or passenger? *Annu. Rev. Anim. Biosci.* 8, 199–220. doi:10.1146/annurev-animal-021419-083952

Ollier, S., Zhao, X., and Lacasse, P. (2013). Effect of prolactin-release inhibition on milk production and mammary gland involution at drying-off in cows. *J. Dairy Sci.* 96, 335–343. doi:10.3168/jds.2012-5955

Peisl, B. Y. L., Schymanski, E. L., and Wilmes, P. (2018). Dark matter in host-microbiome metabolomics: tackling the unknowns–A review. *Anal. Chim. Acta* 1037, 13–27. doi:10.1016/j.aca.2017.12.034

Pluskal, T., Castillo, S., Villar-Briones, A., and Orešič, M. (2010). MZmine 2: modular framework for processing, visualizing, and analyzing mass spectrometry-based molecular profile data. *BMC Bioinforma.* 11, 395. doi:10.1186/1471-2105-11-395

Rakusanova, S., Fiehn, O., and Cajka, T. (2023). Toward building mass spectrometry-based metabolomics and lipidomics atlases for biological and clinical research. *Trends Anal. Chem.* 158, 116825. doi:10.1016/j.trac.2022.116825

Ray, P., Knowlton, K. F., Shang, C., and Xia, K. (2014). Development and validation of a UPLC-MS/MS method to monitor cephapirin excretion in dairy cows following intramammary infusion. *PLoS One* 9, e112343. doi:10.1371/journal.pone.0112343

Reitelseder, S., Tranberg, B., Agergaard, J., Dideriksen, K., Højfeldt, G., Merry, M. E., et al. (2020). Phenylalanine stable isotope tracer labeling of cow milk and meat and human experimental applications to study dietary protein-derived amino acid availability. *Clin. Nutr.* 39, 3652–3662. doi:10.1016/j.clnu.2020.03.017

Ribeiro, M. D., Pereira, J. C., Queiroz, A. C.De, Bettero, V. P., Mantovani, H. C., and Silva, C. J.Da (2009). Influence of intraruminal infusion of propionic acid and forage to concentrate levels on intake, digestibility and rumen characteristics in young bulls. *Rev. Bras. Zootec.* 38, 948–955. doi:10.1590/S1516-35982009000500023

Rosen, B. D., Bickhart, D. M., Schnabel, R. D., Koren, S., Elsik, C. G., Tseng, E., et al. (2020). *De novo* assembly of the cattle reference genome with single-molecule sequencing. *Gigascience* 9, giaa021. doi:10.1093/gigascience/giaa021

Ruegg, P. L. (2017). A 100-Year Review: mastitis detection, management, and prevention. *J. Dairy Sci.* 100, 10381–10397. doi:10.3168/JDS.2017-13023

Rule, R., Quiroga, G., Buschiazzo, H., Lacchini, R., and Mordujovich, P. (1998). Rate of decline of cefotaxime and ceftazidime in milk following intramammary administration to healthy and mastitic dairy cows. *Vet. Rec.* 143, 310–311. doi:10.1136/vr.143.11.310

Saleem, F., Ametaj, B. N., Bouatra, S., Mandal, R., Zebeli, Q., Dunn, S. M., et al. (2012). A metabolomics approach to uncover the effects of grain diets on rumen health in dairy cows. *J. Dairy Sci.* 95, 6606–6623. doi:10.3168/jds.2012-5403

Schmartz, G. P., Hartung, A., Hirsch, P., Kern, F., Fehlmann, T., Müller, R., et al. (2022). PLSDB: advancing a comprehensive database of bacterial plasmids. *Nucleic Acids Res.* 50, D273–D278. doi:10.1093/nar/gkab1111

Segata, N., Izard, J., Waldron, L., Gevers, D., Miropolsky, L., Garrett, W. S., et al. (2011). Metagenomic biomarker discovery and explanation. *Genome Biol.* 12, R60. doi:10.1186/gb-2011-12-6-r60

Steinegger, M., and Söding, J. (2018). Clustering huge protein sequence sets in linear time. *Nat. Commun.* 9, 2542. doi:10.1038/s41467-018-04964-5

Tan, J., McKenzie, C., Potamitis, M., Thorburn, A. N., Mackay, C. R., and Macia, L. (2014). "Chapter three - the role of short-chain fatty acids in health and Disease," in *Adv immunol 21*. Editor F. W. Alt (Academic Press), 91–119. doi:10.1016/B978-0-12-800100-4.00003-9

Van Den Bossche, T., Arntzen, M. Ø., Becher, D., Benndorf, D., Eijsink, V. G. H., Henry, C., et al. (2021). The Metaproteomics Initiative: a coordinated approach for propelling the functional characterization of microbiomes. *Microbiome* 9, 243. doi:10.1186/s40168-021-01176-w

Vasco, K., Nohomovich, B., Singh, P., Venegas-Vargas, C., Mosci, R. E., Rust, S., et al. (2021). Characterizing the cattle gut microbiome in farms with a high and low prevalence of Shiga toxin-producing *Escherichia coli*. *Microorganisms* 9, 1737. doi:10.3390/microorganisms9081737

Vasco, K. A., Carbonell, S., Sloup, R. E., Bowcutt, B., Colwell, R. R., Graubics, K., et al. (2023). Persistent effects of intramammary ceftiofur treatment on the gut microbiome and antibiotic resistance in dairy cattle. *Anim. Microbiome* 5 (15), 56–19. doi:10.1186/S42523-023-00274-4

Wang, M., Carver, J. J., Phelan, V. V., Sanchez, L. M., Garg, N., Peng, Y., et al. (2016). Sharing and community curation of mass spectrometry data with global natural products social molecular networking. *Nat. Biotechnol.* 34, 828–837. doi:10.1038/nbt.3597

Wickham, H. (2011). ggplot2. *Wiley Interdiscip. Rev. Comput. Stat.* 3, 180–185. doi:10.1002/wics.147

Wilson, C., and Gilbert, G. (1986). Pharmacokinetics of cefoperazone in the cow by the intramammary route and its effect on mastitis pathogens *in vitro*. *Vet. Rec.* 118, 607–609. doi:10.1136/vr.118.22.607

Wu, X., Huang, S., Huang, J., Peng, P., Liu, Y., Han, B., et al. (2021). Identification of the potential role of the rumen microbiome in milk protein and fat synthesis in dairy cows using metagenomic sequencing. *Animals* 11, 1247. doi:10.3390/ani11051247

Xu, H., Huang, W., Hou, Q., Kwok, L. yu, Sun, Z., Ma, H., et al. (2017). The effects of probiotics administration on the milk production, milk components and fecal bacteria microbiota of dairy cows. *Sci. Bull. (Beijing)* 62, 767–774. doi:10.1016/J.SCIB.2017.04.019

Xue, M.-Y., Xie, Y.-Y., Zhong, Y., Ma, X.-J., Sun, H.-Z., and Liu, J.-X. (2022). Integrated meta-omics reveals new ruminal microbial features associated with feed efficiency in dairy cattle. *Microbiome* 10, 32. doi:10.1186/s40168-022-01228-9

Zhang, J., Shi, H., Wang, Y., Cao, Z., Yang, H., and Li, S. (2018). Effect of limit-fed diets with different forage to concentrate ratios on fecal bacterial and archaeal community composition in Holstein heifers. *Front. Microbiol.* 9, 976. doi:10.3389/fmicb.2018.00976

Zheng, N., Ruan, J., and Zhang, Y. (2000). Pharmacokinetic study on absorption of stachyose. *Chin. J. Integr. Traditional West. Med.* 20, 444–446.

Frontiers in
Molecular Biosciences

Explores biological processes in living organisms on a molecular scale

Focuses on the molecular mechanisms underpinning and regulating biological processes in organisms across all branches of life.

Discover the latest Research Topics

See more →

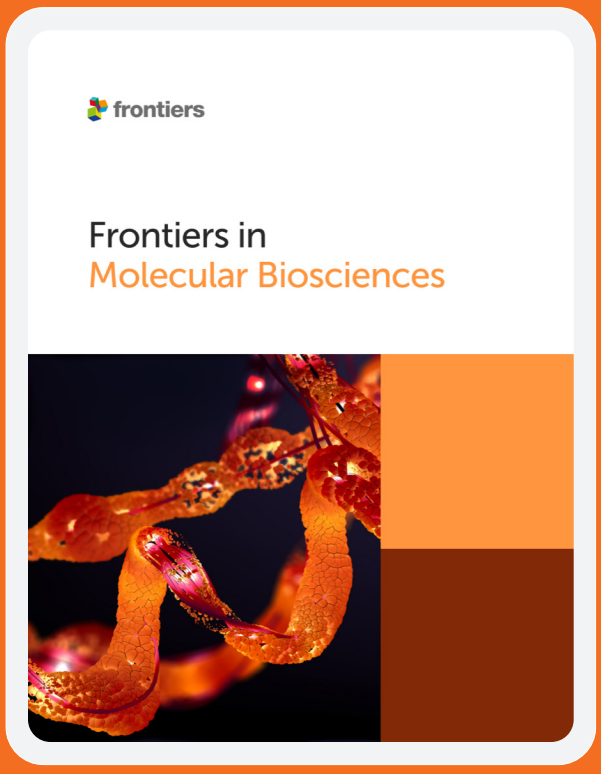

Frontiers

Avenue du Tribunal-Fédéral 34
1005 Lausanne, Switzerland
frontiersin.org

Contact us

+41 (0)21 510 17 00
frontiersin.org/about/contact